ANNUAL REPORT

of

THE INSTITUTE OF PHYSICS

ACADEMIA SINICA

VOLUME 7 DECEMBER 1977

PART B ATMOSPHERIC PHYSICS AND FLUID MECHANICS

THE INSTITUTE OF PHYSICS, ACADEMIA SINICA
NANKANG, TAIPEI, TAIWAN, REPUBLIC OF CHINA

中央研究院物理研究所集刊

編 輯 委 員 會

The Annual Report is published annually by the Institute of Physics, Academia Sinica, Nankang, Taiwan 115, Republic of China. The Annual Report is available on an exchange basis to other scientific, research, and educational institutions.

本集刊每年出版一次

非賣品

中央研究院

物理研究所集刊

第七卷

發行人：林爾康

編輯者：中央研究院物理研究所集刊編輯委員會

出版者：中央研究院物理研究所　臺北市南港區

印刷者：崇文企業有限公司

電話：三七一〇二二〇•三三一二六〇八

中華民國六十六年十二月出版

中央研究院物理研究所集刊

第 七 卷

中央研究院物理研究所印行

CONTENT 目 錄

Annual Report of the Institute of Physics, Academia Sinica, Vol.7, 1977

A Note on Water Drops

Chun-Tsung Wang

Institute of Physics, Academia Sinica

For many years rainfall simulators have been used frequently to accelerate research in surface runoff and in soil erosion problems (Mutchler & Hermsmeier, 1963; Chow & Harbaugh, 1965; Wang & Wenzel, 1970). Of the many simulators used, the method of capillary tube production produces the most uniform size drop. This drop former was constructed by inserting a length of capillary tube through the bottom of a water container. When water slowly flowed from the capillary tube a steady jet did not occur but rather a series of drops were formed because of the surface tension force. If the pressure at the tube entrance is kept constant and the tube has a square sharp edge, the drop formed is a function of the tube tip geometry, the surface tension force between air and water, the flow rate through the tube, and the air drag force on the drop. The relationship between the weight of the drop, tube size, and surface tension can be approximately expressed as

$$\text{Drop weight} = K \cdot \pi d_o \Gamma \qquad (1)$$

where d_o is the outside diameter of the tube, Γ is the surface tension force per unit length and K is an experimental constant varying from 0.59 to 1.00 (Manfre, 1966). When the flow rate through the tube approaches zero, Harkins & Brown (1919) showed that

$$K = \text{function (tube tip condition, capillary constant)} \qquad (2)$$

where capillary constant $=(2\Gamma/\rho)^{\frac{1}{2}}$, ρ is the water density; and K could be experimentally determined as a function of d_o/d, where d is the equivalent drop diameter.

When the flow rate increases, the analysis of drop production becomes a complicated one. Mutchler (1965) obtained an experimental relation assuming

$$\text{Drop weight} = \text{function } (\Gamma, d_o, q, \nu, g) \qquad (3)$$

where q is the flow rate through the tube, ν is the kinematic viscosity of water, g is the gravitational acceleration. Manfre′ & Whorlow (1967) also reported the relation between drop weight and $\rho^2\nu gq/\Gamma^2$ for a specific tube indicating that the drop weight increases to a maximum value as $\rho^2\nu gq/\Gamma^2$ increases. However that relationship tends to hold only for high viscous fluid.

The present experimental study was made by using drop formers constructed

by inserting different sizes of polyethylene tubes through the bottom of a plexiglass container. Tape water was used, and drops produced from the drop former were collected and weighed to 0.001 gm.

Figure 1 presents data on d vs. q for tubes of outside diameter of 0.047 inch and inside diameter of 0.023 inch. Because many capillary tubes were used and temperature during measurements varied between 65° and 74°F, a certain scattering was observed. However it is clearly seen that as the flow rate increases, the drop weight also increases until pulsating occurs. After that drop weight tends to decrease. Worthington (1881) suggested that it might be due to the influx of water through the residual neck into the lower portions after drop has begun to seperate. Many researchers (Manfre′, 1966; Edgerton et. al, 1937) studied drop formation problems, but as the air resistance and dynamic surface tension force remain unclear, the drop formation mechanism also remains unknown.

When the tube wall thickness is small, water tends to adhere to the outside of the tube and then forms drop. Figure 2 shows the relation between d and d_o for the various sizes PE tubings tested. It could be seen that the correlation between d and d_o is better than that of d and d_i. And as d_o increases, d also increases. Thus by chosing suitable tube outside diameter size, drop former could be constructed to produce needed drop sizes. The relationship between d and d_o is approximately

$$d = 8.607\ d_o^{0.308} \qquad (4)$$

References

Chow, V. T. & T. E. Harbough, Raindrop Production for Laboratory Watershed Experimentation, J. Geophysical Res., 70, 6111, 1965.

Edgerton, H. E., E. A. Hauser & W. B. Tucker, Studies in Drop Formation as Reveraled by the High-Speed Motion Camera, J. Phys. Chem., 41, 1017, 1937.

Harkins, W. D. & F. E. Brown, The Determination of Surface Tension, and the Weight of Falling Drops: The Surface Tension of Water and Benzene by the Capillary Height Methods, J. Am. Chem. Soc., 41, 499, 1919.

Manfre′, G., Rheological Aspects of Drop Formation, J. Appl. Phys., 37, 1955, 1966.

Manfre′, G. & R. W. Whorlow, The Rapid Formation of Drops of Viscous Liquids, Brit. J. Appl. Phys., 18, 6, 839, 1967.

Mutchler, C. K., Waterdrop Formation from Capillary Tubes, ARS 41-107, 1965.

Mutchler, C. K., & L. F. Hermsmeier, A Review of Rainfall Simulators, presented at the Winter Meeting of ASAE, Chicago, Dec. 1963.

Wang, C. T. & H. G. Wenzel, Jr., The Mechanics of a Drop After Striking a Stagnant Water Layer, Res. Rept. 30, U. Illinois WRC., Jan. 1970.

Worthington, A. M., On Pendent Drops, Proc. Royal Soc. (London), 32, 362, 1881.

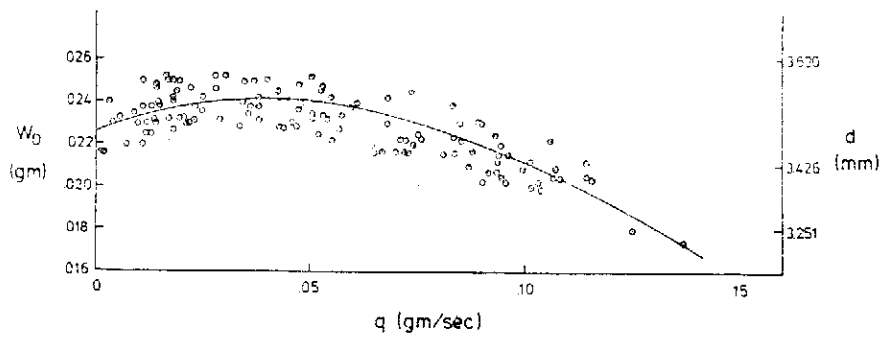

Figure 1 Flow Rate vs. Drop Size Relation

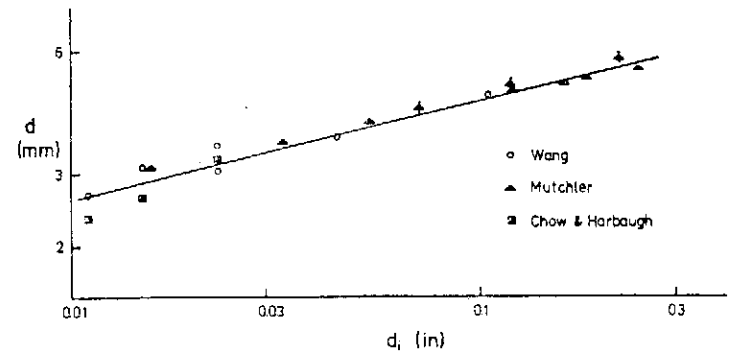

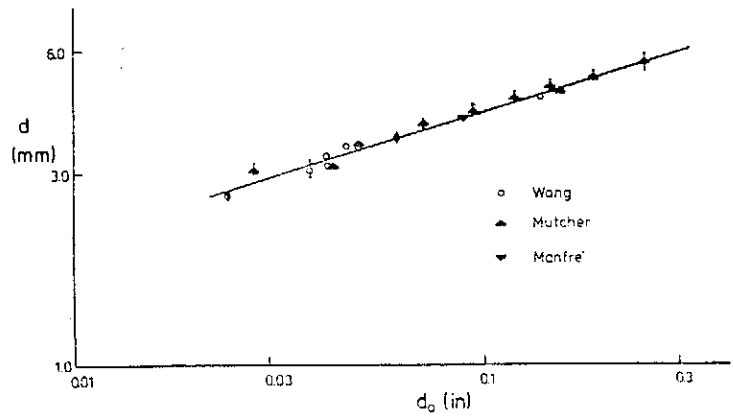

Figure 2. Tube Size vs. Drop Size Relation.

Annual Report of the Institute of Physics, Academia Sinica, Vol.7, 1977

快艇基本設計研究

汪 群 從

中央研究院物理研究所

摘 要

本文由穩定、阻力、空蝕等船用流力觀點，研設30噸級快艇，採用船型爲雙舭型，提供設計線圖、螺槳圖，及設計艇靜水穩定及阻力性能。

橫傾角變化時，滑航艇靜水阻力性能公式直接由滑航面理論推導，考慮海況3波浪中行駛阻力增加值，推估設計艇在2,430HP×850rpm時，可以40節速率行駛。

Ⅰ 緒 言

在國防軍事上一般使用之高速艦艇有三種：快艇（Planing craft），水翼船及氣墊船，到目前爲止使用最多的仍是快艇。由於國防機密的緣故，此方面資料不易獲得，作者於前年在海軍總部支援下，開始展開系列快艇試驗探討工作，先後完成36呎快艇之阻力試驗研究（劉、汪、胡，1975），雙體滑航面分離比對靜水阻力及性能之影響探討（汪、劉、郭，1975），單階滑航艇之靜水阻力探討（汪、呂，1977）等工作。臺灣海峽屬於風浪較大之海域，特別是在冬季，本文擬針對海況較壞情況下，由船用流力觀點，研設30噸級快艇。其設計性能要求爲：

§ 排水噸位：30噸。

§ 速度要求：最大速度爲40kt，一般巡航速度依據排水噸位定爲10kt，以使其體積佛勞數不超過1。

§ 吃　水：定爲2.7ft。

§ 使用海域：定爲3，其有效波高$H^1/_3$=4.6ft, T_w=4.6*sec*, L_w=108.3ft. Wiegel, 1964; Blount & Fox, 1975)

§ 重心平均衝擊加速度：不超過0.4g，使人員仍可工作(Vossers, 1971)

§ 定 傾 高：GM=3 *ft*.

Ⅱ 快艇設計

1.主要尺寸決定

主要尺寸之決定，在使快艇在靜水及波浪中皆有較低阻力，同時顧及該艇之橫向穩度，使其在高速使用及一般低速巡航時，皆能有較佳性能。

1.1.平均衝擊加速度

主要利用Fridsma 1969及1971系列快艇試驗結果爲依據，其計算步驟爲

§ 假設不同船寬B，得

B	$C_\Delta=\frac{\triangle}{WB^3}$	$\frac{1}{C_\Delta^2}$	$\frac{Hy_{\frac{1}{3}}}{B}$	$Cv=\frac{V}{\sqrt{gB}}$
9	1.440	0.48	0.511	3.97
10	1.050	0.91	0.460	3.77
11	0.789	1.60	0.418	3.59
12	0.608	2.69	0.383	3.44
13	0.478	4.34	0.354	3.30

表中W=64 #/ft^3，B爲離艇艉80%L之平均寬

§ 利用B及L/B之變化求平均衝擊加速度

	$B=9$		$B=10$		$B=11$		$B=12$		$B=13$	
L/B	L	$V_k/\sqrt{L}$	L	$V_k/\sqrt{L}$	L	$V_k/\sqrt{L}$	L	$V_k/\sqrt{L}$	L	$V_k/\sqrt{L}$
4	36	6.67	40	6.32	44	6.03	48	5.77	52	5.55
5	45	5.96	50	5.66	55	5.39	60	5.16	65	4.96
6	54	5.44	60	5.16	66	4.92	72	4.71	78	4.53

§ ηcg值〔$\tau=4°, \beta=20°$〕可由 L/B, $1/C_{\Delta}^2$, $H^1/_3/B$ 及 $V/\sqrt{L}$ 關係求得 (Savitsky & Brown; 1975, 1976)

$B=9$ $\quad 1/C_{\Delta}^2=0.48 \quad H^1/_3/B=0.511$

$L/B=$	4	5	6
$V/\sqrt{L}=$	6.67	5.96	5.44
$\eta cg=$	0.48	0.35	0.365

$(\eta cg)_{avg}=0.36g$

$B=10$ $\quad 1/C_{\Delta}^2=0.91 \quad H^1/_3/B=0.46$

$L/B=$	4	5	6
$V/\sqrt{L}=$	6.32	5.66	5.16
$\eta cg=$	0.79	0.61	0.59

$(\eta cg)_{avg}=0.60g$

$B=11$ $\quad 1/C_{\Delta}^2=1.60 \quad H^1/_3/B=0.418$

$L/B=$	4	5	6
$V/\sqrt{L}=$	6.03	5.39	4.92
$\eta cg=$	0.95	0.83	0.90

$(\eta cg)_{avg}=0.89g$

$B=12$ $\quad 1/C_{\Delta}^2=2.69 \quad H^1/_3/B=0.383$

$L/B=$	4	5	6
$V/\sqrt{L}=$	5.77	5.16	4.71
$\eta cg=$	1.07	1.04	1.06

$(\eta cg)_{avg}=1.06g$

$B=13$ $\quad 1/C_{\Delta}^2=4.34 \quad H^1/_3/B=0.354$

$L/B=$	4	5	6
$V/\sqrt{L}=$	5.55	4.96	4.53
$\eta cg=$	1.12	1.17	1.17

$(\eta cg)_{avg}=1.17g$

§ 設快艇橫傾角 $\beta=20°$, 在不同B時保持$(\eta cg)_{avg}=0.4g$, 則 $\tau=4°$, $\beta=20°$

B	$(\eta cg)_{avg}$	$K=\dfrac{0.4g}{(\eta cg)_{avg}}$	$\tau=4K$
9	$0.36g$	1.11	4.44
10	$0.60g$	0.67	2.67
11	$0.89g$	0.45	1.80

1.2 方塊係數C_b

一般滑航艇C_b在0.4至0.5之間，現設計艇吃水定爲2.7 ft，則艇長關係爲

B	C_b=0.4	C_b=0.45	C_b=0.5
9	108	96	86
10	97	86	78
11	88	79	71

1.3 長度決定：長度之決定需同時考慮下列因素

§ 符合平均衝擊加速度之仰角

§ C_b之範圍

§ 一般巡航速度時阻力宜低

初步利用Savitsky (1964) 公式粗估阻力，得下列關係

B	τ	Cv	λ	LCG	L_k	L	C_b	$L/\nabla^{1}/_{3}$
9	4.00	3.968	5.40	27.12	56.1	62	.70	6.1
10	2.42	3.764	6.61	33.36	79.8	88	.44	8.7
11	1.80	3.589	7.00	37.27	97.3	107	.33	10.5

式中L=1.1L_k，一般巡航速度時$L/\nabla^{1}/_{3}$，大於7時，阻力合宜，從而得

合宜艇長爲 L=71 ft.

B=9.3 ft.

C_b=0.6

1.4.橫向穩度

設計艇定傾高GM定爲 3ft. (Savitsky et. al., 1972)

$KB \cong {}^{2}/_{3}d$=1.8 ft (戴堯天等，1974)

KG=4.6 ft (船舶，1976)

則得下敍關係

B	I	BM	KM	GM
9	2372	2.26	4.06	—
10	3254	3.10	4.90	0.30
11	4331	4.13	5.93	1.33
12	5623	5.36	7.16	2.56
12.3	6090	5.80	7.60	3.00
13	7149	6.81	8.61	4.01

式中 I =0.55(${}^{1}/_{12}LB^{3}$)，$BM=\frac{I}{\triangle}$

1.5.主要尺寸決定，由以上考慮，得二種尺寸

§ 不考慮GM=3 ft，則 L=71 ft

B=9.3 ft

LCG=29.2 ft

C_b=0.61

§ 考慮 $GM=3\ ft$，則 $L=127\ ft$

$B=12.3\ ft$

$LCG=41\ ft$

$C_b=0.25$

後者船身太長不合經濟原則，前者因舷寬不够，橫向穩定性能不足。加採用雙舷船型，則可二者兼顧，其主要尺寸爲

$L=71\ ft$

$Bouter=12.3\ ft$

$Binner=9.3\ ft$

$LCG=29.2\ ft$

$\beta=20°$

$\triangle=30\ tons$

	upper chine	*lower chine*
Ap	$794.92\ ft^2$	$583.29\ ft^2$
$Ap/\triangle^{2}/_{3}$	7.695	5.646

如此一般低速巡航時有足够定傾高；高速行駛時，水流在低舷處分離，符合耐波性能。

2.線圖決定

依據上敍決定之主要尺寸，並參照 Series 62, 63, 65等已有快艇設計圖樣，給就船圖，加以重覆整順，決定之線圖如圖1所示。重要特性變化如圖2所示。

3.穩定性能

設計快艇之靜水穩定性能由線圖計算如圖3所示，圖4顯示其穩定性能良好，合乎 Vossers (1971) 各項要求

4.靜水阻力推估

具有不同 deadrise angle 變化之快艇阻力計算，可藉下列公式

$$C_v=\frac{V}{\sqrt{gb}}$$

$$C_{L\beta}=\frac{\triangle}{\frac{1}{2}\rho v^2 b^2}$$

$$\frac{LCG}{b\lambda}=0.75-\left(5.21\frac{C_v^2}{\lambda^2}+2.39\right)^{-1}$$

$$C_{L\beta}=C_{L0}-0.0065\ \beta'\ C_{L0}^{0.6}$$

$$C_{L0}=\tau^{1.1}\left[0.012\lambda^{\frac{1}{2}}+\frac{0.0055\lambda^{2.5}}{C_v^2}\right]$$

$$\frac{V_m}{V}=\left[1-\frac{0.012\tau^{1.1}}{\lambda^{\frac{1}{2}}\cos\tau}\right]^{0.5}$$

$$Re=V_m\lambda b/\nu$$

$$\frac{0.242}{\sqrt{C_f}}=\log_{10}(Re\ C_f)$$

$$D_f={}^{1}/_{2}\rho Vm^2\lambda b^2\ (C_f+\triangle C_f)/\cos\beta_A$$

$$D=\triangle\tan\tau'+D_f/\cos\tau''$$

聯立解得

在斜旗角 (deadrise angle) 不變時，Savitsky (1964)設

$$\begin{cases} b=b_{mean\ aft\ 30\%} \\ \triangle C_f=0.0004 \\ \beta_A=\beta_B=\beta' \\ \tau'=\tau''=\tau \end{cases}$$

在有橫斜角變化時，Blount & Fox (1975) 設

$$\begin{cases} b=bmax \\ \beta'=\beta_5 \\ \tau'=\tau''=\tau \\ \triangle C_f=0.0 \end{cases}$$

Savitsky & Brown (1975) 設

$$\begin{cases} b=b_{mean\ aft\ 80\%} \\ \beta'=\beta_T \\ \triangle C_f=0.0004 \\ \tau'=\tau+0.12\theta \\ \tau''=\tau+0.5\theta \\ \theta: \textit{keel 與 chine 間夾角} \end{cases}$$

本文由基本滑航原理，設快艇在每一單位裁面上

$$\frac{d\ C_{L0}}{dx}=bx^2-ax+al$$

x 方向由艇艉指向艇艏，可得

$$\beta'=\beta_T+\theta\frac{\int_0^{\lambda b} x(bx^2-ax+al)^{0\cdot6}dx}{\int_0^{\lambda b}(bx^2-ax+al)^{0\cdot6}dx}$$

式中 $\frac{bl}{a}=3.273\frac{Cv^3}{\lambda^2}$

如此，公式 a) 可寫爲

$$Cv=\frac{V}{\sqrt{gb}}$$

$$CL\beta=\triangle/{}^1/_2\rho v^2b^2$$

$$\lambda^3-3.0158\frac{LCG}{b}\lambda^2+4.9306Cv^2\lambda-6.5741\frac{LCG\ Cv^2}{b}=0$$

$$\beta'=\beta_T+\theta\frac{\int_0^{\lambda b} x(bx^2-ax+al)^{0\cdot6}dx}{\int_0^{\lambda b}(bx^2-ax+al)^{0\cdot6}dx}$$

$$C_L\beta=C_{L0}-0.0065\beta' C_{L0}{}^{0\cdot6}$$

$$C_{L0}=\tau^{1\cdot1}[0.012\lambda^{0\cdot5}+\frac{0.0055\lambda^{2\cdot5}}{Cv^2}]$$

$$\frac{Vm}{V}=[1-\frac{0.012\ \tau^{1\cdot1}}{\lambda^{0\cdot5}\cos\tau}]^{0\cdot5}$$

$$Re=Vm\lambda\ b/\nu$$

$$\frac{0.242}{\sqrt{C_f}}=\log_{10}(Re\ C_f)$$

$$D_f={}^1/_2\rho Vm^2\lambda b^2(C_f+\triangle C_f)/\cos\beta m$$

$$D=\triangle\tan\tau+D_f/Cr\sec\tau$$

式中

$$\begin{cases} b=b_{mean\ aft\ 80\%} \\ \beta m=\dfrac{\beta_5+\beta_{10}}{2} \\ \triangle C_f=0.0004 \end{cases}$$

聯立解之，可得設計艇之阻力推估值爲（圖5）

Vk (kt)	Cv	λ	β'(°)	τ(°)	D_f(#)=R_{BH}
44	4.29	5.51	18.69	3.34	9.800
42	4.10	5.66	18.74	3.35	9.451
38	3.71	6.03	18.86	3.30	8.708
36	3.51	6.26	18.93	3.23	8.305
34	3.32	6.50	19.02	3.14	7.876
25	1.95	8.35	19.55	2.25	4,576
20	1.46	8.84	19.65	2.02	3.554
15	0.98	9.19	19.71	1.85	2.743

5.波浪中阻力增加推估

設計快艇需在海況3情況下作業，此時 H_{v3}=4.6 ft，風速達 16 kts。快艇阻力推估引用 Fridsma (1971) 系列試驗值，計算過程如下：(Blount & Fox, 1976)

						$(Raw/wb^3)max$				$(V/\sqrt{L})max$	
Vk	σ	τ	β'	$Vk/\sqrt{L}$	b	$H^1/_3/b$=0.2	0.4	0.495	0.6	H_{v3}/b=0.2	0.4&0.6
15	$atm.$	1.98	19.65	1.78	9.3	.027	.049	.0533	.058	4.8	5.3
20.21	2	2.25	19.55	2.40	↓	.028	.0475	.052	.057	4.8	5.2
23.34	1.5	2.43	19.42	2.77	↓	.028	.047	.0518	.057	4.7	5.05
28.58	1.0	2.81	19.11	3.39	↓	.027	.047	.0513	.056	4.4	4.8
33.0	.75	3.07	18.92	3.92	↓	.027	.0455	.0498	.0545	4.5	4.7
40.42	.50	3.34	18.80	4.80	9.3	.027	.045	.049	.054		4.6

$\frac{V}{Vmax}$	$\frac{Raw}{Rawmax}$	E	$\frac{Raw}{wb^3}$	Raw	$Rapp$
.34	.20	2.65	.0282	1,454	
.46	.31	2.07	.0344	1,718	
.55	.43	1.82	.0405	2,087	
.71	.715	1.46	.0532	2,738	579
.83	.893	1.27	.0561	2,890	765
1.04	.995	1.20	.0585	3,012	1.121

$$Rapp=R_{BH}\left(\frac{1}{\eta_A}-1\right)$$

$F\nabla$	1.0	1.5	2.0	2.5	3.0	3.5	4.0	4.5	5.0
η_A	.948	.942	.934	.925	.913	.900	.885	.869	.851

推估阻力示於圖5

6.艉端佈置

由Ducane (1974) 快艇資料可求出船長與舵面積關係，圖6顯示設計快艇艇長71 ft時，宜有8 ft² 之舵面積。如使用雙螺槳、雙舵，舵之寬長比爲4：3時，舵寬爲1.73 ft，舵長爲2.31 ft. 同時設計螺槳軸(shaft)由station 8 4分之1 buttock處伸長。

7.螺槳設計

高速快艇螺槳設計需考慮空蝕問題，系列螺槳方面有SSPA等，設計快艇採用較易購得之 Gawn & Burill's系列螺槳（1957），設EAR=0.82，用3葉片螺槳。$1-t$及$1-w$值使用Blount & Fox（1975）表列實際快艇值。在不同螺槳大小時，快艇性能爲：（圖7）

V_k	R_{BH}	R_{APP}	R_{AW}	R_T	F_D	$1-t$	$1-w$	η_R	σ	K_T/J_T^2	D	η_O	J_T	P/D	P	EHP	SHP	RPM	η_A
28.58	6,570	579	2,738	9,887	2.69	.92	.97	1.0	1.0	.197	2.5	.723[5]	1.03	1.4	3.5	867	1,263	1,091	.92
										.137	3.0	.741	1.23[5]	1.6	4.8		1,234	758	
										.101	3.5	.742	1.57	2.0	7.0		1,232	511	
										.077	4.0	.750	1.637	2.0	8.0	↓	1,219	429	
33.00	7,640	765	2,890	11,295	3.10	.92	.975	1.0	.75	.167	2.5	.718	1.07	1.4	3.5	1,144	1,689	1,218	.909
										.116	3.0	.744	1.30	1.6	4.8		1,630	836	
										.0854	3.5	.750	1.67	2.0	7.0		1,617	558	
										.0654	4.0	.750	1.676	2.0	8.0	↓	1,617	486	
40.42	9,160	1,121	3,012	13,293	3.80	.92	.975	1.0	.50	.131	2.5	.559	.899	1.4	3.5	1,649	3,126	1,776	.89
										.0912	3.0	.696	1.295	1.6	4.8		2,511	1,028	
										.0670	3.5	.694	1.37	1.6	5.6		2,518	833	
										.0513	4.0	.776	1.42	1.6	6.2	↓	2,252	703	

如選擇 $\begin{cases} D=3.4' \\ EAR=0.82 \\ P/D=1.6 \end{cases}$

則在設計速度附近 $Vk=40.42\ kt$ 時

$$\tau_c=\frac{T}{0.5\rho\ A_T\ V^2_{0.7R}}=0.0823$$

$$\sigma_{0.7R}=\sigma\left[\frac{J^2}{J^2+4.84}\right]=0.1375$$

由於

$$\tau_c<0.494(\sigma_{0.7R})^{0.88}$$

因之back cavitation小於 blade area之10%，螺槳設計可行，螺槳線圖可依照圖 8 繪製。

Ⅲ 設計艇性能

設計艇△=30 *fons*, *LCG*=29.2 *ft*, *D*=3.4 *ft*, *EAR*=.82, *P/D*=1.6, N_PR=2, 穩定性能如圖 4 所示，靜水阻力性能如圖 5 所示，在不同速度所需主機馬力爲：

V_K	R_{BH}	*Rapp*	*Raw*	R_T	$F\Delta$	1-*t*	1-w_t	η_R	K_T/J_T^2	σ	η_O	J_T	η_D	*EHP*	*SHP*	*RPM*
10	2743	144	1353	4,240	.93	.92	1.06	1.0	.313	*Atm.*	.656	1.03	.569	130	228[5]	307
15	3554	213	1454	5,221	1.40	.92	1.045	1.0	.176	*Atm.*	.709	1.19	.624	240	385	392
20.21	4610	318	1718	6,646	1.89	.92	1.0	1.0	.135	2	.740	1.24	.681	412	605	486
28.58	6570	579	2738	9,887	2.69	.92	.97	1.0	.107	1.0	.743	1.30	.705	867	1,230	635
33.0	7640	765	2890	11,295	3.10	.92	.975	1.0	.0905	.75	.749	1.36	.707	1,144	1,618	705
40.42	9160	1121	3012	13,293	3.80	.92	.975	1.0	.0710	.50	.697	1.36	.658	1.649	2,507	863

推估馬力及轉速顯於圖 9

Ⅳ 結　　語

本研究由船用流力觀點研討設計30噸級快艇。可以看出爲了增加耐波及穩定性能，船寬需要加大，爲了減少船舶阻力，長度需要加長。然而太長、太寬不合經濟原則，因之使用雙舭船型，快艇線圖如圖 1 所示。

快艇在高速下行駛，螺槳發生空蝕爲不可避免現象，考慮可容忍的空蝕發生，設計螺槳線圖如圖 8 所示。

快艇橫傾角變動時，阻力推估方式有許多種。本文由基本滑航理論推導靜水中滑航艇阻力公式（公式 7），推估設計快艇靜水阻力（圖 5）。

快艇在海況不佳情況下高速行駛時，阻力增加甚大，所需推動之主機馬力亦增加不少。設計快艇在40kts馳行時約需2,430HP×850RPM（圖 9）。

後記：本工作承呂崇湧、陳芳正、徐潮君、張弘岳等先生及造船所同人協助完成，謹致謝意。中正科技基金會及行政院國科會對助理研究人員及計劃執行費用之鼎力支援，一併致謝意。

Ⅴ 參考文獻

（1） 劉衿友、汪群從、胡定宇，「36呎快艇之阻力試驗研究」，NTU-INA-33, 1975.

（2） 汪群從、劉衿友、郭崇霖，「雙體滑航面分離比對靜水阻力及性能之影響探討」，NTU-INA-34, 1975.

(3) 汪群從、呂崇湧，單階滑航艇之靜水阻力探討，NTU-INA 49, 1976, Also 18th ATTC, Annapolis, 1977.

(4) Blount, D. L. et. al., 'Correlation of Full-Scale Trials and Model Tests for a Small Planing Boat', Trans. RINA 1969, Vol.111, P. 165

(5) Blount, D. L. & D. L. Fox, Small Craft power prediction, Marine Tech., 13, 1976, P. 14

(6) Clement, E.P. & D. L. Blount, 'Resistance Tests of a Systematic Series of Planing Hull Forms, SNAME, 71, 1963, P. 491.

(7) Du Cane, P., High Speed Small Craft, Temple Press Ltd., London, 1974.

(8) Fridsma, G., A Systematic Study of the Rough-Water Performance of Planing Boats' Davidson Lab. Rept. R-61275, Nov. 1969.

(9) Fridsma, G., A Systematic Study of the Rough-Water Performance of Planing Boats (Irregular Waves-Part II), Davidson Lab, Rept. R-1495, Mar. 1971.

(10) Gawn, R.W.L. & L.C. Burrill, Effect of Cavitation on the Performance of a Series of 16-Inch Model Propllers, T.I.N.A., 99, 1957.

(11) Hadler, J.B., The Prediction of Power Performnce on Planing Craft. SNAME, 74, 1966, P. 563.

(12) Hadler, J.B. & E. N. Hubble, Prediction of Power Performance of t he Series 62 Planing Hull Forms, SNAME, 79, 1971, P. 366.

(13) Hadler, J. B., Hubble, E. N. & H. D. Holling, Resistance Characteristics of a Sysematic Series of Planing Hull Forms-Series 65, Cheasapeake Sec., SNAME, May, 1974.

(14) Holling, H. D. & E. N. Hubble, Model Resistance Data of Series 65 Hull Forms Applicable to Hydrofoils and Planing Craft, NSRDC Rept. 4121, May, 1974.

(15) Hubble, E. N., 'Resistance of Hard-Chine, Step-less Planing Craft with Systematic Variation of Hull Form, Longitudinal Center of Gravity, and Loading, NSRDC Rept. 4307, Apr., 1974.

(16) Hubble, N., Correlation of Resistance Test Resuits from Fixed-and Free'to-trim Methods for a Dynamic-Lift Craft, NSRDC Rept. 3544, 1972

(17) Lindgren, H., Model Tests With a Family of Three-and Five-Bladed Propllers, SSPA Rept. 47, Sweden, 1961.

(18) Martin, M., Theoretical Determination of Porpoising Instability of High-Speed Planing Boats, D.T. NSRDC Rept. 76-0068, Apr., 1976.

(19) Martin, M., Theoretical Prediction of High-Speed Planing Boats in Waves, D. T. NSRDC Rept. 76-0069, Apr., 1976.

(20) Mercier, J.A. & D. Savitsky, Resistance of Transom-Stern Craft in the Pre-planing Regime, Davidson Lab. Rept. SIT-DL-76-1667, 1973.

(21) Sarchin, T. H. & L. L. Goldberg, Stability and Buoyancy Criteria for U.S. Naval Surface Ships, SNAME, 70, 1962, P. 418.

(22) Savitsky, D. et. al., Hydrodynamic Development of a High Speed Plan ing Hull for

Rough Water, 9th Symposium on Naval Hydrodynamics, Paris, Aug. 1972, P. 419.

(23) Savitsky, D., Hydrodynamic Design of Planing Hulls, Marine Tech., 1, 1964, P. 71.

(24) Savitsky, D., Wetted Length and Center of Pressure of VeeStep Planing Surfaces, Davidson Lad. Rept. SIT-DL-51-378, 1951.

(25) Savitsky, D., & P. W. Brown, Procedures for Hydrodynamic Evaluation of Planing Hulls in Smooth and Rough Water, Hampton Rds. Sec., SNAME, Nov. 26, 1975.

(26) Sibul, O.J., Measurements and Calculations of Ship Resistance in Waves, Part II, Rept. No. NA 71'3, Coll. Engr., U.C. Berkeley, 1971

(27) Sibul, O.J., Ship Resitance in Irreguler Waves, Rept. No. NA-69- 5, Coll. Engr., U. C. Berkeley, 1969.

(28) Vossers, G., Resistance, Propulsion and Steerin g of Ships, C. Behavionr of Ships in Waves, 1971.

(29) Wiegel, R.L., Oceanographical Engineering, Prentice-Hall, Inc., Edglewood Ciffs, N.J. 1964.

(30) Yeh, H.Y.H., Series 64 Resistance Experiments on High-Speed Displacement Forms. SNAME, Chesapeake Section, Dec. 1964.

(31) 戴堯天、劉衿友、陸磐安，造船原理，NTU-INA-19, 1974.

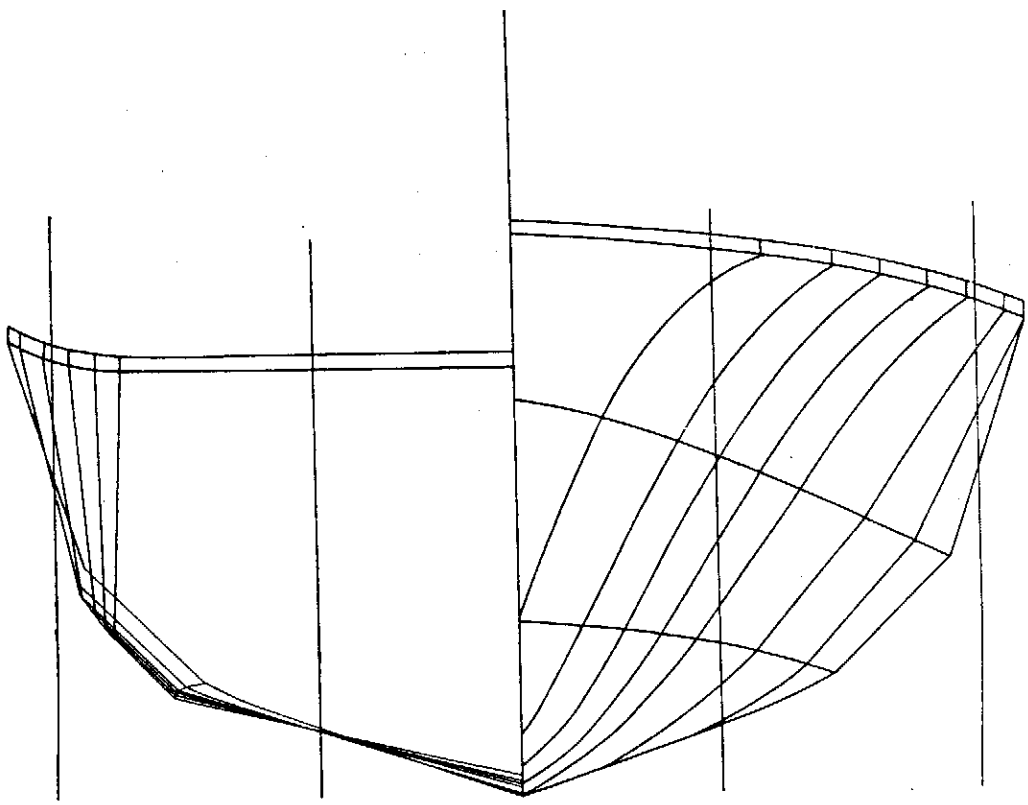

Figure 1. Hull Form Lines

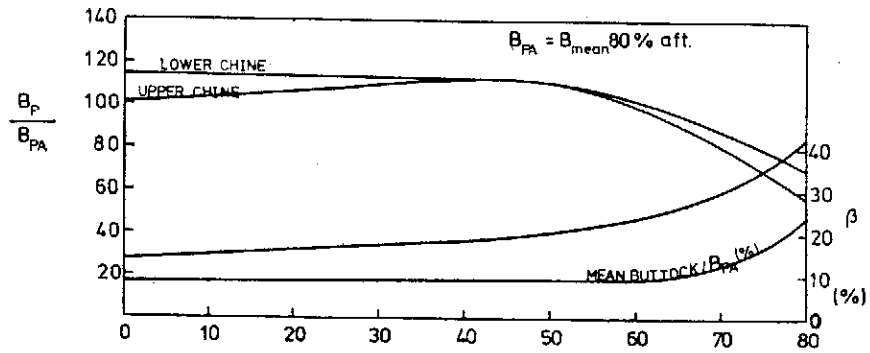

Figure 2. Form Characteristics Curve.

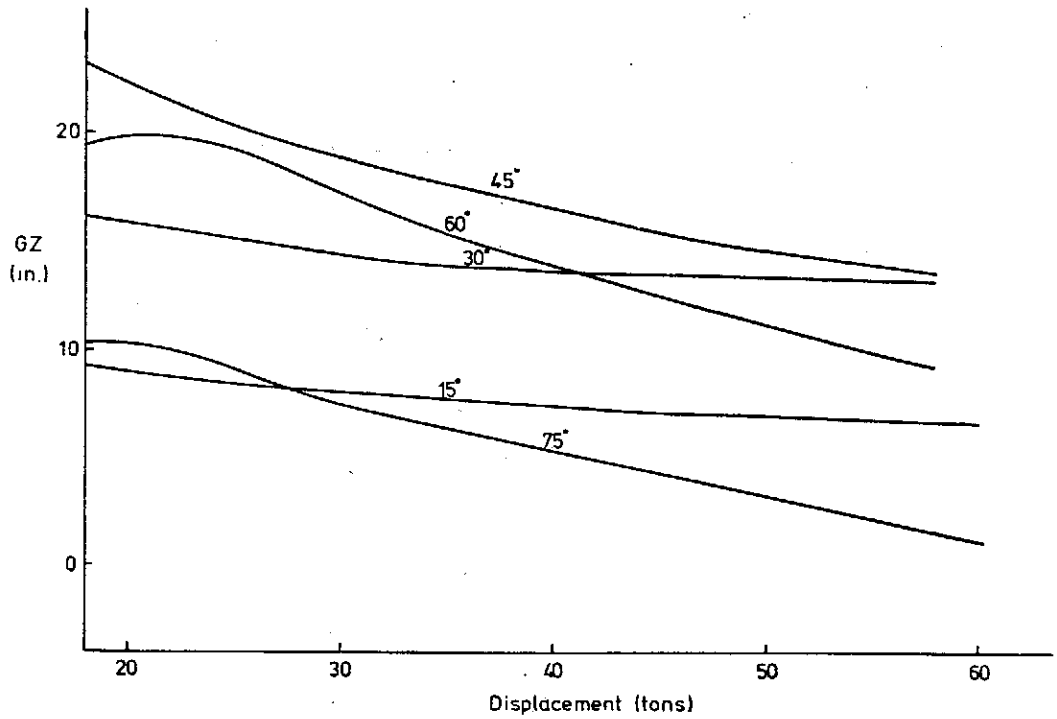

Figure 3. Cross Curve.

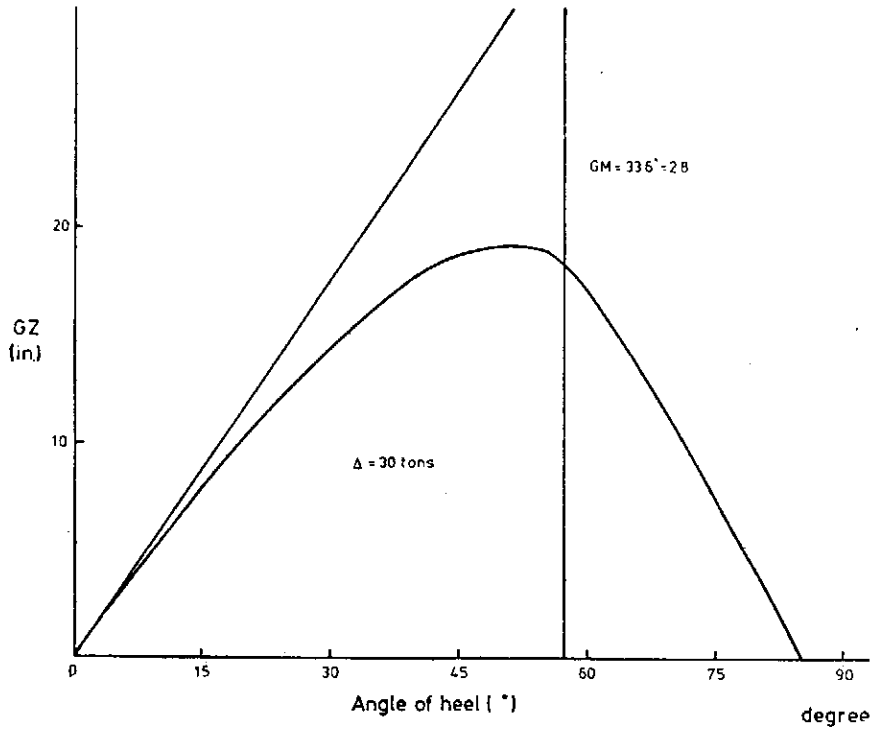

Figure 4. Curve of Static Stability.

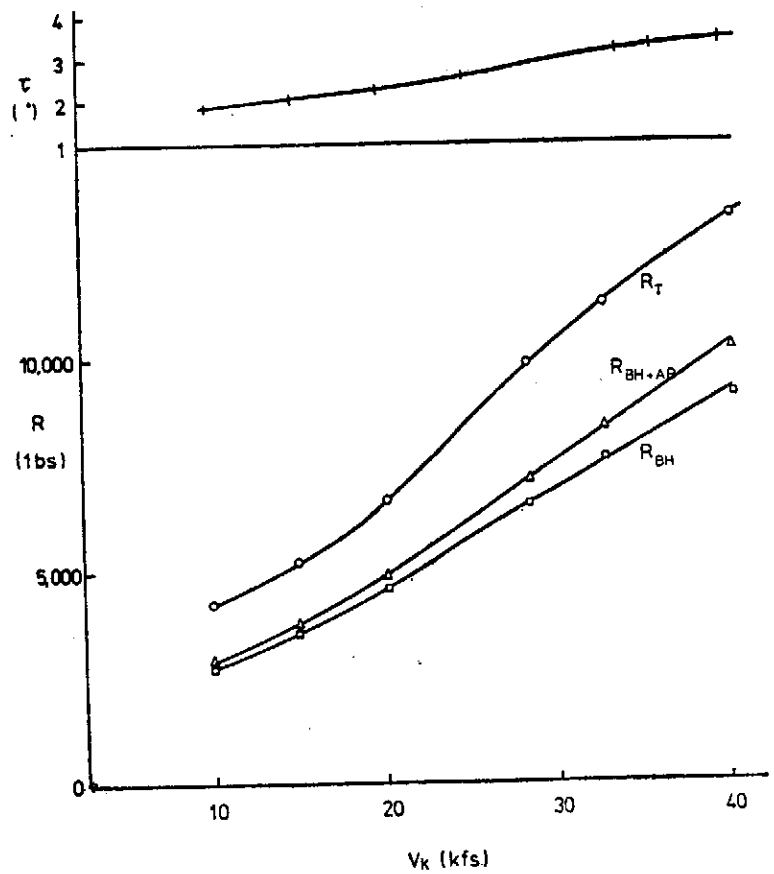

Figure 5. Resistance and Trim.

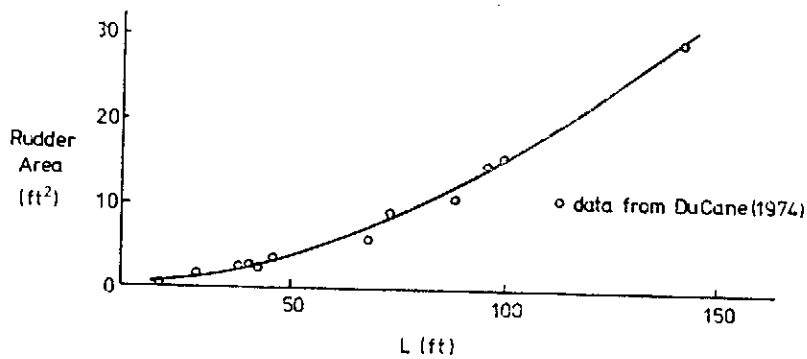

Figure 6. Rudder Area .vs. Ship Length.

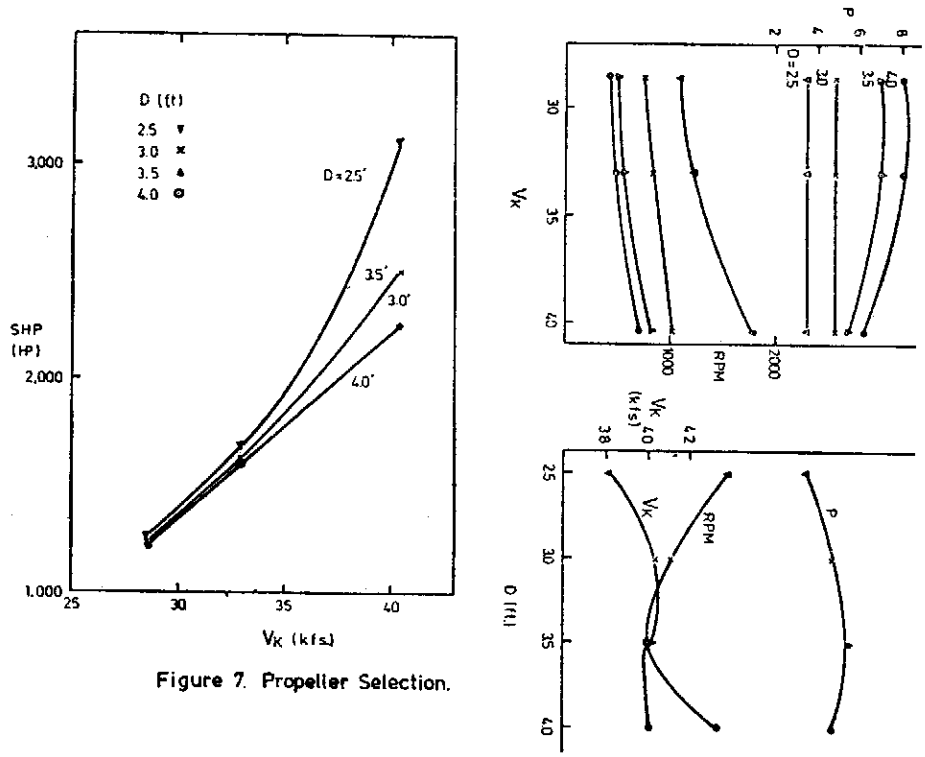

Figure 7. Propeller Selection.

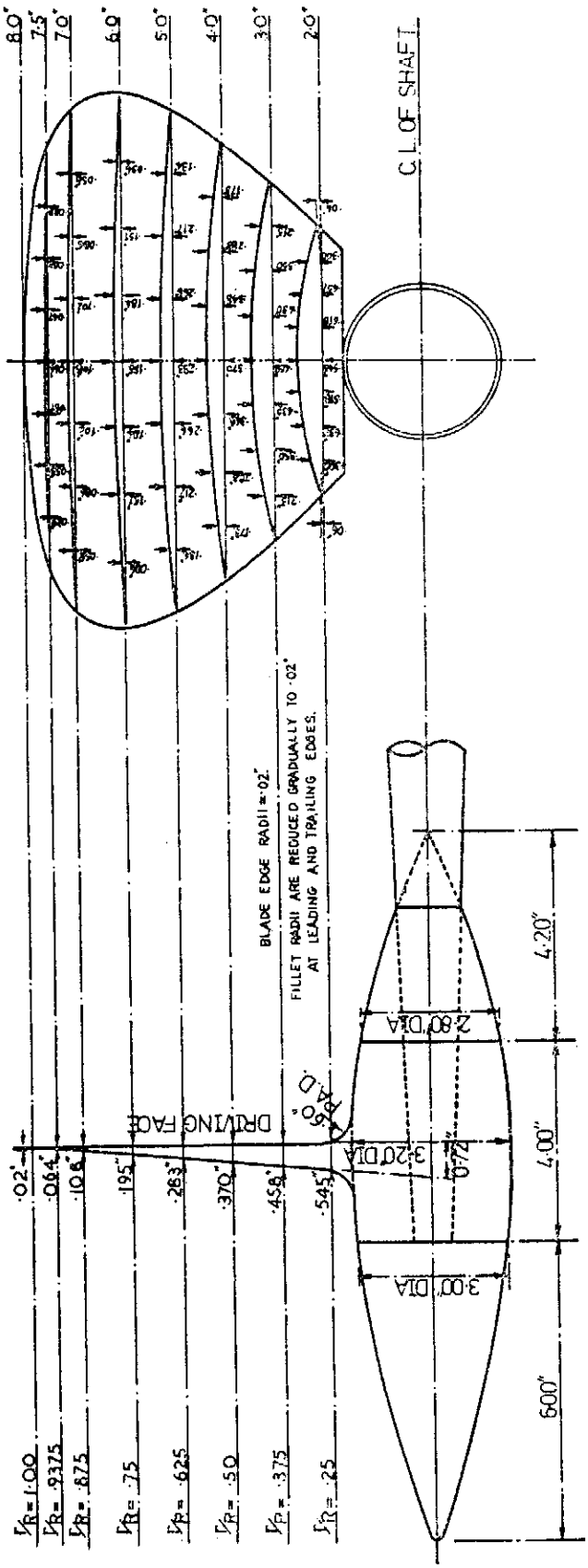

TABLE OF CHORD LENGTHS IN INCHES AND %ω50

B.AR	r/R=·25	r/R=·375	r/R=·50	r/R=·625	r/R=·75	r/R=·875	r/R=·9375	EXP. A.R.
0·50	3·35	4·55	5·555	6·33	6·74	6·32	5·25	0·51
0·65	4·38	5·93	7·25	8·26	8·79	8·25	6·86	0·665
0·80	5·38	7·30	8·92	10·18	10·80	10·16	8·42	0·82
0·95	6·56	8·90	10·87	12·38	13·16	12·37	10·28	1·00
1·10	7·73	10·49	12·80	14·60	15·53	14·58	12·11	1·18
ω/ω50	·604	·819	1·000	1·140	1·212	1·139	·946	

Diameter = 16·00ins. Bt.r.= ·045 d/D = 0·20. Number of Blades = 3 R.H. BAR. = 0·80

Figure 8. Propeller Lines

Annual Report of the Institute of Physics, Academia Sinica, Vol.7, 1977

Numerical Computation of a Moving Two-Dimensional Vortex Past a Barrier

Robert R. Hwang and J. H. Chen

Institute of Physics,
Academia Sinica

ABSTRACT

In this study a moving two-dimensional vortex past a two-dimensional barrier is studied theoretically in terms of the dynamical events encountering with its bloking phenomena. A numerical model involving the full Navier-Stokes equations is developed such that the flow patterns of the combination of a uniform flow and a moving vortex encountering the presence of a barrier are calculated. The moving track of the vortex obtained from laboratory experiments as well as the field data is specified as a given input in the numerical computation.

A finite-difference scheme derived from the partial differential equation with the use of local model solutions is used by applying to the time-dependent vorticity equation. The numerical results show the development of flow patterns and its formation of a secondary vortex behind the barrier. These results were compared favorably to the laboratory as well as well as the field data on the vortex flow when encountering with the barrier considered.

1. Introduction

Flows past obstacles are the most studied subject in the field of fluid mechanics as well as in atmospheric flow problems. The major points of interest are attempted to obtain the flow phenomena associated with the development and the detachment of the secondary vortices behind a barrier. In this study, a numerical method was developed in studying the dynamical events and the blocking phenomena for a two-dimensional potential vortex moving with a uniform flow in the presence of an elliptical barrier. The moving track of the vortex, obtained from the laboratory experiments, was specified in the numerical computation.

Studies of a uniform flow past a barrier have been made extensively in both theoretical and expeimental investigations. For impulsively starting flow past a circular cylinder or a sphere, numerous results concerning the main

features of the flow phenomena over the range of Reynolds numbers have been summarized in papers by Ingham (1968), Jain and Rao (1969),Son and Hanratty (1969), Thoman and Szewczyk (1969). Collins and Dennis (1973), and Dennis (1973), and Coutanceau and Bouard (1977). For uniform flow past obstacles other than circular cylinders and spheres, the survey papers by Berger and Wille (1972), and Lugt and Haussling (1974) should be mentioned. Although the study on uniform flow past an obstacle is numerous, the study on a complex flow, a combination of uniform flow and a vortex for example, in the presence in a barrier seems to be relatively unexplored. Very recently, using a numerical method, Hwang and pao (1977) studied theoretically the effect of an elliptical barrier on a stationary two-dimensional votex in terms of the understanding of the dynamical events associated with its blocking phenomena. The numerical results showed the development of flow seperation in the lee of the barrier and its formation of a secondary vortex behind the barrier. These results were comparably to the laboratory experiments.

In order to study the dynamics of an invading typhoon vortex while interacting with a mountainous island, a simpler numerical model is used here. The flow field is treated by introducing an essentially two-dimensional vortex in a uniform flow which interacts with a two-dimensional elliptical barrier. The moving track of the vortex is obtained from the laboratory experiments and specified as a given input in the numerical computation. In the present study, a numerical scheme involving the full Navier-Stokes equations is developed such that the flow pattern of the combination of a uniform flow and a moving vortex encountering the presence of a barrier are calculated. Results of the numerical computations for the flow pattern are compared with the laboratory experiments and the field data on typhoons when encountering the island of Taiwan.

2. The Flow Problem

The flow field due to a two-dimensional vortex flow in the presence of a two-dimensional elliptical barrier is considered in the two-dimensional laminar motion of an incompressible, viscous fluid. The basic equations governing the fluid motion are the conituity equation and Navier-Stokes equations. They are formulated as follows:

$$\frac{\partial \tilde{u}}{\partial \tilde{x}}+\frac{\partial \tilde{v}}{\partial \tilde{y}}=0 \tag{1}$$

$$\rho\left(\frac{\partial\tilde{u}}{\partial\tilde{t}}+\tilde{u}\frac{\partial\tilde{u}}{\partial\tilde{x}}+\tilde{v}\frac{\partial\tilde{u}}{\partial\tilde{y}}\right)=-\frac{\partial\tilde{p}}{\partial\tilde{x}}+\mu\tilde{\nabla}^2\tilde{u} \tag{2}$$

$$\rho\left(\frac{\partial\tilde{v}}{\partial\tilde{t}}+\tilde{u}\frac{\partial\tilde{v}}{\partial\tilde{x}}+\tilde{v}\frac{\partial\tilde{v}}{\partial\tilde{y}}\right)=-\frac{\partial\tilde{p}}{\partial\tilde{y}}+\mu\tilde{\nabla}^2\tilde{v} \tag{3}$$

where $\tilde{u}$ and $\tilde{v}$ are the Cartesian coordinates $\tilde{x}$ and $\tilde{y}$ respectively, $\tilde{\rho}$ is the density, μ is the viscosity, $\tilde{p}$ is the pressure, $\tilde{t}$ is the time, and $\tilde{\nabla}^2=\partial^2/\partial\tilde{x}^2+\partial^2/\partial\tilde{y}^2$ is the Laplacian operator.

By cross differentiating equations (2) and (3), and then eliminating the pressure, one arrives at the vorticity transport equation

$$\frac{\partial\tilde{\zeta}}{\partial\tilde{t}}+\tilde{u}\frac{\partial\tilde{\zeta}}{\partial\tilde{x}}+\tilde{v}\frac{\partial\tilde{\zeta}}{\partial\tilde{y}}=\nu\tilde{\nabla}^2\tilde{\zeta} \tag{4}$$

where $\nu=\mu/\rho$ is the kinematic viscosity, the vorticity $\tilde{\zeta}$ is defined by

$$\tilde{\zeta}=\partial\tilde{v}/\partial\tilde{x}-\partial\tilde{u}/\partial\tilde{y} \tag{5}$$

A stream function, $\tilde{\Psi}$, which satisfies the continuity equation (1) is introduced as

$$\tilde{u}=\partial\tilde{\Psi}/\partial\tilde{y},\ \text{and}\ \tilde{v}=-\partial\tilde{\Psi}/\partial\tilde{x} \tag{6}$$

and the vorticity can be redefined as

$$\tilde{\zeta}=-\tilde{\nabla}^2\tilde{\Psi} \tag{7}$$

For convenience, equations (4), (6) and (7) will be normalized to give a set of nondimensional equations.

The dimensionless variables are defined as

$$\begin{aligned}&u=\tilde{u}/(\Gamma/\ell),\ v=\tilde{v}/(\Gamma/\ell),\ x=\tilde{x}/\ell\\&y=\tilde{y}/\ell,\ t=\tilde{t}/(\ell^2/\Gamma),\ \Psi=\tilde{\Psi}/\Gamma\\&\zeta=\tilde{\zeta}/(\Gamma/\ell^2),\ R_e=\Gamma/\nu\end{aligned} \tag{8}$$

ℓ, ℓ^2/Γ and Γ/ℓ are the characteristic length, time, and velocity respectively, ℓ is the length of the elliptical cylinder and Γ is the circulatio n of the vortex divided by 2π. The governing equations in demensionless form then become:

$$\frac{\partial\zeta}{\partial t}+u\frac{\partial\zeta}{\partial x}+v\frac{\partial\zeta}{\partial y}=\frac{1}{R_e}\nabla^2\zeta \tag{9}$$

$$\Delta^2\Psi=-\zeta \tag{10}$$

$$u=\partial\Psi/\partial x,\quad v=-\partial\Psi/\partial y \tag{11}$$

$$\zeta=\partial v/\partial x-\partial u/\partial y \tag{12}$$

here R_e is the Reynolds number and $\nabla^2=\partial^2/\partial x^2+\partial^2/\partial y^2$ denotes the Laplacian perator.

3. Numerical Analysis

For numerical computation, equations (9) and (10) will be discretized into table and convergent finite difference forms and then, provided the initial onditions, boundary conditions are adequately defined, one may simulate a ow with the computer.

Discretization of equation (9) presents greater difficulty since one must onsider questions of convergence and of stability. A further difficulty arises rom the nonlinearity involved in equation (9). Experience shows that the onlinearity can produce instability in the computations although stability nalysis based on the locally linearized finite difference system indicates a tablescheme. In this study a finite-difference scheme derived from the partial ifferential equation with the use of local model solutions (Chien, 1976) is used y applying to the time-dependent vorticity equation. The main advantage of his method is there is no apparent stability limition grid size and time step. hese limitations on grid sizes and time steps are directly related to the iscretization errors associated with the derived finite-difference equations. he problem of discretization error and the numerical stability can be minimized r eliminated by making use of local analytical model solutions of the governing artial differential equation in the formulation of a finite difference equation. he finite difference formulation of equation (9) by using local madel solution s given as

$$\frac{\zeta_{i,j}^{n+1}-\zeta_{i,j}^{n}}{\Delta t}\frac{1}{Gt}+u_{i,j}\frac{\zeta_{i+1,j}^{n}-\zeta_{i-1,j}^{n}}{2\Delta x}+v_{i,j}\frac{\zeta_{i,j+1}^{n}-\zeta_{i,j-1}^{n}}{2\Delta y}=$$

$$\frac{1}{R_e}\left(\frac{\zeta_{i+1,j}^{n}+\zeta_{i-1,j}^{n}-2\zeta_{i,j}^{n}}{\Delta x^2}\frac{1}{G_j}+\frac{\zeta_{1,i+1}^{n}+\zeta_{i,j-2}^{n}-2\zeta_{i,j}^{n}}{\Delta y^2}\frac{1}{G_j}\right) \tag{13}$$

$$u_{i,j}=-\frac{1}{2\Delta y}(\Psi_{i,j+1}-\Psi_{i,j-1})$$

$$v_{i,j}=-\frac{1}{2\Delta x}(\Psi_{i+1,j}-\Psi_{i-1,j}) \tag{14}$$

where Δx and Δy are the mesh intervals in the x and y directions, respectively, he subscripts i and j indicate the space coordinates by $x=i\Delta x$ and $y=j\Delta y$, the

superscsipts $n+1$ and n denote the time steps $(n+1)\Delta t$ and $n\Delta t$. Figure 1 displays the arrangement of the mesh and $\Delta x=\Delta y=h$ is considered in this study. Gt, G_i and G_j are so called decay functions used to modify finite differ ence expressions of terms containining derivatives with respect to t, x and y. These functions can be determined by the use of the local time-dependent model solution and the local steady-stase model solution. They can be obtained as

$$Gt=\frac{1-e^{-2\sigma}}{2c}$$

$$G_i=\frac{2}{R_i}\left[1-\frac{2(e^{R_i}-1)}{e^{2R_i}-1}\right] \tag{15}$$

$$G_j=\frac{2}{R_j}\left[1-\frac{2(e^{R_j}-1)}{e^{2R_j}-1}\right]$$

where $c=\left(\frac{1}{\Delta x^2\cdot G_i}+\frac{1}{\Delta y^2\cdot G_j}\right)\cdot\nu\Delta t$, $R_i=\frac{u_{i,j}\Delta x}{\nu}$ and $R_j=\frac{v_{i,j}\Delta y}{\nu}$ are local grid Reynolds numbers in x and y directions, respectively.

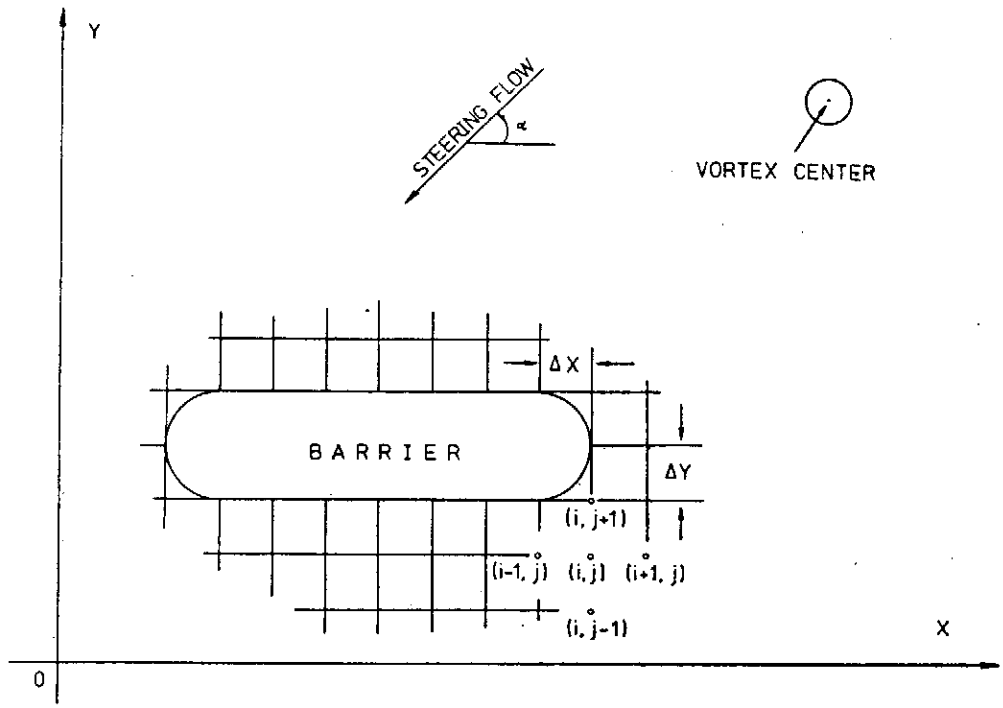

Figure 1. Sketch of grid points, mesh sizes and flow problems.

In equation (10) the derivatives are replaced by central differences to give

$$(\Psi_{i+1,j}-2\Psi_{i,j}+\Psi_{i-1,j})/\Delta x^2+(\Psi_{i,j+1}-2\Psi_{i,j}+\Psi_{i,j-1})/\Delta y^2=-\zeta_{i,j} \tag{16}$$

The system of algebraic equations (16) is solved by the iteration technique of Liebmann relaxation method. The (k+1) th advanced values of Ψ toward convergence of the iteration process is calculated as

$$\Psi_{i,j}^{k+1}=\Psi_{i,j}^{k}+\frac{1+E}{4}S_{i,j}^{k} \tag{17}$$

/here $S_{i,j}^{k}=\Psi_{i+1,i}^{k}+\Psi_{i-1,j}^{k}+\Psi_{i,j+1}^{k}+\Psi_{i,i-1}^{k}-4\Psi_{i,j}^{k}+\Delta x^{2}\ \zeta_{i,j}$ and

he over-relaxation factor, $E=0.6$, is used. The iteration process is halted fter the kth iteration if

$$\left|\Delta^{2}\Psi^{k}-\zeta^{k}\right| \equiv \left|S_{i,j}^{k}\right|<\varepsilon \tag{18}$$

t each grid point, where ε is of the order 10^{-3} for the entire grid points and : is the iteration number in relaxation. The number of iterations depends on he nature of the flow field.

4. Initial and Boundary Conditions

The flow is considered to be started impulsively within an infinitesimal ime interval. Thus at $t=0+$, the motion is assumed to be irrotational except t the body surface, where the no-slip condition produces a vorticity sheet. 'he initial stream function is, therefore set as

$$\Psi_{o}(x,y)=\frac{U_{o}\ell}{\Gamma}(y\cos\alpha-x\sin\alpha)-\ell\mathbf{n}\ \Omega \tag{19}$$

/here $\Omega=z-a$ with a being the location of the vortex center, and α is the ngle of incidence of uniform flow relative to the x-axis. At the barrier surface, he wall vorticity is an extremely important evaluation. The vorticity transport quation (9) for $\partial\zeta/\partial t$ determines how ζ is advected and diffused, but the orticity ζ at interior points is generated from the barrier surface. At the body urface a one-sided difference scheme must be used in order to calculate the orticity at the wall ζ_{b}. Using the Taylor series expansions with no-slip condit-)s and regardless of the wall orientation or boundary value of Ψ, we can /rite firist-order approximation as

$$\zeta_{b}=-\frac{2(\Psi_{b+1}-\Psi_{b})}{\Delta h^{2}}+O(\Delta h) \tag{20}$$

/here Δh is the distance from $(b+1)$ to b, normal to the wall. For Ψ_{b}, the tream function around the elliptical barrier is determined from the average of alues of Ψ evaluated from equation (19) on grid points in which the barrier s occupied. That is

$$\Psi_{b}=\sum_{i=1}^{N}\Psi_{i}/N \tag{21}$$

/here N is th total number of grid points occupied by the elliptical barrier. \t the outer boundaries, which are sufficiently far away from the barrier, the

following conditions are specified as

$$\partial\zeta/\partial x = O \tag{22a}$$

on vertical outer boundaries,

$$\partial\zeta/\partial y = O \tag{22b}$$

on horizontal outer boundaries. The sequential values of stream function on the outer boundaries are calculated directly from equation (19) at the time that the moving vortex is located.

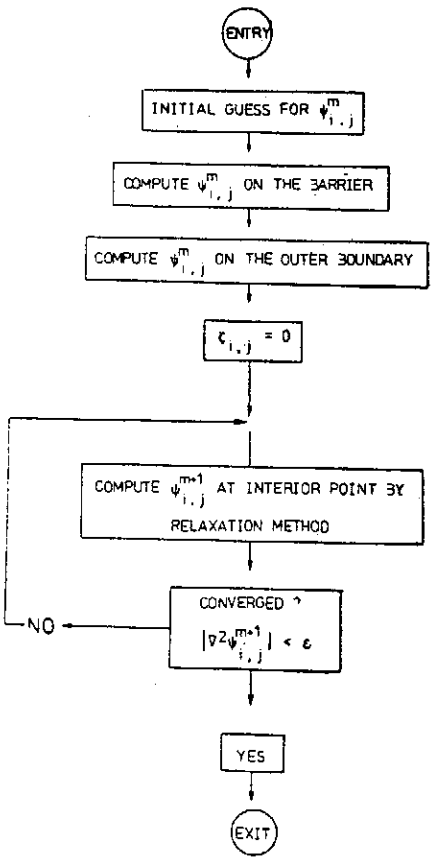

Figure 2. Flow chart for initial solution.

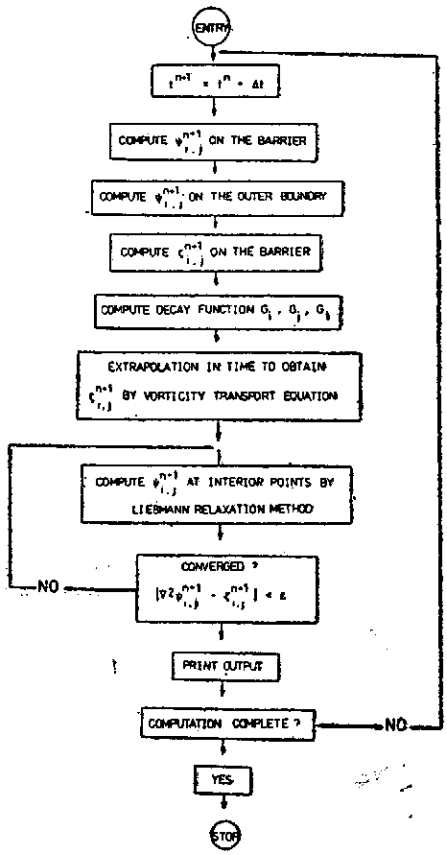

Figure 3. Flow chart for transient solution.

The integration process of the numerical computation is carried out in the following way. The flow is considered to be started impulsively within an infinitesimal time interval while the vortex is moved toward the barrier at a distance sufficiently far away to be interacted with the barrier. Thus at $t=O$, the motion is assumed irrotational except at the center of the vortex. The initial flow is then obtained from the calculation of Ψ_b and appropriate boundary conditions incorporporated in solving the Laplace equation of $\Delta^2\Psi = O$ by using the calculation of equation (19) as the initial input for the Ψ field. The vorticity $\zeta^{n+1}_{i,j}$, for the advanced time step $n+1$ is computed at the interior points according to equations (14) and (15) while the movement of the

center of the vortex is prescribed. The stream function $\Psi_{i,j}^{n+1}$ is then calculcula-ted with the aid of equation (16) for the time step $(n+1)$. The cycle concludes with the calculation of ζ_b^{n+1} from equation (20).

5. Results and Discussion

The flow problem of a moving vortex with a uniform flow past a barrier in which the moving track of the vorex was specified in the numerical computation has been studied numerically. Two approaching tracks of the moving vortex were chosen and specified in the numerical computation.

Before the numerical calculation starts, the time increment and mesh sizes must be determined. Althgh there is no apparent stability limitation on the time increment and the space mesh size in the use of local model solutions, an iterative process is always needed for the calculation of vorticity due to the nonlinearity of the equation and boundary conditions. If a large time increment is chosen, it is to be expected, for a given time iterval, a large number of iterations will be required. Otherwise, for a small time increment, fewer iterations will be needed but a great number of time steps will be required in carring out the calculculation. There is no way to determine analytically the optimum time increment. The only accessible way is to conduct a numerical experiment and to find out the optimum time increment experimentally. The time increment in this study is quite dependent on the circulation of vortex and the velocity of the steering flow. As to the space mesh size, small mesh size will increase computer storage in the calculation and the limitation in computer storage requires the computation field to be small in space. On the other hand, for large mesh size, the increase in truncation was too great and over-shadowed the advantage of a larger computation field. In this study, computation domain is divided into 60×40 square meshes with mesh size $\Delta x=\Delta y=0.125$ and Δt in a range of 0.02 to 0.045 depends on the flow conditions. Computation results are presented as follows.

Figure 4(a) is one of moving track of the vortex specified in the numerical computation in which $\Gamma/\nu=8\times10^3$, $U_\infty\ell/\Gamma=0.4$ and $\alpha=O^o$. The flow is considered to be started impulsively within infinitesimal time interval when the moving vortex is at the inition. Thus at $t=0+$, the motion is assumed to be irrotational except at the body surface and the initial flow pattern is shown in figure 4(b).

Figures 5(a) to 5(i) are the computational results of stream function, and 5(a*) to 5(i*) are of vorticity at time steps for which the moving vortex was

moved as specified in figure 4(a). In figure 5(a) the flow pattern at $t=0.3$ is shown. Two eddies are being formed at lee sides on both tips of the barrier. As the main vortex is moving around the tip, the induced eddy at the front tip is drifting away from the barrier as shown in figures 5(b) through 5(e). In the meantime, the eddy on the trailing edge has initially a tendency to grow in size but it is quickly constrained in growth under the influence of the main vortex. As the main vortex is moving downstream further near the tip of the trailing edge, it overtakes the induced eddy. At this time, these two vortices behave very much like a vortex pair with, of course, different strengths. This can be noted from figure 5(f). It is seen that as the main vortex is passed over the rear edge of the barrier, the induced eddy is drifting away from the barrier and then quickly overtaken by the main vortex in moving downstream as shown in figures 5(g) through 5(i).

Figures 5(a*) to 5(i*) are the computational results of vorticity at different time steps corresponding to the flow pattern mentioned previously. Vorticity of the vortex flow is initially confined to the region of the body surface. When the main vortex is moving toward the barrier, it diffuses toward upstream at the front edge and downstream at the rear edge of the barrier. This is illustrated in figures 5(a*) to 5(d*). As the main vortex is moving around the barrier, we can seen that vorticity is not only diffused toward the flow from the body surface but also convected to the downstream direction under the influence of the motion of the main vortex. This can be seen from figures 5(e*) to 5(i*).

For the purpose of comparison. a sequence of streamline pictures showing the flow pattern of a moving vortex past the barrier obtained from the experimental observation is shown in figure 6. It is seen that the resemblance of the flow pattern between the numerical computations and laboratory is striking. This fact is also confirmed in the comparison with surface flow of typhoon Wendy, 1974. Figures 7 show the com parison between field data and the computational results. It can be seen that the agreement is remarkable.

Another track of a moving vortex flow past the barrier as shown in figure 8(a) with $\Gamma/\nu=8\times10^3$, $U_\infty\ell/\Gamma=0.4$ and $\alpha=100°$ is also carried out in this numerical calculation through the flow field. The initial flow pattern for the main vortex far from the barrier is shown in figure 8(b). Computation results of stream function and vorticity of the vortex flow at different time steps corresponding to various positions of the main vortex are illustrated at figures 9(a) to 9 (i)

and figures 9(a*) to 9(i*) respecitivelly. These results show the development of the flow pattern and the formation of the secondary vortex at the lee side of the barrier during the time of the main vortex past the barrier. In the comparison with experimental results, we also found that the flow pattern in the numerical study resembles those in the laboratory as well as the field as shown in figures 10 and figures 11.

The main purpose of this study is used a simpler numerical model to study the dynamical phenomena of an invading typhoon vortex while inteacting with a mountainous barrier in which the flow field is treated by introducing an essentially two-dimensional moving vortex in a uniform flow which interacts with a two-dimensional barrier. The numerical computaion is of from satisfactory for actual application to typhoon flow field. But the results obtained from this numerical study are very encouraging for the precusor of a longer course far research in typhoon problems. It does provide qualitative flow features of a tyhoon when encountering with the mountainous island.

Acknowledgments. This work was supported by the Institute of physics, Academia Sinica and the National Science Councial of ROC. The computer calcultions were carried out on CDC-CYBER-72 computer of Chung-Shan Institute computer of Chung-Shlogy.

References

1. Berger, E. and Wille, R. 1972: periodic flow phenomena. Ann. Rev. Flúid Mech., 4, 313-340.
2. Chien, J. C. 1976: A general finite-difference formulation with application to Navier-Stokes equations. J. Comput. phys. 20, 268-278.
3. Collins, W. M. and Dennis, S. C. R. 1973: Flow past an impulsively started circular cylinder. J. Fluid Mech., 60,105-127.
4. Coutanceau, M. and Bouard, R. 1977: Experimental determination of the main features of the viscous flow in the wake of a circular cylinder in uniform translation. part 1 and part part 2. J. Fluid Mech. 79, 231-256 and 257-272.
5. Davis, A. M.J. and O'Nell, M. E. 1977: Separation in a slow linear shear flow past a cylinder and a plane. J. Fluid Mech., 81, 551-564.
6. Fromm, J. 1964: The time dependent flow of an incompressible viscous fluid. Topices selected from Methods in Computational physics, edited by B. Alder. Acabemic Press. PP. 345-382.

7. Hamielec, A. E. and Raal, J. D. 1969: Numerical studies of viscous flow around circular cylinders. phys. Fluids, 12, 11-17.
8. Hwang, R.R. and Pao, H. P. 1977: Numerical computation of a stationary two-dimensional vortex flow in the presence of a barrier. Atmosperic Sciences (Meteor. Soci. of R.O.C.) 4, 28-37.
9. Hwang, R. R., Pao, H. P., and Wang, C. T. 1977: Laboratory study of the effects on typhoons when encountering the mountains of Twain island. Tech. Rept., Inst. of phys., Academia Sinica, R. O. C.
10. Ingham, D. B. 1968: Note on the numerical solution for unsteady viscous flow past a circular cylinder. J. Fluid Mech. 31, 815-821.
11. Jain, P. C. and Rao, K. S. 1969: Numerical solution of unsteady viscous incompressible fluid past a circular cylinder. Phys. Fluids Suppl., 12, II 57.
12, Lugt, H. J. and Haussling, H. J. 1974: Laminar flow past an abruptly accelerated elliptic cylinder. J. Fluid Mech., 65, 711-734.
13. Pao, H. P. and Hwang, R. R. 1977: The effects of mountains on a typhoon vortex. proc. of the National Sc. Council, 10, Part 1, 251-258.
14. Son, J.S. and Hanratty, T. J. 1969: Numerical solution for the fow around a cylinder. J. Fluid Mech. 369-383.
15. Thoman, D. C. and Szewczyk, A. A. 1969: Time-dependent viscous flow over a circular cylinder. Phys. Fluids Suppl. 12, II 76-88.

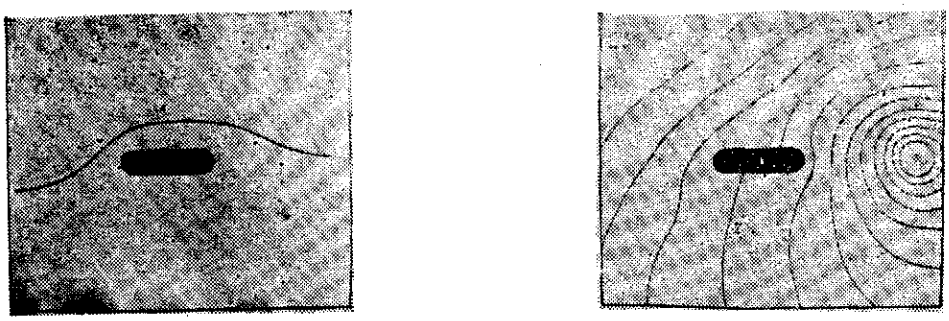

(a) (b)

Figure 4. Moving track and inital flow pattern of a vortex flow.

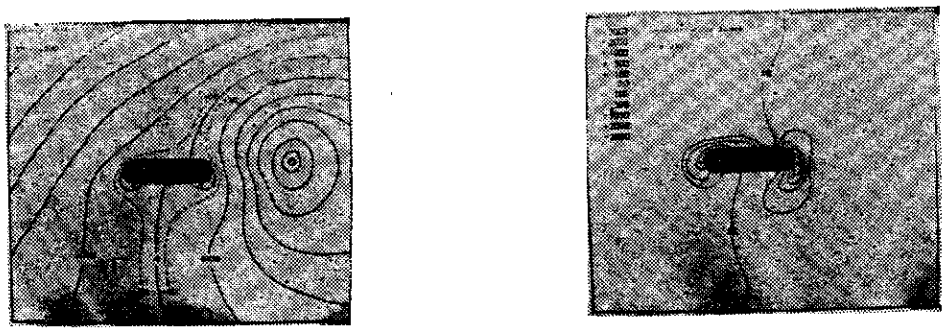

(a) (a*)

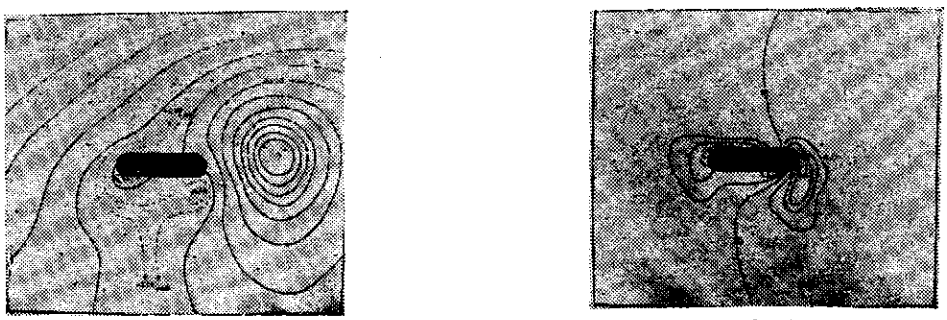

(b) (b*)

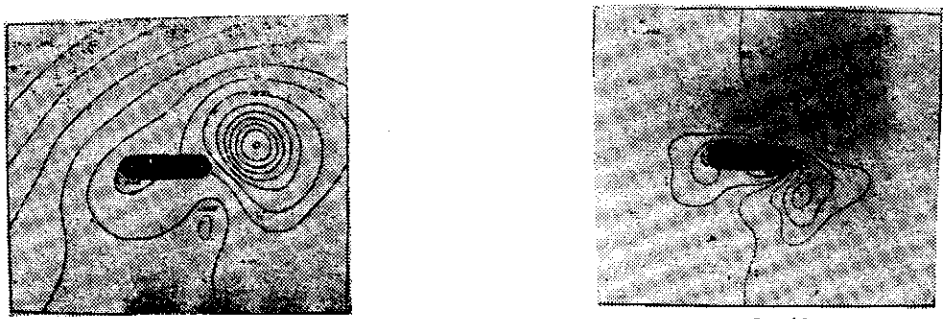

(c) (c*)

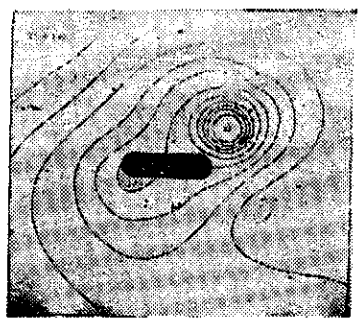

(d)

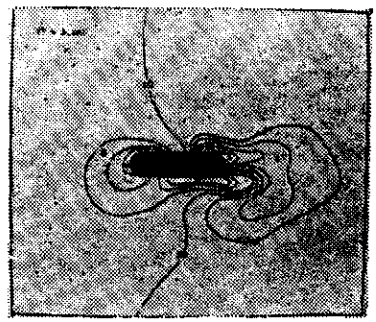

(d*)

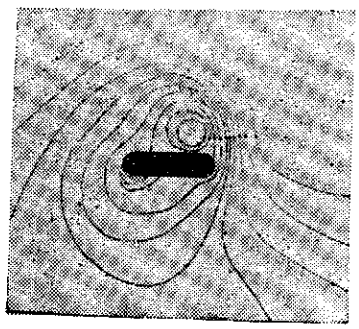

(e)

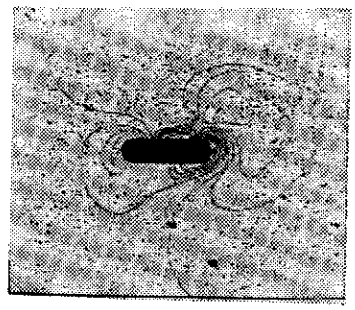

(e*)

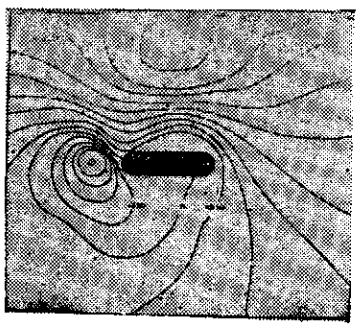

(f)

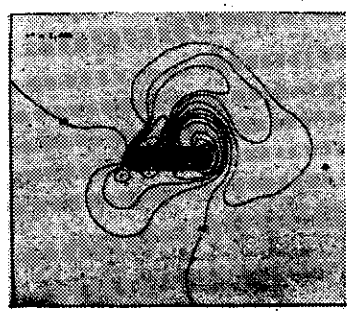

(f*)

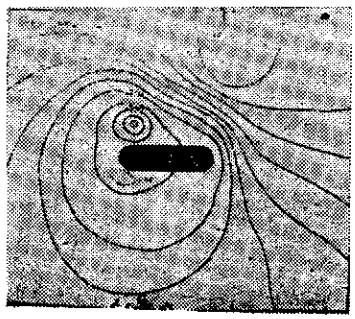

(g)

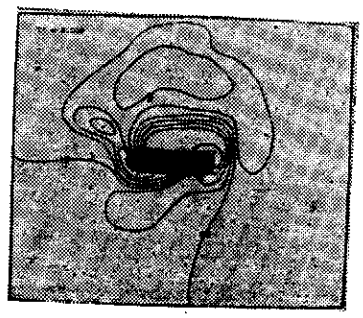

(g*)

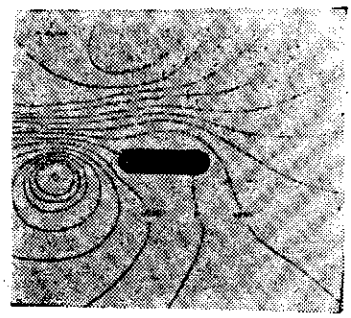

(h)

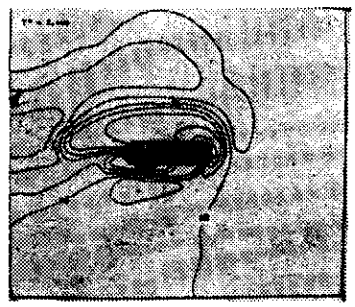

(h*)

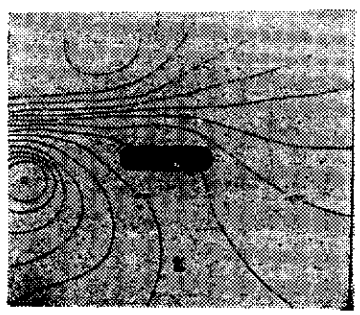

(i)

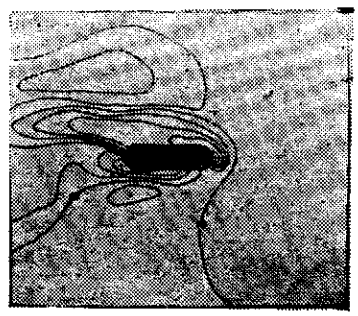

(i*)

Figure 5. Sequence of streamlines and equi-vorticity lines for a vortex flow at various times.

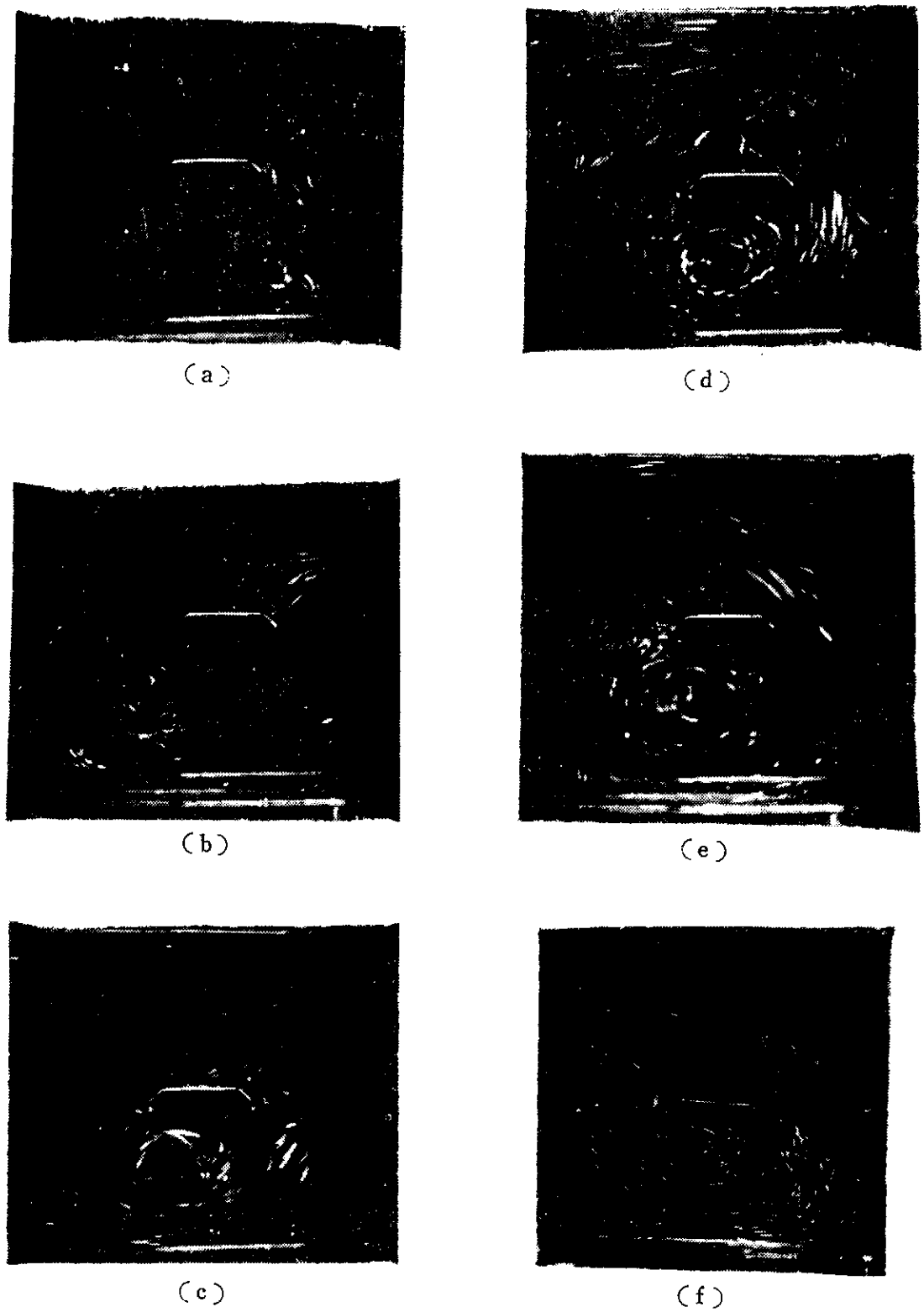

Figure 6. Laboratory experiment of a moving vortex past a barrier. Angle approach $\alpha=0°$, U=2.0cm/sec.

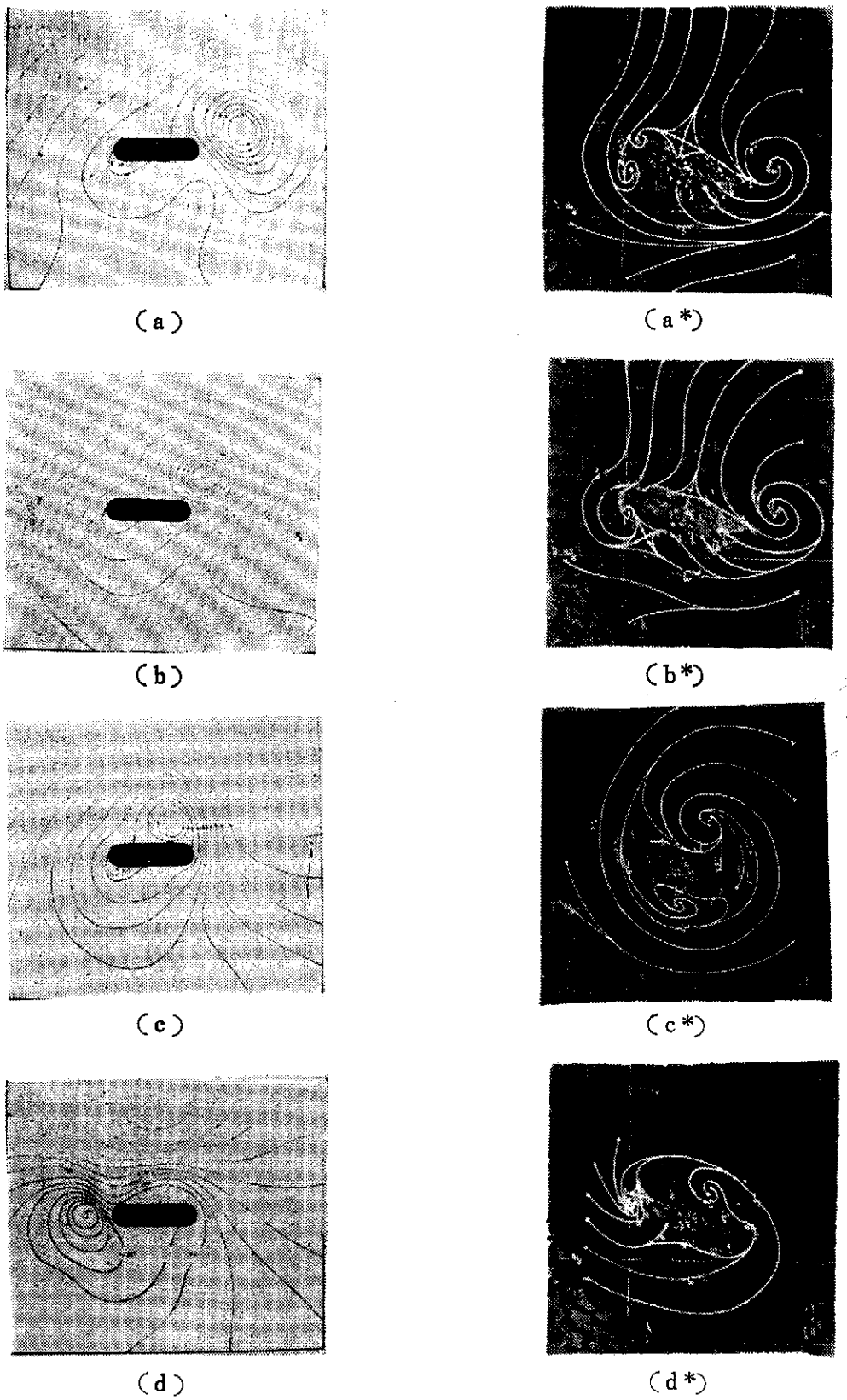

Figure 7. Comparison of some flow lines obtained in numerical compution for a moving vortex past a barrier to field data of typhoon Wendy, 1974.

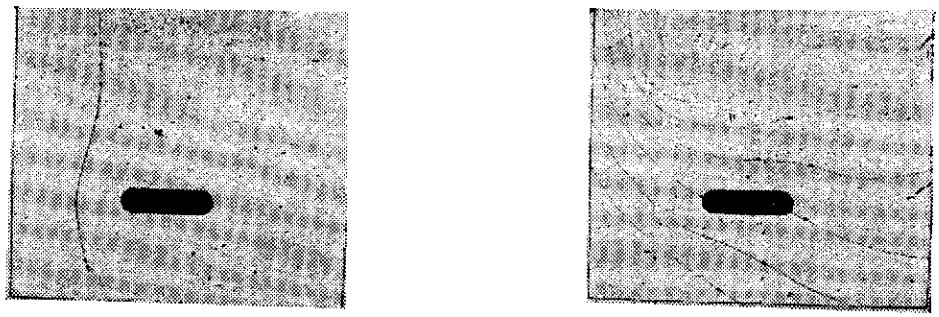

(a) (b)

Figure 8. Moving track and initial flow pattern of a vortex flow.

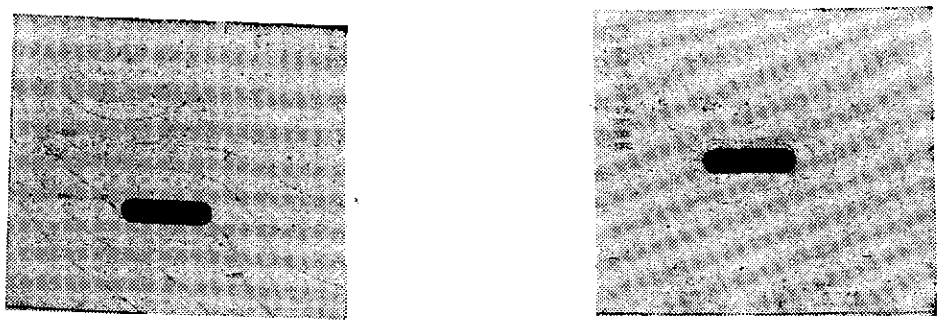

(a) (a*)

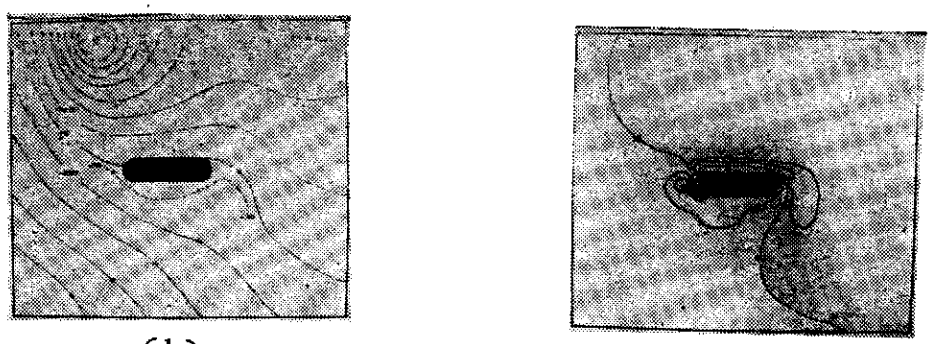

(b) (b*)

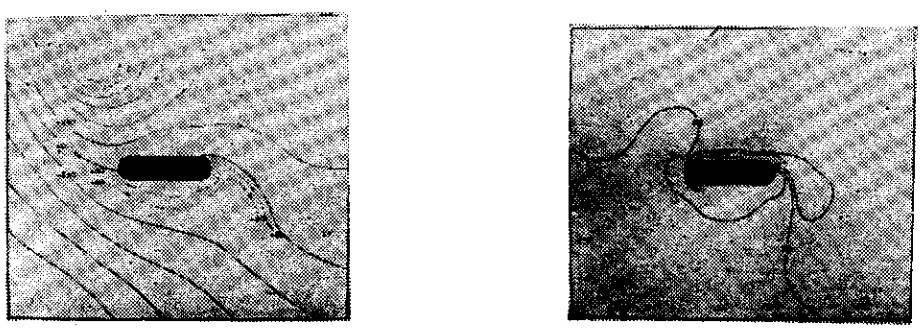

(c) (c*)

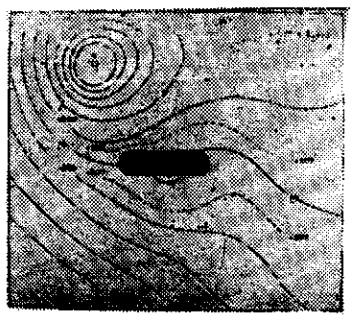

(d)

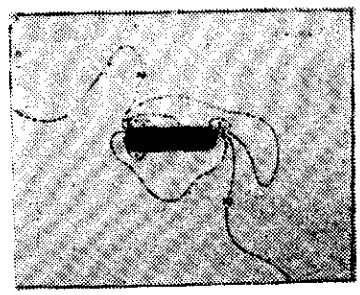

(d*)

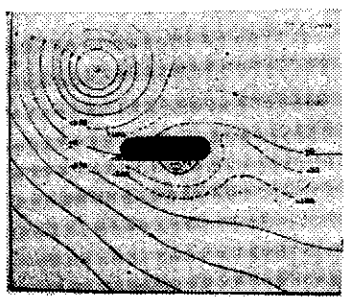

(e)

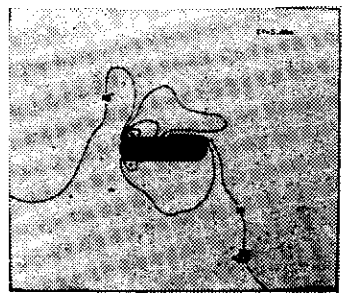

(e*)

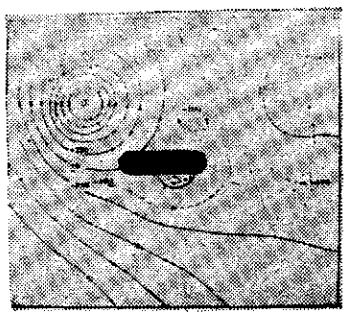

(f)

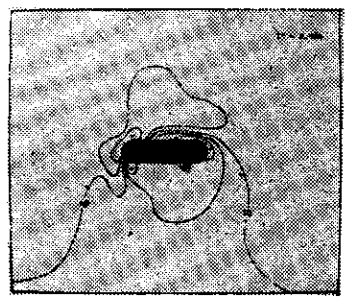

(f*)

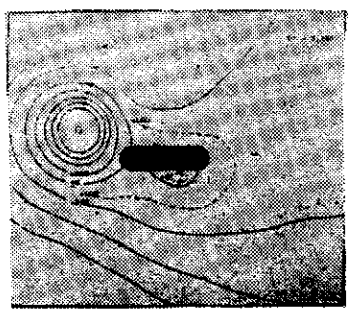

(g)

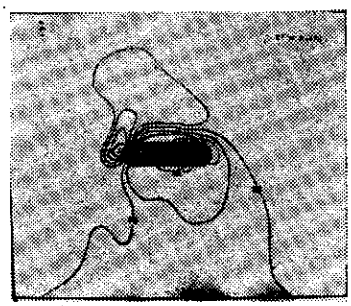

(g*)

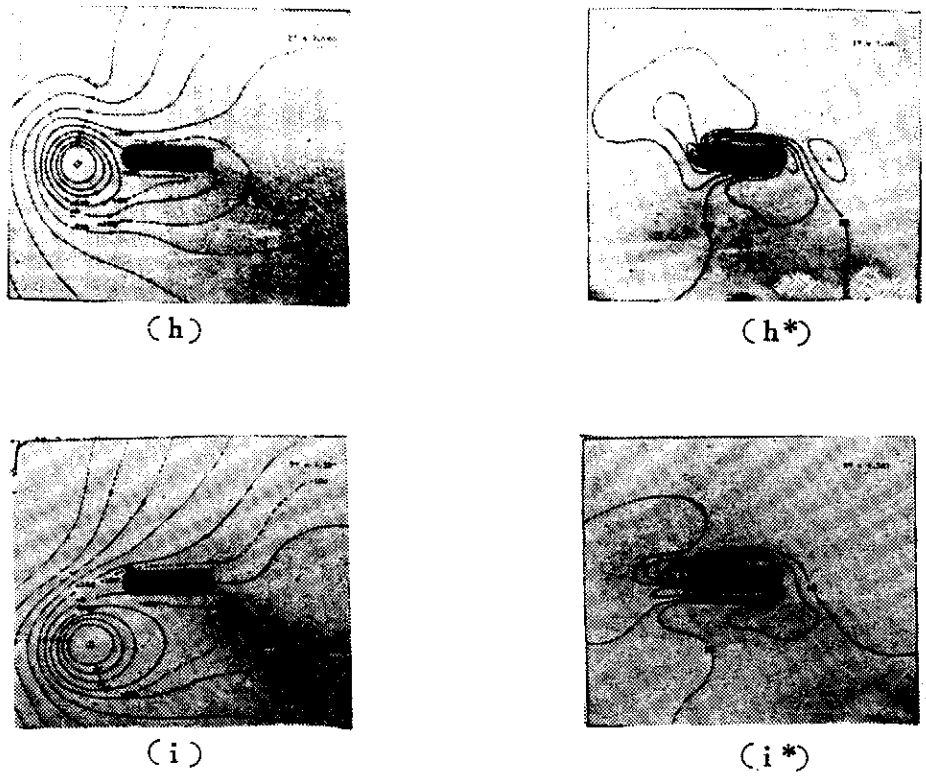

Figure 9. Streamlines and equi-vorticity lines for a vortex flowat various times.

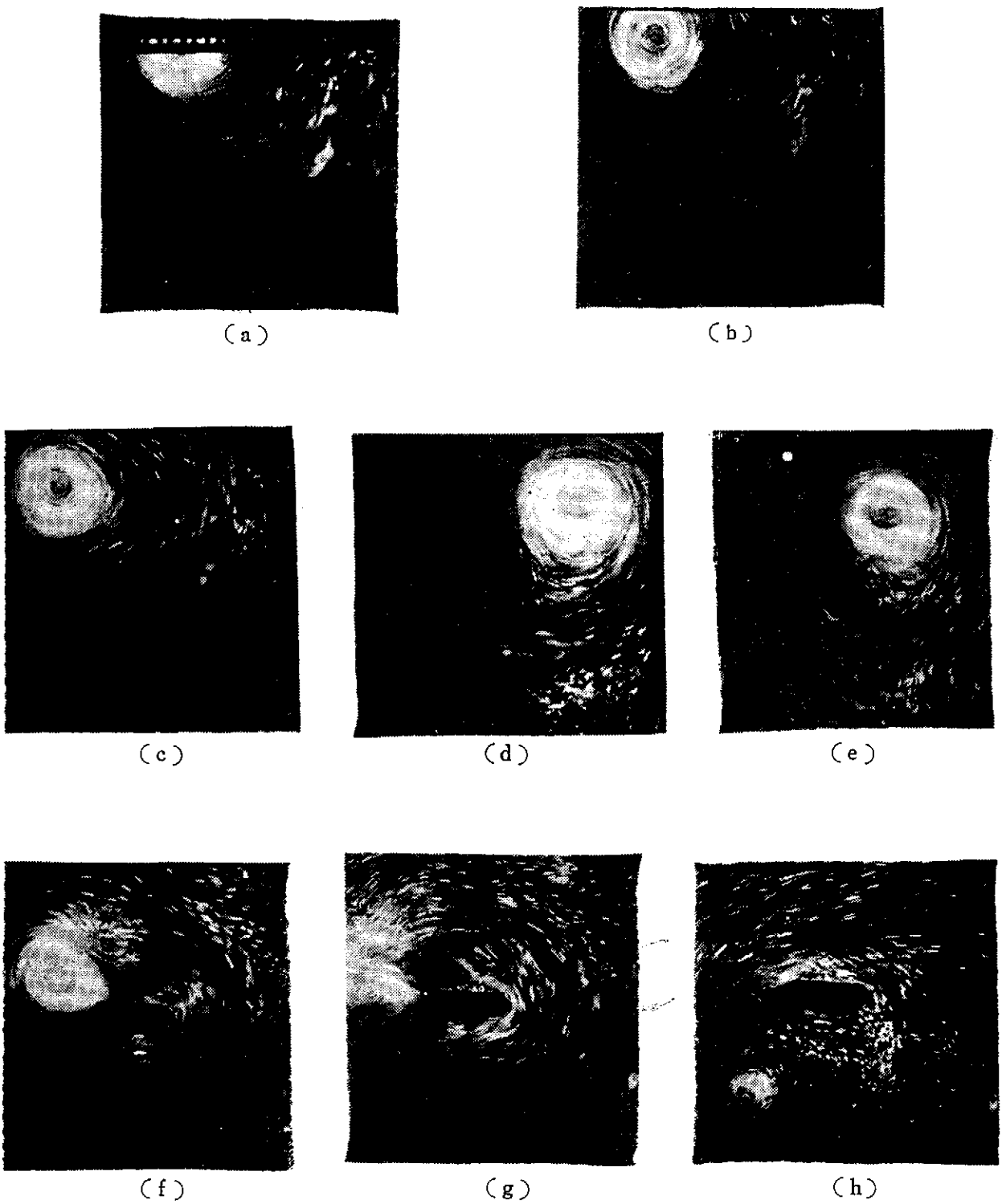

Figure 10. Laboratory experiment of a moving vortex past a barrier. Angle of approach $\alpha=100°$, U=2·0cm/sec.

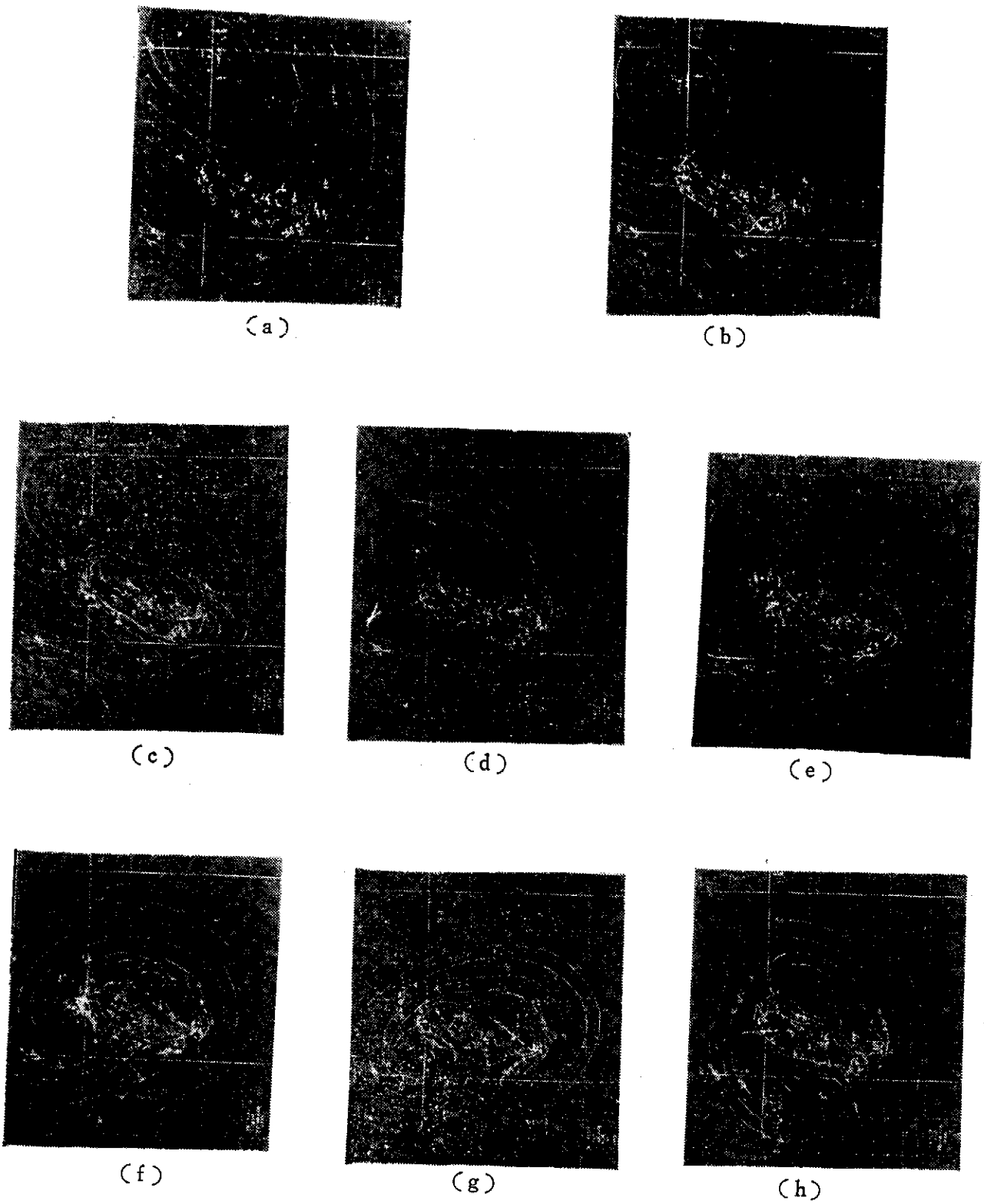

Figure 11. Some surface flow lines of typhoon Trix, 1960.

Annual Report of the Institute of Physics, Academia Sinica, Vol.7, 1977

利用原始方程式進行變分客觀分析之研究

A Variational Optimization Analysis Scheme Using the Primitive Equations as Dymamic Constraints

曾 忠 一

中央研究院物理研究所

摘 要

本研究利用變分最佳化法設計一個可以分析高度，溫度和風的程式。除了動量方程式和靜水方程式之外，本研究又利用連續方程式和熱力學方程式做爲動力條件進行變分分析，使所得的氣象場能維持內部一致。所得的分析方程式是聯立二階橢圓型偏微分方程式，可用緩和法來求解。本研究詳細討論分析方程式的動力學並且進行個案研究以了解這個分析程式的適用性。

1. 導言與研究目的

自從 1958 年 Sasaki 提出利用變分原理來從事客觀分析的理論基礎以來，到現在已有五十篇論文和研究報告（詳細目錄見 Tseng 1976a）進行理論的研究和應用於實際的客觀分析上。早期的研究偏重於變分分析理論的建立，諸如動力條件的功能，濾波器的特性以及權重的估計。最近七年來的研究偏重於實際的應用，諸如變分分析在初期狀態值，客觀分析以及四維資料同化和有限差分程式設計等各方面之應用。 Stephens (1970) 利用平衡方程式爲動力條件來研究數值預報的初期狀態問題，他發現用這種方法可以減少許多隨機的和持續的誤差。 Lewis (1972a) 利用動量方程式爲動力條件來分析海平面氣壓和風場 。 Lewis (1972b) 利用廣義溫度風的關係式和靜水方程式進行變分分析， 使用太平洋周圍陸地上較爲密集測站的資料和海洋中少量的測站資料，重建了太平洋上的溫度場和風場。 Groll (1975) 利用上述 Lewis 的變分分析程式來分析地中海區域的溫度場和風場，發現利用控制大氣大規模運動的流體力學方程式爲動力條件來進行變分分析確能濾除氣象場中的短波，得到最佳的分析結果。 Wei (1975) 也利用 Lewis 的變分分析程式來分析大氣氣團變性實驗 (AMTEX) 的天氣資料。Tseng (1976b) 利用動量方程式和靜水方程式爲動力條件來分析東亞與西太平洋地區的天氣資料，發現逐次校正法所得的客觀分析值若經過變分分析的校正以後會更接近主觀的分析場 。 Sasaki (1976) 利用能量守恆的積分條件來控制數值天氣預報積分過程中產生的截斷誤差，因此能避免在積分過程中產生短波和高頻雜波。Ritchie (1975) 利用線型平衡方程式和連續方程式來從事四維資料同化的實驗，以消除遙感儀器所測得的溫度和風等非定時 (asynoptic) 資料納入數值天氣預報模式後所產生的短波和高頻雜波。由上述的研究結果顯示，變分分析能把動力的，能量的甚至統計的或經驗的條件納入一個望佳止步的過程中，以進行氣象變數的分析，使校正後的氣象變數之間能維持內部一致，而且控制短波和高頻雜波的形成。

本研究繼續去年的研究成果 (Tseng 1976b) ，除了動量方程式和靜水方程式外，也把連續方程式和熱

力學方程式納入望佳止步的過程中，利用這些所謂原始方程式爲動力條件，校正網格點上的氣象變數值，使校正後的氣象變數值能滿足原始方程式，也就是使這些氣象變數值之間能維持內部一致，代表大氣大規模的特性。

現在一般測站所觀測的主要氣象變數有高度（或地面氣壓），溫度和風。不論用主觀分析或一般客觀分析法來從事這些氣象變數的分析時，雖然會參考一些簡單的動力條件如地轉風和溫度風的關係式，可是實際上每個氣象變數都是獨立分析的，因此這些變數不能滿足數值天氣預報的模式，也不能完全代表大氣大規模的運動，也就是說這些變數之間不能維持內部一致。假如這些變數直接使用在預報模式裏，會因爲氣象變數之間不能保持平衡而產生慣性重力波，終至影響數值積分的結果和預報的精度。爲了解決這些問題，人們設計了許多由高度求得其他變數的方法，這就是所謂初期狀態值問題。假如高度有誤差，這些誤差會立即出現在風場和溫度場上。測站上所測得的各種氣象變數值，雖然其精度有大小之分，可是在分析天氣時都是重要的資訊。要如何儘量利用這些資訊，來互相校正氣象變數值，以求得內部一致的氣象場，是各種客觀分析法努力的目標之一。本研究儘量利用所有的觀測資料，利用動量方程式，靜水方程式，連續方程式以及熱力學方程式，進行氣象變數的變分分析，使最後得到的氣象場之間能維持內部一致，滿足控制大氣大規模運動的原始方程式。

2. 研究方法

在進行變分最佳化的過程中，我們所做的假設是這樣的：

$$u\simeq\tilde{u},\ v\simeq\tilde{v},\ T\simeq\tilde{T},\ z\simeq\tilde{z} \tag{1}$$

$$\frac{\partial u}{\partial t}\simeq o,\ \frac{\partial v}{\partial t}\simeq o,\ \frac{\partial T}{\partial t}\simeq o \tag{2}$$

其中u是x方向的速度分量，v是y方向的速度分量，T是絕對溫度，z 是高度。$\tilde{u}$, $\tilde{v}$, $\tilde{T}$ 和 $\tilde{z}$ 分別是 u, v, T, z 的觀測值。第(2)式代表經過變分分析以後所得到的 u, v, T, z 值與觀測值 $\tilde{u}$, $\tilde{v}$, $\tilde{T}$, $\tilde{z}$ 相差很小。雖然校正後的值與原來的觀測值相差很小，假如這些校正值若只當做診斷用途實際上並無多大的意義，但是若當做預報用途，則這些氣象變數值的微小改變意義就非常重大，因爲不但觀測值有誤差，而且這些變數之間不能維持內部一致，假如不加校正，則在預報模式積分時會產生重力波，終致影響預報的精度。此外在利用水平風速計算鉛直速度和發散量以及研究能量收支問題時，這種校正也是必要的。第(2)式的假設是代表大氣大規模運動的準定常特性，有了這個假設可以濾去高頻雜波。(1)式和(2)式這兩個條件在變分原理中叫做 Weak constraints，因此我們的變分公式是這樣的

$$\delta J\equiv\delta\int\int\int\{[\tilde{\alpha}(u-\tilde{u})^2+\tilde{\alpha}(v-\tilde{v})^2+\tilde{\beta}(RT-R\tilde{T})^2+\tilde{\gamma}(\phi-\tilde{\phi})^2]$$
$$+[\alpha(\frac{\partial u}{\partial t})^2+\alpha(\frac{\partial v}{\partial t})^2+\beta(\frac{\partial RT}{\partial t})^2]\}dxdydp/m^2=0 \tag{3}$$

其中 δ 是變分運算子，ϕ是 geopotential ($\phi=gz$，g是重力加速度(，R是氣體常數。$\tilde{\alpha}$，$\tilde{\beta}$，$\tilde{\gamma}$ 分別是風速，溫度和高度的觀測權重，α, β 分別是風速傾向和溫度傾向的動力權重，m是image scale factor。

(3)式中的變分原理的意義是很清楚的。第一個中括弧內的意義是強迫分析值 u, v, RT, ϕ 分別與 $\tilde{\alpha}$, $\tilde{\alpha}$, $\tilde{\beta}$, $\tilde{\gamma}$ 成比例趨近於原有的觀測值，換句話說就是使分析值和觀測值兩者差的平方爲最小，因此這和最小二乘方的意義相類似。$\tilde{\alpha}$, $\tilde{\beta}$ 和 $\tilde{\gamma}$ 這些觀測權重是事先決定的，而不是變分分析中的未知數。這些觀測權重與風速，溫度，高度的精確度有關係。假如某一變數觀測值的誤差很大，那麼它的觀測權重很小，

這樣一來這個變數的觀測值比較不影響最後的分析結果。反之若某一變數的觀測值比較準確，那麼它就會決定最後的分析結果。各種氣象變數觀測值的精確度與觀測系統有關係，在 Bengtsson (1975) 一書中有詳細的介紹。

(3)式中第二個中括弧內的意義是使溫度和風速的時間變化爲最小，這樣可以濾去高頻雜波而維持大氣大規模運動的準定常特性。動力權重 α，β 的值愈大，代表大氣運動愈趨向於定常，因此動力權重 α，β 代表大氣運動趨向於定常的程度。

所有的權重在本研究中都假設爲常數，又(3)式中用RT而不用T，用ϕ而不用 z，是爲了導出分析方程式的方便，並不影響分析結果。此外(3)式中加上m^2 表示所有的權重是在地球面上而不是在地圖上決定的。

(3)式中每個變數並不是互相獨立的，而是藉動力條件而互相影響的。本研究所使用的動力條件是原始方程式，即動量方程式，靜水方程式，連續方程式以及熱力學方程式

$$-\frac{\partial u}{\partial t}=u\frac{\partial u}{\partial x}+v\frac{\partial u}{\partial y}-fv+m\frac{\partial \phi}{\partial x} \tag{4}$$

$$-\frac{\partial v}{\partial t}=u\frac{\partial v}{\partial x}+v\frac{\partial v}{\partial y}+fu+m\frac{\partial \phi}{\partial y} \tag{5}$$

$$RT=-p\frac{\partial \phi}{\partial p} \tag{6}$$

$$m^2\frac{\partial}{\partial x}\left(\frac{u}{m}\right)+m^2\frac{\partial}{\partial y}\left(\frac{v}{m}\right)+\frac{\partial \omega}{\partial p}=0 \tag{7}$$

$$-\frac{\partial RT}{\partial t}=u\frac{\partial RT}{\partial x}+v\frac{\partial RT}{\partial y}+\sigma\omega \qquad \sigma=\frac{RT}{\theta}\frac{\partial \theta}{\partial p} \tag{8}$$

其中 ω 是鉛直速度，σ 是靜力穩定度，θ 是乘上R後的位溫

$$\theta=RT\left(\frac{p_0}{p}\right)^{R/c_p}$$

在(4)，(5)二式中我們已做了若干假設。(4)，(5)和(8)等三式是非線型方程式，假如就用這些式子當作動力條件，所得到的分析方程式非常複雜，不易求解。現在爲了求解方便起見，但仍希望保留非線型項的效應，我們採用 Lewis (1972a,b) 的方法，非線型的平流項使用觀測值，靜力穩定度也使用觀測值來求得，因此(4)，(5)，(8)三式改寫爲

$$-\frac{\partial u}{\partial t}=\tilde{A}-fv+m\frac{\partial \phi}{\partial x} \tag{9}$$

$$-\frac{\partial v}{\partial t}=\tilde{B}+fu+m\frac{\partial \phi}{\partial y} \tag{10}$$

$$-\frac{\partial RT}{\partial t}=\tilde{C}+\tilde{\sigma}\omega \tag{11}$$

其中

$$\tilde{A}=m\tilde{u}\frac{\partial \tilde{u}}{\partial x}+m\tilde{v}\frac{\partial \tilde{u}}{\partial y}$$

$$\tilde{B}=m\tilde{u}\frac{\partial \tilde{v}}{\partial x}+m\tilde{v}\frac{\partial \tilde{v}}{\partial y}$$

$$\tilde{C}=m\tilde{u}\frac{\partial \tilde{RT}}{\partial x}+m\tilde{v}\frac{\partial \tilde{RT}}{\partial y}$$

$$\tilde{\sigma}=\frac{R\tilde{T}}{\tilde{\theta}}\frac{\partial\tilde{\theta}}{\partial p}$$

$$\tilde{\theta}=R\tilde{T}\left(\frac{P_o}{p}\right)^{P/C_p}$$

(6)，(9)，(10)，(11)等四式可直接代入(3)式中，除了這些以外我們還有一個 Strong constraint ，就是(7)式的連續方程式。跟據變分原理， Strong constraint 可隨意加進(3)式積分式內 ， 但前面必須乘上一個 Lagrangian multiplier。 Lagrangian multiplier 在變分最佳化過程中是一個未知數，而且具有固定的物理意義，爲了使 Lagrangian multiplier 的物理意義更清楚起見，我們使用 $2\tilde{\alpha}\lambda$ ， 其中加上係數 2 的目的是使分析方程式沒有不必要的常數，加上 $\tilde{\alpha}$ 的目的是使 λ 的物理意義更清楚。因此(3)式可改寫爲

$$\begin{aligned}\delta\int\int\int\{&\tilde{\alpha}(u-\tilde{u})^2+\tilde{\alpha}(v-\tilde{v})^2+\tilde{\beta}(p\frac{\partial\phi}{\partial p}+R\tilde{T})^2\\&+\tilde{\gamma}(\phi-\tilde{\phi})^2+2\tilde{\alpha}\lambda[m^2\frac{\partial}{\partial x}\frac{u}{m}+m^2\frac{\partial}{\partial y}\frac{v}{m}+\frac{\partial\omega}{\partial p}]\\&+\alpha(\tilde{A}-fv+m\frac{\partial\phi}{\partial x})^2+\tilde{\alpha}(B+fu+m\frac{\partial\phi}{\partial y})^2\\&+\beta(\tilde{C}+\tilde{\sigma}\omega)^2\}\,dxdydp/m^2=0\end{aligned}$$

由上式我們可以得到下列 Euler-Lagrange 方程式：

$$\tilde{\alpha}\left(\frac{u}{m}-\frac{\tilde{u}}{m}\right)+\alpha f\left(\frac{\tilde{B}}{m}+\frac{fu}{m}+\frac{\partial\phi}{\partial y}\right)-\tilde{\alpha}\frac{\partial\lambda}{\partial x}=0 \tag{12}$$

$$\tilde{\alpha}\left(\frac{v}{m}-\frac{\tilde{v}}{m}\right)-\alpha f\left(\frac{\tilde{A}}{m}-\frac{fv}{m}+\frac{\partial\phi}{\partial x}\right)-\tilde{\alpha}\frac{\partial\lambda}{\partial y}=0 \tag{13}$$

$$\beta\tilde{\sigma}(\tilde{C}+\tilde{\sigma}\omega)-\tilde{\alpha}\frac{\partial\lambda}{\partial p}=0 \tag{14}$$

$$\begin{aligned}&\frac{\tilde{\gamma}}{m^2}(\phi-\tilde{\phi})-\frac{\partial}{\partial x}[\alpha(\frac{\tilde{A}}{m}-\frac{fv}{m}+\frac{\partial\phi}{\partial x})]\\&-\frac{\partial}{\partial y}[\alpha(\frac{\tilde{B}}{m}+\frac{fu}{m}+\frac{\partial\phi}{\partial y})]-\frac{\partial}{\partial p}[\frac{\tilde{\beta}}{m^2}(p\frac{\partial\phi}{\partial p}+R\tilde{T})p]=0\end{aligned} \tag{15}$$

$$\frac{\partial}{\partial x}\left(\frac{u}{m}\right)+\frac{\partial}{\partial y}\left(\frac{v}{m}\right)+\frac{1}{m^2}\frac{\partial\omega}{\partial p}=0 \tag{16}$$

(16)式就是原來的連續方程式。由(12)式和(13)式我們可以看出，λ 的單位和速度勢函數是一樣的，假如我們所考慮的大氣是定常的，也就是說當(12)式和(13)式中的第二項爲零時，λ 是一種速度勢函數，因此我們的Lagrangian multiplier 採用 $2\tilde{\alpha}\lambda$ 使 λ 的意義更清楚一點。此外採用這個 Lagrangian multiplier 在以後用緩和法求解時比較可以控制 λ 的大小，以免浪費計算時間。由(12)，(13)和(14)式我們可以得到下列結果：

$$u=\frac{1}{\tilde{\alpha}+\alpha f^2}\left[\tilde{\alpha}\tilde{u}+\tilde{\alpha}m\frac{\partial\lambda}{\partial x}-\alpha f\tilde{B}-\alpha fm\frac{\partial\phi}{\partial y}\right] \tag{17}$$

$$v=\frac{1}{\tilde{\alpha}+\alpha f^2}\left[\tilde{\alpha}\tilde{v}+\tilde{\alpha}m\frac{\partial\lambda}{\partial y}+\alpha f\tilde{A}+\alpha fm\frac{\partial\phi}{\partial x}\right] \tag{18}$$

$$\omega=\frac{\tilde{\alpha}}{\beta\tilde{\sigma}^2}\frac{\partial\lambda}{\partial p}-\frac{\tilde{C}}{\tilde{\sigma}} \tag{19}$$

假如 λ 和 ϕ 的值已經求到，而且 $\tilde{\sigma}$ 不爲零，則以上三式可以用來求校正後的u，v值以及鉛直速度 ω。由(17)(18)二式我們可以看出，校正後的u，v值是四種速度的加權平均，即觀測風，某種速度勢函數所得到的風，平流項和地轉風。由速度勢函數所得到的風可使水平風速和鉛直速度滿足連續方程式的動力條件。

假如 $\tilde{\alpha}$ 趨近於無窮大時，也就是說觀測風相當準確時，我們得到

$$u=\tilde{u}+m\frac{\partial\lambda}{\partial x} \tag{20}$$

$$v=\tilde{v}+m\frac{\partial\lambda}{\partial y} \tag{21}$$

由(19)式我們爲了使 ω 保持有限，必須使 $\partial\lambda/\partial p$ 的值爲零，即

$$\frac{\partial\lambda}{\partial p}=O \tag{22}$$

(20)，(21)，(22)三式再加上連續方程式所得的方程式系可以用來分析水平風速和求出鉛直速度。這組方程式系原來的變分原理就是

$$\delta\int\int\int\{(u-\tilde{u})^2+(v-\tilde{v})^2+2\lambda[m^2\frac{\partial}{\partial x}\frac{u}{m}+m^2\frac{\partial}{\partial y}\frac{v}{m}+\frac{\partial\omega}{\partial p}]\}$$
$$dxdydp/m^2=O$$

這個變分原理的意義就是強迫觀測風滿足連續方程式的動力條件。這組方程式系已有許多人應用來求鉛直速度做爲診斷的用途（如 O'Brien 1970）。

假如(17)式和(18)式中 $\tilde{\alpha}$ 很小時，也就是說觀測風較不準確時，則校正後的風速完全由動力條件決定。

現在我們回到本研究的主題。將(17)，(18)和(19)等三式代入(16)式，我們可以得到 λ 的分析方程式：

$$\nabla\cdot(\mu\nabla\lambda)+\frac{1}{m^2}\frac{\tilde{\alpha}}{\beta}\frac{\partial}{\partial p}(\frac{1}{\tilde{\sigma}^2}\frac{\partial\lambda}{\partial p})+\nabla\cdot\frac{\mu\tilde{V}}{m}-k.\nabla\times\frac{\alpha}{\tilde{\alpha}}\frac{\mu\tilde{D}}{m}$$
$$+J(\phi,\frac{\alpha}{\tilde{\alpha}}\mu f)-\frac{1}{m^2}\frac{\partial}{\partial p}\frac{\tilde{C}}{\tilde{\sigma}}=O \tag{23}$$

其中

$$\mu=\frac{\tilde{\alpha}}{\tilde{\alpha}+\alpha f^2}$$

$$\tilde{V}=u\boldsymbol{i}+v\boldsymbol{j}$$

$$\tilde{D}=\tilde{A}\boldsymbol{i}+\tilde{B}\boldsymbol{j}$$

假如 α 爲零時，也就是說我們不用動量方程式爲動力條件時，$\mu=1$，此時(23)式變爲

$$\nabla^2\lambda+\frac{1}{m^2}\frac{\tilde{\alpha}}{\beta}\frac{\partial}{\partial p}(\frac{1}{\tilde{\sigma}^2}\frac{\partial\lambda}{\partial p})+\nabla\cdot\frac{\tilde{V}}{m}-\frac{1}{m^2}\frac{\partial}{\partial p}\frac{\tilde{C}}{\tilde{\sigma}}=O \tag{24}$$

上式也可以用來分析水平風速和求出鉛直速度，由(17)和(18)我們可得

$$u=\tilde{u}+m\frac{\partial\lambda}{\partial x} \tag{25}$$

$$v=\tilde{v}+m\frac{\partial\lambda}{\partial y} \tag{26}$$

現在(24)，(25)和(26)式再加上(19)式是一個完整的方程式系，λ 由(24)求得以後，風速和垂直速度立即可由(25)，(26)和(19)式分別求得。或者將(24)式對 p 微分，利用(19)式消去 λ，我們可以得 ω 的分析方程式。這組方程式系同時利用連續方程式和熱力學方程式求得鉛直速度，並且校正水平風速，因此值得在此提出，以便有興趣的人能試用這個程式。

現在若將(17)，(18)二式代入(15)式，我們可以得到 ϕ 的分析方程式

$$\nabla\cdot(r\nabla\phi)+\frac{\tilde{\beta}}{m^2}\frac{\partial}{\partial p}\left(p^2\frac{\partial\phi}{\partial p}\right)-\frac{\tilde{r}}{m}\phi$$

$$=-\frac{\tilde{r}}{m^2}\tilde{\phi}-\frac{\tilde{\beta}}{m^2}\frac{\partial}{\partial p}(pR\tilde{T})-\boldsymbol{k}\cdot\nabla\times\frac{rf\tilde{\boldsymbol{V}}}{m}-J(\lambda,rf)-\nabla\cdot\frac{r\tilde{\boldsymbol{D}}}{m} \tag{27}$$

其中

$$r=\frac{\alpha\alpha}{\tilde{\alpha}+\alpha f^2}$$

(23)式 Jacobian 項中有 ϕ，(27)式 Jacobian 項中有 λ，因此(23)式和(27)二式是聯立方程式，而且 λ 和 φ 也是經由這兩個 Jacobian 項來互相影響的。由(27)式中我們可以看出，假如高度觀測權重 $\tilde{\gamma}$ 值很大時，則校正後的高度完全由它的觀測值決定。假如 $\tilde{\beta}$ 很大時，也就是說溫度的觀測值比較準確時，校正後的高度場大部份由觀測溫度決定。此外我們也可以由(27)式看出，風的資訊完全由動力權重 α 和觀測權重 $\tilde{\alpha}$ 所合併起來的 r 來決定。假如 $\tilde{\alpha}$ 保持固定而讓 α 增加，則 γ 會增加，反之若 α 保持固定而讓 $\tilde{\alpha}$ 增加，則 γ 也會增加。因此假如觀測風的準確度增加時（即 $\tilde{\alpha}$ 增加），或是風的定常性增加時（即 α 增加），都會使風的資訊在高度分析值的重要性增加。假如 $\tilde{\beta}$，$\tilde{\gamma}$ 比 γ 小得很多時高度分析值完全由風的資訊決定。此外我們也可以發現，使風速滿足連續方程式的動力條件是經由 Jacobian 項決定的。假如觀測權重 $\tilde{\alpha}$ 或動力權重 α 很大時，連續方程式的動力條件對高度分析值的決定性較大。仔細考察(27)式的右邊，我們可以發現有五項對 ϕ 的解有關係。第一項代表觀測高度的影響，第二項代表觀測溫度的影響，第三項是觀測風的渦度，第四項是連續方程式動力條件的影響，第五項的物理意義較難解釋，但可當做觀測風場的曲率的影響。

自然邊界條件隨變分最佳化的過程而產生。本研究的自然邊界條件是 $\delta\phi=0$ 和 $\lambda=0$，也就是上下和四周邊界的 ϕ 值不加校正而等於原來的觀測值 $\tilde{\phi}$，而且 λ 在上下和四周的邊界的值皆爲零。(23)式和(27)式是橢圓型二階偏微分方程式，可用緩和法來求解，由於這二式是聯立方程式，必須重覆運算數次以求得兩個值的穩定解。

3. 研究結果

在進行數值解之前，首先必須決定觀測權重 $\tilde{\alpha}$，$\tilde{\beta}$，$\tilde{\gamma}$ 和動力權重 α，β。第一次權重決定以後就可以同時由(23)式和(27)式解出 λ 和 ϕ，然後由(17)式和(18)式解出 u，v，再重新計算權重，如此類推，重覆計算，經過四五個周期之後會趨近於一定值。雖然總共有五個權重，但只有四個是互相獨立的，另外一個可以假設

爲1

第一次的觀測權重採用下列各值

$$\tilde{\alpha}=1/\ (2m/sec)^2$$

$$\tilde{\beta}=1/\ (R\times 2)^2 \tag{28}$$

$$\tilde{r}=1/(9.8\times 10)^2$$

這種觀測權重的決定就是假設觀測風的誤差爲 2m/sec，觀測溫度的誤差爲 2°K，而觀測高度的誤差爲 10m，動力權重 α，β 可以採用下列式子估計：

$$\alpha=2\Big/\overline{\left[\left(\frac{\partial u}{\partial t}\right)^2+\left(\frac{\partial v}{\partial t}\right)^2\right]} \tag{29}$$

$$\beta=1\Big/\overline{\left(\frac{\partial RT}{\partial t}\right)^2} \tag{30}$$

其中一長橫線代表所有網格點上變數值的平均。(29)式和(30)式中的 $\partial u/\partial t$，$\partial v/\partial t$ 和 $\partial RT/\partial t$ 分別可由(9)，(10)和(11)三式求得，由於第一次計算時 u，v，ϕ，ω 都是未知數，我們可以用觀測值代替，ω 沒有觀測值，只好利用大氣大規模運動的 ω 值了，即

$$-\frac{\partial u}{\partial t}=\tilde{A}-f\tilde{v}+m\frac{\partial\tilde{\phi}}{\partial x} \tag{31}$$

$$-\frac{\partial v}{\partial t}=\tilde{B}+f\tilde{u}+m\frac{\partial\tilde{\phi}}{\partial y} \tag{32}$$

$$-\frac{\partial RT}{\partial t}=\tilde{C}+\tilde{\sigma}\tilde{\omega} \qquad \tilde{\omega}=\pm 10^{-3}mb/sec$$

由於 ω 值可能爲負，我們可再做一次估計

$$\beta=1/(\tilde{C}+\tilde{\sigma}\tilde{\omega})^2=1/(\overline{\tilde{C}^2}+\overline{2\tilde{\sigma}\tilde{\omega}\tilde{C}}+\overline{\tilde{\sigma}^2\tilde{\omega}^2})$$

現在假設 $\overline{\tilde{\sigma}\tilde{\omega}\tilde{C}}=0$，則我們的 β 估計值爲

$$\beta=1/(\overline{\tilde{C}^2}+\overline{\tilde{\sigma}^2\tilde{\omega}^2}) \tag{33}$$

權重 $\tilde{\alpha}$，$\tilde{\beta}$，$\tilde{r}$ 代表觀測值的可靠度，若$(u-\tilde{u})$，$(v-\tilde{v})$，$(RT-R\tilde{T})$與$\phi-\tilde{\phi}$等項愈趨近於零，則其權重 $\tilde{\alpha}$，$\tilde{\alpha}$，$\tilde{\beta}$，$\tilde{r}$ 應該愈大，由(28)式中我們可以看出，決定第一次權重時我們已假設高度的觀測值的誤差爲最小，其次爲溫度，誤差最大的是風。動力權重 α 和 β 是由 $\partial u/\partial t$，$\partial v/\partial t$ 和 $\partial R/\partial t$ 趨近於零的程度決定的，假如 α 和 β 的值愈大則代表大氣大規模運動愈趨近於定常。

第二次以後的觀測權重是由校正值和原來的觀測值決定的

$$\tilde{\alpha}=2/\overline{[(u-\tilde{u})^2+(v-\tilde{v})^2]}$$

$$\tilde{\beta}=1/(RT-R\tilde{T})^2$$

$$\tilde{r}=1/(\phi-\tilde{\phi})^2$$

$$\alpha=2/\left[\overline{\left(\frac{\partial u}{\partial t}\right)^2}+\overline{\left(\frac{\partial v}{\partial t}\right)^2}\right]$$

這樣決定的權重實際代表校正值與觀測值兩者差的平方平均的倒數，由這樣決定權重除了代表某一變數的可信度之外，另外也會使(3)式中每項的單位一致。

除了觀測和動力權重之外，網格點上之觀測值 $\tilde{u}$, $\tilde{v}$, $\tilde{T}$, $\tilde{\phi}$ 也必須事先決定。 這些觀測值可以由主觀分析和其他各種客觀分析法得到。本研究使用逐次校正法所得到的網格點上的高度、溫度和風速分量。本研究使用民國64年9月21日格林尼治標準時間零時的五個定壓層的高空天氣資料 。 當時中度颱風貝蒂在北緯21.8度，東經129.5度，此外在庫頁島有一低壓中心，冷鋒由該處向西南延伸經過日本海到達黃海。 本研究的考察範圍包括整個東亞和西太平洋地區。

在進行變分分析時，計算的步驟如下：

(1)利用(28)式估計第一次 $\tilde{\alpha}$, $\tilde{\beta}$, $\tilde{r}$ 值

(2)利用(29)式和(31)，(32)式估計第一次 α 值

(3)利用(33)式求 β 值

(4)由(23)和(27)式用緩和法解出入和 ϕ。由於(23)中 Jacobian 項有 ϕ，第一次計算時尚未求出 ， 因此在此項中第一次採用觀測值

(5)求出 λ 和 ϕ 以後由(17)和(18)二式分別求出 u, v, 再由靜水方程式求出T

(6)重新計算權重

如此反覆運算可以得到校正後的高度，溫度和風。由於本研究中一共有五個權重，因此最後的校正值與權重的大小很有關係， 尤其是動力權重在計算過程中值的大小變動很大無法得到收斂的解。 這個情形在前文（Tseng 1976b）中也發現同樣的情形，動力學上的原因尚不能明瞭，因此在本文中仍是把兩個動力權重固定不變，而讓觀測權重跟據上述的步驟重新計算，得到了穩定解。表一所列的就是高度溫度，風速與其觀測值的 rms 值以及相對權重之值。

$\sqrt{\overline{(u-\tilde{u})^2}}$	$\sqrt{\overline{(v-\tilde{v})^2}}$	$\sqrt{\overline{(T-\tilde{T})^2}}$	$\sqrt{\overline{(z-\tilde{z})^2}}$	$\tilde{\alpha}/\alpha$	$\tilde{\beta}/\alpha$	$\tilde{r}/\alpha$	β/α
$5.5m/s$	$4.3m/s$	$2.10k$	$8.3m$	7.1×10^{-6}	5.4×10^{-10}	7.4×10^{-8}	1.1×10^{-1}

表一：α 與 β 保持固定時所得到的風速，溫度，高度與其觀測值的rms值與相對權重之值

主觀分析高度場分別在圖 1（700mb），圖 9（500mb），圖 17（300mb）。逐次校正法所得的高度場分別在圖 2（700mb），圖 10（500mb），圖 18（300mb）。只利用動量方程式和靜水方程式爲動力條件的變分分析高度場分別在圖 3（700mb），圖 11（500mb），圖 19（300mb）。以上的情形在前文（Tseng 1976b）中已討論過了。本研究所得的高度場分別在圖 4（700mb），圖 12（500mb），圖 20（300mb）。本研究所得的高度場比逐次校正分析場更加合理，也更接近主觀分析的結果。本研究的程式（以下簡稱B程式）所得的結果也比只用動量方程式和靜水方程式爲動力條件的變分分析程式（以下簡稱A程式）較爲合理。比較圖 1 至 4 我們可以發現圖 4 的颱風中心位置比圖 2 和圖 3 更靠近圖 1 主觀分析的颱風中心位置。此外圖20中 9720m 的等高線形狀也比較像主觀分析的的等高線形狀。這些改進很顯然的是由於溫度和風的資訊影響高度場的結果。 其他方面和主觀分析顯著的差異是由於輸入值，即網格點上的觀測值， 的品質較差的緣故，由於東南亞和西太平洋測站稀少，由逐次校正法所得的網格點上的值無法得到令人滿意的結果，尤其是在邊界附近的分析與主觀分析相差更大。因此一般客觀分析法如逐次校正法或最佳內插法仍值再研究，以求得較佳的分析場，不但對數值天氣預報而且對變分分析也有很大的關係。

主觀分析溫度場分別在圖 5（700mb），圖 13（500mb），圖 21（300mb）。逐次校正法所得的溫度場分別在圖 6（700mb），圖 14（500mb），圖22（300mb）。A程式所得的溫度場分別在圖 7（700mb），圖 15（500mb），圖 23（300mb）。本研究（B程式）所得的溫度場分別在圖 8（700mb），圖 16（

500mb），圖 24（300mb）。比較這些用各種不同的方法所得的溫度場，我們可以發現本研究（B程式）的結果比較接近主觀分析場，但是因爲邊界值未加校正，所以在靠近邊界的地方溫度場仍無改進，距離邊界較遠處本研究的結果的確改進了逐次校正法或A程式中不合理的溫度場。由於本研究的溫度場完全由靜水方程式得到，因此高度與溫度互相影響，最後得到較合理的結果。

因此本研究所得的高度場和溫度場，除了在邊界附近之外，比較接近主觀分析值。不但如此，本研究利用動量方程式、靜水方程式，連續方程式和熱力學方程式爲動力條件，進行高度場，溫度場和風場的變分分析，使這些變數滿足所謂原始方程式，因此所得的分析場是內部一致的，分析值可以當做初期狀態值使用。除此之外本研究所得到的程式也可以用來進行診斷研究之用，因爲這個分析程式可以改進各種分析值的品質。

4. 結　　語

本研究利用變分最佳化法設計一種可以同時分析高度，溫度和風的程式。除了動量方程式和靜水方程式之外，本研究又利用連續方程式和熱力學方程式爲動力條件，進行變分分析，以校正網格點上的氣象變數值，使校正後的氣象變數值能滿足原始方程式，也就是使氣象場能維持內部一致，代表大氣大規模運動的特性。本研究儘量利用現有的觀測資訊進行氣象變數的分析，使其滿足原始方程式的動力條件，最後使校正值在水平方向和鉛直方向在力學上均能一致。

本研究最後進行東亞西太平洋地區天氣資料的個案研究以探討設計出來的分析程式的適用性，發現這個程式可以改進一般客觀分析法所得到的氣象變數分析值的品質。由於本研究所得的分析程式已維持內部一致，因此分析結果可當做數值預報的初期狀態值使用。

5. 致　　謝

本研究是在國家科學委員會 NSC-66M 0202 02C(01)「東亞天氣資料變分客觀分析之研究」專題計劃補助下完成的。本研究所使用的天氣資料由中央氣象局和空軍氣象中心提供，對上述的機關著者深表謝意。

References

Bengtsson, L., 1975: 4-dimensional assimilation of meteorological observations. GARP Publication Series No.15, WMO-ICSU Joint Organizing Committee, 76 pp.

Groll, A., 1975: NVA upper air temperature and wind analysis for a 12-level European area model. ENVPREDRSCHFAC Technical Note No. 21, Environmental Prediction Research Facility, Monterey, California, 53 pp.

Lewis, J. M., 1972a: The adjustment of surface wind and pressure by Sasaki's variational matching technique. J. Appl. Meteor., 11, 586-597.

Lewis, J. M., 1972b: An operational upper air analysis using the variational method. Tellus, 24, 514-530.

O'Brien, J. J., 1970: Alternative solutions to the classical vertical velocity problem. J. Appl. Meteor., 9, 197-203.

Ritchie, A. A., 1975: A variational optimization analysis approach to continuous data

assimulation. Ph. D. Dissertation, University of Oklahoma, Norman, Oklahoma, 98 pp.

Sasaki, Y., 1958:An objective analysis based on the variational method. J. Meteor. Soc. Japan.36, 77-88.

Sasaki, Y,. 1976: Variational design of the finite difference scheme for initial value problem of an integral constraint. J. Comp. Phys., 21, 270-278.

Stephens, J. J., 1970: Variational initialization with the balance equation. J. Appl. Meteor., 9, 732-739.

Tseng, C. Y., 1976a: Variational optimization analysis—a bibliography. Institute of physics, Academia Sinica, 4 pp.

Tseng, C. Y., 1976b: Variational objective analysis of meteorological fields in East Asia area. (In Chinese) Annual Report of the Institute of Physics, Academia Sinica, 6, 161-178.

Wei, A. M., 1975: An application of a numerical variational analysis to the AMTEX data. Master's Thesis, University of Oklahoma, Norman, Oklahoma, 68 pp.

A Variational Optimization Analysis Scheme Using the Primitive Equations as Dynamic Constraints

The variational optimization technique is used to develop a scheme to analyze the height, temperature and wind. In addition to the hydrostatic equation and horizontal momentum equations, the continuity equation and thermodynamic equation are also used as dynamic constraints to ensure the internal consistency. The resulting analysis equations for the geopotential and the velocity potential are two coupled second order elliptic equations, which may be solved simultaneously by relaxation method. The dynamics of the analysis equations has been dicussed in detail and a case study has been made to investigate the applicability of the proposed analysis scheme to synoptic data.

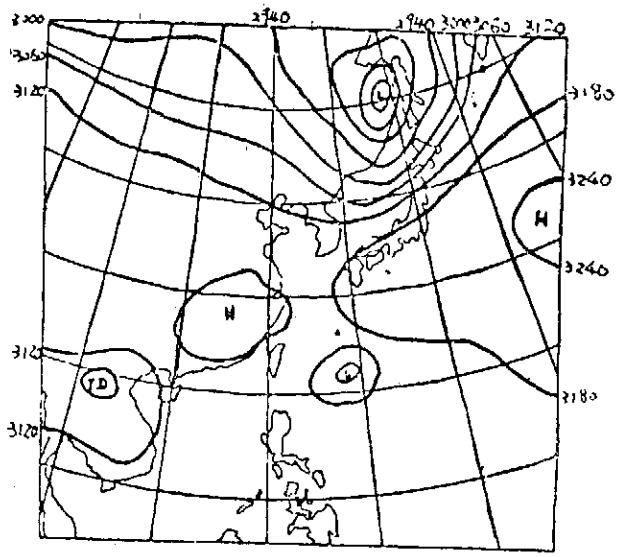

圖1　700mb 主觀分析高度場

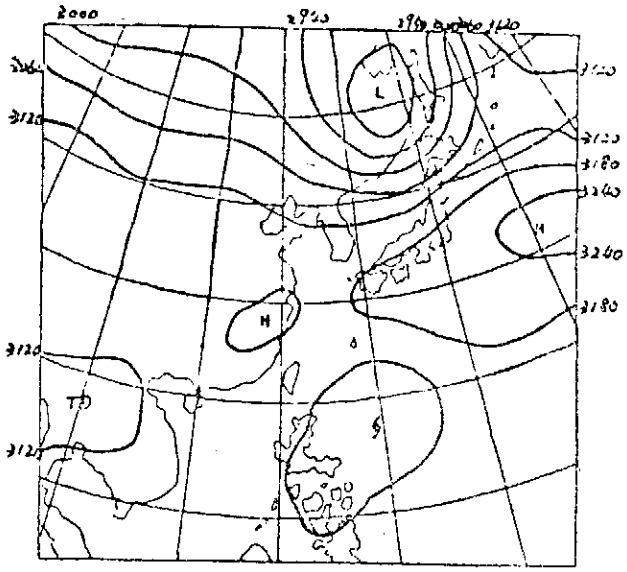

圖2　700mb 逐次校正分析高度場

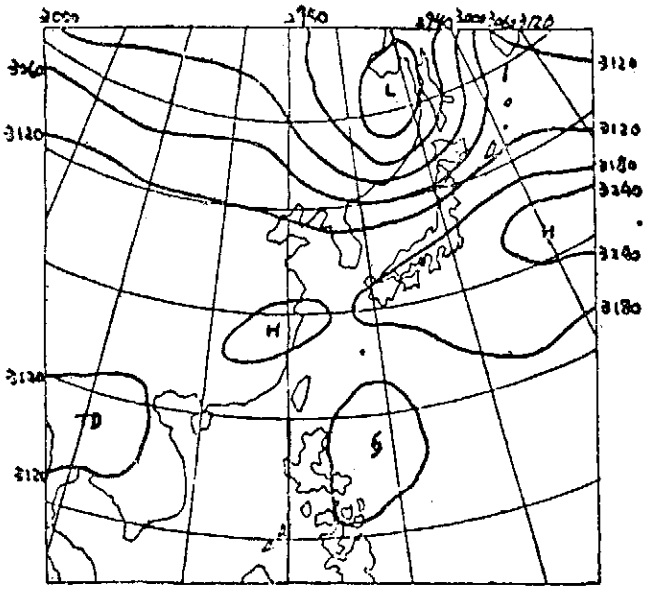

圖3　700mb 變分分析高度場

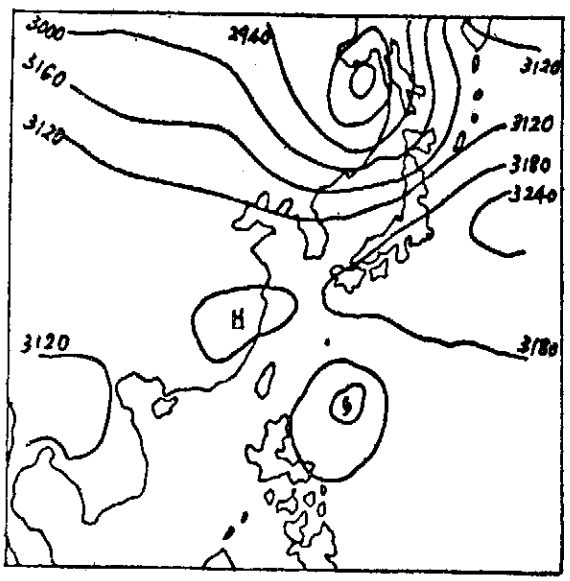

圖4　本研究所得700m高度場

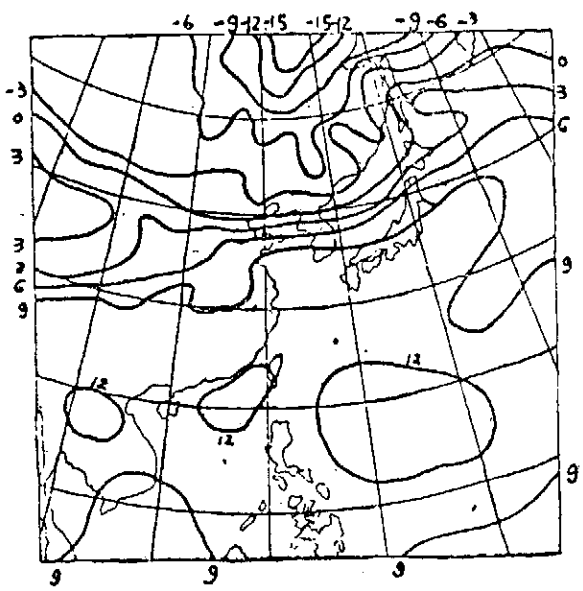

圖 5　700主觀分析溫度場

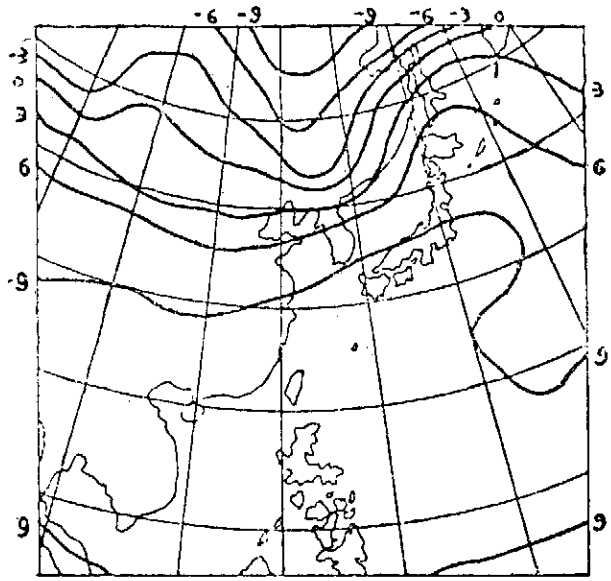

圖 6　700mb逐次校正分析溫度場

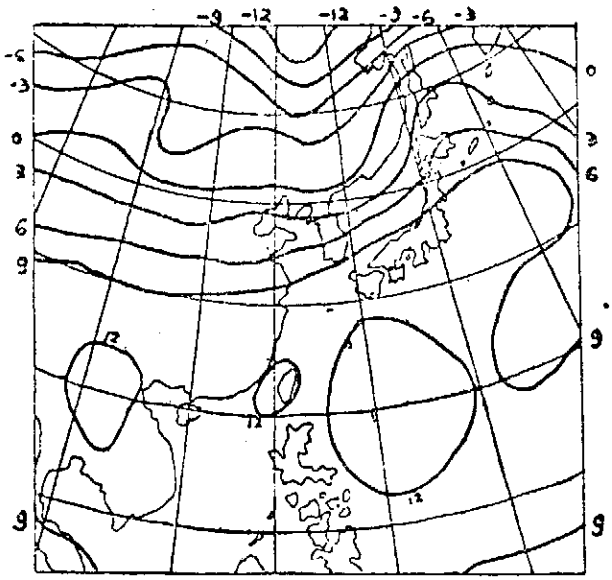

圖 7　700mb變分分析溫度場

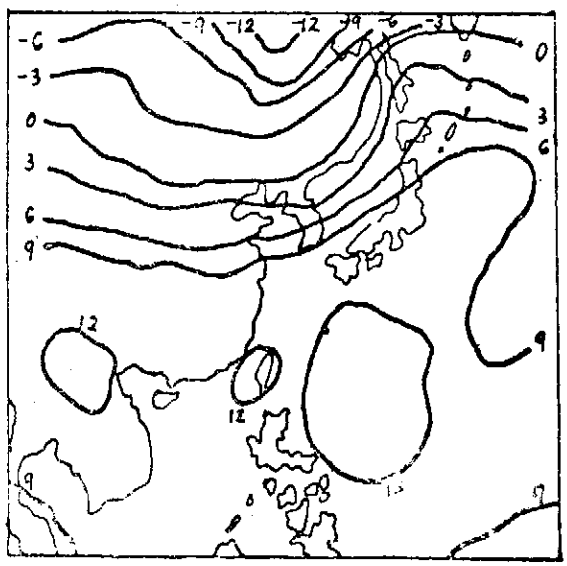

圖 8　本研究所得700mb溫度場

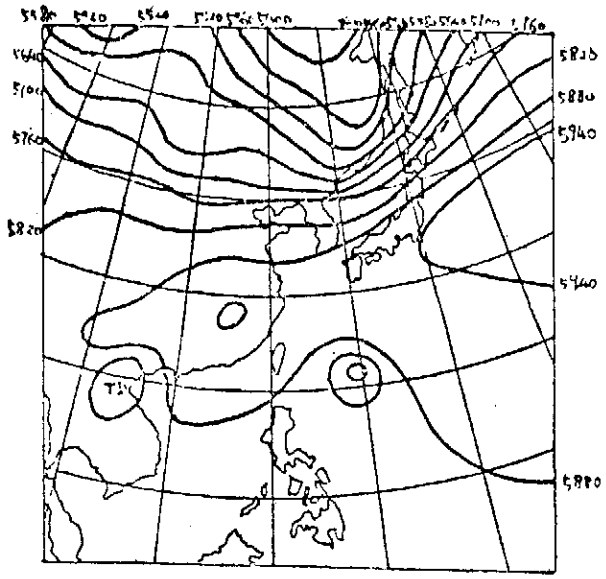

圖 9　500mb主觀分析高度場

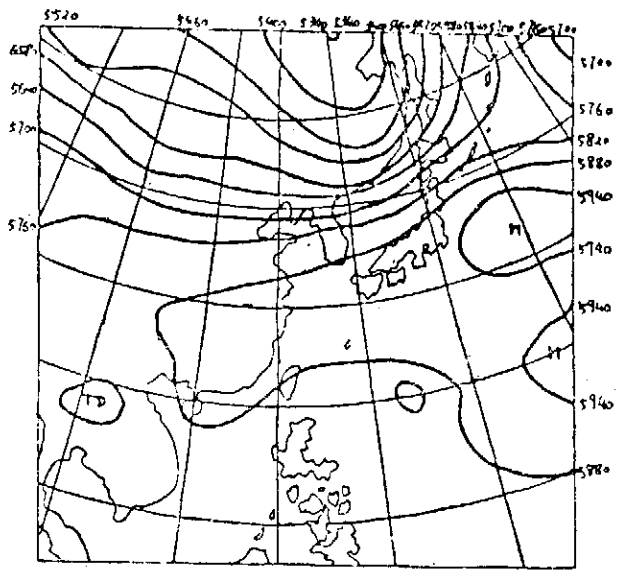

圖10　500mb逐次校正分析高度場

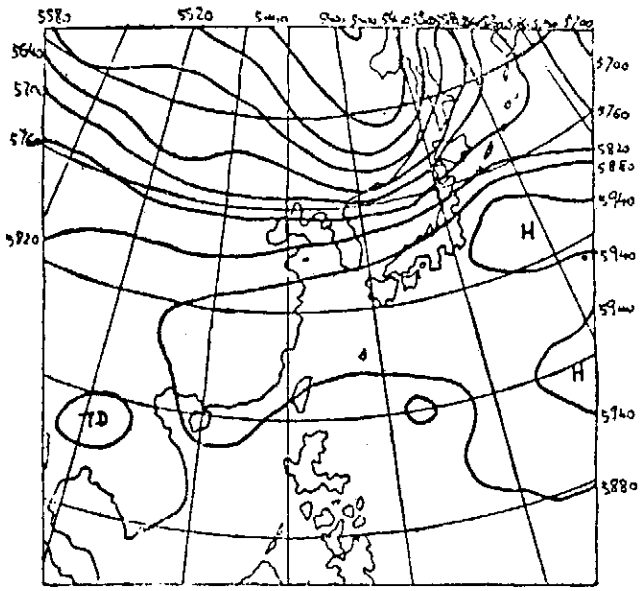

圖11　500mb變分分析高度場

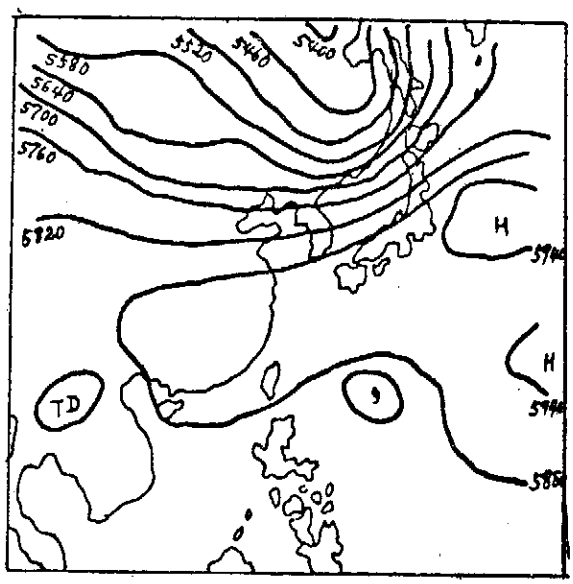

圖12　本研究所得500mb高度場

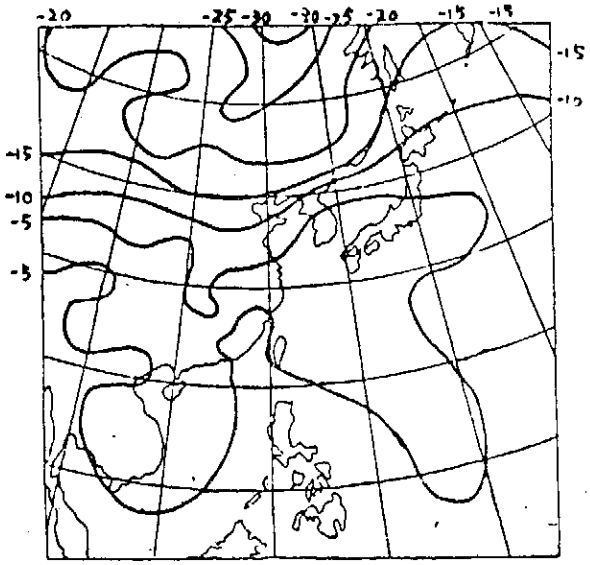

圖13　500mb主觀分析溫度場

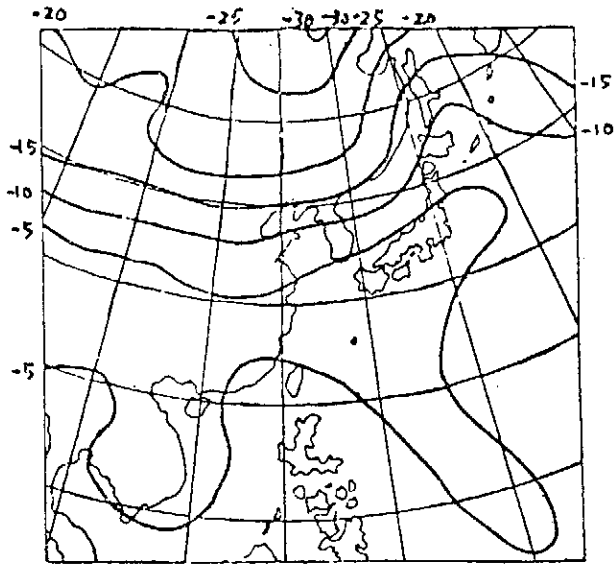

圖14　500mb逐次校正分溫析度場

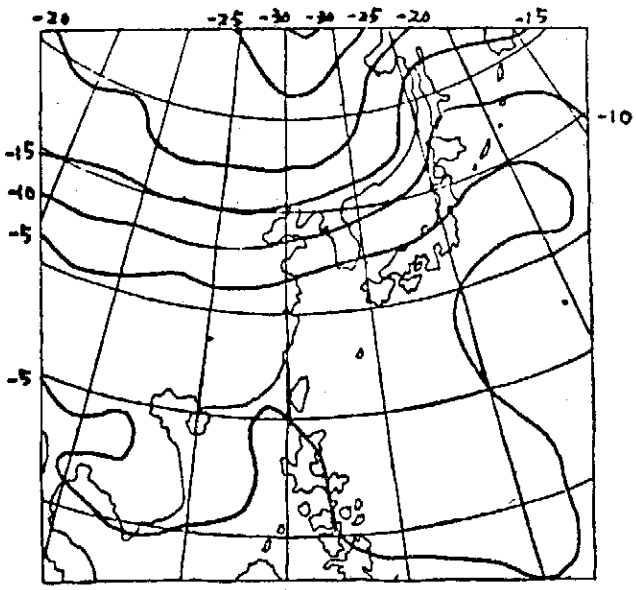

圖15　500mb 鞿分分析溫度場

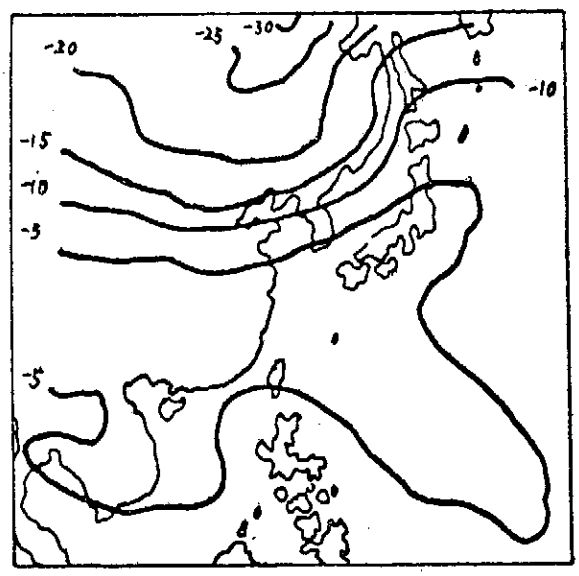

圖16　本研究所得 500mb溫度場

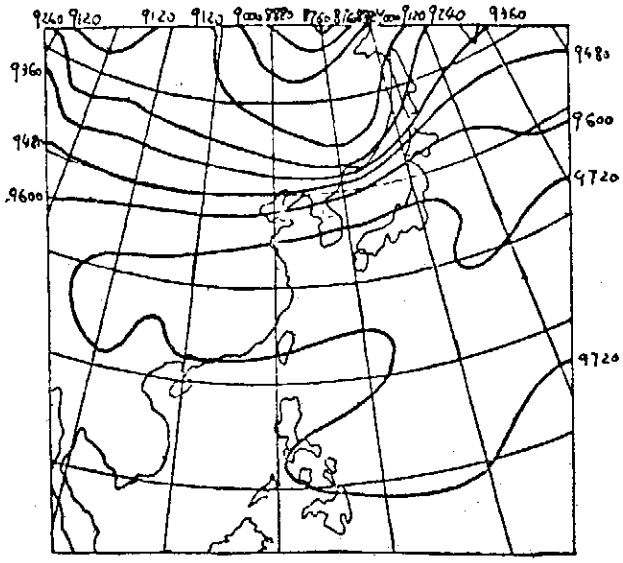

圖17　300主觀分析高度場

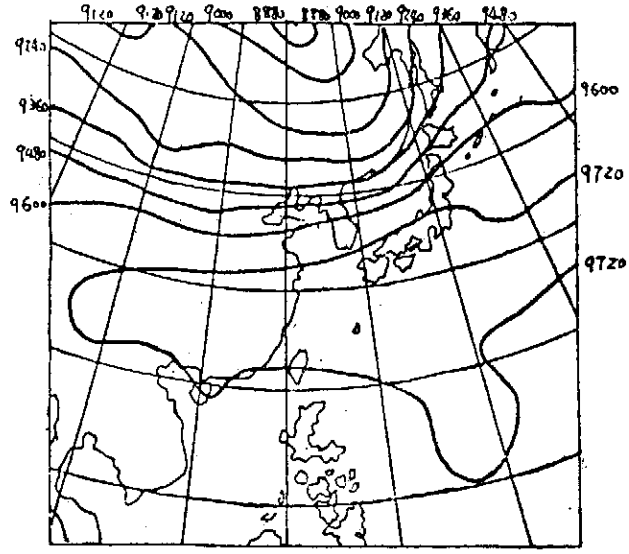

圖18　300mb逐次校正分析高度場

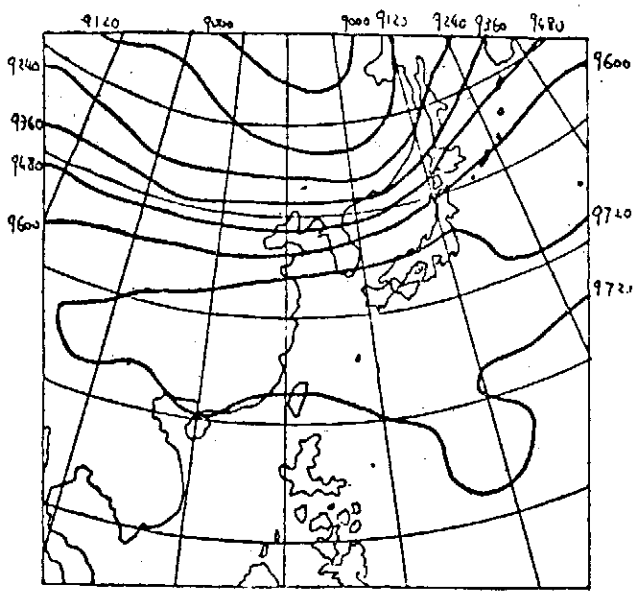

圖19　　變分分析高度場

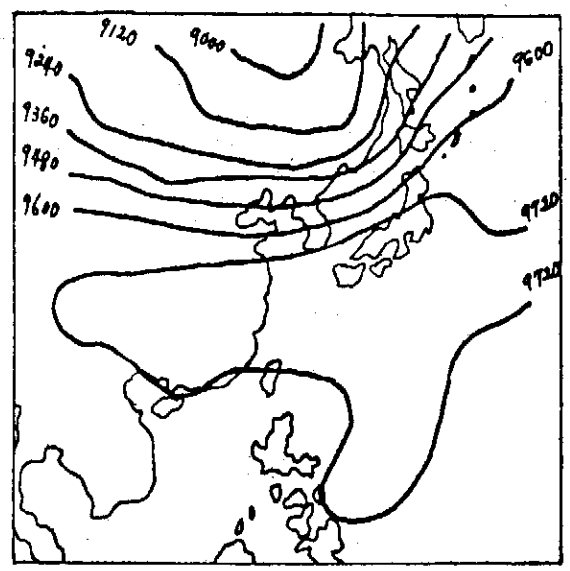

圖20　本研究所得300mb高度場

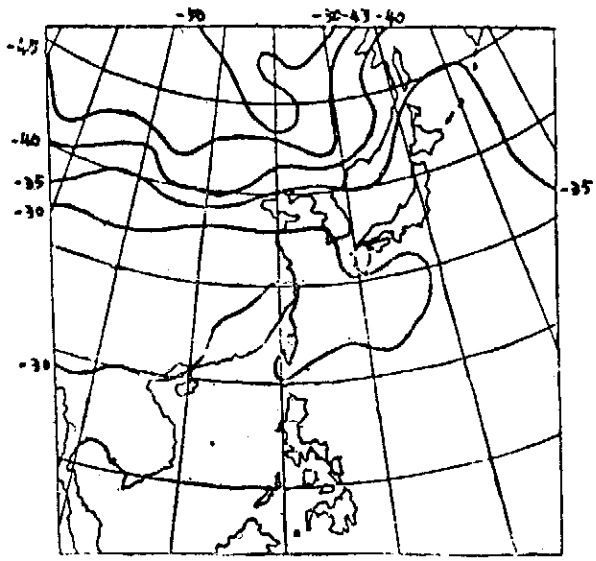

圖21　300mb主觀分析溫度場

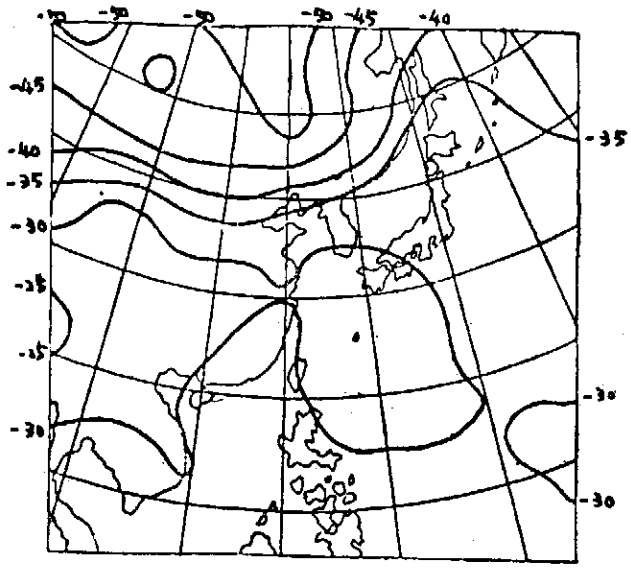

圖22　300mb逐次校正分析溫度場

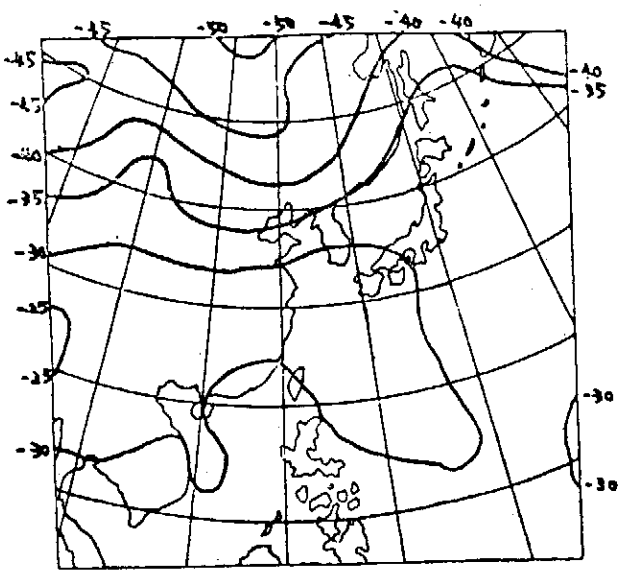

圖23　300mb 變分分析溫度場

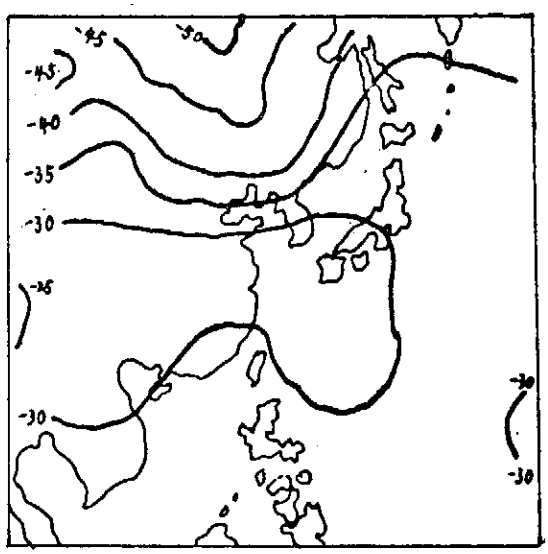

圖24　本研究所得300mb溫度場

Annual Report of the Institute of Physics, Academia Sinica, Vol.7, 1977

正壓原始方程式計算不穩定之研究

曾忠一　張德青

中央研究院物理研究所

摘　要

本研究探討正壓原始方程式預報模式之非線型計算不穩定。本研究進行三種空間差分程式和兩種時間差分程式之數值試驗。在六種試驗中均無計算不穩定的情形存在。使用Euler backward時間積分程式確比跳蛙式時間積分程式會更有效控制計算不穩定。

§1. 導言與模式

本研究所使用的模式爲淺水方程式，又叫做正壓原始方程式。這是代表廻轉系中具有自由面的正壓流體運動的方程式。

$$\begin{aligned}&\frac{\partial u}{\partial t}+u\frac{\partial u}{\partial x}+v\frac{\partial u}{\partial y}-fv=-\frac{\partial \varphi}{\partial x}\\&\frac{\partial v}{\partial t}+u\frac{\partial v}{\partial x}+v\frac{\partial v}{\partial y}+fu=-\frac{\partial \varphi}{\partial y}\\&\frac{\partial \varphi}{\partial t}+u\frac{\partial \varphi}{\partial x}+v\frac{\partial \varphi}{\partial y}+\varphi\left(\frac{\partial u}{\partial x}+\frac{\partial v}{\partial y}\right)=0\end{aligned}\tag{1}$$

其中φ是重力位，其他符號與通常使用的相同。這組方程式可以描述許多海洋運動的現象，同時也可以來用預測溫帶地區的500mb 等高線的變化（見Gerrity and McPherson 1969）。此外這組方程式中不但具有位相速度緩慢的羅士培波，同時也有快速運行的慣性重力波。在中緯度地區這種慣性重力波的幅度遠比現有的高空觀測網所能測得的大氣現象的幅度小得很多，因此通常被認爲是大幅度預報的雜波。但是由於這種雜波的位相速度很快，若不加以有效的控制，會污染整個預報場。上述這組淺水方程式比一般原始方程式簡單，而且具有慣性重力波，因此在從事數值天氣預報的研究時，常使用這組方程式來探討雜波的控制法。例如數值差分程式的設計，計算不穩定的控制，四維資料同化的研究以及差分程式的變分設計等等經常使用這組方程式來進行慣性重力波的控制工作。因此本研究首先利用這組方程式探討計算不穩定的控制，設計預報模式，以作爲未來研究四維資料同化和差分程式變分設計的基礎。

這組方程式可以寫成 flux form

$$\begin{aligned}&\frac{\partial}{\partial t}(\varphi u)+\frac{\partial}{\partial x}(\varphi u^2)+\frac{\partial}{\partial y}(\varphi uv)-f\varphi v=-\varphi\frac{\partial \varphi}{\partial x}\\&\frac{\partial}{\partial t}(\varphi v)+\frac{\partial}{\partial x}(\varphi uv)+\frac{\partial}{\partial y}(\varphi v^2)+f\varphi u=-\varphi\frac{\partial \varphi}{\partial y}\\&\frac{\partial \varphi}{\partial t}+\frac{\partial}{\partial x}(\varphi u)+\frac{\partial}{\partial y}(\varphi v)=0\end{aligned}\tag{2}$$

也可以寫爲 invariant form

$$\frac{\partial u}{\partial t}+\frac{\partial}{\partial x}\frac{u^2+v^2}{2}-v\left(f+\frac{\partial v}{\partial x}-\frac{\partial u}{\partial y}\right)=-\frac{\partial \varphi}{\partial x}$$

$$\frac{\partial v}{\partial t}+\frac{\partial}{\partial y}\frac{u^2+v^2}{2}+u\left(f+\frac{\partial v}{\partial x}-\frac{\partial u}{\partial y}\right)=-\frac{\partial \varphi}{\partial y} \tag{3}$$

$$\frac{\partial \varphi}{\partial t}+\frac{\partial}{\partial x}(\varphi u)+\frac{\partial}{\partial y}(\varphi v)=0$$

由(1)(2)(3)三式的淺水方程式可以設計多種數值差分程式。一般說來(1)式是最常見的型式，(3)式在導出能量方程式，渦度和位渦方程式時比較方便，(2)式又叫 momentum form 在斜壓原始方程式的差分程式中經常使用。以上三式具有質量守恒積分式

$$\frac{d}{dt}\int\int \varphi dxdy=0 \tag{4}$$

和能量守恒積分式

$$\frac{d}{dt}\int\int \frac{1}{2g}\left[\varphi(u^2+v^2)+\varphi^2\right]dxdy=0 \tag{5}$$

數值預報模式的時間積分數值差分程式對預報結果的影響很大。除了差分程式的一致性穩定性以及收斂性之外，一般設計的差分程式並不會滿足上面兩個守恒積分式。Arakawa（一九六六）指出了差分程式必須滿足某些守恒積分式的重要性。假如一組方程式的差分程式能滿足該方程式的守恒積分式，計算不穩定就能得到有效的控制。Sasaki（一九七六）利用變分原理使淺水方程式時間積分過程中的每一變數如u,v,φ滿足上面兩個守恒積分式來控制計算不穩定。

其他的差分程式是由(1)，(2)，(3)三式得到，並未滿足(4)(5)兩個守恒積分式。本研究探討三個不同的差分程式，同時進行六個數值試驗，以了解如何控制計算不穩定。

§2. 差分程式

本研究所使用的差分程式有三種，第一種是 Shuman and Vanderman′ (1966) 所使用的，後來NMC也一直用這種差分程式 (Shuman and Hovermale 1968) 來進行斜壓原始方程式的時間積分：

$$\bar{u}_t^t+\overline{\bar{u}^x\bar{u}_x^y+\bar{u}^y\bar{u}_y^x+\bar{\varphi}_x^y-\bar{f}^y\bar{v}^y}^{xy}=0$$

$$\bar{v}_t^t+\overline{\bar{u}^x\bar{v}_x^y+\bar{v}^y\bar{v}_y^x+\bar{\varphi}_y^x\bar{f}^y\bar{u}^y}^{xy}=0$$

$$\bar{\varphi}_t^t+\overline{(\bar{u}^y\bar{\varphi}^y)_x+\bar{v}^x\bar{\varphi}^x)_y}^{xy}=0$$

南北的邊界條件是

$$u_y=0 \qquad \bar{v}^y=0 \qquad \phi_y=0$$

第二種差分程式是 Grimmer and Shaw (1967) 使用的

$$(\overline{\varphi u})_t^t+(\overline{\phi u^x}\bar{u}^x)_x+(\overline{\varphi v^y}\bar{u}^y)_y-f\varphi v+\varphi\bar{\varphi}_x^x=0$$

$$(\overline{\varphi v})_t^t+(\overline{\varphi u^x}\bar{v}^x)_x+(\overline{\varphi v^y}\bar{v}^y)_y+f\varphi u+\varphi\bar{\varphi}_y^y=0$$

$$\bar{\phi}_t^t+(\overline{\varphi u})_x^x+(\overline{\varphi v})_y^y=0$$

南北的邊界條件是

$$v=0 \qquad \bar{\varphi}_y^y=0 \qquad \bar{u}_y^y=0$$

第三種差分程式是一種能量守恒程式：

$$\bar{u}_t^t+\left(\overline{\frac{u^2+v^2}{2}+\varphi}\right)_x^x-v\left(f+\bar{v}_x^x-\bar{u}_y^y\right)=0$$

$$\bar{v}_t^t+(\overline{\frac{u^2+v^2}{2}}+\varphi)_y^y+u(f+\bar{v}_x^x-\bar{u}_y^y=0$$

$$\bar{\varphi}_t^t+(\overline{\varphi u})_x^x+(\overline{\varphi v})_y^y=0$$

南北的邊界和第二種差分程式一樣。東西邊界是Cyclic boundary condition. 以上的三種差分程式中我們所用的符號和 Shuman 1962 一樣，即

$$F_x=\frac{F_{i+\frac{1}{2},j}-F_{i-\frac{1}{2},j}}{\Delta x}$$

$$\overline{F}^x=\frac{F_{i+\frac{1}{2},j}+F_{i-\frac{1}{2},j}}{2}$$

初期高度場在這研究中採用Grammeltvedt 1969 (見圖1.) ，即

$$h(x,y)=H_0+H_1,tanh\frac{9(y-D/2)}{2D}+H_2sech^2\frac{9(y-D/2)}{D}[0.8\ sin\frac{\partial\pi x}{L}+0.5sin\frac{12\pi x}{L}]$$

其中

$H_0=2000m$　　$L=6000km$

$H_1=-220m$　　$D=4000km$

$H_2=133m$　　$f_0=10^{-4}\ sec^{-1}$

$g=9.8m/sec^2$　　$\beta=1.5\times10^{-11}/m\text{-}sec$

本研究使用31×23的網格，初期風場直接由地轉風的關係式得到，即

$$u=-\frac{g}{f}\bar{h}_y^y \qquad v=\frac{g}{f}\bar{h}_x^x$$

其中

$$f=f_0+\beta(y-D/2)$$

時間積分方面使用跳蛙式程式和 Euler backward程式。Euler backward 程式具有消滅高頻雜波的特性，在時間積分時時常被使用到 。 本研究進行三種空間積分程式和兩種時間積分程式，總共進行六個實驗。

在檢定差分程式的穩定度時，我們在時間積分的每一個過程都計算有效能量，即

$$\frac{1}{2g}\sum_i\sum_j\{\varphi_{ij}(u_{ij}^2+v_{ij}^2)+(\varphi_{ij}-gH_0)^2\}$$

這個有效能量根據(5)式應當是保持固定的，假如有效能量愈來愈大表示計算不穩定，慣性重力波污染了預報場。

§3. 結果與討論

由於計算機時間的限制，上述六個試驗只進行六十小時的預報，六個試驗的有效能量均保持穩定 (見圖2) ，不會愈來愈大，因此計算不穩定獲得有效的控制 ， 至少在六十個小時內如此 。 此由圖2可見 Euler backward 時間積分程式具有消滅高頻雜波的特性。

第一種空間差分程式的六十小時後的高度場在圖3和圖4。圖3是用跳蛙式的時間積分 ， 圖4是用 Euler backward 的時間程式。由這兩圖可見大規模波動的振幅用跳蛙式時間積分比 Euler backward 時間積分大，可是兩者的位相幾乎一樣，此外 Euler backward 時間積分似具修勻與濾波的特性。

第二種空間差分程式的六十小時後的高度場在圖 5 和圖 6 。第三種空間差分程式所得的高度場在圖 7 和圖 8。由這些圖中可見跳蛙式和 Euler backward 兩程式結果的差異，即大規模波動的振幅跳蛙式的結果較大，而跳蛙式和 Euler backward 所得的位相幾乎一樣。

此外三種空間程式所得到的預報場並不相符，大規模波動的位相並不一樣，由於這個起始值問題並無準確解作爲比較之用，無法說明這三種空間積分的優劣。

由本研究所進行的六個試驗的結果，計算不穩定可說獲得有效的控制，至少在六十小時之內確是如此。邊界條件、初期狀態問題也會影響預報結果，本研究當繼續從事這方面的探討。此外本研究所得的結果將作爲設計斜壓原始方程式預報模式之用，也可以作爲未來研究差分程式變分設計和四維資料同化等研究之基礎。

§4. 致　謝

本文承陳鈞珍小姐進行繪圖工作，著者深表謝意。

參考文獻

Gerrity, J.P. and R. D. McPherson, 1969: Development of a fine mesh, limited area prediction model. Mon. Wea. Rev.,97, 665-669.

Grammelvedt,A., 1969:A survey of finite difference schemes for the primitive equations of a barotropic fluid. Mon. Wea.Rev., 97, 384-404.

Shuman, F.G., and J.B.Hovermale, 1968: An operational six layer primitive equation model. J. Appl.Meteor., 7, 525-547.

Shuman, F.G., and L. W. Vanderman, 1966: Difference system and boundary conditions for the primitive equation barotropic forecast. Mon Wea. Rev., 94, 329-335.

Sasaki, Y. K., 1976:Variational design of finite difference scheme for initial value problem with an integral constraint. J. Computational Physics, 21, 270-278

Shuman, F. G., 1962:Numerical experiments with the primitive equations. Proc. International Symposium on NWP. Tokyo, 1960.

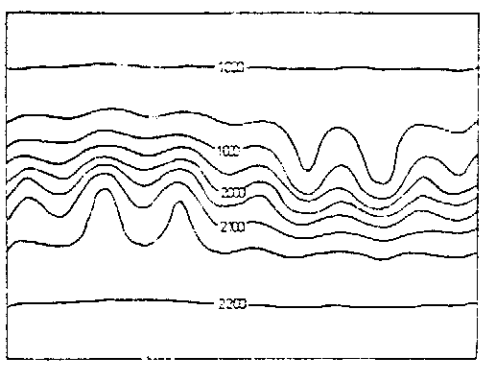

圖一　本研究所用的初期高度場，單位爲公尺，等高線間隔五十公尺。

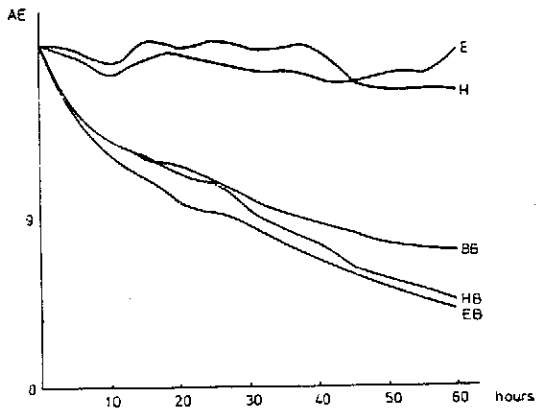

圖二　各種試驗有效能量的時間變化。
E　第三種空間差分程式，跳蛙式時間差分程式
EB同上但時間差分程式爲 Euler Backward
BB第二種空間差分程式Euler Backward時間差分程式
H　第一種空間差分程式，跳蛙式時間差分程式
HB同上但時間差分程式爲 Backward

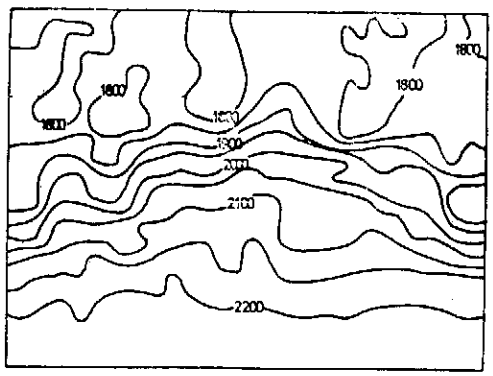

圖三　第一種空間差分程式六十小時後的高度場。時間積分程式爲跳蛙式。

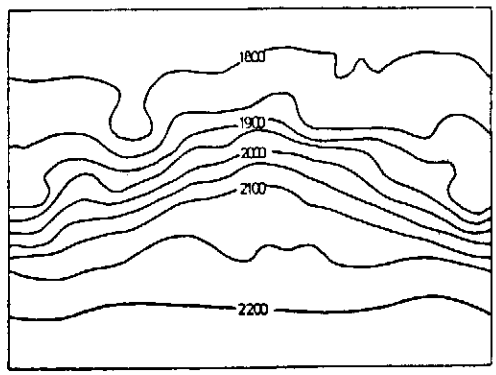

圖四　同圖三。但時間積分程式爲 Euler Backward。

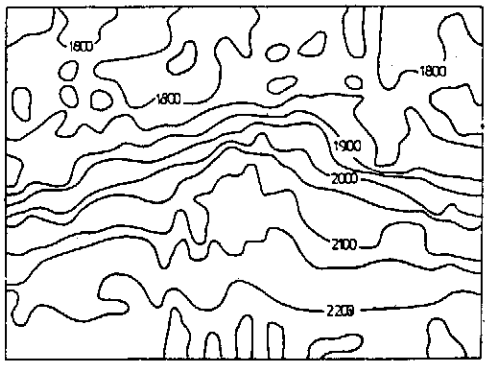

圖五　第二種空間差分程式六十小時後的高度場。時間積分程式爲跳蛙式。

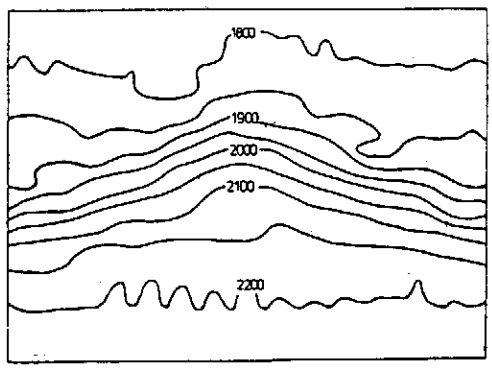

圖六　同圖五。但時間積分程式爲 Euler Backward。

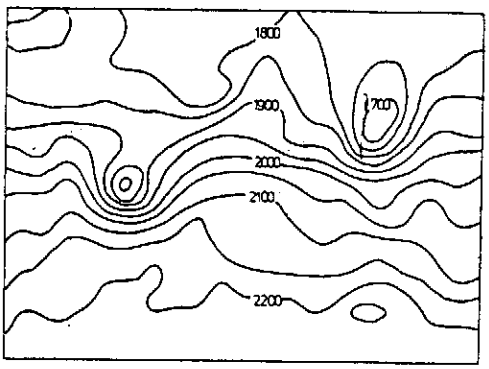

圖七　第三種空間差分程式六十小時後的高度場。時間積分程式爲跳蛙式。

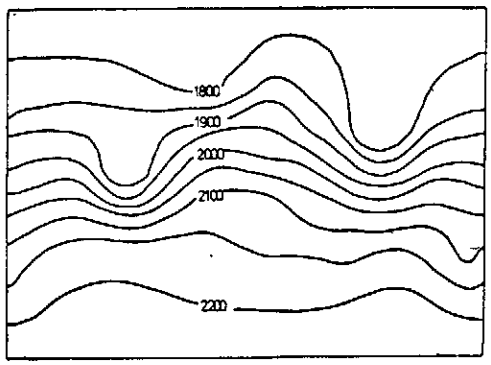

圖八　同圖七。但時間積分程式爲 Euler Backward。

Annual Report of the Institute of Physics, Academia Sinica, Vol.7, 1977

The Generalization of Kuo's Parameterization of Cumulus Convection Part I. Diagnostic Studies

Wen-Jey Liang

Institute of Physics Academia Sinica and
Dept. of Mech. Eng., National Taiwan University

ABSTRACT

In this study, a new parameterization of cumulus convection is developed from the moisture conservation equation. It is shown that the scheme can be considered as the generalization of Kuo's parameterization concepts and Kuo's (1965 and 1974) schemes can be reduced from it as two special cases. For realizing the flexibility of this scheme, the diagnostic investigation is performed utilizing the combination of the parameterization formula and the large-scale heat and moisture budgets. Compared with the observations, the results of the diagnostication show that the generalized scheme gives better estimations on the latent heat released and the pressure of the cloud top, and reveals that the adiabatic subsidence of the environmental atmosphere and the vertical transport of moisture inside the clouds are both significant in the parameterization of cumulus convection.

1. Introduction

The atmospheric motion consists of a great deal of atmospheric systems of different scales. Among those, cumulus convection may be one of the most interesting phenomenon. It is well known that convective system plays an important role in vertical transport of heat, moisture and horizontal momentum, provides a large portion of the annual precipitation, accounts for the greatest weather damage in many areas, and reveals the obvious intereaction among disturbances of large, medium and small scales. Furthermore, clouds are reflectors and modifiers of shortwave radiation and emitters and absorbers of longwave radiation. Consequently, studies of clouds and convection naturally become an important topics in atmospheric science. Recently, increasing attention is being focused on the mean effects of cumulus clouds to develop the larger scale systems in the tropics and the middle latitudes. However, because of its smallness, cumulus convection can not be resolved in the present observational network. This mechanism should be parameterized in terms of larger scale

variables. Indeed, since Riehl and Malkus (1958) concluded from their budget studies that cumulus convection is a dominant mechanism in the tropics, parameterization of cumulus convection has been studied by many investigators. In the past decade, many parameterization schemes have been developed. Each scheme has its significance for the purpose for which it has been proposed. Still, because of the complexity of the relevant phenomenon of convective motion, the completely satisfactory parameterization scheme is out of sight.

Currently, two types of cumulus parameterizations are used. One, based on the hypothesis of convective adjustment (Manabe et al., 1965), is utilized in general circulation and synoptic-scale prediction models. The idea of convective adjustment is based on the assumption that thermal convection develops when the lapse rate of temperature exceeds a certain neutral value. The other, based on the hypothesis of penetrative convection (Ooyama, 1964; Kuo, 1965), is also utilized in general circulation models; but the scheme is primarily applied to the study of the development of tropical cyclones and of the synoptic-scale numerical prediction. Here, penetrative convection is assumed to occur when cumulus clouds penetrate deeply into an unsaturated atmosphere in areas of low-level mass convergence. Although both types of cumulus parameterization have practical significance, the latter appears to be more attractive because the existence of low-level convergence is involved as triggering mechanism. Acoording to Ceselski's (1973) numerical prediction experiments, convective adjustment scheme is less desirable for real data forecasting because of no consideration of the link between the motion disturbance and total saturation.

Based on the hypothesis of penetrative convection, the parameterization procedure consists of two significant mechanisms involved in the interaction between convection and the environment: (1) adiabatic warming due to the downward motion of the environmental air which compensates for the upward motion inside convective elements, (2) lateral mixing of cloud substance into the environment. Among such parameterization schemes, Kuo's (1965) scheme is one of the most representative. Kuo's parameterization is based on a non-steady deep cumulus model; the temperature difference between the cloud and the surrounding atmosphere, and the large-scale low-level convergence of moisture are the key indicators. Recently, some arguments about it arose (e.g., Ceselski, 1974). It has been stated that Kuo has neglected the heating by adiabatic compression of the slowly decending environment. Also, the reality of the horizontal mixing process involved in his scheme has been questioned.

The Generalization of Kuo's Parameterization of Cumulus Convection
Part I. Diagnostic Sudies

Yanai et al (1973) determined the bulk properties of tropicalclond clusters from large-scale heat and moisture budgets using 1956 Marshall Islands data. They showed that the cloud mass flux exceeds the mean vertical mass flux required by the large-scale convergence, thus causing a compensating sinking motion between active clouds, and concluded that the large-scale heating of the environmental air is primarily due to its adiabatic compression in the compensating downward motion. In order to clarify those arguments, Kuo (1974) gave his scheme a new derivation and explained that both the adiabatic heating of the descending branch and the adiabatic cooling of the ascending branch of the convective cell have been taken into consideration. He also states that the horizontal mixing mechanism is achieved simply by the horizontal averaging of the randomly distributed convective elements over the representative area of the large-scale system, even though vigorous horizontal mixing will undoubtedly also be accomplished physically by these randomly distributed and ever-changing convection cells. However, it is believed that if in Kuo's formulation the terms which account for departures from the area mean, as well as the precipitation terms, are examined carefully, a better explanation can be obtained.

Kuo's scheme is applicable in those situations where a deep conditionally unstable layer and large-scale low-level convergence are in existence. The former condition makes it possible for huge cumuli to penetrate into the upper troposphere or the lower stratosphere, while the latter condition provides a lifting mechanism to trigger the convective instability. Therefore, in some situations, although the computed fractional area of coverage may be near unity, only shallow or even no clouds may develop. Investigations of moisture convergence and its relationship to the middle-latitudes severe storm, hurricane and tropical cylone occurrence (e.g., Charney and Elliassen, 1964; Sasaki, 1973) indicate that unstable conditions, downward momentum transport, and other factors, which may be important to the severe weather development, are implicitly shown in the moisture convergence patterns. Because the large-scale moisture convergence in a conditionally unstable region is believed to be a key mechanism in the development of deep convection, we would like to investigate the applicability of Kuo's scheme and to generalize it so that the scheme becomes dynamically and practically plausible.

Recently, Liang (1975) has proposed a modification of Kuo's parameterization. In this modified scheme, the large-scale moisture suply and the vertical transport of moisture and dry static energy inside the cloud are considered, and

a two-layer cloud ensemble model is combined. Diagnostic investigations of modified and Kuo's schemes have been carried out by combining the large-scale heat and moisture budgets and the expressions of the latent heat released of the tested schemes. The results of tests indicate that the added mechanisms serve surprisingly well in the modified parameterization. The precipitation rate, the mean top of clouds, and the level of the maximum latent heat released agree much better with observed values than those from Kuo's scheme. The tests also conformed the foregoing statement that the eddy terms which account for departures from the area mean, as well as the precipitation terms, plays an important role in the vertical transport of heat and moisture inside the cloud, and, therefore, fosters the low-level moisture convergence to produce a high level release of latent heat. However, because the modified scheme is based on physically intuitive consideration, the rigorous relationship between the modified and Kuo's schemes is vague. Theoretical and practical interests stimulate one to ponder further.

This study developes a new parameterization of cumulus convection from the moisture conservation equation. The scheme can be considered as a generalization of Kuo's parameterization concepts, and Kuo's (1965, 1974) schemes can be reduced from it as two special cases. In order to realize its applicability, the new parameterization is diagnosed similar to the procedures proposed by Liang (1975). The results are compared to those from Kuo's schemes, and the mechanisms involved are discussed.

2. Generalization of Kuo's parameterization

For convenience, let us define the dry static energy and the moist static energy as

$$s \equiv C_p T + gz, \text{ and}$$
$$h \equiv C_p T + gz + Lq,$$

where T is temperature, z the height, q the mixing ratio, C_p the specific heat of dry air, L the latent heat of condensation, and g the acceleration of gravity. It is obvious that the static energy is the sum of enthalpy and potential energy and the moist static energy is the sum of the static energy and latent energy. For the clarification of the essential points of the parameterization problem, the large-scale variables are represented as the average values over a hypothesized area, and the actual values are the sum of the average values and the departures. The hypothesized area is taken to be large enough such

that a great deal of cumulus clouds may be surrounded, and to be small enough thus the large-scale motion may be described by the area mean values of its variables. This quasi-homogeneous assumption is based on the fact that the physical properties of the large-scale system may approximately be homogeneous over a suitablly chosen area. For prediction of the synoptic scale motion, for example, the grid area may reasonablly be taken as the hypothesized area. Furthermore, based on the assumption of the feasibility of the parameterization of cumulus convection, the location and time of the convection occurrence are random distributed and the distribution may be estimated in term of the large-scale variables.

For the description of the large-scale motion, the equations of heat and moisture continuity are averaged over the hypothesized area:

$$\frac{\partial \bar{s}}{\partial t}+\overline{\nabla \cdot s\vec{V}}+\frac{\partial \overline{s\omega}}{\partial p}=Q_R+Q_c, \tag{1}$$

$$\frac{\partial \bar{q}}{\partial t}+\overline{\nabla \cdot q\vec{V}}+\frac{\partial \overline{q\omega}}{\partial p}=-\frac{Q_c}{L} \tag{2}$$

$$Q_c=L(c-e) \tag{3}$$

where $\vec{V}$ is the wind velocity, ω the vertical p- velocity, Q_R the radiation heating, Q_c the latent heat released by net condensation, c the condensation rate, and e the re-evaporation. The equations are expressed in (x, y, p, t) coordinates, and the area averages are denoted by $\overline{(\ )}$. As the variables are represented by the area mean values and the departures, (1) and (2) become

$$Q_1 \equiv \frac{\partial \bar{s}}{\partial t}+\overline{\nabla \cdot s\vec{V}}+\frac{\partial \overline{s\omega}}{\partial p}=Q_R+Q_c-\frac{\partial}{\partial p}\overline{s'\omega'}, \tag{4}$$

$$-\frac{Q_2}{L}=\frac{\partial \bar{q}}{\partial t}+\overline{\nabla \cdot q\vec{V}}+\frac{\partial \overline{q\omega}}{\partial p}=-\frac{Q_c}{L}-\frac{\partial}{\partial p}\overline{q'\omega'} \tag{5}$$

where $(\ )'$ denotes the departure. In the above, Q_1 is called the apparent heat source of the large-scale system and Q_2 is called the apparent moisture sink. According to Kuo (1974), the average of the vertical eddy transport of any variable x can be expressed as:

$$\overline{\omega' x'}=\frac{\sigma}{1-\sigma}(\omega_c-\bar{\omega})\ (x_c-\bar{x}),$$

where σ is the fractional area covered by the active clouds, and the subscript c denotes the flow variables in σ. Since ω_c is much larger than $\bar{\omega}$ and σ is much smaller than unity, (5) can be approximated by

$$\overline{\omega' x'}=-M_c\ (x_c-\bar{x}), \tag{6}$$

where

$$M_c = -\sigma\ \omega_c. \tag{7}$$

The substitution of (6) into (4) and (5) leads to

$$\frac{\partial \bar{s}}{\partial t} + \overline{\nabla \cdot s\vec{V}} + \frac{\partial \overline{s\omega}}{\partial p} = Q_R + Q_c + \frac{\partial}{\partial p}[M_c(s_c - \bar{s})], \tag{8}$$

$$\frac{\partial \bar{q}}{\partial t} + \overline{\nabla \cdot q\vec{V}} + \frac{\partial \overline{q\omega}}{\partial p} = -\frac{Q_c}{L} + \frac{\partial}{\partial p}[M_c(q_c - \bar{q})], \tag{9}$$

where $\overline{\nabla \cdot \bar{s}\vec{V}}$ and $\overline{\nabla \cdot q\vec{V}}$ can be separated as

$$\overline{\nabla \cdot s\vec{V}} = \nabla \cdot (\bar{s}\ \bar{\vec{V}}) + \overline{\nabla \cdot s'\vec{V}'},$$

and

$$\overline{\nabla \cdot q\vec{V}} = \nabla \cdot (\bar{q}\ \bar{\vec{V}}) + \overline{\nabla \cdot q'\vec{V}'}.$$

The horizontal diffusion terms $\overline{\nabla \cdot s'\vec{V}'}$ and $\overline{\nabla \cdot q'\vec{V}'}$ may be parameterized in terms of large-scale variables by the use of nonlinear horizontal diffusion coefficients similar to those used by Smagorinsky et al. (1965) and Manabe et al. (1965). Therefore, the apparent heat source Q_1 and the apparent moisture sink Q_2 can be determined from the large-scale observations. In order to clarify the physical meaning of each mechanism involved, (9) is rewriten as

$$\frac{\partial \bar{q}}{\partial t} + (c - e) = -[\overline{\nabla \cdot q\vec{V}} + \frac{\partial}{\partial p}(\overline{\omega q})] + \frac{\partial}{\partial p}[M_c(q_c - \bar{q})] \equiv \dot{q}_T \tag{10}$$

It is obvious that $\dot{q}_T$ is the total moisture supply from the large-scale and the subgrid scale motions. According to (10), this amount of moisture is utilized to increase the local moisture content of the mean flow $\bar{q}$ and to produce the net precipitation, (c-e). The local increasing of the moisture of environmental air is based on two processes. One is the mixing process of the cloud mass and the environmental air, and the other is the transport process directly from the large-scale motion. In other words, the local change of the mixing ratio of environmental air can be considered as the sum of this two sources:

$$\frac{\partial \bar{q}}{\partial t} = \frac{\sigma}{\tau}(q_c - \bar{q}) + b^*, \tag{11}$$

where τ is the time scale for growth and decay of the cumulus convection cell, and σ/τ is the cloud mass producing rate. The terms in the right of (11) are corresponding to the two processes, respectively. Also, according to Kuo, the latent heat released can be expressed in terms of the cloud mass producing rate and the temperature difference between clouds and the environment as

$$Q_c = \frac{\sigma}{\tau}(s_c - \bar{s}) \tag{12}$$

The substitution of (11) and (12) into (10) leads to

$$\frac{\sigma}{\tau}\frac{(h_e-\bar{h})}{L}=\dot{q}_T-b^*, \tag{13}$$

or,

$$\frac{\sigma}{\tau}=\frac{B\dot{q}_T}{h_e-\bar{h}}, \tag{14}$$

$$B=L(1-b^*/\dot{q}_T).$$

Since the environmental air requires $(\delta q_1+\delta q_2)$ to creat a unit cloud mass, where

$$\delta q_1=(s_e-\tilde{s})/L,$$

$$\delta q_2=q_e-\tilde{q},$$

Eq (14) shows that the producing rate of cloud mass, σ/τ, is determined from the effective moisture supply $B\dot{q}_T$ divided by the moisture requirement of a unit cloud mass. The factor B denotes the effect coefficient of cumulus convection in moisten processes. After substituting (14) into (12), we have

$$Q_e=\frac{B\dot{q}_T(s_e-\bar{s})}{h_e-\bar{h}}, \tag{15}$$

It will be shown in the following paragraphs that the parameterization formulas of latent heat released in Kuo's (1965 and 1974) schemes can be deduced from (15). Therefore, (15) is reasonablly considered as the basic formula of the generalization of Kuo's parameterization of cumulus convection, and the scheme is considered as the generalization of Kuo's concepts.

Now, let us integrate (13) from the top of the atmosphere, p_t, to the ground surface, p_s, and assume the cloud mass producing rate to be a constant during the integration, we get

$$\frac{\sigma}{\tau}=\frac{(1-b)M_t}{M_L} \tag{16}$$

where b, M_t, and M_L are defined as

$$b=\int_{p_t}^{p_s} b^*\,dp/\int_{p_t}^{p_s}\dot{q}_T\,dp,$$

$$M_t=-\frac{1}{g}\int_{p_t}^{p_s}\overline{\nabla\cdot q\vec{V}}\,dp+p_0\,C_D\,V_*(q_*-q_0),$$

and

$$M_L=\frac{1}{gL}\int_{p_t}^{p_s}[C_p\,(T_e-\bar{T})+L(q_e-\bar{q})]dp.$$

During the above derivation, $\overline{\omega}$ is assumed to be zero both at the ground surface and at the top of the atmosphere, and $\overline{\omega's'}$ is assumed to be zero at and above

the cloud top and is approximated, at the ground surface, by

$$-(\overline{\omega' s'})_s = \rho_o g C_D V_o (q_s - q_o),$$

where the subscript o denotes the values at a reference level above which is representative of the surface boundary layer, and the subscript s are values at ground surface. The combination of (12) and (16) leads to

$$Qc = \frac{(1-b)M_t}{M_L}(s_c - \bar{s}) \tag{17}$$

It is obvious that (17) can be reduced to Kuo's (1965) formula of parameterization scheme if b is assumed to be negligiblly small. Also, it can be shown that if b_1 is defined as

$$b_1 = \int_{p_t}^{p_s} \frac{\partial \bar{q}}{\partial t} dp \Big/ \int_{p_t}^{p_s} q_r dp,$$

the integration from p_t to q_s of the combination of (10) and (12) leads to

$$\frac{\sigma}{\tau} = \frac{(1-b)L\ M_t}{\int_{p_t}^{p_s} (s_c - \bar{s}) dp},$$

where σ/τ is still assumed to be a constant during the integration. Substituting the above expression into (12), we have

$$Q_c = \frac{(1-b_1)L\ M_t(s_c - \bar{s})}{\int_{p_t}^{p_s} (s_c - \bar{s})\ dp} \tag{18}$$

Eq. (18) is essentially the same as that derived by Kuo (1974).

3. The procedure for diagnosticating cumulus parameterization schemes

a. Basic Procedure

Here, a procedure is proposed to diagnosticate and evaluate the mechanisms involved in a parameterization scheme. The method is based on the concept that utilization of an accurate expression for the latent heat released by cumulus should lead to good evaluations of other characteristics of the cloud ensemble. It will be shown below that when Q_c, the latent heat released by cumulus, is expressed in terms of certain cloud ensemble properties, the cloud ensemble properties may be determined from the large-scale budget equations if the time derivatives of dry static energy and mixing ratio in the environment is specified. In other words the cloud ensemble properties computed from this procedure should directly reflect the quality of the expression, for the latent heat released, which is utilized in the parameterization scheme. Furthermore, if the large-scale budgets and the parameterization scheme are both perfect, the latent heat

released, as computed from the parameterization scheme and as determined using the diagnosticating procedure, should be exactly the same. In the following discussion, any quantity, except the vertical velocity, in the environment is approximated by the area-mean value of that quantity.

First, let us define the saturation moist static energy of the environment, $\tilde{h}^*$, as

$$\tilde{h}^* \doteq C_p\,\overline{T} + g\overline{z} + L\overline{q}^* \equiv \bar{h}^*,$$

where $\bar{q}^*$ is the saturation mixing ratio at temperature $\overline{T}$, and $\tilde{(\ )}$ is the values of the environmental variables. Then, after Arakawa (1969), we have

$$s_c = \bar{s} + \frac{1}{1+r}(h_c - \bar{h}^*), \tag{19}$$

$$q_c = \bar{q}^* + \frac{r}{(1+r)L}(h_c - \bar{h}^*), \tag{20}$$

where $r \equiv \frac{L}{C_p}\left(\frac{\partial \bar{q}^*}{\partial \overline{T}}\right)_p$.

If Q_c is expressed in terms of the other variables, combination of (8), (9), (19) and (20) gives four equations for the four unknowns, s_c, q_c, M_c, and h_c. They can be solved provided that the observed large-scale heat and moisture budgets over the area considered are known. The associated boundary conditions are

$$\frac{\Delta p}{g}(Q_1 - Q_R) = S_s - \frac{M_{cb}}{g}(s_{cb} - \bar{s}_b),$$

$$-\frac{\Delta p}{g}Q_2 = LE_s - \frac{M_{cb}}{g}L(q_{cb} - \bar{q}_b),$$

$$S_s/LE_s = C_p(\overline{T}_s - \overline{T}_o)/[L(\bar{q}_s - \bar{q}_o)],$$

where the subscript b denotes values at cloud base, S_s and E_s are, respectively, the supply of sensible heat and the rate of evaporation from surface, and $\Delta p = p_s - p_b$. Defining Y as $-\overline{\omega' h'}$, adding (8) and (9) and integrating the resultant equation, we get

$$Y(p) = \int_{p_t}^{p} (Q_1 - Q_2 - Q_R)\,dp,$$

$$= M_c(h_c - \bar{h}) + Y(p_{ct}),\ if\ p \leq p_b, \tag{21}$$

where p_{ct} is the pressure at the top of clouds, and $Y(p_t)$ and $M_c(p_{ct})$ are assumed to be zero. Utilizing (21), the boundary conditions are explicitly expressed as

$$M_{cb}=\frac{a_1-(1+r_b)a_2}{\bar{h}_b^*-h_b} \tag{22}$$

$$h_{cb}=\bar{h}_b+\frac{a_1}{M_{cb}}, \tag{23}$$

where

$$a_1=g(S_s+LE_s)-\Delta P(Q_1-Q_R-Q_2),$$
$$a_2=gs-\Delta p(Q_1-Q_R),$$

and

$$S_s+LE_s=Y(P_s).$$

During the diagnosticating procedure, the cloud base is assumed to be at the lifted condensation level representative of the surface layer, and the top of cloud is assumed to be at a level where the temperature of the clouds is equal to that of the environment or at a level where M_c is zero.

b. Equations for diagnosticating Kuo's scheme

In preceding section, it has been shown that Kuo's (1965) and Kuo's (1974) schemes are essentially the same. Therefore we would like to investigate Kuo's (1965) scheme only, and the results and conclusions should be able to apply to both schemes. According to Kuo (1965), Q_c is specified as

$$Q_c=\frac{M_t}{M_c}(s_c-\bar{s}). \tag{24}$$

After elimination of s_c, q_c and h_c from (8), (9), (19) and (20), an ordinary nonlinear differential equation is obtained:

$$\frac{dU}{dp}=F+G/U, \tag{25}$$

where

$$U=M_c\left(\frac{\bar{h}^*+\bar{h}}{1+Y}\right),$$

$$F=-Q_1+Q_R-\frac{B(\bar{h}^*+\bar{h})}{1+r}+\frac{\partial}{\partial p}\left[\frac{Y-Y(p_{ct})}{1+r}\right],$$

$$G=-\frac{B_1(h^*-h)[Y-Y(p_{ct})]}{(1+r)^2}, \text{ and}$$

$$B_1=\frac{M_t}{M_L},$$

where Y is determined from (21) as a function of Q_1, Q_2, and Q_R.

Eq. (25) can be reduced to Abel's equation of the first kind and can be solved analytically if the ratio of the two coefficients, G and F, is constant, or it can be solved numerically even if the coefficients are variable. However,

because the producing rate of cloud air, B_1, depends on M_c, and the pressure at cloud top, p_{ct}, is unknown before the solution is obtained, the equation is an nonlinear integral-differential equation. A Runge-Kutta method and an iterative technique are utilized to solve it. After the solution is obtained, M_c, h_c, s_c, q_c and Q_c can be computed according to (25), (21), (19), (20) and (24), respectively, and T_c is determined by

$$T_c \equiv \bar{T} + \frac{s_c - \bar{s}}{C_p} \tag{26}$$

c. Equation for diagnosticating the generalized scheme

Similar procedure described above can also be used to diagnosticate the mechanisms involved in the generalized scheme. According to (15), Q_c is specified as

$$Q_c = \frac{B\dot{q}_T\ (s_c - \bar{s})}{h_c - \bar{h}}.$$

After elimination of s_c, q_c, and h_c from (8), (9), (19) and (20), an ordinary nonlinear differential equation is obtained:

$$(F_0 + F_1 U)\frac{dU}{dp} = G_0 + G_1 U, \tag{27}$$

where

$$U = \frac{M_c}{1+r}\ (\bar{h}^* - \bar{h}),$$

$$F_0 = Y - Y(p_{ct}) - \frac{B[Y - Y(p_{ct})]}{L(1+r)},$$

$$F_1 = \frac{B}{L},$$

$$G_0 = [Y - Y(p_{ct})](-Q_1 + Q_R) + \frac{BQ_3}{1+r}[Y - Y(p_{ct})]$$

$$+ [Y - Y(p_{ct})]\frac{d}{dp}\left[\frac{Y - Y(p_{ct})}{1+r}\right]$$

$$G_1 = -BQ_3,$$

$$Q_3 = -\nabla \cdot \bar{q}\bar{\vec{V}}_3 - \frac{\partial}{\partial p}(\bar{q}\,\bar{\omega}) + \frac{d}{dp}\left\{\frac{r[Y - Y(p_{ct})]}{(1+r)L}\right\}.$$

Since the pressure at cloud top is unknown before the solution is obtained, (27) should be solved utilizing the Rung-Kutta method and an iterative procedure. While the solution is determined, M_c, h_c, s_c, q, T_c and Q_c can be computed according to (25), (21), (19), (20), (26) and (15), respectively.

4. Large-scale mass, heat, and moisture budgets

a. Data

All data are from the second NASA Atmospheric Variability Experiment (AVE II) except for the radiation data. There were fifty-four rawinsonde stations participating in the AVE II Pilot Experiment as shown in Fig. 1. Soundings were made at three-hour intervals at each station beginning at 1200 GMT 11 May 1974, and ending at 1200 GMT 12 May 1974. The data were obtained during a period when convective activity was present, large horizontal temperature gradients were evident and rapid changes in weather patterns were occurring. The data area is over the eastern United States east of approximately 105° W longitude. Radar data were obtained from eleven stations located near the center of the observational area, and as much data as possible were collected from the NIMBUS 5, NOAA-3, ATS-3, and DMSP (DAPP) satellites.

The radiation climatological data are from Rodger's results (1967), which are available in the region 0-70 N, 1000-10 mb, and for the months of January, April, July and October. Because the AVE II pilot experiment was held in May, an average of the data for April and July will be utilized in this study.

The synoptic situation of 2100 GMT 11 May 1974 is shown in Figs. 2-3. We choose this particular time because a deep conditionally unstable layer exists over a wide area of the southern United States. There is layer exists over a wide area of the southern United States. There is a cold front across the central part of the country and a warm front extends through the northern states. Three lows and two precipitation areas appear on the map at the analysis time. Also, there is a deep trough in the upper levels extending from north to south across the central United States.

The grid system is shown in Fig. 4; the polar stereographic projection is utilized. The standard latitude and the standard longitude are 60°N and 100°W, respectively. The 11 by 13 computational grid is oriented so that the y-axis is perpendicular to the standard longitude. The map scale is 1:15,000,000, the upper-left-hand corner grid point is located at $x=12.6$ in and $y=0.97$ in (the origin is at the North pole), and the grid interval is 190.5 km on the image plane. The procedures for the interpolation of each field variables from stations to grid points and the variational optimization of the wind field for the estimation of mass divergence, moisture divergence and vertical velocity are described in detail in Liang (1976). The optimization scheme is designed such that the integrated continuity equation and the global boundary condition are satisfied.

Also, a low-pass filter is simultaneously incorporated in the optimization scheme to ensure that the filtered field satisfies the above constraints.

b. Static energy

The tests are performed around Mississippi valley where a deep unstable layer exists from the lifted condensation level of the surface layer up to the 100-mb level. The average values of each variable at grid points (7, 9), (8, 9) and (8, 10) are utilized to represent the meteorological situation of the tested area. The horizontal diffusion terms $\overline{\nabla\cdot\vec{V}'s'}$ and $\overline{\nabla\cdot\vec{V}'q'}$ in (8) and (9) are computed by the use of nonlinear horizontal diffusion coefficients similar to those used by Smagorinsky et al. (1965) and Manabe et al. (1965); i.e.,

$$\overline{\nabla\cdot\vec{V}'s'}=\nabla\cdot(K_s\nabla\bar{s}),$$

$$\overline{\nabla\cdot\vec{V}'q'}=\nabla\cdot(K_q\nabla\bar{q}),$$

$$K_q=K_s=\frac{1}{2}k_0^2\dot{\Delta}^2(D_1^2+D_2^2)^{\frac{1}{2}},$$

where

$$D_1=\frac{\partial\bar{u}}{\partial x}-\frac{\partial\bar{v}}{\partial y},$$

$$D_2=\frac{\partial\bar{v}}{\partial x}+\frac{\partial\bar{u}}{\partial y}$$

k_0 is the Karman constant (0.4 in this study), and Δ is the grid length. The results show that values of these horizontal diffusion terms are one or two orders of magnitude smaller than those of the other terms appeared in the apparent heat source, Q_1, and the apparent moisture sink, Q_2. The local time changes of the dry static energy and the mixing ratio are determined from observations at 1800 GMT and at 2400 GMT 11 May 1974. Results show that these two terms are not negligible. The lifted condensation level is computed according to Inman's (1969) approximate formula. The dry static energy $\bar{s}$, the moist static energy $\bar{h}$, and the saturation moist static energy $\bar{h}^*$ are shown in Fig. 5. In the lower troposphere, $\bar{h}$ is much larger than $\bar{s}$ due to the presence of moisture. In the upper troposphere $\bar{h}$ approaches $\bar{s}$ and the difference between the two curves becomes negligible above the 180 mb level. There is a minimum of $\bar{h}$ at 700 mb. According to Riehl and Malkus (1958), the development of the deep cumulus convection prefers to the existence of such a minimum of $\bar{h}$ with the upward increase of $\bar{h}$ in the upper troposphere. It is also interesting to mention that the difference between $\bar{h}$ and $\bar{h}^*$ is larger in the lower and middle

troposphere than that in the upper troposphere because of the upward decrease of temperature in the upper troposphere.

c. Apparent heat source, apparent moisture sink and derived vertical eddy heat flux

The apparent heat source Q_1 and the apparent moisture sink Q_2 are shown in Fig. 6. The Q_1 has a maximum (26.6 c/day) at 400 mb and a secondary maximum (19.8 c/day) at 200 mb level, while the Q_2 has a maximum (19.6 c/day) at 500 mb and a secondary maximum (10.5 c/day) at 900 mb level. These values are about three times larger than those of tropics as determined by Yanai et al (1973). It is interesting to mention that the minimum value (−10.49 c/day) of Q_2 at 700 mb may reflect the existence of shallow clouds and the re-evaporation of rain drops or the melting of ice crystals falling from the higher levels.

The derived vertical eddy heat flux Y can be determined from (21) provided that Q_R is known. Because the direct measurements of Q_R are not available, Rodgers' climatological results are utilized in the computation. The profile of Q_R is shown in Fig. 6. In the troposphere, it is about the order of 10 c/day. Compared to the profiles of Q_1 and Q_2 this value is about a half times smaller. Utilizing those values in (21), Y is determined and is shown in Fig. 7. The profile shows a relative maximum (1849 ℓy/day) at 800 mb, a minimum (1839 ℓy/day) at 900 mb, and a largest value (1906.4 ℓy/day) at the ground surface. These values are about five times larger than those of tropics determined by Yanai et al (1973).

In order to obtain a better comparison between the observations and the results computed from the diagnosticating procedures, the required precipitation is determined from the large-scale heat and moisture budgets. Assuming the vertical eddy heat flux and the vertical eddy moisture flux to be zero at the cloud tops. i.e.,

$$M_c(s_c-\bar{s})_{p=p_{ct}}=0\,,$$

$$M_c(q_c-\bar{q})_{p=p_{ct}}=0\,,$$

and integrating (24), we have

$$\frac{1}{g}\int_{p_{ct}}^{p_s}(Q_1-Q_R)dp=LP_0+S_s\,,$$

where P_0 is the total precipitation inside the clouds, and S_s is the rate of transport of sensible heat from the surface. Since the observed tops of clouds

are near 300 mb, computations based on the large-scale heat and moisture budgets indicate that the required P_0 is about 0.03 in·hr^{-1}, This amount of precipitation is reasonable compared with observations from the National Weather Service radar charts (2035 GMT 11 May 1974) and Service A teletype reports.

5. Results of diagnostication of parameterization schemes

As mention before, Kuo's two parameterization schemes of cumulus convection (1965 and 1974) are essentially the same. The results presented here are computed from Kuo's (1965) scheme with b set to be zero. Also, since the effect coefficient B in the generalized parameterization should be specified before the diagnostication, it will be assumed to be a constant throughout the investigation. In other words, the effect of the moisten process directly due to the large-scale transport, b^*, is assumed to be proportional to the total moisture supply, $\dot{q}_T$:

$$b^*=K\dot{q}_T \tag{28}$$

where

$$K=1-\frac{B}{L}.$$

Theoretically, because b^* is unknown, the parameterization scheme is still unclosed. The flexibility of the scheme essentially depends on the parameterization of b^*. Therefore, (28) can be considered as a kind of simple parameterization of b^* to close the generalized scheme in this study. Of course, the other kinds of parameterization of b^* may also be useful in the numerical weather prediction.

a. Results of diagnostication of Kuo's parameterization of cumulus convection

Figs. 8-9 shows the excess temperature T_e-$\overline{T}$, the excess mixing ratio, q_e-$\overline{q}$, the released latent heat Q_e, the cloud mass flux M_e, and the residual mass flux in the environment, $\tilde{M}=-\omega-M_e$, from the diagnostication of Kuo's scheme. The results show that the cloud top is at 609.7 mb level. The excess temperature is of the order of 0.5~1C and a maximum (0.829 C) occurs at 700 mb. The excess mixing ratio is monotonically decreasing upward from the maximum (2.26 gm·kg^{-1}) at cloud base to the minimum (0.497 gm·kg^{-1}) at cloud top. The released latent heat is of the order of 5~10C·day^{-1} and the maximum (10.902C·day^{-1}) is located at 700 mb corresponding to the maximum excess temperature. The cloud mass flux is of the order of 5 μb·sec^{-1}. It has a relative maximum

(6.18 $\mu b \cdot sec^{-1}$) at 800 mb and a minimum (4.595 $\mu b \cdot sec^{-1}$) at 700 mb due to the existence of the maximum excess temperature. The residual mass flux in the environment is of the order of -3 $\mu b \cdot sec^{-1}$, and a maximum (-0.829 $\mu b \cdot sec^{-1}$) at 700 mb corresponding to the occurence of the minimum cloud mass flux.

The precipitation rate computed from the diagnostication of Kuo's scheme is 0.00996 $in \cdot hr^{-1}$. Compared to the required precipitation 0.03 $in \cdot hr^{-1}$, this value is about three times smaller. The result is mainly due to the smallness of the excess temperature and the lowness of the cloud top. Physically, the buoyancy force produced by the mechanisms involved in Kuo's scheme sounds too weak compared with that of the real situation.

b. Results of diagnostication of the generalized parameterization of cumulus convection

Figs. 10-11 shows the excess temperature $T_e - \overline{T}$, the excess mixing ratio $q_e - \overline{q}$,the released latent heat Q_e, the cloud mass flux M_e, and the residual mass flux in the environment $\tilde{M}$ computed from the diagnostication of the generalized scheme. The cloud top determined from these procedures is at 487.6 mb. The excess temperature is of the order of 5 C and a maximum (9.742 C) is at 700 mb level. The excess mixing ratio is of the order of 5 $gm \cdot kg^{-1}$ and has a maximum (6.21 $gm \cdot kg^{-1}$) at 600 mb. The released latent heat is of the order of 10 $C \cdot day^{-1}$ and the maximum occurs at 700 mb corresponding to the maximum excess temperature. The cloud mass flux is of the order of 5 $\mu b \cdot sec^{-1}$. There is a relative maximum (6.215 $\mu b \cdot sec^{-1}$)at 800 mb and a minimum (2.99 $\mu b \cdot sec^{-1}$) at 700 mb due to the existence of the maximum excess temperature. The residual mass flux in the environment is of the order of -3 $\mu b \cdot sec^{-1}$. It has a relative maximum (0.776 $\mu b \cdot sec^{-1}$) at 700 mb corresponding to the occurence of the minimum cloud mass flux.

The precipitation rate computed from the diagnostication of the generalized scheme is 0.025 $in \cdot hr^{-1}$. Compared to the required precipitation, this value is acceptable and is much closer than that from Kuo's scheme. Physically, the discard of the assumption that the cloud mass producing rate σ/τ is a constant permits the coorperation of the adiabatic subsidence of the environmental atmosphere and the vertical transport of the moisture inside the cloud into the parameterization. The results shows that both mechanisms are important in the latent heat released processes.

6. Conclusions and Recommendations

This study developes a new parameterization of cumulus convection from

the moisture conservation equation. The analysis shows that the scheme can be considered as a generalization of Kuo's parameterization concepts, and Kuo's (1965 and 1974) schemes are reduced from it as two special cases. It also has been shown that Kuo's two scheme are essentially the same.

In order to realize its plausibility, the new parameterization is diagnostically investigated by the combination of the parameterization formula and the large-scale heat and moisture budgets. In addition to the latent heat released and the pressure of the cloud top, the diagnostication determines the average properties of the cloud essemble including the temperature, the mixing ratio, and the mass flux of clouds. Furthermore, the vertical integration of the latent heat released computed from the diagnostic investigation gives the total precipitation rate. This value and the pressure of cloud top are compared with the observations and with those of Kuo's scheme to reveal the flexibility and the improvement of the generalized parameterization scheme.

The generalized scheme is closed after the effect coefficient B (or b^*) is specified. So far, there is no any rigorously theoretical basis can be utilized to specify b^*. However, because b^* is the effect of the moisten process directly due to the large-scale transport, it sounds reasonable, from the physical point of view, to assume b^* to be proportional to the total moisture supply from the large-scale and the subgridscale motions. Of course, the other kinds of the specification of b^* should be investigated if one required deeper understanding about the generalized parameterization scheme.

Results of the diagnostic investigation show that the new scheme make significant improvements. The values of the computed precipitation rate and the pressure of the cloud top are much closer to the observations. However, they are still unsatisfactory. The results show that the pressure of the cloud top is about 180 mb lower and the precipitation rate is about 17% smaller than those of the observational values. Also, the maximum excess temperature at 700 mb is too high. The shortcomings may come from the unsatisfactory parameterization of b^*. Indeed, the tests using other kinds of the specification of b^* are in progress. The investigation results will be presented in the future.

The data used in diagnostic investigation is AVE 11 data. The data area is over the eastern United States. Since the weather systems are typically of the middle latitudes, the diagnostic investigation mainly reveals the mechanisms involved in this area. Although the generalization procedure is shows that the generalized scheme surpasses this restriction, it is meaningful to examine the

flexibility of the scheme utilizing the other sets of data. For example, 1956 Marshall Islands data set, which is used in the study by Yanai et al (1973), may be one of the most interesting sets.

References

Arakawa, A., 1969: Parameterization of cumulus convection. Proc. WMO/IUGG Symp. Numerical Prediction, Tokyo, IV 8, 1-6.

Ceselski, B. F., 1973: A comparison of cumulus Parameterization techniques. Tellus, 25, 459-478.

Ceselski, B. F., 1974: Cumulus convection of weak and strong tropical disturbances. J. Atmos. Sci., 31, 1241-1255.

Charney, J. G., and Elliassen, 1964: On the growth of the hurricane depression. J. Atmos. Sci., 21, 68-75.

Inman, R. L., 1969: Computation of temperature at the lifted condensation level. J. Appl. Meteor., 8, 155-158.

Kuo, H. L., 1965: On the formation and intensification of tropical cyclones through latent heat release by cumulus convection. J. Atmos. Sci., 22, 40-63.

Kuo, H. L., 1974: Further studies of the parameterization of the influence of cumulus convection of large-scale flow. J. Atmos. Sci., 31, 1232-1240.

Liang, W. J., 1975: The modification and application of Kuo's parameterization of cumulus convection in middle latitudes. Ph. D. thesis, Dept. of Meteorology, University of Oklahoma, 90 pp.

Liang, W. L., 1976: The variational optimization of wind field for the estimation of vertical velocity, Annual Report of the Institute of Physics, Academia Sinica, 6, 179-198.

Manabe, S., J. Smagorinsky, and R. F. Strickler, 1965: Simulated climatology of a general circulation model with a hydrologic cycle. Mon. Wea. Rev., 93, No. 12, 769-798.

Ooyama, K., 1964: A dynamical model for the study of tropical cyclone development. Geofisica Intern. (Mexico), 127-198.

Riehl, H., and J. S. Malkus, 1958: On the heat balance of the equatorial trough zone. Geophysica, 6, 503-538.

Rodgers, C. D., 1967: The radiative heat budget of the troposphere and lower stratosphere. Report No. A2, Department of Meteorology, Massachusetts Inst. of Technology.

Sasaki, Y., 1973: Final report of investigation of an operational scheme of analysis and short range prediction of local severe weather. The University of Oklahoma Research Inst.

Smagorinsky, J., S. Manabe, and J. L. Holloway, 1965: Numerical results from a nine-level general circulation model of the atmosphere. Mon. Wea. Rev., 93, 727-768.

Yanai, M., S. Eskensen and J. Chu, 1973: Determination of bulk properties of tropical cloud clusters from large-scale heat and moisture budgets. J. Atmos. Sci., 30, 611-627.

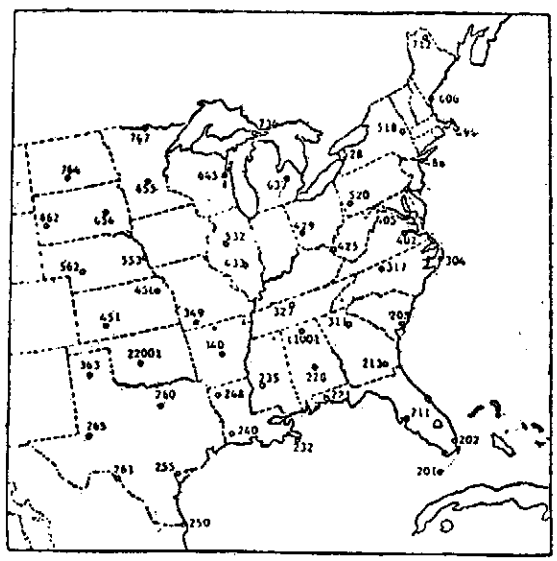

Fiig. 1. Rawinsonde stations for AVE II pilot Experiment.

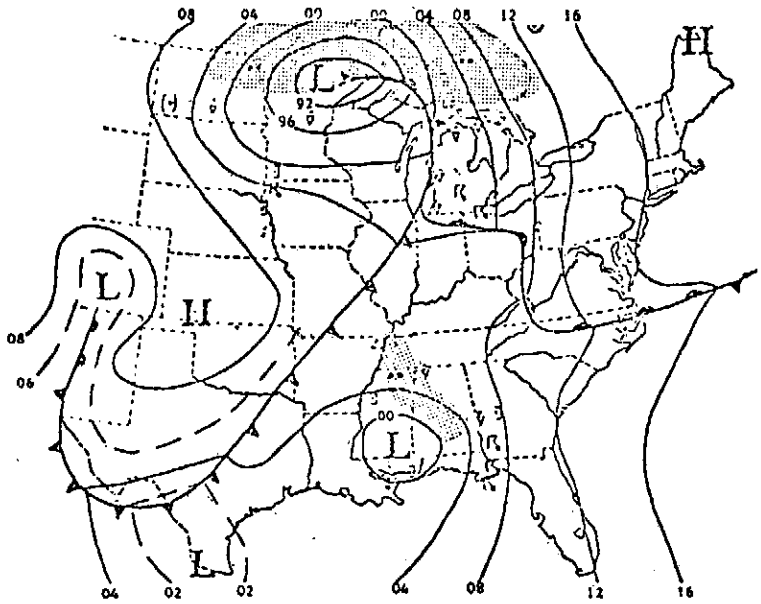

Fig. 2. Surface chart for 2100 GMT 11 may 1974. Isobars are drawn at 4 mb intervals.

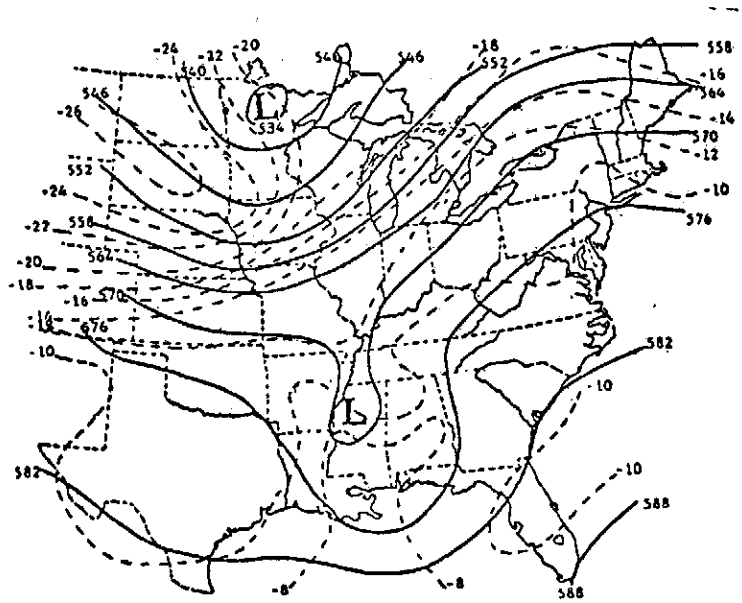

Fig. 3. 500mb chart for 2100 GMT 11 may 1974. Height (solid) contours are drawn at 60 m intervals. Isotherms (dashed) are constructed at 2°C intervals.

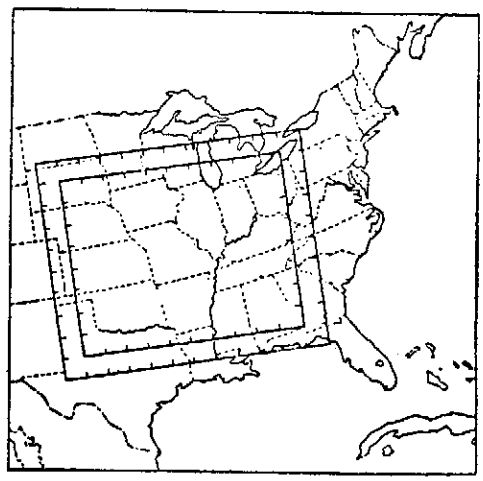

Fig. 4. Data grid and interior working grid.

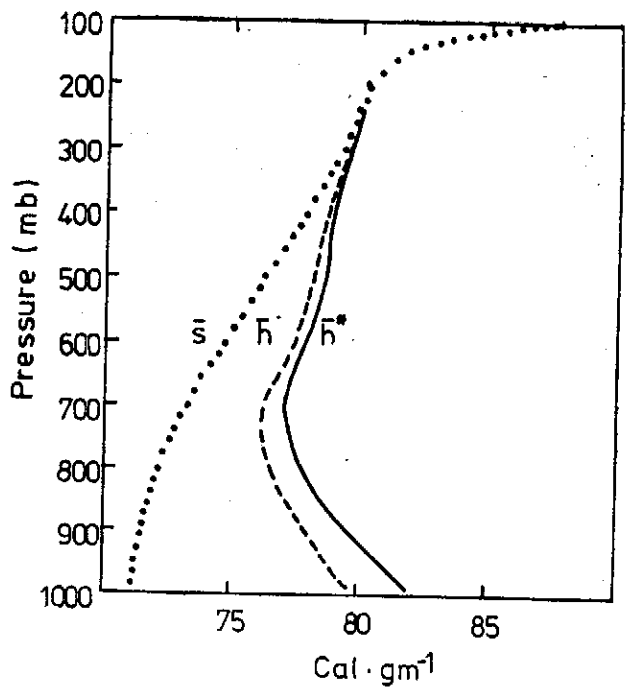

Fig. 5. The dry static energy, $\bar{s}$ (dotted), moist static energy, $\bar{h}$ (dashed), and saturation moist static energy., $\bar{h}^*$ (solid), of environment.

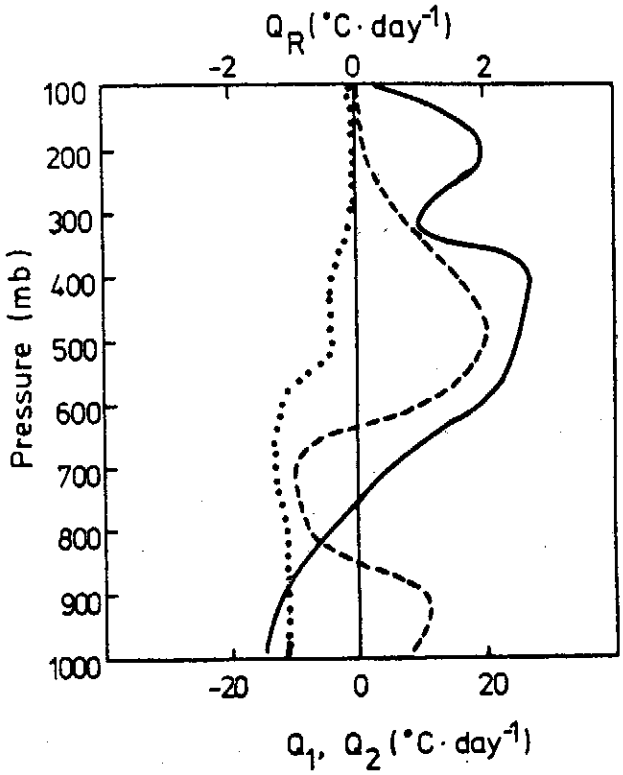

Fig. 6. The apparent heat source, Q_1 (solid), the apparent moist sink, Q_2 (dashed), and the radiational heating from Rodger's results (1967), Q_R (dotted).

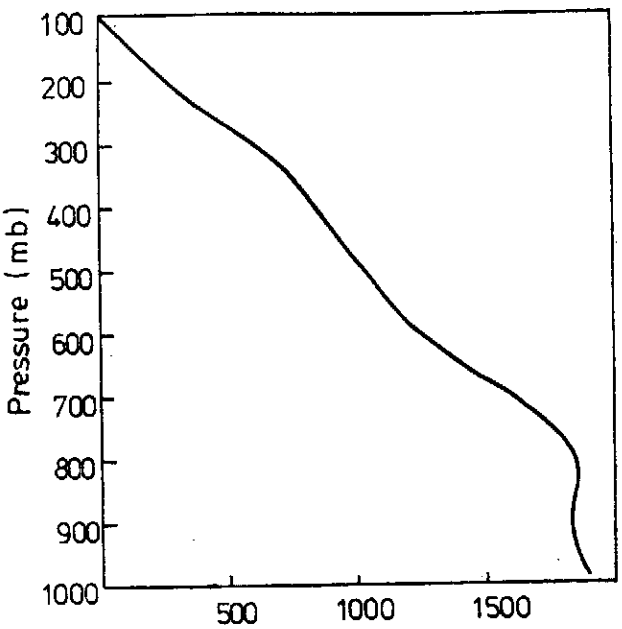

Fig. 7. The derived vertical eddy heat flux, Y.

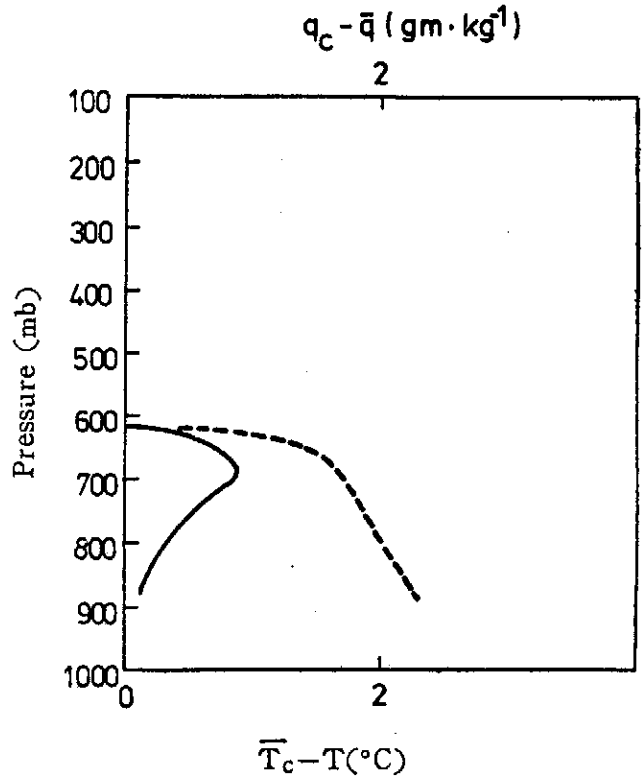

Fig. 8, The excess temperature, $\overline{T}_c$-T (solid), and the excess mixing ratio, $q_c - \overline{q}$ (dashed), from the diagnostic results of kuo's scheme.

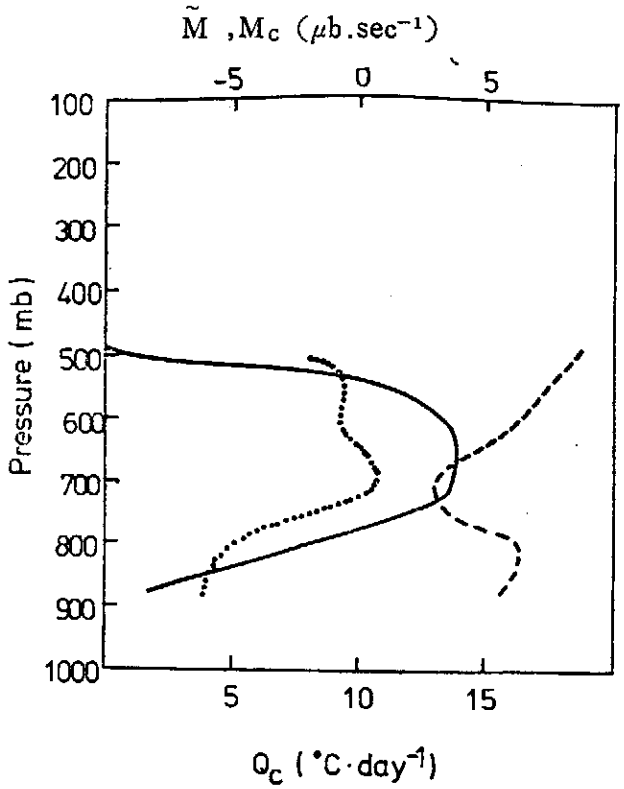

Fig. 9, Released latent heat, Q_c(solid), cumulative mass flux distribution within clouds, M_c (dashed), and the corresponding environmental mass flux, $\tilde{M}$ (dotted) from the diagnostic results of Kuo's scheme.

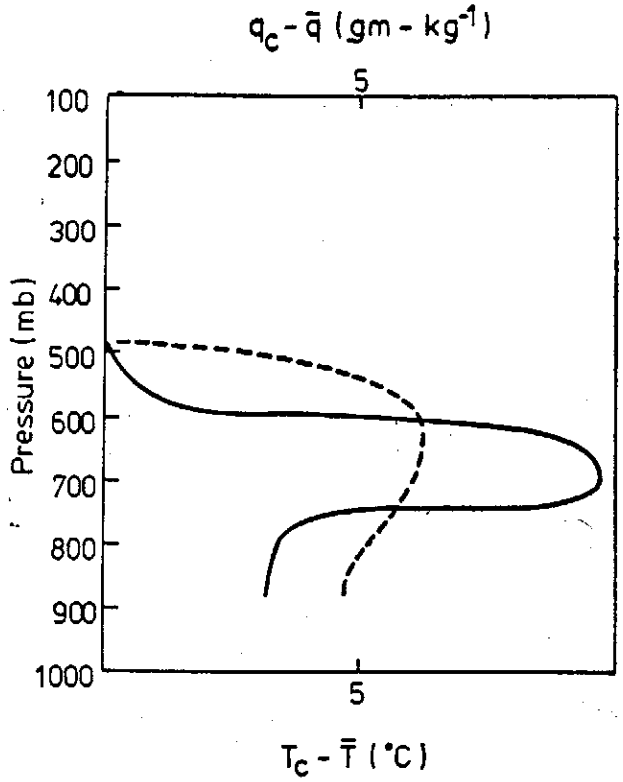

Fig. 10, The excess temperature, $T_c - \overline{T}$ (solid), and the excess mixing ratio, $q_c - \overline{q}$ (dashed), from the diagnostic results of generalized scheme.

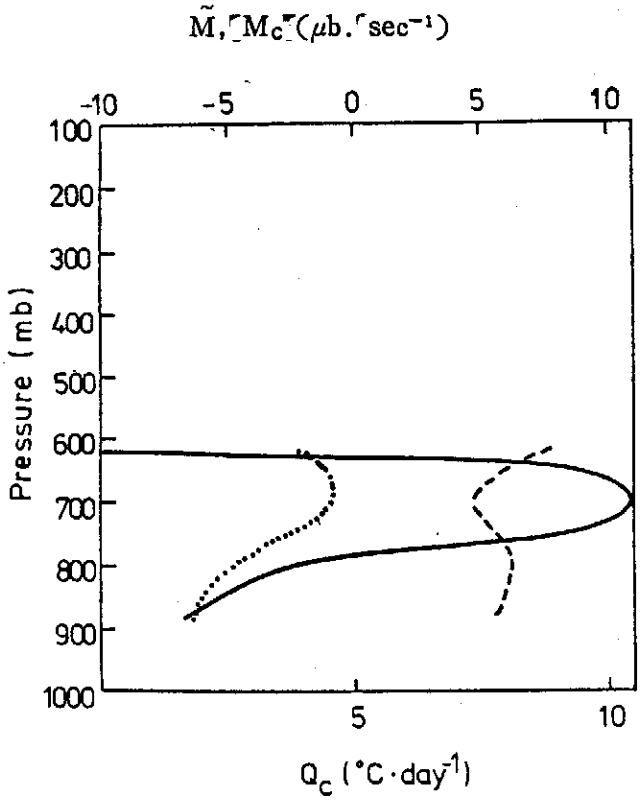

Fig. 11, Released latent heat, Q_c (solid), cumulative mass flux distribution within clouds, M_c (dashed), and the corresponding environmental mass flux, $\tilde{M}$ (dotted), from the diagnostic results of the generalized scheme.

Annual Report of the Institute of Physics, Acodemia Sinica, Vol.7, 1977

The Initial Flow Past an Impulsively Started Circular Cylinder

Lai-Chen Chien

Institute of Physics
Academia Sinica
Nankang, Taipel, Taiwan

The flow field of an incompressible, viscous fluid around an impulsively started circular cylinder is studied in detail. The analytical solution for the initial flow field stream function, by the method of matched asymptotic expansion, in term of exponential and error fnnctions for the inner flow field and of circular function for the outer, is obtained to the third order from which a uniformly valid composite solution is found. The initial separation time as a function of Reynolds number shows close agreement to Collins and Dennis (1973a, b) and is much better than second order expansion. Also presented are the vorticity, pressure, separation point and drag. These quantities agree with the numerical computations of Collins and Dennis.

1. Introduction

Numerous scholors have investigated the incompressible viscous flow over an impulsively started cylinder. As reviewed by Yang and Bar-lev (1976), there are four different approaches to the theoretical investigation of this problem. The first is the boundary layer solution which is first studied by Blasius (1908), and later extended by Goldstein and Rosenhead (1936). The second approach is the the matched asymptotic expansions of the time dependent Navier-Stokes equations for the flow field. Wang (1967, 1968) employed the method of inner and outer expansions to solve the two-dimensional unsteady Navier-Stokes equations in an atempt to extended the boundary layer theory to lower value of Reynolds number. Although his work is conceptually sound, he did not carry enough terms in the expansion to describe the flow porperties accurately. Collins and Dennis (1973a) improved Wang's analysis by expanding stream function and vorticity in powers of time from the start of motion and obtained the development of flow properties at early time. Bar-lev (1974) got a perturbation solution for the vorticity equation by the method of matched asymptotic expansion to the third term for this problem. Flow propertis were presented in detail. Unfortunately there are some minor errors found in his third order inner solution.

The third class is the numerical solution. The recent advent of high-speed computers with large memory is making the numerical solution of the

Navier-stokes solution possible. A number of papers on this problem has been published in the past years as reviewed in Roache (1975, 1976).

The fourth is the potential flow model in which the unifow over an impulsively started cylinder contains two symmetric potential vortices in the wake is considered. Potential flow models are proposed by Bryson (1959), Sarpkaya (1968), Yang and Bar-lev (1976).

The objetive of this study is to obtain a new solution for the problem of the incompressible viscous flow over an impulsively started cylinder. The outer solutions to the third order and the inner solution to the second order by the previous investigators are recapitulated. The third order solution, obtalned by Bar-lev (1974), was repeated. The solution is in term of polynomials involving error function and exponential function. The polynomials, with their derivatives and integrals, are written in general forms. The streamlines, tangetial velocity profiles are depicted from which separation and eddy formation behind the circle cylinder are discernible. Vorticity on the of the cylinder for small time is sufficient accurte. The initial separation time, the progression of the separation point are plotted for various Reynolds numbers and tabulated comparing with the existing solutions. Also presented are pressure distribution on the surface of the cylinPer and time history of drag coefficient.

2. Formulation

The governing vorticity transport equation for time-dependnt, incompressible, viscous flow, Bar-lev and Yang (1975), in nondimensional form is

$$\frac{\partial \vec{w}}{\partial t} - \epsilon \nabla \times (\vec{V} \times \vec{w}) = \epsilon^2 \alpha \nabla^2 w, \tag{2-1}$$

where

$$\epsilon = U_\circ T_\circ / l, \quad \alpha = (\epsilon R_e)^{-1}, \quad t = t^*/T_\circ \tag{2-2}$$

In (2-2), $l_\circ$, $T_\circ$ and $U_\circ$ are the reference length, time and velocity, t^* is the dimensional time, $R_e = U_\circ l_\circ/\nu$ Reynolds number. Here, the reference length $l_\circ$ is the radius of the cylinder. For the initial flow. ε is a a small quantity, $\alpha = O(1)$ (Chien, 1977). The time variable may be expressed by the relation

$$\epsilon t = \frac{U_\circ t^*}{l_\circ} = T, \qquad \epsilon(\alpha t)^{\frac{1}{2}} = (T/R_e)^{\frac{1}{2}}. \tag{2-3}$$

Here T is a new non-dimensional time.

For the problem of viscous flow over an impulsivly started cylinder, the velocity components (u_r, u_θ) may be expressed in term of stream function,

$$u_r = -\frac{1}{r}\frac{\partial \Psi}{\partial \theta}, \qquad u_\theta = \frac{\partial \Psi}{\partial r}. \tag{2-4}$$

By the above equation, we get a poisson equation relating the vorticity to the stream function

$$\nabla^2 \Psi = w. \tag{2-5}$$

The vorticity equation (2-1) becomes

$$\left[\frac{\partial}{\partial t} + \epsilon\frac{1}{r}\left(\frac{\partial \Psi}{\partial r}\frac{\partial}{\partial \theta} - \frac{\partial \Psi}{\partial \theta}\frac{\partial}{\partial r}\right)\right]\nabla^2 \Psi = \epsilon^2 \alpha \nabla^4 \Psi, \tag{2-6}$$

in which

$$\nabla^2 = \frac{\partial^2}{\partial r^2} + \frac{1}{r}\frac{\partial}{\partial r} - \frac{1}{r^2}\frac{\partial^2}{\partial \theta^2}.$$

3. Outer expansions

The fluid in contact with the cylinder is at rest to the surface, while the adjacent layer of fluid is slipping past the boundary with a velocity determined by the potential flow theory. There is thus inititially a vortex sheet in the fluid coincident with the surface of the cylinder. The vorticity in the vortex sheet is diffused from the boundary further into fluid forming a thin visous layer. The outer inviscid region, without any vorticity at the start of the motion, will remain irrotional by virture of Helmholtz's theorem. Thus, for an initial interval of time the motion of the fluid is irrotational everywherer except within the thin viscous layer adjoining the cylinder surface. (Batchelor, 1970, P. 321).

Assume the outer expansion for the stream function to be of the form

$$\Psi^o(r, \theta, t, \varepsilon) = \sum_{n=1} \delta_n(\varepsilon)\, \Psi^o_n(r, \theta, t), \tag{3-1}$$

where $\delta_n(\varepsilon)$ are the gauge functions. It may be determined by the asymptoic matching principle between the inner and the outer expansion solutious. Bar-lev and Yang (1975) gave

$$\delta_n(\varepsilon) = \varepsilon^{n-1}, \qquad n = 1, 2, 3. \tag{3-2}$$

Substituting the above into equation (2-5), Provided $\omega = 0$ becuase of the irrotationality at outer region, we have

$$\nabla^2 \Psi^o_n = 0 \qquad n = 1, 2, 3 \ldots. \tag{3-3}$$

Introducing equations (3-1) and (3-2) into vorticity transport equation (2-6) gets

$$\left\{\frac{\partial}{\partial t}+\frac{\varepsilon}{r}\left[\frac{\partial}{\partial r}\left(\sum_{n=1}^{}\varepsilon^{n-1}\Psi_n^o\right)\frac{\partial}{\partial\theta}-\frac{\partial}{\partial\theta}\left(\sum_{n=1}\varepsilon^{n-1}\Psi_n^o\right)\frac{\partial}{\partial r}\right]\right\}$$

$$\nabla^2\left(\sum_{n=1}\varepsilon^{n-1}\Psi_n^o\right)-\varepsilon^2\alpha\nabla^4\left(\sum_{n=1}\varepsilon^{n-1}\Psi_n^o\right)=0. \tag{3-4}$$

Expanding the above equation and collecting the terms of the same order, we have equation for the first order

$$\frac{\partial}{\partial t}\nabla^2\Psi_1^o=0, \tag{3-5}$$

equation for the second order

$$\frac{\partial}{\partial t}\nabla^2\Psi_2^o=\frac{1}{r}\left[\frac{\partial\Psi_1^o}{\partial\theta}\frac{\partial}{\partial r}-\frac{\partial\Psi_1^o}{\partial r}\frac{\partial}{\partial\theta}\right]\nabla^2\Psi_1^o, \tag{3-6}$$

and equation for the third order

$$\frac{\partial}{\partial t}\nabla^2\Psi_3^o=\frac{0}{r}\left[\frac{\partial\Psi_1^o}{\partial\theta}\frac{\partial}{\partial r}-\frac{\partial\Psi_1^o}{\partial r}\frac{\partial}{\partial\theta}\right]\nabla^2\Psi_2^o$$

$$+\frac{1}{r}\left[\frac{\partial\Psi_2^o}{\partial\theta}\frac{\partial}{\partial r}-\frac{\partial\Psi_2^o}{\partial r}\frac{\partial}{\partial\theta}\right]\nabla^2\Psi_1^o+\alpha\nabla^4\Psi_1^o. \tag{3-7}$$

The leading term in the outer stream function expansion is that of a uniform potential flow over a circular cylinder,

$$\Psi_1^o=(r-r^{-1})\sin\theta \tag{3-8}$$

The second and the third order expansions are governed by equation (3-6) and (3-7). The boundary conditions at infinity for the second and the third order expansion are

$$\Psi_n^o=0 \qquad n=2,\ 3, \tag{3-9}$$

as $r\to\infty$. The inner boundary conition will be determined from the matching with the inner expansions.

The second and the third order stream functions were obtained by Wang (1967). The second order solution is

$$\Psi_2^o=-\frac{4}{\sqrt{\pi}}\frac{\sqrt{\alpha t}}{r}\sin\theta \tag{3-10}$$

The effect is equivalent that of a doublet whose strength grows with the square root of time.

The third order solution is of the fom

$$\Psi_3^o=-\alpha t r^{-1}\sin\theta-8t\sqrt{\alpha t}\pi^{-\frac{1}{2}}\left(1+\frac{4}{9\pi}-\frac{4\sqrt{2}}{2}\right)\sin\theta\cos\theta \tag{3-11}$$

The effect of the first part of the third order expansion is equivalent doublet whose strength increases with time, while that of the second part is a quadrupole whose strength grows as $\sqrt{t^3}$

The contribution of equations (3-8), (3-10) and (3-11) to the outer stream fnuction, through equations (2-3), is

$$\Psi^o=(r-r^{-1})\sin\theta-\frac{4}{\sqrt{\pi}}\frac{\sqrt{T}}{\sqrt{Re}}\frac{1}{r}\sin\theta$$
$$-\frac{T}{Re}\frac{1}{r}\sin\theta-\frac{8}{\sqrt{\pi}}\frac{T\sqrt{T}}{\sqrt{Re}}\left(1+\frac{4}{9\pi}-\frac{4\sqrt{2}}{3}\right)r^{-2}\sin\theta\cos\theta. \tag{3-12}$$

4. Inner Solution to Second Order

The region of non-uniformity near the surface of the cylinder should be stretched such that that the boundary are comparable to those normal to it. Let the stretched radial coordiante be

$$R=\frac{r-1}{\varepsilon} \tag{4-1}$$

In order to magnify the inner-flow stream function Ψ^i, which is a function of stretched radial variable R, we set

$$\Psi^i(r,\theta,t;\varepsilon)=\varepsilon\bar{\Psi}^i(R,\theta,t). \tag{4-2}$$

Assume the inner stream function to be of the form

$$\Psi^i(r,\theta,t;\varepsilon)=\sum_{n=1}\Delta_m(\varepsilon)\bar{\Psi}^i_m(R,\theta,t) \tag{4-3}$$

in which $\Delta_m(\varepsilon)$ are gauge functions. Bar-lev and Yang (1975), determined

$$\Delta_m(\varepsilon)=\varepsilon^m, \qquad m=1,2,3. \tag{4-4}$$

Substuting the equations (4-3) and (4-4) into the vorticity transport equation (2-6), and letting the coefficients of ε's vanish, we have

$$\bar{\Psi}^i_{1RRt}-\alpha\bar{\Psi}^i_{1RRR}=0 \tag{4-5}$$

for the first order;

$$\bar{\Psi}^i_{2RRt}-\alpha\bar{\Psi}^i_{2RRR}=\bar{\Psi}^i_{1\theta}\bar{\Psi}^i_{1RRR}-\bar{\Psi}^i_{1R}\bar{\Psi}^i_{1RRR\theta}+2\bar{\Psi}^i_{1RRR}$$
$$-\bar{\Psi}^i_{1Rt} \tag{4-6}$$

for the second order; and

$$\overline{\Psi}^i_{3RRt}-\alpha\overline{\Psi}^i_{3RRR}=-\overline{\Psi}^i_{2Rt}+R\overline{\Psi}^i_{1Rt}-\overline{\Psi}^i_{1\theta\theta t}$$
$$-\overline{\Psi}^i_{1R}\overline{\Psi}^i_{2RR\theta}-\overline{\Psi}^i_{2R}\overline{\Psi}^i_{1RR\theta}+\overline{\Psi}^i_{1\theta}\overline{\Psi}^i_{2RRR}-\overline{\Psi}^i_{1R}\overline{\Psi}^i_{1R\theta}$$
$$+R\overline{\Psi}^i_{1R\theta}\overline{\Psi}^i_{1RR\theta}+\overline{\Psi}^i_{1\theta}\overline{\Psi}^i_{1RR}-R\overline{\Psi}^i_{1\theta}\overline{\Psi}^i_{1RRR}$$
$$+\overline{\Psi}^i_{2\theta}\overline{\Psi}^i_{1RRR}+\alpha\Big[2\overline{\Psi}^i_{2RRR}-2R\overline{\Psi}^i_{1RRR}+2\overline{\Psi}^i_{1RR\theta\theta}$$
$$-\overline{\Psi}^i_{1RR}\Big] \qquad (4\text{-}7)$$

for the third order.

The boundary conditions for the inner solutions are

(1) No-slip of the tangential velocity at the surface of the cylinder,

$$\overline{\Psi}^i_{mR}(0,\ \theta,\ t)=0 \qquad (4\text{-}8)$$

(2) Vanishing of the normal velocity or the cylinder surface being a streamline,

$$\overline{\Psi}^i_{m}(0,\ \theta,\ t)=0 \qquad (4\text{-}9)$$

(3) The tangential veiocity for the inner expansion at $R\to\infty$ being identical that of the outer expansion *at* $r\to 0$.

By the equation for the first order expansion (4-5), we see that at the beginning of motion, the diffusion effect is dominating and that convection is negligible in comparison. Integrating equation (4-5) with respect to R and making the use of matching principle get

$$\overline{\Psi}^i_{1Rt}-\alpha\overline{\Psi}^i_{1RRR}=0. \qquad (4\text{-}10)$$

This equation is exactly the same as that of governing the Rayleigh problem provided the uniform flow for the plate replaced by potential flow over a circuar cylinder. The solution found is

$$\overline{\Psi}^i_{1R}=2\mathrm{erf}\ \eta\ \sin\theta \qquad (4\text{-}11)$$

where $\eta=\dfrac{R}{2\sqrt{\alpha t}}$, is the inner stretched variable.

The second order inner expansion is obtained by wang (1967)

$$\overline{\Psi}^i_{2R}=2\sqrt{\alpha t}\Big[\frac{2}{\sqrt{\pi}}[1-\exp(-\eta^2)]-2\eta+3\eta\mathrm{erfc}\eta\Big]$$
$$\sin\theta+4tf(\eta)\ \sin\theta\ \cos\theta \qquad (4\text{-}12)$$

where

$$f(\eta)=(\eta^2-\frac{1}{2})\mathrm{erfc}^2\eta+\Big[-(3+\frac{4}{3\pi})\eta^2+(\frac{1}{2}-\frac{2}{3\pi})\Big]\mathrm{erfc}\eta-\frac{3}{\sqrt{\pi}}\eta\exp(-\eta^2)\mathrm{erfc}\eta+\frac{1}{\sqrt{\pi}}\Big[(4+\frac{4}{3\pi})\eta-\frac{1}{3\sqrt{\pi}}\Big]\exp(-\eta^2)+\frac{2}{\pi}\exp(-2\eta^2) \tag{4-13}$$

is Blasius' solution.

To get the stream function for the first and the second order inner expansion, we integrate (4-11) and (4-12),

$$\overline{\Psi}_1^i=4\sqrt{\alpha t}\Big[\mathrm{erf}\,\eta-\frac{1}{\sqrt{\pi}}[1-\exp(-\eta^2)]\Big]\sin\theta \tag{4-14}$$

$$\overline{\Psi}_2^i=\Big[-4\alpha t\eta^2+\frac{4}{\sqrt{\pi}}\alpha t[2\eta+\frac{\sqrt{\pi}}{4}(6\eta^2-1)-\mathrm{erfc}\eta-\frac{3}{2}\eta\exp(-\eta^2)]\Big]\sin\theta+\Big[8t\sqrt{\alpha t}\int_0^\eta f(\zeta)d\zeta\Big]\sin\theta\cos\theta. \tag{4-15}$$

5. Third Order Inner Solution

The right hand side of equation (4-7) is a function of the derivatives of the first and the second order expansions. Bar-lev (1974) integrated (4-12) to obtain the second order stream function. Unfortunately, he put an extra factor $\frac{1}{\pi}$ in the first term of equation (4-15), which caused a minor error in the third order inner solution.

The outer boundary condition for the third order inner expansion is obtained by making use of the matching condition for the tangential velocity between the the third order inner and outer expansions. By the matching procedure (Van Dyke, (1975), Bar-lev (1974) obtained the outer boundary condition for the third order inner expansion,

$$\overline{\Psi}_{3R}^i(\infty,\ \theta,\ \mathrm{t})=(12\eta^2-\frac{16}{\sqrt{\pi}}\eta+1)\alpha t\ \sin\theta+\frac{16}{\sqrt{\pi}}(1+\frac{4}{9\pi}-\frac{4\sqrt{2}}{3})t\sqrt{\alpha t}\ \sin\theta\cos\theta \tag{5-1}$$

The inner boundary conditios are non-slip at the surface of the cylinder and the cylinder surface as a stream line,

$$\overline{\Psi}_{3R}^i(0,\ \theta,\ t)=0, \tag{5-2}$$

$$\overline{\Psi}_3^i(0,\ \theta,\ t)=0. \tag{5-3}$$

Substituting the first and the second order inner expansions (4-14), (4-15) into the right hand side of the third order equation (4-7), and integrating with respect to R, we have

$$\overline{\Psi}^{i}_{3Rt}-\alpha\overline{\Psi}^{i}_{3RRR}=H(\eta)\ \sin\theta+8\sqrt{\alpha t}\ I(\eta)\ \sin\theta\cos\theta$$
$$-8t\theta(\eta)\sin^{3}\theta+8t\left[\Theta(\eta)+\phi(\eta)\right]$$
$$\sin\theta\ \cos^{2}\theta \tag{5-5}$$

where

$$H(\eta)=-\frac{8}{\sqrt{\pi}}\eta+7\,\mathrm{erfc}\,\eta-\frac{6}{\sqrt{\pi}}\exp(-\eta^{2})-5, \tag{5-5a}$$

$$I(\eta)=2\eta\mathrm{erfc}^{2}\eta+\left[-(4+\frac{2}{3\pi})\eta+\frac{3}{2\sqrt{\pi}}+\frac{5}{2\sqrt{\pi}}(1+2\eta^{2})\right.$$
$$\left.\exp(-\eta^{2})\right]\mathrm{erfc}\eta-\frac{4}{\sqrt{2\pi}}\mathrm{erfc}\sqrt{2}\eta+\frac{1}{\sqrt{\pi}}\left[-\frac{9}{2}\eta^{2}\right.$$
$$\left.+\frac{17}{3\sqrt{\pi}}\eta-(\frac{3}{2}-\frac{2}{3\pi})\right]\exp(-\eta^{2})-\frac{5}{\pi}\eta\exp(-2\eta^{2})$$
$$+\frac{1}{\sqrt{\pi}}(3+\frac{4}{3\pi}-\frac{8}{\sqrt{2}}), \tag{5-5b}$$

$$\Theta(\eta)=(-\eta^{2}+\frac{1}{2})\mathrm{erfc}^{3}\eta+\left[(4+\frac{4}{3\pi})\eta^{2}-(1-\frac{2}{3\pi})\right.$$
$$\left.+\frac{1}{\sqrt{\pi}}(\frac{3}{2}\eta^{3}+4\eta^{2})\exp(-\eta^{2})\right]\mathrm{erfc}^{2}\eta$$
$$+\left[-(3+\frac{4}{3\pi})\eta^{2}+\frac{2}{3\pi}+\frac{2}{3\sqrt{\pi}}[(3+\frac{4}{3\pi})\eta^{3}\right.$$
$$\left.-12\eta^{2}]\exp(-\eta^{2})+\frac{1}{3\pi}(4\eta^{2}-17)\exp(-2\eta^{2})\right]$$
$$\mathrm{erfc}\eta+\frac{1}{\sqrt{\pi}}(4\eta^{2}+\frac{4}{3}\eta-1-\frac{4}{3\pi})\exp(-\eta^{2})$$
$$-\frac{1}{3\pi}\left[(6+\frac{8}{3\pi})\eta^{2}+(19+\frac{8}{3\pi})\right]\exp(2\eta^{2})$$
$$-\frac{2}{3\sqrt{\pi^{3}}}\eta\exp(-3\eta^{2})+(1+\frac{4}{3\pi}), \tag{5-5c}$$

$$\phi(\eta)=(\eta^{2}+\frac{1}{2})\mathrm{erfc}^{3}\eta+\left[-4(1+\frac{1}{3\pi})\eta^{2}+\frac{2}{\sqrt{\pi}}\eta\right.$$
$$\left.+(-1+\frac{2}{3\pi})+\frac{2}{\sqrt{\pi}}\eta^{3}\exp(-\eta^{2})\right]\mathrm{erfc}^{2}\eta+\left[(3+\frac{4}{\pi})\eta^{2}\right.$$
$$-\frac{2}{\sqrt{\pi}}(3+\frac{4}{3\pi})\eta+(\frac{1}{2}-\frac{2}{3\pi})+\frac{1}{\sqrt{\pi}}[-4\eta^{3}$$

$$+\frac{14}{3\sqrt{\pi}}\eta^2+3\left(1+\frac{4}{3\pi}\right)\eta+1\Big]\exp(-\eta^2)$$

$$-\frac{1}{\pi}(4\eta^2+1)\exp(-2\eta^2)\Big]\operatorname{erfc}\eta+2\eta^2$$

$$+\frac{1}{\sqrt{\pi}}\left(6-\frac{2}{3\pi}\right)\eta+2+\frac{1}{\sqrt{\pi}}\left(1+\frac{4}{3\pi}\right)+\frac{1}{\sqrt{\pi}}\Big[2\eta^3$$

$$-\frac{14}{3\sqrt{\pi}}\eta^2+\left(1+\frac{4}{3\pi}\right)\eta+\frac{1}{\sqrt{\pi}}\left(\frac{5}{3}+\frac{8}{3\pi}\right)\Big]\exp(-\eta^2)$$

$$+\frac{1}{\pi}\Big[4\eta^2-\frac{7}{3\sqrt{\pi}}\eta-\frac{4}{3\pi}\Big]\exp(-2\eta^2)$$

$$+\frac{2}{\sqrt{\pi^3}}\eta\exp(-3\eta^2). \qquad (5\text{-}5d)$$

Suppose the solution for $\overline{\Psi}^i_{3R}$ be of the form

$$\overline{\Psi}^i_{3R}=\alpha t f_1(\eta)\sin\theta+8t\sqrt{\alpha t}\,g_3(\eta)\sin\theta\cos\theta$$

$$+8t^2F_3(\eta)\sin\theta\cos^2\theta-8t^2f_3(\eta)\sin^3\theta. \qquad (5\text{-}6)$$

Substituting the above expansion into equation (5-5) gives (5-5)

$$f_1''(\eta)+2\eta f_1'-4f_1=-4H(\eta), \qquad (5\text{-}7)$$

$$g_3''(\eta)+2\eta g_3'-6g_3=-4I(\eta), \qquad (5\text{-}8)$$

$$f_3''(\eta)+2\eta f_3'-8f_3=-4\theta(\eta), \qquad (5\text{-}9)$$

$$F_3''(\eta)+2\eta F_3'-8F_3=-4\Big[\theta(\eta)+\phi(\eta)\Big]. \qquad (5\text{-}10)$$

Equations (5-9) and (5-10) were solved solved by Goldstein and Rosenhead (1936) and later corrected by Wundt (1955). $f_3(\eta)$ and $F_3(\eta)$ will be written in general form, equation (6-7), and the constant coefficients are listed in Tables 3 and 4. Equations (5-7) and (5-8) were solved by Chien (1977)

$$f_1(\eta)=12\eta^2-\frac{16}{\sqrt{\pi}}\eta+1-(16\eta^2+1)\operatorname{erfc}\eta$$

$$+\frac{13}{\sqrt{\pi}}\eta\exp(-\eta^2), \qquad (5\text{-}11)$$

$$g_3(\eta)=-\left(\eta^3-\frac{1}{2}\eta\right)\operatorname{erfc}^2\eta+\Big[\left(-\frac{133}{24}+\frac{14}{9\pi}-4\sqrt{2}\right)\eta^3$$

$$+\left(\frac{69}{16}+\frac{5}{3\pi}-6\sqrt{2}\right)\eta+\frac{1}{\pi}\Big]\operatorname{erfc}\eta$$

$$+\frac{1}{\sqrt{\pi}}\left(\frac{11}{3}\eta^2+\frac{5}{3}\right)e^{-\eta^2}\operatorname{erfc}\eta-\frac{4\sqrt{2}}{3\sqrt{\pi}}\operatorname{erfc}\sqrt{2}\eta$$
$$+\frac{1}{\sqrt{\pi}}\left(2+\frac{8}{9\pi}-\frac{8\sqrt{2}}{3}\right)+\frac{1}{\sqrt{\pi}}\left[-\left(\frac{169}{24}+\frac{14}{9\pi}-4\sqrt{2}\right)\eta^2\right.$$
$$\left.+\frac{34}{15\sqrt{\pi}}\eta-\left(\frac{14}{3}+\frac{8}{9\pi}-4\sqrt{2}\right)\right]e^{-\eta^2}-\frac{8}{3\pi}\eta e^{-2\eta^2}. \qquad (5\text{-}12)$$

To sum up, the solution of the third order inner flow is equation (5-6), provided $f_1(\eta)$ given by (5-11) $g_3(\eta)$by (5-12), $f_3(\eta)$ and $F_3(\eta)$ by (6-7).

6. Composite Solution

We have presented the solution of the perturbation problem by an inner and an outer expansion. The former is valid in the inner region, and the latter in the outer. Since there is a common region we can construct a composite solution which is uniformly valid throughout the flow field. Carrying out the algebra for the inner limit of the outer solution or the outer limit of the inner expansion of the tangtial velocity, we have

$$\text{Common Part}=2\sin\theta+\varepsilon\left(4\eta\sqrt{\alpha t}\eta+\frac{4}{\sqrt{\pi}}\sqrt{\alpha t}\right)\sin\theta$$
$$+\varepsilon^2\left[\alpha t\left(12\eta^2-\frac{16}{\sqrt{\pi}}\eta+1\right)\sin\theta\right.$$
$$\left.+\frac{16}{\sqrt{\pi}}t\sqrt{\alpha t}\left(1+\frac{4}{9\pi}-\frac{4\sqrt{2}}{3}\right)\sin\theta\cos\theta\right] \qquad (6\text{-}1)$$

Constructing the composite solution to third order expansion contributing to tangential velocity, by adding the inner solution to the outer solution and subtracting the common part, we get a uniformly valid Ψ_r for the flow field as follow,

$$\Psi_r(r,\ \theta,\ t)=\left\{1+r^{-2}-2\operatorname{erfc}\eta+\frac{4}{\sqrt{\pi}}\frac{\sqrt{T}}{\sqrt{Re}}\left(r^{-2}\right.\right.$$
$$\left.+\frac{3\sqrt{\pi}}{2}\eta\operatorname{erfc}\eta-e^{-\eta^2}\right)+\frac{T}{Re}\left[r^{-2}\right.$$
$$\left.\left.-(16\eta^2+1)\operatorname{erfc}\eta+\frac{13}{\sqrt{\pi}}\eta\ e^{-\eta^2}\right]\right\}\sin\theta$$
$$+\left\{4Tf(\eta)+8\frac{T\sqrt{T}}{\sqrt{Re}}\left[g_3(\eta)\right.\right.$$
$$\left.\left.+\frac{2}{\sqrt{\pi}}\left(1+\frac{4}{9\pi}-\frac{4\sqrt{2}}{3}\right)(r^{-2}-1)\right]\right\}\sin\theta\cos\theta$$
$$+8T^2\left[F_3(\eta)\sin\theta\cos^2\theta-f_3(\eta)\sin^3\theta\right] \qquad (6\text{-}2)$$

Integrating the above equation, one gets the composite solution for the stream function.

$$\Psi(r,\ \theta,\ t)=\Big\{r-r^{-1}-\frac{4}{\sqrt{\pi}}\frac{\sqrt{T}}{\sqrt{Re}}(r^{-1}+\sqrt{\pi}\,\eta\mathrm{erfc}\eta$$
$$-e^{-\eta^2})-\frac{T}{Re}\Big[r^{-1}-(6\eta^2+1)\mathrm{erfc}\eta$$
$$+\frac{6}{\sqrt{\pi}}e^{-\eta^2}\Big]-2\Big(\frac{T}{Re}\Big)^{\frac{3}{2}}\Big[\Big(\frac{16}{3}\eta^3+\eta\Big)\mathrm{erfc}\eta$$
$$-\frac{1}{\sqrt{\pi}}\Big(\frac{16}{3}\eta^2-\frac{1}{6}\Big)\,e^{-\eta^2}-\frac{1}{6\sqrt{\pi}}\Big]\Big\}\sin\theta$$
$$+8\frac{T\sqrt{T}}{\sqrt{Re}}\Big[\int_0^\eta f(\zeta)\mathrm{d}\zeta-\frac{1}{\sqrt{\pi}}\Big(1+\frac{4}{9\pi}-\frac{4\sqrt{2}}{3}\Big)$$
$$(r^{-2}+2r-3)+2\frac{\sqrt{T}}{\sqrt{Re}}\int_0^\eta g_3(\zeta)d\zeta\Big]\sin\theta\cos\theta$$
$$+16\frac{T^2\sqrt{T}}{\sqrt{Re}}\Big[\int_0^\eta F_3(\zeta)d\zeta$$
$$\sin\theta\cos^2\theta-\int_0^\eta f_3(\zeta)d\zeta\sin^3\theta\Big] \qquad (6\text{-}3)$$

We shall use following eqation in this study

$$\Psi rr(r_o,\ \theta,\ t)=\Big[\frac{2}{\sqrt{\pi}}\frac{\sqrt{Re}}{\sqrt{T}}+1-\frac{2T}{Re}-\frac{1}{2\sqrt{\pi}}\frac{\sqrt{T}}{\sqrt{Re}}\Big]\sin\theta$$
$$+\Big[2\sqrt{TRe}\,f'(0)+4Tg_3'(0)$$
$$-\frac{48}{\sqrt{\pi}}\frac{T\sqrt{T}}{\sqrt{Re}}\Big(1+\frac{4}{9\pi}-\frac{4\sqrt{2}}{3}\Big)\Big]\sin\theta\cos\theta$$
$$+4T\sqrt{TRe}\Big[F'(0)\sin\theta\cos^2\theta$$
$$-f_3'(0)\sin^3\theta\Big] \qquad (6\text{-}4)$$

$f(\eta)$, $g_3(\eta)$, $f_3(\eta)$ and $F_3(\eta)$, together with their integration and differentiation are complicated functions involving error function and exponential function. Here, we write the general formula for each function and tabulate the constants for the convenience of computation.

$f(\eta)$, $f'(\eta)$ and $\int_0^\eta f(\zeta)d\zeta$ are of the form

$$\left.\begin{matrix} f(\eta) \\ f'(\eta) \\ \int_0^\eta f(\zeta)d\zeta \end{matrix}\right\} = \begin{cases} (A_3\eta^3+A_2\eta^2+A_1\eta+A_0)\mathrm{erfc}^2\eta \\ +(B_3\eta^4+B_2\eta^2+B_1\eta+B_0)\mathrm{erfc}\eta \\ +C_0\ \mathrm{erfc}\sqrt{2}\eta+(D_2\eta^2+D_1\eta+D_0)\frac{1}{\sqrt{\pi}}\exp(-\eta^2)\mathrm{erfc}\eta \\ +(E_2\eta^2+E_1\eta+E_0)\frac{1}{\sqrt{\pi}}\exp(-\eta^2) \\ +(F_1\eta+F_0)\frac{1}{\pi}\exp(-2\eta^2)+G_0 \end{cases} \quad (6\text{-}5)$$

The coefficienss in the above equation are tabulated in Table 1.

The general formula for $g_3(\eta)$, $g'3(\eta)$ and $\int_0^\eta g_3(\zeta)d\zeta$ can be expressed as follow:

$$\left.\begin{matrix} g_3(\eta) \\ g_3'(\eta) \\ \int_0^\eta g_3(\zeta)\,d\zeta \end{matrix}\right\} = \begin{cases} (A_4\eta^4+A_3\eta^3+A_2\eta^2+A_1\eta+A_0)\mathrm{erfc}^2\eta \\ +(B_4\eta^4+B_3\eta^3+B_2\eta^2+B_1\eta+B_0)\mathrm{erfc}\eta \\ +(C_3\eta^3+C_2\eta^2+C_1\eta+C_0)\frac{1}{\sqrt{\pi}}\exp(-\eta^2)\mathrm{erfc}\eta \\ +(D_1\eta+D_0)\ \mathrm{erfc}\sqrt{2}\eta \\ +(E_3\eta^3+E_2\eta^2+E_1\eta+E_0)\frac{1}{\sqrt{\pi}}\exp(-\eta^2) \\ +(F_2\eta^2+F_1\eta+F_0)\frac{1}{\pi}\exp(-2\eta^2) \\ +G_1\eta+G_0 \end{cases} \quad (6\text{-}6)$$

The coefficients are listed at Table 2.

$F_3(\eta)$ and $f_3(\eta)$ are written in general form and the cofficients are tabulated by Wundt (1955). Bar-lev (1974) did not integrate these functions because an extensive integral table of the form $\int_0^\eta \zeta^i \exp(-j\zeta^2)\ \mathrm{erfc}k\zeta d\zeta$, where i, j and k are integers, was not available. Wang (1966) listed some in his work. Chien (1977) have derived additional formulas for this study. The integral $\int_0^\eta \exp(-2\zeta^2)\ \mathrm{erc}\zeta d\zeta$ is the only one which can not be integrated analytically. It is numerically integrated by using quadrature formula (IBM, 1970).

The Initial Flow Past an Impulsively Started Circular Cylinder

The general form for $F_3(\eta)$ and $f_3(\eta)$, together with their deririvatives and integrals, is as follows.

$$
\left.\begin{matrix} f_3(\eta) \\ f'_3(\eta) \\ \int_0^\eta f_3(\zeta)d\zeta \\ F_3(\eta) \\ F'_3(\eta) \\ \int_0^\eta F_3(\zeta)d\zeta \end{matrix}\right\} =
\begin{cases}
-(A_5\eta^5+A_4\eta^4+A_3\eta^3+A_2\eta^2+A_1\eta+A_0)\mathrm{erfc}^3\eta \\
+(B_4\eta^4+B_3\eta^3+B_2\eta^2+B_1\eta+B_0)\frac{2}{\pi}\exp(-\eta_2)\mathrm{erfc}^2 \\
-(C_3\eta^3+C_2\eta^2+C_1\eta+C_0)\frac{4}{\pi}\exp(-2\eta^2)\mathrm{erfc}\eta \\
+(D_4\eta^4+D_3\eta^3+D_2\eta^2+D_1\eta+D_0)\frac{8}{\pi\sqrt{\pi}}\exp(-3\eta^2) \\
-(E_5\eta^5+E_4\eta^5+E_3\eta^3+E_2\eta^2+F_1\eta+E_1\eta+E_0)\mathrm{erfc}\sqrt{3}\,\eta \\
-(F_1\eta+F_0)\frac{2}{\sqrt{\pi}}\exp(-\eta^2)\mathrm{erfc}\sqrt{2}\,\eta \\
+(G_5\eta^5+G_4\eta^4+G_3\eta^3+G_2\eta^2+G_1\eta+G_0)\mathrm{erfc}^2\eta \\
-(H_4\eta^4+H_3\eta^3+H_2\eta^2+H_1\eta+H_0)\frac{2}{\sqrt{\pi}}\exp(-\eta^2)\mathrm{erfc}\eta \\
+(I_3\eta^3+I_2\eta^2+I_1\eta+I_0)\frac{4}{\sqrt{\pi}}\exp(-2\eta^2) \\
-(K_5\eta^5+K_4\eta^4+K_3\eta^3+K_2\eta^2+K_1\eta+K_0)\mathrm{erfc}\eta \\
+(L_4\eta^4+L_3\eta^3+L_2\eta^2+L_1\eta+L_0)\frac{1}{\sqrt{\pi}}\exp(-\eta^2) \\
-M_0\mathrm{erfc}\sqrt{2}\,\eta+N_0\mathrm{erfc}\eta\ \ \mathrm{erfc}\sqrt{2} \\
+P_0\frac{4}{\pi}\int_0^\eta\exp(-2\zeta^2)\mathrm{erfc}\zeta d\zeta+Q_0
\end{cases}
\qquad (6\text{-}7)
$$

The coefficients are listed at Table 3 for $F_3(\eta)$, an Table 4 for $f_3(\eta)$.

Table 1 Coefficients for $f(\eta)$, $f'(\eta)$ and $\int_0^\eta f(\zeta)d\zeta$

	$f(\eta)$	$f'(\eta)$	$\int_0^\eta f(\zeta)d\zeta$
A_3	0	0	$\frac{1}{3}$
A_2	1	0	0
A_1	0	2	$-\frac{1}{2}$
A_0	$-\frac{1}{2}$	0	0
B_3	0	0	$-1-\frac{4}{9\pi}$
B_2	$-3-\frac{4}{3\pi}$	0	0
B_1	0	$-6-\frac{8}{3\pi}$	$\frac{1}{2}-\frac{2}{3\pi}$
B_0	$\frac{1}{2}-\frac{2}{3\pi}$	0	$\frac{2}{3\sqrt{\pi}}$
C_0	0	0	$-\frac{8}{3\sqrt{2\pi}}$
D_2	0	2	$-\frac{2}{3}$
D_1	-3	0	0
D_0	0	-1	$\frac{11}{6}$
E_2	0	-2	$1+\frac{4}{9\pi}$
E_1	$4+\frac{4}{3\pi}$	$\frac{8}{3\sqrt{\pi}}$	0
E_0	$-\frac{4}{3\sqrt{\pi}}$	$3+\frac{8}{3\pi}$	$\frac{4}{9\pi}-\frac{3}{2}$
F_1	0	-2	$\frac{1}{3}$
F_0	2	0	0
G_0	0	0	$\frac{1}{\sqrt{\pi}}(-1+3\sqrt{\frac{8}{2}}-\frac{4}{9\pi})$

Table 2 Coefficients for $g_3(\eta)$, $g'_3(\eta)$ and $\int_0^\eta g_3(\zeta)d\zeta$

	$g_3(\eta)$	$g'_3(\eta)$	$\int_0^\eta g_3(\zeta)d\zeta$
A_4	0	0	$-\frac{1}{4}$
A_3	-1	0	0
A_2	0	-3	$\frac{1}{4}$
A_1	$\frac{1}{2}$	0	0
A_0	0	$\frac{1}{2}$	$-\frac{39}{48}$
B_4	0	0	$\frac{133}{96}+\frac{7}{18\pi}-\sqrt{2}$
B_3	$\frac{133}{24}+\frac{14}{9\pi}-4\sqrt{2}$	0	0
B_2	0	$\frac{133}{8}+\frac{14}{3\pi}-12\sqrt{2}$	$\frac{69}{32}+\frac{5}{6\pi}-3\sqrt{2}$
B_1	$\frac{69}{16}+\frac{5}{3\pi}-6\sqrt{2}$	0	$\frac{1}{\sqrt{\pi}}$
B_0	$\frac{1}{\sqrt{\pi}}$	$\frac{69}{16}+\frac{5}{3\pi}-6\sqrt{2}$	$\frac{253}{128}+\frac{1}{8}-\frac{3\sqrt{2}}{4}$
C_3	0	$-\frac{10}{3}$	$\frac{1}{2}$
C_2	$\frac{11}{3}$	0	0
C_1	0	2	$-\frac{19}{12}$
C_0	$\frac{5}{3}$	0	0
D_1	0	0	$-\frac{8}{3\sqrt{2\pi}}$

Table 2 Coefficients for $g_3(\eta)$, $g'_3(\eta)$ and $\int_0^\eta g_3(\zeta)d\zeta$ (Continued)

	$g_3(\eta)$	$g'_3(\eta)$	$\int_0^\eta g_3(\zeta)d\zeta$
D_0	$-\frac{8}{3\sqrt{2\pi}}$	0	0
E_3	0	3	$-\frac{133}{96}-\frac{7}{18\pi}+2$
E_2	$-\frac{169}{24}-\frac{14}{9\pi}+4\sqrt{2}$	$-\frac{68}{15\sqrt{\pi}}$	0
E_1	$\frac{34}{15\sqrt{\pi}}$	$-\frac{107}{8}-\frac{14}{3\pi}+12\sqrt{2}$	$-\frac{137}{192}-\frac{23}{36\pi}+\frac{5\sqrt{2}}{2}$
E_0	$-\frac{14}{3}-\frac{8}{9\pi}+4\sqrt{2}$	$\frac{4}{15\sqrt{\pi}}$	$-\frac{32}{15\sqrt{\pi}}$
F_2	0	$\frac{10}{3}$	$-\frac{1}{4}$
F_1	$-\frac{8}{3}$	0	0
F_0	0	$\frac{2}{3}$	$\frac{31}{12}$
G_1	0	0	$\frac{1}{\sqrt{\pi}}(2-\frac{8\sqrt{2}}{3}+\frac{8}{9\pi})$
G_0	$\frac{1}{\sqrt{\pi}}(2-\frac{8\sqrt{2}}{3}+\frac{8}{9\pi})$	0	$-\frac{149}{128}+\frac{3\sqrt{2}}{4}-\frac{23}{40\pi}$

Table 3 Coefficients for $F_3(\eta)$, $F'_3(\eta)$ and $\int_0^\eta F_3(\zeta)d\zeta$

	$F_3(\eta)$	$F'_3(\pi)$	$\int_0^\eta F_3(\zeta)d\zeta$
A_5	0	0	$-\frac{1}{15}$
A_4	$-\frac{1}{3}$	0	0
A_3	0	$-\frac{4}{3}$	$-\frac{1}{3}$
A_2	-1	0	0
A_1	0	-2	$\frac{1}{4}$
A_0	$\frac{1}{4}$	0	0
B_4	0	$\frac{1}{3}$	$\frac{1}{10}$
B_3	$-\frac{2}{3}$	0	0
B_2	0	$-\frac{1}{3}$	$-\frac{11}{30}$
B_1	-2	0	0
B_0	0	$-\frac{5}{4}$	$\frac{121}{120}$
C_3	0	$\frac{1}{3}$	$-\frac{1}{20}$
C_2	$-\frac{5}{12}$	0	0
C_1	0	$-\frac{1}{6}$	$-\frac{7}{60}$
C_0	$-\frac{7}{6}$	0	0

Table 3 Coefficients for $F_3(\eta)$, $F'3(\eta)$ and $\int_0^\eta F_3(\zeta)d\zeta$

	$F_3(\eta)$	$F_3^{\eta}(\eta)$	$\int_0^\eta(\eta)(\zeta)d\zeta$
D_4	0	0	$\frac{9}{200}$
D_3	$\frac{9}{40}$	0	0
D_2	0	$\frac{59}{60}$	$\frac{251}{1200}$
D_1	$\frac{133}{240}$	0	0
D_0	0	$\frac{14}{15}$	$\frac{353}{1800}$
E_5	0	0	$\frac{9\sqrt{3}}{25}$
E_4	$\frac{9\sqrt{3}}{25}$	0	0
E_3	0	$\frac{36\sqrt{3}}{5\pi}$	$\frac{9\sqrt{3}}{5\pi}$
E_2	$\frac{27\sqrt{3}}{5\pi}$	0	0
E_1	0	$\frac{54\sqrt{3}}{5\pi}$	$\frac{27\sqrt{3}}{20\pi}$
E_0	$\frac{27\sqrt{3}}{20\pi}$	0	0
F_1	0	$-\frac{16}{15}\sqrt{\frac{2}{\pi}}$	0
F_0	$\frac{8}{15}\sqrt{\frac{2}{\pi}}$	0	0
G_5	0	0	$-\frac{1}{6}+\frac{2}{45\pi}$
G_4	$-\frac{5}{6}+\frac{2}{9\pi}$	0	0
G_3	0	$-\frac{10}{3}+\frac{8}{9\pi}$	$-\frac{5}{6}+\frac{2}{9\pi}$

Table 3 Coefficients for $F_s(\eta)$, $F_s'(\eta)$ and $\int_0^\eta F_s(\zeta)d\zeta$ (Continued)

	$F_s(\eta)$	$F_s'(\eta)$	$\int_0^\eta F_s(\zeta)d\zeta$
G_2	$-\frac{5}{2}+\frac{2}{3\pi}$	0	$-\frac{2}{3\sqrt{\pi}}$
G_1	$-\frac{4}{3\sqrt{\pi}}$	$-5+\frac{4}{3\pi}$	$\frac{3}{8}-\frac{1}{2\pi}$
G_0	$\frac{3}{8}-\frac{1}{2\pi}$	$-\frac{4}{3\sqrt{\pi}}$	$\frac{1}{3\sqrt{\pi}}$
H_4	0	$\frac{1}{2}-\frac{2}{9\pi}$	$-\frac{1}{6}+\frac{2}{45\pi}$
H_3	$-\frac{13}{12}+\frac{1}{3\pi}$	$-\frac{4}{3\sqrt{\pi}}$	0
H_2	$\frac{2}{3\sqrt{\pi}}$	$-\frac{13}{6}-\frac{2}{9\pi}$	$-\frac{5}{8}+\frac{13}{90\pi}$
H_1	$-\frac{73}{24}+\frac{23}{18\pi}$	$-\frac{2}{3\sqrt{\pi}}$	$-\frac{1}{\sqrt{\pi}}$
H_0	$-\frac{1}{3\sqrt{\pi}}$	$-\frac{55}{24}+\frac{5}{18\pi}$	$\frac{61}{48}-\frac{259}{180\pi}$
I_3	0	$\frac{1}{4}-\frac{1}{9\pi}$	$-\frac{1}{24}+\frac{1}{90\pi}$
I_2	$-\frac{1}{3}+\frac{1}{9\pi}$	$-\frac{1}{3\sqrt{\pi}}$	0
I_1	$\frac{1}{3\sqrt{\pi}}$	$-\frac{3}{8}-\frac{5}{18\pi}$	$-\frac{5}{48}+\frac{1}{60\pi}$
I_0	$-\frac{5}{6}+\frac{4}{9\pi}$	0	$-\frac{1}{3\sqrt{\pi}}$
K_3	0	0	$-\frac{1}{10}-\frac{2+27\sqrt{3}}{75\pi}-\frac{64}{675\pi^2}$
K_2	$-\frac{1}{2}-\frac{2+27\sqrt{3}}{15\pi}-\frac{64}{135\pi^2}$	0	0
K_1	0	$-2-\frac{8+108\sqrt{3}}{15\pi}-\frac{256}{135\pi^2}$	$-\frac{1}{2}-\frac{2+27\sqrt{3}}{15\pi}-\frac{64}{135\pi^2}$

Table 3 Coefficients for $F_3(\eta)$, $F_3'(\eta)$ and $\int_0^\eta F_3(\zeta)d\zeta$ (Continued)

	$F_3(\eta)$	$F_3'(\eta)$	$\int_0^\eta F_3(\zeta)\,d\zeta$
K_2	$-\frac{3}{2}-\frac{2+27\sqrt{3}}{5\pi}-\frac{64}{45\pi^2}$	0	$-\frac{2}{\sqrt{\pi}}-\frac{8}{9\pi\sqrt{\pi}}$
K_1	$-\frac{4}{\sqrt{\pi}}-\frac{16}{9\sqrt{\pi}\pi}$	$-3-\frac{4+54\sqrt{3}}{5\pi}-\frac{128}{45\pi^2}$	$\frac{1}{8}-\frac{46+81\sqrt{3}}{60\pi}-\frac{16}{45\pi^2}$
K_0	$\frac{1}{8}-\frac{46+81\sqrt{3}}{60\pi}-\frac{16}{45\pi^2}$	$-\frac{4}{\sqrt{\pi}}-\frac{16}{9\pi\sqrt{\pi}}$	$\frac{3+8\sqrt{2}}{15\sqrt{\pi}}-\frac{43}{45\pi\sqrt{\pi}}$
L_4	0	$\frac{1}{2}$	$-\frac{1}{20}-\frac{2+27\sqrt{3}}{150\pi}-\frac{32}{675\pi^2}$
L_3	$-\frac{1}{2}-\frac{2+27\sqrt{3}}{30\pi}-\frac{32}{135\pi^2}$	$-\frac{4}{3\sqrt{\pi}}$	0
L_2	$\frac{2}{3\sqrt{\pi}}$	$\frac{1}{6}+\frac{28-162\sqrt{3}}{45\pi}-\frac{128}{135\pi^2}$	$-\frac{1}{10}-\frac{6+81\sqrt{3}}{100\pi}-\frac{16}{75\pi^2}$
L_1	$-\frac{19}{12}-\frac{22+81\sqrt{3}}{36\pi}-\frac{16}{27\pi^2}$	$-\frac{6+16\sqrt{2}}{15\sqrt{\pi}}+\frac{16}{45\pi\sqrt{\pi}}$	$-\frac{4}{3\sqrt{\pi}}-\frac{4}{9\pi\sqrt{\pi}}$
L_0	$-\frac{17+8\sqrt{2}}{15\sqrt{\pi}}-\frac{16}{15\pi\sqrt{\pi}}$	$-\frac{35}{24}-\frac{62+162\sqrt{3}}{45\pi}$	$\frac{181}{240}-\frac{31+81\sqrt{3}}{225\pi}$
		$-\frac{128}{135\pi^2}$	$-\frac{64}{675\pi^2}$
M_0	0	0	$-\frac{2\sqrt{2}}{\sqrt{\pi}}+\frac{64\sqrt{2}}{45\pi\sqrt{\pi}}$
N_0	0	0	$\frac{8\sqrt{2}}{15\sqrt{\pi}}$
P_0	0	0	$\frac{18}{5}$
O_0	0	0	$-\frac{1}{\sqrt{\pi}}\left(\frac{67}{60}+2\sqrt{2}+\frac{1}{\pi}\right.$
			$\left.\frac{169}{150}-\frac{64\sqrt{2}}{45}-\frac{18\sqrt{3}}{25}\right)$
			$-\frac{128}{675\pi^2}$

Table 4 Coefficients for $f_3(\eta)$, $f'_3(\eta)$ and $\int_0^\eta f_3(\zeta)d\zeta$

	$f_3(\eta)$	$f'_3(\eta)$	$\int_0^\eta f_3(\zeta)d\zeta$
A_5	0	0	$\frac{1}{15}$
A_4	$\frac{1}{3}$	0	0
A_3	0	$\frac{4}{3}$	0
A_2	0	0	0
A_1	0	0	$\frac{1}{4}$
A_0	$\frac{1}{4}$	0	0
B_4	0	$-\frac{1}{6}$	$\frac{1}{10}$
B_3	$\frac{7}{12}$	0	0
B_2	0	$\frac{23}{12}$	$-\frac{11}{120}$
B_1	$-\frac{3}{8}$	0	0
B_0	0	$\frac{3}{8}$	$\frac{113}{240}$
C_3	0	$-\frac{1}{6}$	$\frac{1}{20}$
C_2	$-\frac{1}{3}$	0	0
C_1	0	$\frac{19}{12}$	$-\frac{11}{120}$
C_0	$-\frac{5}{12}$	0	0

Table 4 Coefficients for $f_3(\eta)$, $f'_3(\eta)$ and $\int_0^\eta f_3(\zeta)d\zeta$ (Continued)

	$f_3(\eta)$	$f'_3(\eta)$	$\int_0^\eta f_3(\zeta)d\zeta$
D_4	0	0	$-\frac{9}{800}$
D_3	$-\frac{9}{160}$	0	0
D_2	0	$-\frac{4}{15}$	$-\frac{17}{320}$
D_1	$-\frac{31}{320}$	0	0
D_0	0	$-\frac{7}{30}$	$-\frac{17}{300}$
E_5	0	0	$-\frac{9\sqrt{3}}{100\pi}$
E_4	$-\frac{9\sqrt{3}}{20\pi}$	0	0
E_3	0	$\frac{9\sqrt{3}}{5\pi}$	$-\frac{9\sqrt{3}}{20\pi}$
E_2	$-\frac{27\sqrt{3}}{20\pi}$	0	0
E_1	0	$-\frac{27\sqrt{3}}{10\pi}$	$-\frac{27\sqrt{3}}{80\pi}$
E_0	$-\frac{27\sqrt{3}}{80\pi}$	0	0
F_1	0	$-\frac{16}{15}\sqrt{\frac{2}{\pi}}$	0
F_0	$\frac{8}{15}\sqrt{\frac{2}{\pi}}$	0	0
G_5	0	0	$\frac{3}{10}+\frac{2}{15\pi}$
G_4	$\frac{3}{2}+\frac{2}{3\pi}$	0	0
G_3	0	$6+\frac{8}{3\pi}$	$\frac{1}{6}+\frac{2}{9\pi}$

Table 4 Coefficients for $f_3(\eta)$, $f_3'(\eta)$ and $\int_0^\eta f_3(\zeta)\,d\zeta$ (Continued)

	$f_3(\eta)$	$f_3'(\eta)$	$\int_0^\eta f_3(\zeta)\,d\zeta$
G_2	$\frac{1}{2}+\frac{2}{3\pi}$	0	0
G_1	0	$1+\frac{4}{3\pi}$	$\frac{5}{8}-\frac{1}{6\pi}$
G_0	$\frac{5}{8}-\frac{1}{6\pi}$	0	0
H_4	0	$-\frac{1}{2}-\frac{2}{9\pi}$	$\frac{3}{10}+\frac{2}{15\pi}$
H_3	$\frac{7}{4}+\frac{7}{9\pi}$	0	0
H_2	0	$\frac{13}{2}+\frac{2}{\pi}$	$-\frac{13}{120}+\frac{1}{10\pi}$
H_1	$-\frac{1}{8}+\frac{5}{6\pi}$	0	0
H_0	0	$\frac{9}{8}+\frac{1}{2\pi}$	$\frac{139}{240}-\frac{29}{60\pi}$
I_3	0	$-\frac{1}{4}-\frac{1}{9\pi}$	$\frac{3}{40}+\frac{1}{30\pi}$
I_2	$\frac{1}{2}+\frac{2}{9\pi}$	0	0
I_1	0	$\frac{15}{8}+\frac{7}{18\pi}$	$-\frac{23}{240}-\frac{1}{180\pi}$
I_0	$-\frac{1}{4}+\frac{2}{9\pi}$	0	0
K_5	0	0	$\frac{7}{30}+\frac{24+9\sqrt{3}}{100\pi}+\frac{32}{135\pi^2}$
K_4	$\frac{7}{6}\quad\frac{24+9\sqrt{3}}{20\pi}\quad\frac{32}{45\pi^2}$	0	0
K_3	0	$\frac{14}{3}+\frac{24+9\sqrt{3}}{5\pi}+\frac{128}{45\pi^2}$	$\frac{1}{6}+\frac{136+81\sqrt{3}}{180\pi}+\frac{32}{45\pi^2}$

Table 4 Coefficients for $f_3(\eta)$, $f_3'(\eta)$ and $\int_0^\eta f_3(\zeta)\,d\zeta$ (Continued)

	$f_3(\eta)$	$f_3'(\eta)$	$\int_0^\eta f_3(\zeta)\,d\zeta$
K_2	$\frac{1}{2}+\frac{136+81\sqrt{3}}{60\pi}+\frac{32}{15\pi^2}$	0	0
K_1	0	$1+\frac{136+81\sqrt{3}}{30\pi}+\frac{64}{15\pi^2}$	$\frac{3}{8}+\frac{56+81\sqrt{3}}{240\pi}+\frac{8}{15\pi^2}$
K_0	$\frac{3}{8}+\frac{56+81\sqrt{3}}{240\pi}+\frac{8}{15\pi^2}$	0	$-\frac{2+8\sqrt{2}}{15\sqrt{\pi}}-\frac{8}{45\pi\sqrt{\pi}}$
L_4	0	0	$\frac{7}{60}+\frac{24+9\sqrt{3}}{200\pi}+\frac{16}{225\pi^2}$
L_3	$\frac{7}{12}\ \frac{24+9\sqrt{3}}{40\pi}\ \frac{16}{45\pi^2}$	0	0
L_2	0	$\frac{8}{3}+\frac{72+27\sqrt{3}}{30\pi}+\frac{64}{45\pi^2}$	$\frac{1}{40}+\frac{1144+729\sqrt{3}}{3600\pi}+\frac{8}{25\pi^2}$
L_1	$-\frac{5}{24}+\frac{40+27\sqrt{3}}{48\pi}+\frac{8}{9\pi^2}$	$\frac{4-16\sqrt{2}}{15\sqrt{\pi}}+\frac{16}{45\pi\sqrt{\pi}}$	0
L_0	$-\frac{2+8\sqrt{2}}{15\sqrt{\pi}}-\frac{8}{45\pi\sqrt{\pi}}$	$\frac{1}{6}+\frac{32+27\sqrt{3}}{30\pi}+\frac{64}{45\pi^2}$	$\frac{19}{60}+\frac{4}{225\pi}+\frac{9\sqrt{3}}{100\pi}+\frac{32}{225\pi^2}$
M_0	0	0	$-\frac{11\sqrt{2}}{15\sqrt{\pi}}+\frac{32\sqrt{2}}{45\pi\sqrt{\pi}}$
N_0	0	0	$\frac{8}{15}\sqrt{\frac{2}{\pi}}$
P_0	0	0	$\frac{9}{5}$
Q_0	0	0	$-\frac{1}{\sqrt{\pi}}\left[\frac{11}{20}+\frac{11\sqrt{2}}{15}+\frac{1}{\pi}\left(\frac{109}{150}+\frac{9\sqrt{3}}{50}-\frac{32\sqrt{2}}{45}\right)+\frac{64}{225\pi^2}\right]$

7. Flow Patterns and Velocity Profiles

Stream function expressed by equation (6-3) is plotted in Figure 1 for Re= 250. When $T=0$, equation (6-3) reduces to the stream function for potential flow. For $T=0.2$, the flow in the the front half stream is similar to that of the potential flow, and the streamlines are displaced outward in the rear half. At $T=0.4$ besides $\Psi=0$ at the boundary, there appeares another zero streamline. The region between these two stream lines is of negative value and is called "bubble" by Mehta and Lavan (1975). At $T=0.6$, we can see recirculating region behind the cylinder.

The tangential velocity, $u_\theta=\Psi_r$, is expressed by equation (6-2). The development of the tangential velocity component versus the angle at Re=250 is plotted in Figure 2. The time history of the tangential velocity profiles is thus exhibited. At the short time after start, Figure2(a), T=0.1, the velocity profiles along the cylinder are almost fore-and-aft symmetric with respect to the top of the cylinder. The velocity increases abruptly in a thin viscous layer from zero to almost the value of that abtained by potential flow theory. As time goes on, the maximum points of the profiles displace away from the surface as the viscous layer thickness. and the profiles become smooth. At time up to 0.4, the profiles show the occurance of separation. At $T=0.6$, it shows the start of back flow and the separation point progresses to $\theta=150°$.

8. Vorticity Distribution on the Surface of the Cylinder

Vorticity distribution on the surface of the cylinder is one of the interesting characteristics of the problem we are studying. Due to the non-slip condition on the surface of the cylinder, we require both tangential and radial velocity components vanish, i. e. $\Psi_r=0$ and $\Psi_\theta=0$. On the cylinder surface the vorticity is

$$\omega(r_0)=\left[\frac{\sqrt{Re}}{\sqrt{\pi}}\frac{\sqrt{Re}}{\sqrt{T}}+1-\frac{1}{2\sqrt{\pi}}\frac{\sqrt{T}}{\sqrt{Re}}-2\frac{T}{Re}\right]\sin\theta$$
$$+\left[2\sqrt{T}\sqrt{Re}f'(0)+4Tg'(0)-\frac{48}{\sqrt{\pi}}\frac{T\sqrt{T}}{Re}\right.$$
$$\left.\left(1+\frac{4}{9\pi}-\frac{4\sqrt{2}}{3}\right)\right]\sin\theta\cos\theta$$
$$+4T\sqrt{T}\sqrt{Re}\left[F_3'(0)\sin\theta\cos^2\theta-f_3'(0)\sin^3\theta\right] \qquad (8\text{-}7)$$

where $f'(0)$, $g'(0)$, $F_3'(0)$ and $f_3'(0)$ are the value at r_0.

The vorticity distribution on the surface of the cylinder is plotted in Figures 3 to 5. At the impulsive start, $T=0+$, a singularity is present in the first term in equation (8-1). And a vortex sheet forms on the surface at this time. The figures show the vorticity at $T=0.2$, the larger the Reynolds number, the larger the vorticity on the surface. As time goes on, the vorticity diffused into the fluid, and reduced its magnitude. The gradient of the vorticity at the rear stagnation point, which is negative at first, becomes positive at some time after start. The vorticity at the region near stagnation point becomes negative for T greater than 4.0. Separation occurs on the surface and the recirculating flow appears in this region.

Table 5 compares the vorticity distribution $\omega/\sqrt{Rd}=\omega/\sqrt{2Re}$ on the cylinder $Re=\infty$ of the present analytic results with those of Collins and Dennis (1973a, b) at $T=0.2$, 0.4 and 1.0 The numerical computation of Belcher, Burggraf, Cook, Robins and Stewartson (1972) is also included. The agreement is seen to be very good.

The computed surface vorticites on $\theta=0$ (45) 180 at $t=0.3$ and 1.0 at $Re=$ 250 are shown in Tabie 6, where they are compared with those of Wang (1967), Sons and Harantty (1969), Dennis and Staniforth (1970), and Panikker and Levan (1975). The table shows that the agreement between the seven studies is satisfactory before separation at $T=0.3$. At $T=1.0$, the surface vorticity values of the seven studies do not agree. Wang's solution exhibits the largest difference since his expansion is already inaccurate at this time. The present analytic solution is not expected to be valid at $T=1.0$, the agreement is less satisfactory, particulary in the rear separation region.

Table 5 Comparison of the Vorticity Distribution $\omega/\sqrt{Rd}=\omega/\sqrt{2Re}$ on the Cylinder at $Re=\infty$

θ	0	45	90	135	180
			$T=0.2$		
Collins & Dennis (1973a)	0	1.74	1.80	0.73	0
Collins & Dennis (1973b)	0	1.77	1.80	0.72	0
Present	0	1.754	1.803	0.735	0
			$T=0.4$		
Collins & Dennis (1973a)	0	1.56	1.30	0.13	0
Collins & Dennis (1973b)	0	1.57	1.30	0.11	0
Present	0	1.562	1.308	0.127	0
			$T=1.0$		
Belcher et. al. (1972)	0	1.52	1.00	-0.79	0
Collins & Dennis (1973a)	0	1.50	1.00	-0.78	0
Collins & Dennis (1973b)	0	1.50	1.00	-0.78	0
Present	0	1.520	1.025	-0.749	0

Table 6 Comparsion of the Vorticity Distribution on the Cylinder at $Re=2Re=500$

θ	0	45	90	135	180
			$T=0.3$		
Wang (1967)	0	37.0	33.0	10.0	0
Son & Hanratty (1969)	0	37.5	34.0	9.0	0
Dennis et. al. (1970)	0	35.0	31.5	10.5	0
Panikker & Lavan (1975)	0	34.0	39.5	11.5	0
Present (Analytic)	0	35.13	34.26	11.01	0
Potential Flow Start	0	37.59	35.18	10.58	0
			$T=1.0$		
Wang (1967)	0	37.5	17.5	-13.0	0
Son & Hanratty (1969)	0	33.5	20.0	-7.5	0
Dennis et. al. (1970)	0	32.0	19.0	-5.4	0
Panikker & Lavan (1975)	0	27.0	16.5	-5.0	0
Present (Analytic)	0	28.78	23.08	-10.25	0
Potential Flow Start	0	32.60	22.00	-4.58	0

9. Separation Time

As described in the last Section, at small values of T, the vorticity of the fluid is within a thin layer surrounding the cylinder. As Reynolds number increases, the more vorticity is carried to the rear of the cylinder, the vorticity being of negative sign. Ultimately, there is more vorticity at the rear of the cylinder than needed for the satisfaction of the non-slip condition. A backward flow is induced near the surface. The backward flow counters the forwards-moving fluid and deflects it away from the rear of the cylinder. Therefore, there exists a separation point on the surface of the cylinder where vorticity vanishes. And the points where $\omega=0$ at the cylinder surface can read from vorticity distribution over the cylinder surface, Figures 3 to 5.

To find the separation point, we set the vorticity on the cylinder equation (8-1) to zero. Differentiating with respect to the tangential co-ordinate θ, Bar-lev and Yang (1975) showed that the separation starts always at the rear stagnation point, i. e. $\theta=\pi$. Equation (7-2) becomes

$$\frac{2}{\sqrt{\pi}}\frac{\sqrt{Re}}{\sqrt{T}}+1+\left[\frac{14}{\sqrt{\pi}}\frac{1}{\sqrt{Re}}-\frac{4}{\sqrt{\pi}}\left(1+\frac{4}{3\pi}\right)\sqrt{Re}\right]\sqrt{T}$$

$$-\left[\frac{2}{Re}+4\left(\frac{93}{8}-6\sqrt{2}-\frac{24}{\pi}+\frac{34}{\pi\sqrt{\pi}}\right)\right]T$$

$$+\frac{48}{\sqrt{\pi}}\left(1+\frac{4}{9\pi}-\frac{4\sqrt{2}}{3}\right)\frac{1}{\sqrt{Re}}-\frac{8}{\sqrt{\pi}}\left(\frac{-89+108\sqrt{3}}{30\pi}\right.$$

$$\left.+\frac{128}{135\pi^2}-\frac{11}{12}\right)\sqrt{Re}\Big]T\sqrt{T}=0$$

By Newton's method, we can solve for T for a given Reynolds number. The time of initial separation at the rear stagnation point is plotted in Figure 6. Also plotted for comparison are the curve of Wang (1967), which uses the second-order expansion, and the results obtained by Collins and Dennis (1973a, b). The third-order expansion curve is close to that predicted by Collins and Dennis, although somewhat lower.

For the limiting case $Re\to\infty$, the classical analytical boundary layer solution of Blasius (1908) gives the initial separation time $T=0.351$, which was also obtained by Wang (1967). The third order solution is the same as that of

Goldstein and Rosenhead (1936), which was also obtained by Collins and Dennis (1973a, Equation 75), $T=0.3195$. Thus, the inadequacy of the second order expansion is made up by the third order expansion. Collins and Dennis considered the approximation up to the seventh order and obtained $T=0.322$.

After the flow separates at the rear stagnation point, the point of separation moves along the surface of the cylinder and should asymptotically reach a position consistent with that determined from steady boundary layer theroy. Terrill (1960) gave the steady position at angle 104.5° from the fore of the stagnation point for infinite Reynolds number.

The progress of separation time for various Reynolds numbers is shown in Figure 7 . The extremum of the separation point obained in this study is at angle 106° measured from the front stagntion point of the cylinger at $T=2.475$ for $Re=\infty$. The trend of the results is consistant with those of Son and Hanratty (1969), Thoman and Szewczyk (1969), and Collins and Dennis (1973b, Figure 6). From Figure 7 it is seen that the higher the Reynolds number, the sooner the separation angle reaches its steady value. For low Reynolds number, especially for $Re=20$, the curve seems to intersect with that of $Re=40$. Probably, in these low Reynolds number range, our expansion is not valid.

10. Pressure Distribution on the Cylinder

One of the principal quantities of interest in the solution to a flow problem is the pressure, since the integral of the pressure around the surface of the body yeilds the lift and the pressure drag acting on the body. The usual way of expressing the pressure is by means of a dimensionless pressure coefficient. It is therefore of interest to obtain an expression for pressure coefficient for this study.

The pressure coefficient C_p is defined in the following way,

$$C_p=\frac{P-P_\infty}{\frac{1}{2}\rho U^2} \tag{10-1}$$

Here, P_∞ is the pressure far from the cylinder, and P is that on the cylinder surface. Integrating tne equation of motion and using the definition of pressure coefficient, we have the formula

$$C_p=\left[-\frac{4}{\sqrt{\pi}}\frac{1}{\sqrt{ReT}}-\frac{2}{Re}+\frac{47}{\sqrt{\pi}}\frac{\sqrt{T}}{Re\sqrt{Re}}+8\frac{T}{Re^2}-8f'_3(0)\right.$$
$$\left.\frac{T\sqrt{T}}{\sqrt{Re}}\right](1-\cos\theta)+\left[f''(0)+2\frac{\sqrt{T}}{\sqrt{Re}}\{f'(0)\right.$$

$$+g_3''(0)\}+4g_3(0)\frac{T}{Re}+\frac{144}{\sqrt{\pi}}\left(1+\frac{4}{9\pi}-\frac{4\sqrt{2}}{3}\right)$$

$$\frac{T\sqrt{T}}{Re\sqrt{Re}}\Big]\sin^2\theta+\frac{8T\sqrt{T}}{3\sqrt{Re}}\Big[F_3'(0)+f_3'(0)\Big](1-\cos^2\theta) \qquad (10\text{-}2)$$

The square-root time singularity in the first term is due to the impulve start. The pressure coefficient is plotted in figure 8 for $Re=250$. We note in particular that the pressure is nearly uniform near the rear stagnation point of the cylinder. The larger the Reynold number, the larger the pressure near the stagnatlon point. In the limiting case, $Re\to\infty$, we have

$$C_p=f''(0)\ \sin\theta \qquad (10\text{-}3)$$

The pressure coefficient is identical to that of the potential flow as expected. See Batchelor (1970, P. 340).

11. Drag Coefficient

The most practical significant quantity is the total force exerted on the body by the fluid. Contributions to the total force are friction and pressure. The force due to the tangential stress is firction drag and that due to pressure is pressure drag.

The pressure drag coefficient is defined by

$$C_{dp}=-\int_0^\pi C_p\ \cos\theta d\theta \qquad (11\text{-}1)$$

where C_p is given by epuation (10-2). Integrating by parts, equation (11-1) becomes

$$C_{dp}=-\frac{2}{Re}\int_0^\pi\left(\frac{\partial\omega}{\partial\tau}\right)r_0\ \sin\theta d\theta \qquad (11\text{-}2)$$

Using the vorticity gradient on the cylinder surface, we have

$$C_{dp}=\frac{2\sqrt{\pi}}{\sqrt{Re}\sqrt{T}}+\frac{\pi}{Re}-\frac{47\sqrt{\pi}}{2}\frac{\sqrt{T}}{Re\sqrt{Re}}+\frac{4\pi T}{Re^2}+\frac{\pi T\sqrt{T}}{\sqrt{Re}}$$

$$\Big[F_3'(0)-3f_3'(0)\Big] \qquad (11\text{-}3)$$

The square-root singularity in time is again the result of the impulsive start nature of the cylinder motion. As stated in section 10, at the begining of the motion, the cylinder displaces the fluid on the surface of the cylinder with infinite acceleration. The cylinder experiences an infinite resistance of the fluid to its impulsive motion.

The frictional contribution to the drag coefficient is obtained as follows

$$C_{df}=\frac{4}{Re}\int_0^\pi(\omega)_{r_0}\ \sin\theta d\theta \qquad (11\text{-}4)$$

The skin friction drag is

$$C_{df}=\frac{2\sqrt{\pi}}{\sqrt{Re}\sqrt{T}}+\frac{\pi}{Re}+\frac{\sqrt{\pi}\sqrt{T}}{2Re\sqrt{Re}}-\frac{2\pi T}{Re^2}+\frac{\pi T\sqrt{T}}{\sqrt{Re}}\left[F_3'(0)-3f_3'(0)\right] \qquad (2\text{-}11\text{-}5)$$

At the start of the motion, there is a discontinuity in tangential velocity near the cylinder surface. This discontinuity causes an infinite shear stress and consequently gives rise to infinite skin friction drag as indicated by the first term in equation (11-5). After the start, the velocity jump near the cylinder surface spreads over the boundary layer because of the vorticity diffusion. The magnitude of the shear stress reduces and skin friction drag decreases.

Equation (11-3) and (11-5) show that the contribution of skin friction drag and pressure drag to the total drag are equal at the start of the motion. And the total drag coefficient is

$$C_d\sim\frac{4\sqrt{\pi}}{\sqrt{Re}\sqrt{T}} \qquad \text{as } t\to 0 \qquad (2\text{-}11\text{-}6)$$

By estimating the rate of decrease of momentum, Payne (1958) obtained exactly the same result.

The drag coefficient for various Reynolds number is plotted in Figure 9. It is essentially the same as that of Collins and Dennis (1973a).

Conclusion

The major objective of this study has been to solve the problem of the viscous flow field over an impulsively started circular cylinder. The singular behavior of fhe flow properties at the small time was treated by the analytic solution, using the method of matched asymptotic expansion to the third order. The expansion is valid for $T \ll 1$ and $Re \gg 1$ only. For later time, the solution will be continued by numerical integration.

To assure that the analytic solution is correct, the complicated mathematical operation is repeated with great care. In this study, we compare our results quantitatively with the existing solutions. The initial separation time, progression of separation point and the vorticity distribution on the surface of the cylinder agree with the computations of Collins and Dennis (1973a, b). Separation of the viscous layer starts at the rear stagnation point and progresses along the cylinder asymptotically to a steady separation angle. The higher the Reynolds number, the sooner the separation angle reaches its steady value.

The flow patterns, tangential velocity profiles and vorticity distribution over

the cylinder surface were plotted and studied at various time. By the figures, we can see the development of these flow properties.

REFERENCES

Bar-ley, M. (1974). "Impulsively Started Circular Cylinder," Ph.D. Dissertation, Department Aerospace Engineering, University of Southern California.

Bar-lev, M. and Yang, H. T. (1975). "Initial Flow Field Over an Impulsively Started Circular Cylinder," Journal of Fluid Mechanics, Vol. 72, Part 4, PP. 625-647.

Batchelor, G. K. (1970). **An Introduction to Fluid Dvnamics** University Press, Cambridge.

Belcher, R. J., Burggraf, O. R., Cooke, J. C., Robins, A. J. and Stewartson, K. (1972). **Recent Research on Unsteady Boundary Layers**, Vol. 2 (Ed. E. A. Eichlbrenner.) Laval University Press, Quebec.

Blasius, H. (1908). "Small Perturbation Solution of Boundary Layer," NACA TM, 1256, Washington, D.C.

Bryson, A. E. (1959). "Symmetic Vortex Separation on Circular Cylinders and Cones," Journal of Applied Mechanics, Vol. 26, PP. 643-648.

Carslaw, H. S. and Jagger, J. C. (1959). **Conduction of Heat in Solids**, Clarendon Press, Oxford.

Chien, L. C. (1977) "Impulsively Started Viscons Flow over a Cirulor Cylider," PH. D. Dissertation, Univerity of Soutern California.

Collins, W. M. and Dennis, S. C. R. (1973a). "The Initial Flow Past an Impulsively Started Circular Cylinder," Quarterly Journal of Mechanics and Applied Mathematics, Vol. 26, PP. 53-75.

Collins, W. M. and Dennis, S.C.R. (1973b). "Flow Past an Impulsively Started Circular Cylinder," Journal of Fluid Mechanics, Vol. 60, Part 1, PP. 105-127.

Crank, J. (1975). **The Mathematics of Diffusion**. Clarendon Press, Oxford.

Dennis, S. C. R. and Staniforth (1970). "Numerical Method for Calculating the Initial Flow Pass a Cylinder in a Viscous Fluid," in Proceedings of the Second International Conference on Numerical Methods in Fiuid Dynamics, (Ed. M. Holt), Springer-Verlag, New York.

Goldstein S, and Rosenhead, L. (1936). "Boundary Layer Growth," Proceedings of Cambridge Phylosphy Society, Vol. 32, PP. 392-401.

IBM (1970). **Scientific Subroutine Package**. GH20-0205-4, International Bussiness Machines Corporation, New York.

Mehta, U. B. and Lavan, Z. (1975). "Starting Vortex, Separaion Bubbles and Stall: A Numerical Study of Laminar Unsteady Flow Around an Airfoil," Journal of Fluid Mechanics, Vol. 67, Part 2, PP. 227-256.

Payne, R. B. (1958). "Calculation of Unsteady Viscous Flow Past a Circular Cylinder," Journal of Fluid Mechanics, Vol. 4, Part 1, PP. 81-86.

Proudman, I. and Johnson, K. (1962). "Boundary Layer Growth Near a Rear Stagnation Point," Journal of Fluid Mechanics, Vol. 12, Part 2, PP. 161-168.

Panikker, P. K. G. and Lavan, Z. (1975). "Flow Past Impultively Started Bodies Using Green's Function," Journal of Computational Physics, Vol. 18, PP. 46-65.

Rosenhead, L. (1963). **Laminar Boundary Layers**. Clarendon Press, Oxford.

Roache, P.J. (1975). "Recent Developments and Problem Areas in Computational Fluid Dynamics," in Lecture Notes in Mathematics, Vol. 461, Springer-Verlag, New York.

Roache, P. J. (1976). **Computaional Fluid Dynamics**. Hermosa Publishers, New Mexico.

Sarpkaya, T. (1963). "Lift Drag and Add Mass Coefficients for a Circular Cylinder Immersed in a Time Dependent Flow," Journal of Applied Mechanics, Vol. 30, PP. 13-15.

Sarpkaya, T. (1966). "Separated Flow about Lifting Bodies and Impulsive Flow about Cylinders," AIAA Journal, Vol. 4, PP. 414-420.

Sarpkaya, T. (1968). "An Analytic Study of Separated Flow Over Circular Cylinders," Journal of Basic Engineering, Vol. 90, PP. 511-518.

Schlichting, H. (1968). **Boundary Layer Theory**. McGraw- Hill, Now York.

Sears, W. R. and Telionis, D. P. (1975). "Boundary Separation in Unsteady Flow," SIAM Journal of Applied Mathematics, Vol. 28, PP. 215-235.

Son, J. S. and Hanratty. T. J. (1969). "Numerical Solution of Flow Around a Cylinder at Reynolds Number of 40, 200 and 500," Journal of Fluid Mechanics, Vol. 35, Part 2, PP. 369-386.

Terrill, R. M. (1960). "Laminar Boundary-Layer Flow Near Separation with and without Suction," Philosphy Transaction, Vol. A211, PP. 55-100.

Thoman, D. C. and Szewczyk, A. A. (1969). "Time-Dependent Flow over a Circular Cylinder," Physics of Fluids, Vol. 12, PP. II-76 to II-87.

Thwaites, B. (1960). **Incompressible Aerodynamics**. Clarendon Press, Oxford.

Van Dyke, M. (1975). **Perturbation Methods in Fluid Mechanics**. Parabolic

Press, Stanford, California.

Wang, C. Y. (1967). "The Flow Past a Circular Cylinder Which is Started from Rest," Journal of Mathemtics and Physics, Vol. 46, PP. 195-202.

Wang, C. Y. (1968) "A Note on the Drag of an Impulsively Started Cylinder," Journal of Mathematics and Physics, Vol. 47, PP. 451-455.

Wundt, H. (1955). "Washstum der Laminaren Grenzschicht an Schraeg Angestroemten Zylinder bei Anfahrt ous der Ruhe," Ingen. Arch. Vol. 23, PP. 212-230.

Yang, H. T. (1974). Impulse Flow Analogy of Slender Bodies at High Incidence, Naval Weapon Center, Technical Memorandom 2416, China Lake, California.

Yang, H. T. and Bar-lev, M. (1976). "Potential Flow Model for an Impulsively Started Cylinder," Journal of Applied Mechanics, Vol. 98, PP. 213-216.

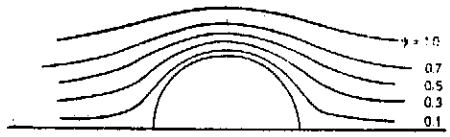

Figure 1(a) Flow Pattern at Re = 250 at T=0.1

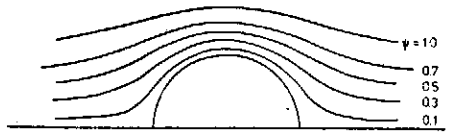

Figure 1(b) Flow Pattern at Re = 250 at T = 0.2.

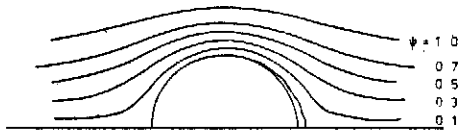

Figure 1(c) Flow Pattern at Re = 250 for T = 0.4

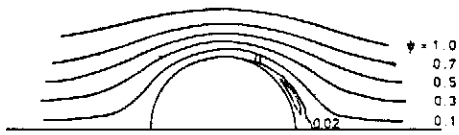

Figure 1(d) Flow Pattern at Re = 250 for T = 0.6.

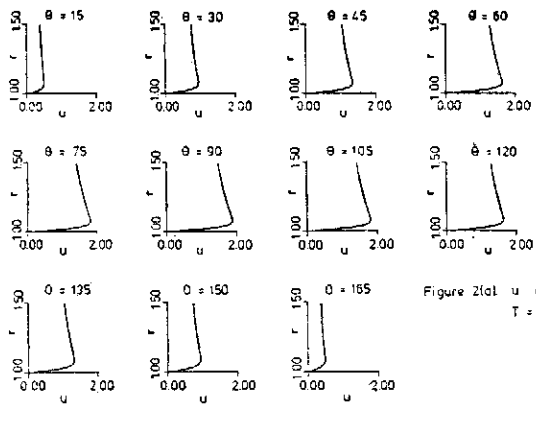

Figure 2(a) u at Re = 250
T = 0.1

Figure 2(b) u at Re = 250
T = 0.2

Figure 2(c) u at Re = 250
T = 0.3

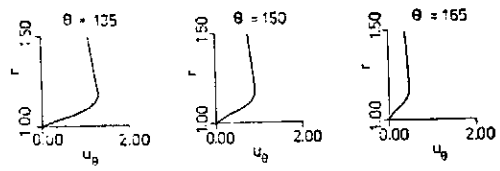

Figure 2(d) u_θ at Re = 250
T = 0.4

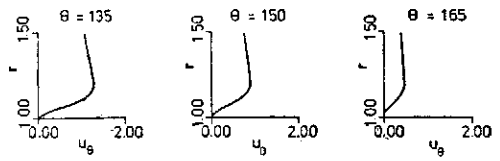

Figure 2(e) u_θ at Re = 250
T = 0.5

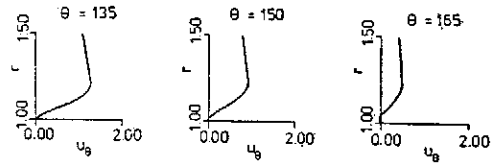

Figure 2(f) u_θ at Re = 250
T = 0.6

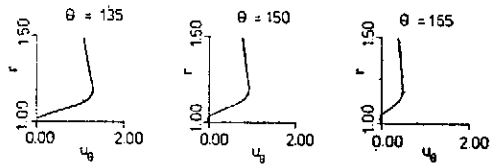

Figure 2(g) u_θ at Re = 250
T = 0.7

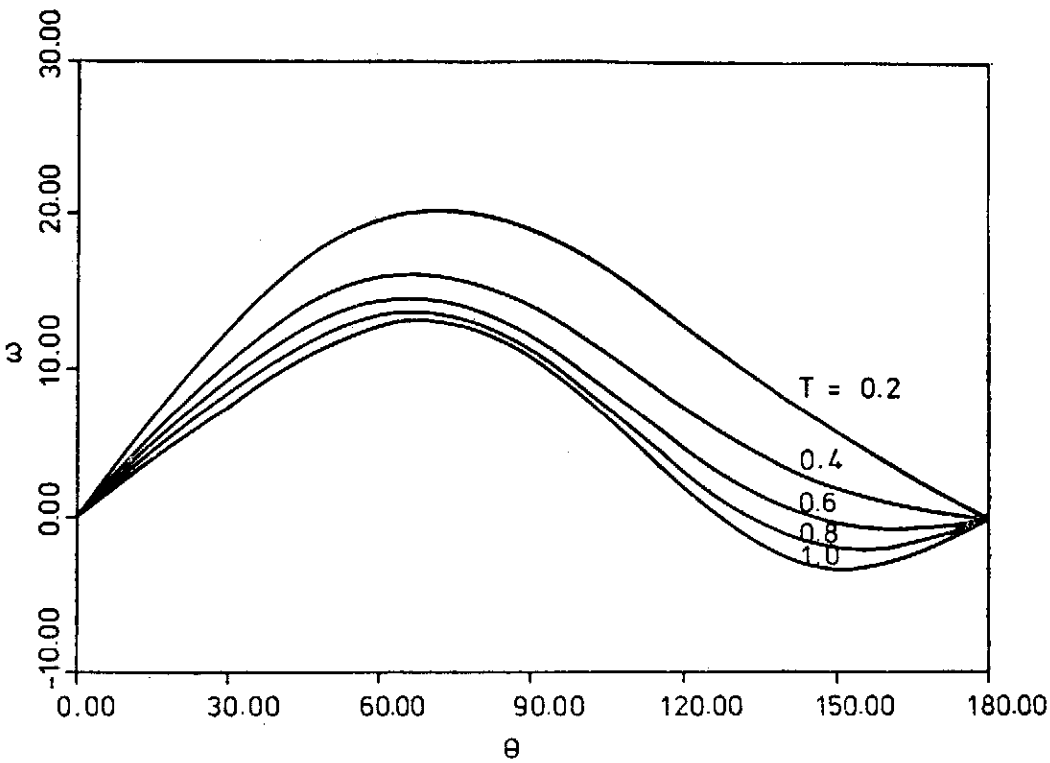

Figure 3. Vorticity Distribution on the Cylinder at Re = 50.

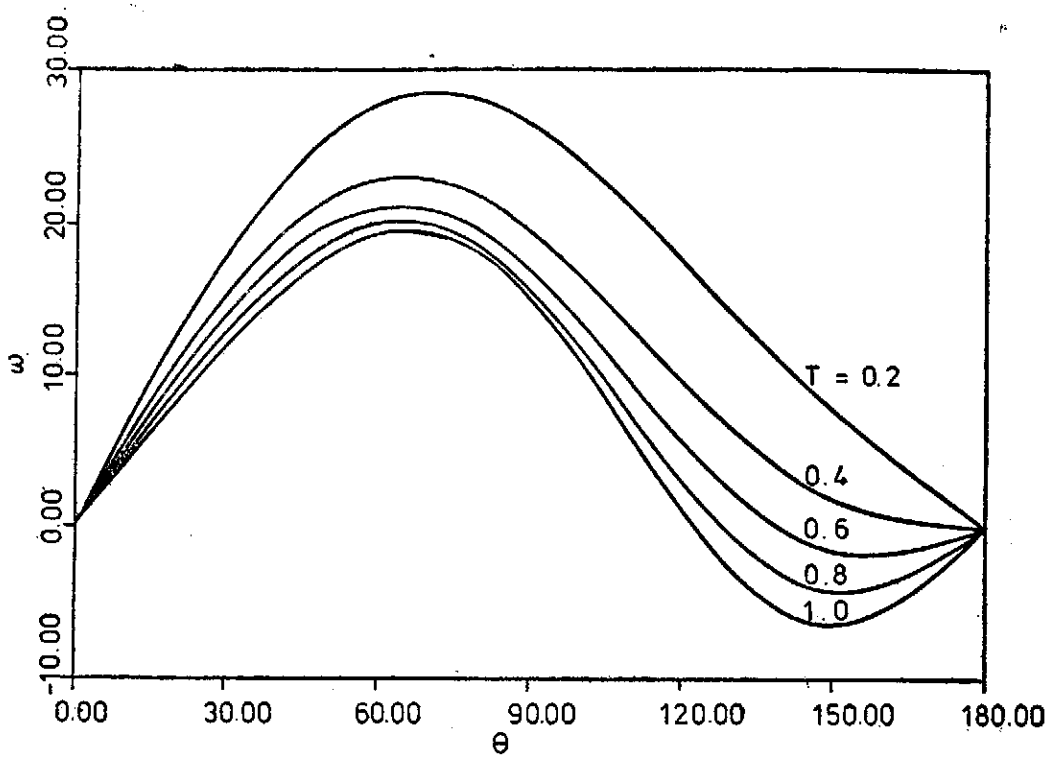

Figure 4. Vorticity Distribution on the Cylinder at Re = 100.

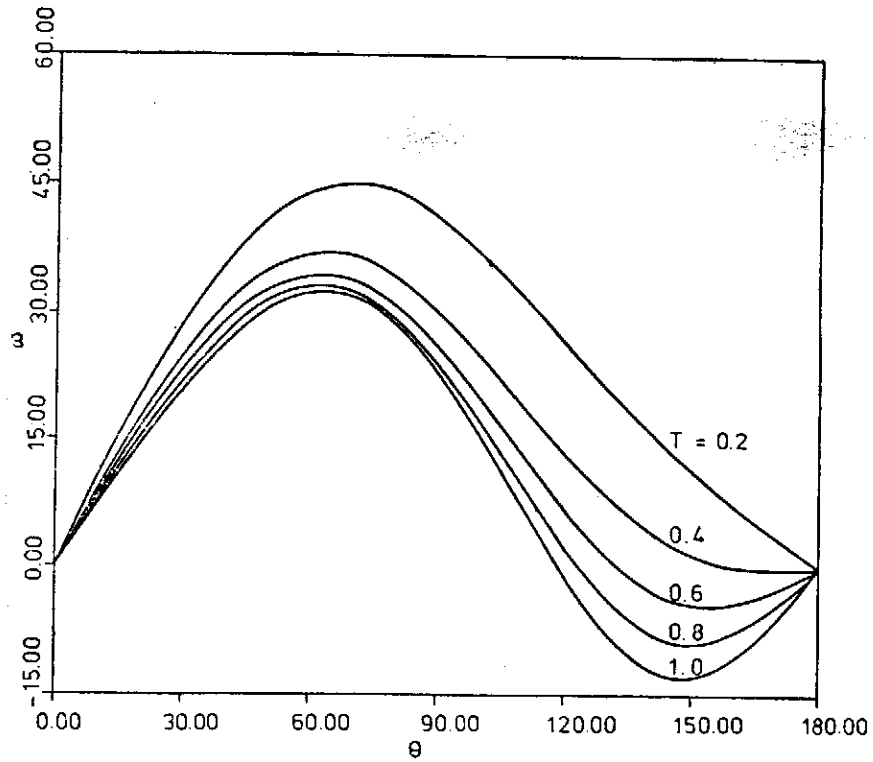

Figure 5. Vorticity Distribution on the Cylinder at Re = 250.

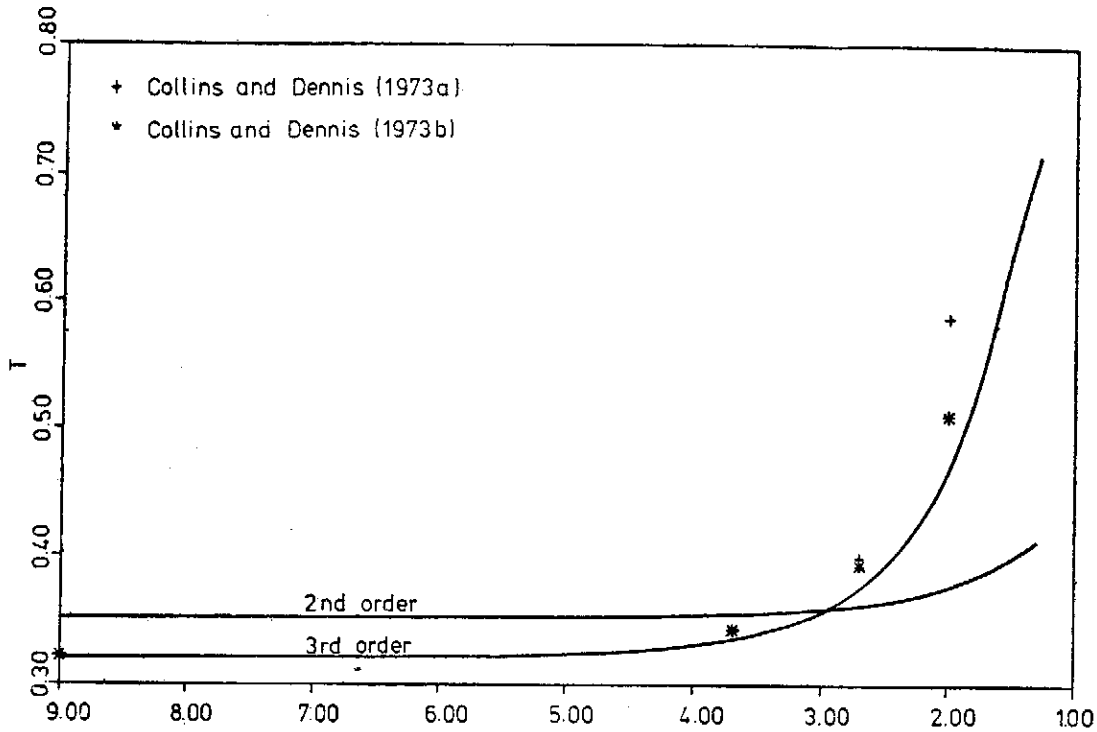

Figure 6. Variation of the Initial Separation Time with Re.

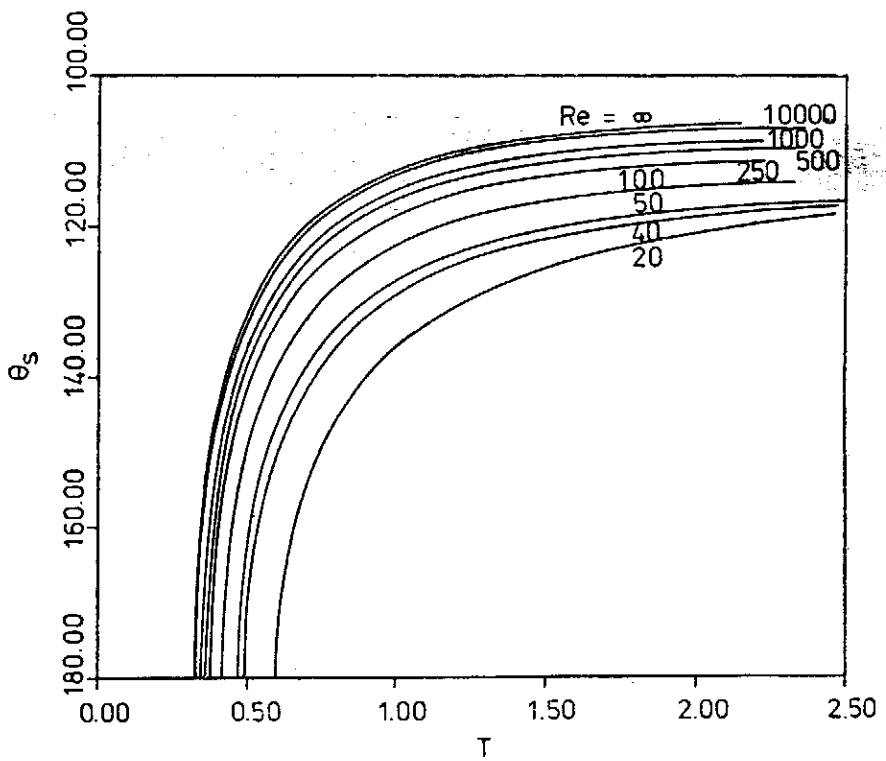

Figure 7. Progression fo Separation Time.

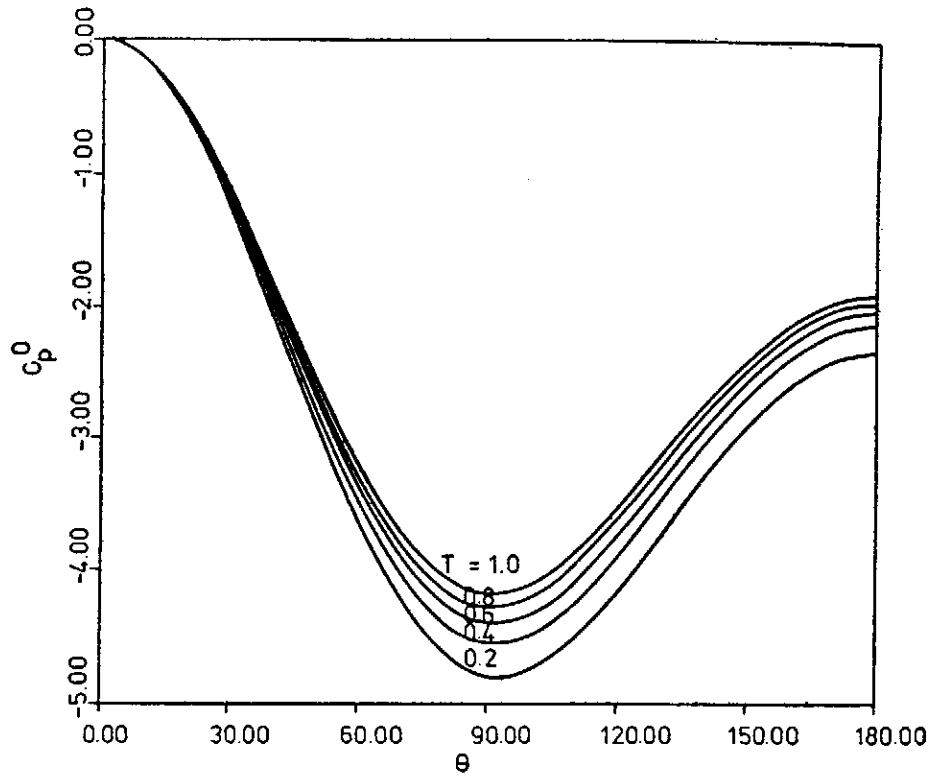

Figure 8. Pressure Coefficient at Re = 250.

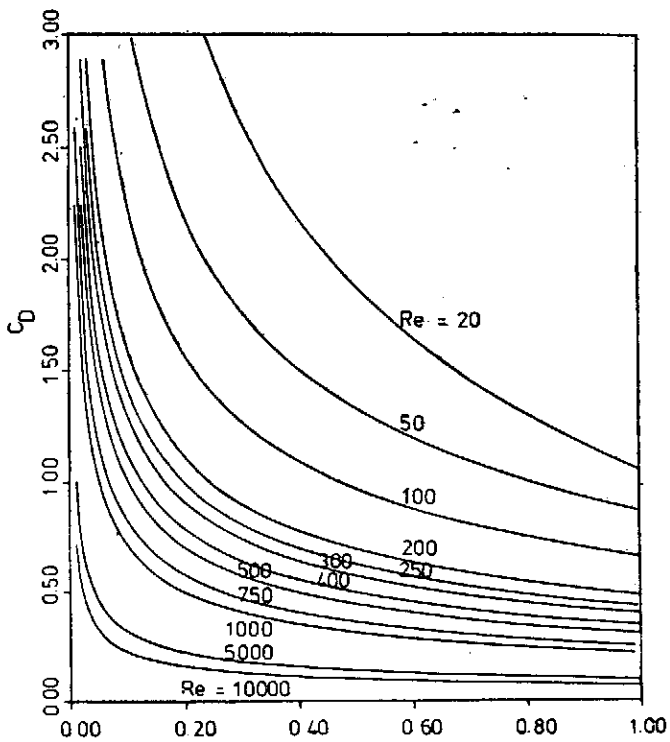

Figure 9. Drag Coefficient at Re = finite.

Annual Report of the Institute of Physics, Academia Sinica, Vol. 7, 1977

Analytic Solution of a Backward Boundary Layer Equation

H. T. Yang and L. C. Chien*

University of Southern California
Los Angeles, California

Analytic solution in terms of Weber parabolc cylinder function is presented for the backward boundary layer equation $f'''(\gamma)-ff''-f'^2+1=0$, subject to the boundary conditions $f(0)=-\gamma$, $f'(0)=0$, and $f'(\infty)=1$. The result agrees with new numerical solution obtained for $\gamma=0$ by employing an adaptive finite difference solver. Comparisons are also made with existing numerical solutions.

1. Introduction

In Rosenhead (1963) the solutions with similar velocity profiles of the steady two-dimensional boundary layer equations were treated. The governing ordinary differential equation is

$$f'''(\eta)+\alpha ff''+\beta(1-f'^2)=0 \tag{1}$$

subject to the boundary conditions

$$f(0)=\gamma/\alpha,\ f'(0)=0,\ f'(\infty)=1. \tag{2}$$

Here η is the similarity boundary layer ordinate, $f(\eta)$ the similarity stream function, $f'(\eta)$ the velocity, and $f''(\eta)$ the shear stress. The parameters α and β are related to the pressure gradient, and γ to the suction (considered positive) or blowing velocity. The case to be studied in the present work is $\alpha=-1$, $\beta=1$. (1) and (2) become:

$$f'''-ff''-f'^2+1=0 \tag{3}$$

$$f(0)=-\gamma,\ f'(0)=0,\ f'(\infty)=1 \tag{4}$$

After double integration, (3) reduces to a Riccati equation

$$f'-\tfrac{1}{2}f^2=-\tfrac{1}{2}\gamma^2+f''(0)\eta-\tfrac{1}{2}\eta^2 \tag{5}$$

subject to the boundary conditions

$$f'(0)=-\gamma,\ f'(\infty)=1. \tag{6}$$

A form of analytic solution in terms of parabolic cylinder function is indicated in Rosenhead,

*Present affiliation; Institute of Physics, Academia Sinica, Taiwan, Republic of China

$$f(\eta)=\gamma-2\frac{U'(a,\eta-A)}{U(a,\eta-A)} \tag{7}$$

where $a=\frac{1}{4}(\gamma^2-A^2)$, $A=f''(0)$. (8)

Without pursuing (7) further, numerical solution is given the last column of Table V.4 there.

Goldstein (1965), pointing out its application to flow in converging passages, showed that for (1) and (2) with $\alpha=-1$, $-\infty<\beta<2$, $\gamma=0$, there are no solutions satisfying the more stringent condition at infinity

$$\eta^N(f'-1)\longrightarrow 0 \qquad as\ \eta\longrightarrow\infty \tag{9}$$

for any real N. He also stated that with the less stringent condition $(2)_3$, an admissible solution could exist for which $\beta>0$.

Evans (1968) odtained numerical solution for (3) and (4) with $\gamma=0$ as shown in figure 6.2.

Burggarf, Stewartson, and Belcher (1971) studied the same system. Their equation (12) and boundary conditions are the same as (3) and (4) with $\gamma=0$ by noting their $\Psi(\eta)$ is the present $-f(\eta)$. Numerical solution is shown in their figure 2(a).

In the present work, analytic solution for (3) and (4) or equivalently (5) and (6) will be obtained in terms of parabolic cylinder function. The results will be compared with new numerical solution and existing ones reviewed above, all for $\gamma=0$.

2. Analytic Solution

The analysis parallels that of § 3 of Yang and Chien (1975), but with important differences. To solve (3) and (4), we transform the non-linear first order Riccati equation (5) to a linear second order parabolic cylinder equation (15). First, let

$$f(\eta)=-2\frac{u'(\eta)}{u(\eta)} \tag{10}$$

then (5) and (6) become

$$u''(\eta)-\tfrac{1}{2}[\tfrac{1}{2}\gamma^2-f''(0)\eta+\tfrac{1}{2}\eta^2]u=0 \tag{11}$$

$$\frac{u'(0)}{u(0)}=\frac{\gamma}{2},\quad \frac{u'(\infty)}{u(\infty)}=-\tfrac{1}{2}[\gamma^2-2f''(0)\eta+\eta^2+1]^{\frac{1}{2}} \tag{12}$$

The minus of the square root is taken because $f(\infty)>0$ in (10). Let

$$z=\eta-f''(0),\ z_0=-f''(0) \tag{13}$$

$$u(\eta)=w(z) \tag{14}$$

Then (11) and (12) transform into

$$w''(z)-(\tfrac{1}{4}z^2+a)w=0 \tag{15}$$

where $$a\equiv\tfrac{1}{4}\{\gamma^2-[f''(0)]^2\} \tag{8}$$

The general solution of (15) is

$$w(z)=c_1U(a,z)+c_2V(a,z) \tag{16}$$

Where the parabolic cylinder functions have the following asymptotic expansions, Abramowitz and Stegun (1972, p. 689)

$$U(a,z)\sim e^{-\frac{1}{4}z^2}z^{-a-\frac{1}{2}}\left[1-\frac{(a+\frac{1}{2})(a+3/2)}{2z^2}+\frac{(a+\frac{1}{2})(a+3/2)(a+5/2)(a+7/2)}{8z^4}\cdots\cdots\right] \tag{17}$$

$$V(a,z)\sim\sqrt{\frac{2}{\pi}}e^{\frac{1}{4}z^2}z^{a-\frac{1}{2}}\left[1+\frac{(a-\frac{1}{2})(a-3/2)}{2z^2}+\frac{(a-\frac{1}{2})(a-3/2)(a-5/2)(a-7/2)}{8z^4}+\cdots\right] \tag{17}$$

In view of the boundary condition $(12)_2$ at infinity and the asymptotic behavior of parabolic cylinder functions (17), we require

$$c_2=0.$$

The solution (10) then becomes, through (13) and (14)

$$f(\eta)=-2\frac{U'(a,\eta-A)}{U(a,\eta-A)} \tag{18}$$

where a and A given by (8) are to be determined. Comparing (18) with (7), we see that there is an extra constant term γ in the formal solution given in Rosenhead.

To pursue further the analytic solution, the major task is to determine $A=f''(0)$. By the recurrence relation Abramowitz and Stegun (1972, P. 688)

$$U'(a,z)=-\tfrac{1}{2}zU(a,z)-(a+\tfrac{1}{2})U(a+1,z) \tag{19}$$

and boundary condition $(12)_1$ We have

$$(2a+1)U(a+1,z_0)+(z_0+\gamma)U(a,z_0)=0 \tag{20}$$

where a is given by (8) and z_0 by $(13)_2$. For a given γ, $-z_0=f''(0)$ may be solved from (20). The relationship between $f''(0)$ and γ is plotted on the computer as shown in figure 1, see §3.

In evaluating parabolic cylinder functions, connection with confluent hypergeometric functions is utilized, Abramowitz and Stegun (1972, P. 691).

$$U(a,\pm z)=\frac{\pi^{\frac{1}{2}}2^{-\frac{1}{4}-\frac{1}{2}a}e^{\frac{1}{2}z^2}}{\Gamma(3/4+\frac{1}{2}a)}M(\tfrac{1}{2}a+\tfrac{1}{4},\tfrac{1}{2},\tfrac{1}{2}z^2)\pm\frac{\pi^{\frac{1}{2}}2^{\frac{1}{4}-\frac{1}{2}a}ze^{-\frac{1}{4}z^2}}{\Gamma(\frac{1}{4}+\frac{1}{2}a)}M(\tfrac{1}{2}a+3/4,3/2,\tfrac{1}{2}z^2) \tag{21}$$

The confluent hypergeometric funcion $M(a,b,z)$ is already programmed in the work of Yang and Chien (1975). For $|z|>2\sqrt{|a|}$ and $|z|>5$, the asymptotic expansion formula (17) has been employed.

3. Velocity Profiles

For a given value of γ, $A=f''(0)=-z_0$ and $a=\frac{1}{4}(\gamma^2-A^2)$ is to be determined from (20) as shown in figure 1. For example,

$$\begin{aligned} \gamma&=0 && f''(0)=1.08637574 \\ &=\sqrt{2} && =1.98064050 \\ &=-\sqrt{2} && =0.57495317 \end{aligned} \tag{22}$$

From(8) a and A are obtained. The stream function $f(\eta)$ is computed from the analytic solution (18) and the velocity profile $f'(\eta)$ from (5). From (18), (19), (17), and (5), it is seen that

$$f'(\eta)\sim 1-\tfrac{1}{2}\{\gamma^2+2-[f''(0)]^2\}\frac{1}{\eta^2}+\cdots \tag{23}$$

The findings of Goldstein (1965) are confirmed, i. e., the boundary condition $(6)_1$ is satisfied by algebraic approach. There are no solutions satisfying the exponential approach (9).

From (23), if the free-stream velocity is to be approached from below, it is required that

$$f''(0)<\sqrt{\gamma^2+2} \tag{24}$$

In figure 1 for $-4<\gamma<4$, we show only that $f''(0)$ which satisfies (24). In this sense, the solution is unique, if one imposes the side condition

$$f'(\eta)<1 \qquad \text{for} \qquad 0<\eta<\infty \tag{25}$$

The velocity profiles for the three different values of γ in (22) are plotted as shown in figure 2. All three velocity profiles approach the free-stream value from below algebraically. The suction will steepen the profile, increase skin friction and decrease displacement thickness, while blowing will have the opposite effect.

4. Comparison with Numerical Solutions

New numerical solution to the nonlinear ordinary differential equation (3) subject to the boundary conditions with $\gamma=0$

$$f(0)=0, f'(0)=0, f'(12)=0.99665841 \tag{26}$$

was obtained by V. Pereyra employing an adaptive finite difference solver for nonlinear two point boundary problems with mild boundary layers. See Lentini and Pereyra (1977). The third value in (26) is supplied from analytic solution. The number of mesh points in this range $0\leq\eta\leq12$ is 79. The analytic solution and the new numerical solution agree with each other to six significant figures as shown in Table 1. Also shown are the existing numerical solutions in

Rosenhead (1963, p. 250, last column of Table V.4), Evans (1968, p. 73, Fig. 6.2, $\beta=1.0$), and Burggarf, Stewartson, and Belcher (1971, p. 1827, Fig. 2, Limit). It is seen the agreement between the present analytic result and the numerical solution of Terrill in Rosenhead is excellent.

5. Conclusion

In boundary layer theory, analytic solutions are of rare occurence. In the present work, analytic solutions to the backward layer equation (3) and boundary conditions (4) are found for any γ in terms of parabolic cylinder functions. These solutions parallel those found recently to the Falkner-Skan equation for $\beta=-1$ and $\gamma\geq 0$ by Yang and Chien (1975).

The analytic result for $\gamma=0$ agrees with new numerical solution obtained by Pereyra. They both agree with that of Terrill in Rosenhead. Comparison is made with other existing numerical solutions.

Acknowledgement

The authors wish to thank professor V. Pereyra for obtaining numerical solutions to the present problem employing his adaptive finite difference solver.

REFERENCES

Abramowitz, M. & Stegun, I. A., 1972, Handbook of Mathematical Functions. Washington, D. C.: U. S. Government printing Office

Burggraf, O. R., Stewartson, K. & Belcher, R., 1971, phys. Fluids. 14, 1821.

Evans. H. L., 1968, Laminar Boundary-Layer Theory. Reading: Addison-Wesley.

Goldstein, S., 1965, J. Fluid Mech. 21, 33.

Lentini, M. & Pereyra, V., 1977, SIAM J.Numer. Anal., 14,

Rosenhead, L., 1963, Laminar Boundary Layer. Oxford: Clarendon press.

Yang, H. T. & Chien, L. C., 1975, SIAM J. Appl. Math., 29, 558.

CAPTION OF FIGURES

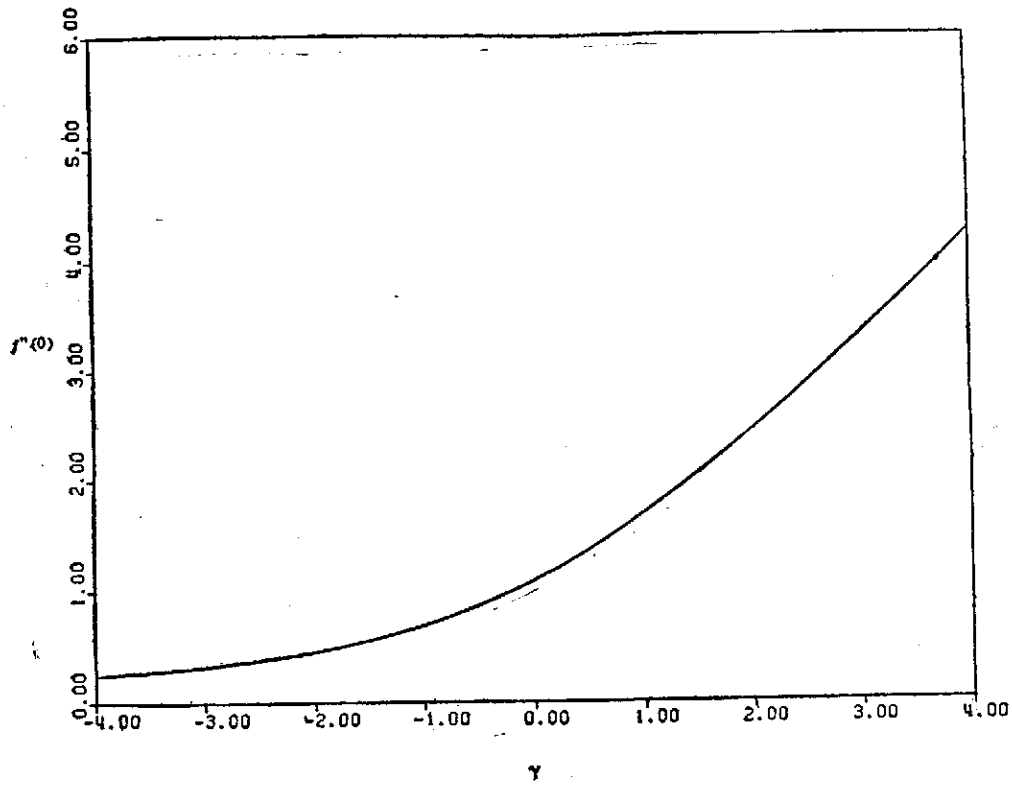

Figure 1 Variation of $f''(0)$ with γ.

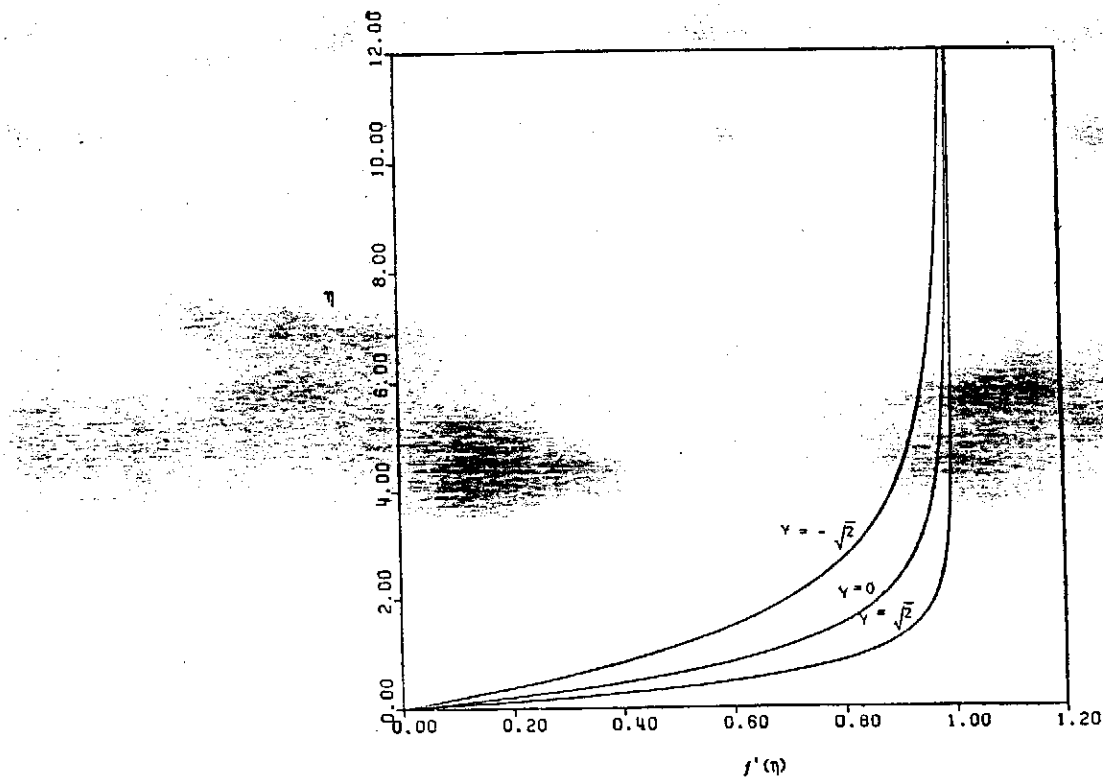

Figure 2 Velocity profiles for three γ's.

TABLE 1

COMPARISON BETWEEN ANALYTIC SOLUTION AND NUMERICAL SOLUTIONS FOR $\gamma=0$

η	$f'(\eta)$			
	Rosenhead	Evans	Burggraf et al	Analytic
0	0	0	0	0
0.1	0.104	0.153	0.103	0.103651
0.2	0.197	0.274	0.163	0.197483
0.3	0.282	0.349	0.214	0.281900
0.4	0.357	0.435	0.271	0.357476
0.5	0.425	0.529	0.393	0.424878
0.6	0.485	0.598	0.471	0.484821
0.7	0.538	0.685	0.535	0.538022
0.8	0.585	0.716	0.593	0.585178
0.9	0.627	0.748	0.650	0.626946
1.0	0.664	0.784	0.721	0.663934
1.2	0.726	0.848	0.743	0.725729
1.4	0.774	0.895	0.786	0.774350
1.6	0.813	0.930	0.814	0.812789
1.8	0.843	0.955	0.831	0.843362
2.0	0.868	0.974	0.871	0.867849
2.4	0.904	0.989	0.907	0.903668
2.8	0.928	0.999	0.928	0.927687
3.2	0.944	1.000	0.943	0.944280
3.6	0.956	1.000	0.957	0.956067
4.0	0.956	1.000	0.971	0.964658
4.4	0.971	1.000	0.974	0.971065
4.8	0.976	1.000	0.978	0.975944
5.2	0.980	1.000	0.981	0.979729
5.6	0.983	1.090	0.984	0.982714
6.0	0.985	1.000	0.985	0.985104
6.4	0.986		0.986	0.987044
6.8			0.987	0.988637
7.2			0.988	0.989959
7.6			0.989	0.991068
8.0			0.990	0.992006
8.4			0.991	0.992806
8.8			0.992	0.993494
9.2			0.993	0.994089
9.1			0.994	0.994607
9.6			0.995	0.995060
10.0				

Annual Report of the Institute of Physics, Academia Sinica, Vol. 7, 1977

原始方程式預報模式之研究*

—模式之建立—

蕭 錫 璋

摘 要

本文將日本氣象廳現行的原始方程式模式引進，用之於東南亞地區。文中數值模式爲通量形式（Flux form）的原始方程式模式。其垂直坐標爲 Sigma 坐標（Phillip, 1957）。預測的應變數（Dependent variable）包括水平風場、氣溫場、地表壓力和比濕。垂直速度場是由連續方程式經診斷求得（Calculated diagnostically）。各變數在空間交錯分佈（Staggered in space）。邊界條件爲設 $V_{normal}=0$ 及 $\frac{\partial\theta}{\partial t}=\frac{\partial q}{\partial t}=0$。爲簡便起見，文中暫不考慮加熱、摩擦和擴散等作用之影響。使用1975年梅雨末期的氣象資料作24小時的預測研究。其時間積分採 Euler-backward 及 Leap-frog 方法合併使用。

24小時的計算結果相當穩定，可見其在有限區域內的計算是可行的。本模式能够方便地求得地表壓力的變化，其結果合理。由於是絕熱系統，700mb 以下的天氣系統受加熱作用影響較大，故其計算結果較差。700mb 以上的計算結果較好。

本文並用相同的氣象資料，以P坐標原始方程式模式（非絕熱系）作24小時的探討，其結果良好。

1. 引 言

由於電子計算機及各種數值模擬方法之發展，許多國家數值天氣預報已被廣泛採用爲日常作業，而且數值天氣預報之模式也不斷地研究與改進，以適合當時、當地之需要。

數值天氣預報始於英人 L. F. Richardson，可惜由於觀測資料之不足，以及由聲波與重力波所引起的數值不穩定問題，使他的嘗試終歸失敗，也使得爾後許多年中數值預報不再爲人所試。直至一九四八年 J. G. Charney 證明大氣運動之動力方程式可藉由流體靜力及地轉假設濾去聲波及重力波而簡化之。此即爲準地轉模型之基礎。在許多試驗中顯示出此模型在中緯度地區約可得10～20%以內的準確度。近年來由於準確度之要求日益增高，準地轉模型已不敷應用。更有進者，若欲使用此模型於低緯度地區，由於地轉假設不佳，流線函數需從頗爲複雜之平衡方程式求得，使求解過程耗時耗力，就所耗之時間，所遭遇之困擾與所得之準確度相較，顯得頗不經濟。近年來由於數值模擬方法之發展，短波之壓制及時間積分之穩定問題已可初步解決，原始方程式模式之數值預報乃應運而生。

在原始方程式模式中，仍假設大氣運動合乎流體靜力穩定近似，因此等壓坐標仍然可用，此坐標有下列諸優點：

(1)一般氣象資料皆在等壓面上。

(2)連續方程式之形態極爲簡單。

(3)大氣密度不顯然出現。

(4)聲波完全被濾去。

只是這些優點因地表邊界條件之困擾而大爲失色，此缺點在 σ 坐標內不復出現。在 σ 坐標中，垂直坐標 σ 的定義爲

* 本文承行政院國家科學委員會支助完成，謹致謝意。

$$\sigma \equiv (P-P_T)/(P_S-P_T)$$

此處P爲壓力，P_T及 P_S 分別表示大氣層頂及地表之壓力。其中很自然地就包括了地表邊界層的情況在內。

本文將日本現行之原始方程式模式引進（Itoo, 1971），爲限於計算機容量及經費，先以東南亞地區爲計算範圍，作有限區域24小時的絕熱計算，與本所設計的P坐標原始方程式模式之計算結果作一比較，並將逐步修正，使合乎此區特有的地理環境、天氣型態，期能供實際預報作業之用。

2. 基本方程式

σ 坐標系統能够自然，方便地考慮地形的效應。在此σ的定義如下：

$$\sigma \equiv (P-P_T)/(P_S-P_T) \tag{2.1}$$

P爲壓力，P_T 爲模式中大氣層頂之壓力，在此設爲 100mb，P_S 爲地表面之壓力。

本文所使用的基本方程式包括運動方程式，流體靜力方程式、連續方程式、熱力方程式、水汽方程式及狀態方程式，分別如下：

$$\begin{aligned}
&\left(\frac{\partial}{\partial t}+\boldsymbol{V}\cdot\nabla+\dot{\sigma}\frac{\partial}{\partial\sigma}\right)\boldsymbol{V}+f\boldsymbol{K}\times\boldsymbol{V}+\left(\nabla-\frac{\sigma}{\pi}\nabla\pi\frac{\partial}{\partial\sigma}\right)\phi+F=0\\
&\frac{\partial\phi}{\partial\sigma}+\pi\alpha=0\\
&\frac{\partial\pi}{\partial t}+\nabla\cdot(\pi\boldsymbol{V})+\frac{\partial}{\partial\sigma}(\pi\dot{\sigma})=0\\
&\left(\frac{\partial}{\partial t}+\boldsymbol{V}\cdot\nabla+\dot{\sigma}\frac{\partial}{\partial\sigma}\right)\theta=\frac{\theta}{C_pT}(Q+D_T)\\
&\left(\frac{\partial}{\partial t}+\boldsymbol{V}\cdot\nabla+\dot{\sigma}\frac{\partial}{\partial\sigma}\right)q=E-M\\
&\theta-(P_0^{\kappa}/R)(\pi\sigma+P_T)^{1/\gamma}\alpha=0
\end{aligned} \tag{2.2}$$

其中$\boldsymbol{V}$爲風速（向量），$\boldsymbol{K}$爲垂直方向單位向量，ϕ爲重力高度場。

F表示摩擦力，α爲比容，$\dot{\sigma}$爲σ坐標上的垂直風速；θ爲位溫，T爲氣溫，C_P爲等壓比熱，Q爲加熱率，D_T爲溫度由於 sub-grid eddies 所造成的水平擴散。

q爲比濕（specific humidity），E爲水汽擴散，M爲凝結率。

P_0爲1000mb，R爲氣體常數。

爲使定差過程（differencing scheme）的動量守恒，運動方程式中不用$\boldsymbol{V}$作 dependent variable，而用$\pi\boldsymbol{V}$，其法爲（$2\cdot3_3$）式乘上$\boldsymbol{V}$，（$2\cdot2_1$）式乘上π，再相加，即得x,y二分量上之水平運動方程式：

$$\begin{aligned}
\frac{\partial}{\partial t}\left(\frac{\pi u}{m^2}\right)=&-\frac{\partial}{\partial x}\left(\frac{\pi u}{m}u\right)-\frac{\partial}{\partial y}\left(\frac{\pi v}{m}u\right)-\frac{\partial}{\partial\sigma}\left(\frac{\pi\dot{\sigma}}{m^2}u\right)\\
&+\frac{\pi v}{m^2}\left[f-\left(v\frac{\partial m}{\partial x}-u\frac{\partial m}{\partial y}\right)\right]\\
&-\frac{\pi}{m}\left(\frac{\partial\phi}{\partial x}-\frac{\sigma}{\pi}\frac{\partial\phi}{\partial\sigma}\frac{\partial\pi}{\partial x}\right)+\frac{\pi}{m^2}F_x
\end{aligned} \tag{2.3}$$

$$\begin{aligned}
\frac{\partial}{\partial t}\left(\frac{\pi v}{m^2}\right)=&-\frac{\partial}{\partial x}\left(\frac{\pi u}{m}v\right)-\frac{\partial}{\partial y}\left(\frac{\pi v}{m}v\right)-\frac{\partial}{\partial\sigma}\left(\frac{\pi\dot{\sigma}}{m^2}v\right)\\
&-\frac{\pi u}{m^2}\left[f-\left(v\frac{\partial m}{\partial x}-u\frac{\partial m}{\partial y}\right)\right]\\
&-\frac{\pi}{m}\left(\frac{\partial\phi}{\partial y}-\frac{\sigma}{\pi}\frac{\partial\phi}{\partial\sigma}\frac{\partial\pi}{\partial y}\right)+\frac{\pi}{m^2}F_y
\end{aligned} \tag{2.4}$$

其中m爲地圖投影放大因子，F_x, F_y爲摩擦力在x, y方向上之分量，同理連續方程式可寫爲

$$\frac{\partial}{\partial t}\left(\frac{\pi}{m^2}\right)=-\frac{\partial}{\partial x}\left(\frac{\pi u}{m}\right)-\frac{\partial}{\partial y}\left(\frac{\pi v}{m}\right)-\frac{\partial}{\partial \sigma}\left(\frac{\pi \dot{\sigma}}{m^2}\right) \tag{2.5}$$

熱力方程式可寫爲

$$\begin{aligned}\frac{\partial}{\partial t}\left(\frac{\pi}{m^2}T\right)=&-\frac{\partial}{\partial x}\left(\frac{\pi v}{m}T\right)-\frac{\partial}{\partial y}\left(\frac{\pi v}{m}T\right)-\frac{\partial}{\partial \sigma}\left(\frac{\pi \dot{\sigma}}{m^2}T\right)\\&+\frac{\sigma}{C_p}\pi\alpha\left[\frac{\partial}{\partial t}\left(\frac{\pi}{m^2}\right)+\frac{u}{m}\frac{\partial \pi}{\partial x}+\frac{v}{m}\frac{\partial \pi}{\partial y}\right]\\&+\frac{1}{C_p}\left(\frac{\pi^2\alpha\dot{\sigma}}{m^2}+\frac{\pi}{m^2}D_T+\frac{\pi}{m^2}Q\right)\end{aligned} \tag{2.6}$$

水汽方程式可寫爲

$$\begin{aligned}\frac{\partial}{\partial t}\left(\frac{\pi}{m^2}q\right)=&-\frac{\partial}{\partial x}\left(\frac{\pi u}{m}q\right)-\frac{\partial}{\partial y}\left(\frac{\pi v}{m}q\right)-\frac{\partial}{\partial \sigma}\left(\frac{\pi \dot{\sigma}}{m^2}q\right)+\frac{\pi}{m^2}M\\&+\frac{\pi}{m^2}E\end{aligned} \tag{2.7}$$

爲簡便起見，本文暫不考慮加熱、摩擦等作用；爲一絕熱系統，同時爲探討綜觀幅度 (synoptic scale) 天氣系統的變化，吾人也暫不考慮 subgrid eddies 所造成的擴散作用。

3. 邊界條件

在地表，垂直風速$\dot{\sigma}$爲零，並假設模式在大氣層頂的垂直風速$\dot{\sigma}$也爲零，即

$$\dot{\sigma}=0 \qquad at\ \sigma=1\ and\ 0 \tag{3.1}$$

由此條件對 (2.5) 式作垂直積分（地表至大氣層頂），可得地表壓力趨勢方程式：

$$\frac{\partial}{\partial t}\left(\frac{\pi}{m^2}\right)=-\int_0^1\left[\frac{\partial}{\partial x}\left(\frac{\pi u}{m}\right)+\frac{\partial}{\partial y}\left(\frac{\pi v}{m}\right)\right]d\sigma \tag{3.2}$$

又由 (2.5) 式及 (3.2) 式，可估計垂直風速$\dot{\sigma}$

$$\frac{\pi\dot{\sigma}}{m^2}=-\sigma\frac{\partial}{\partial t}\left(\frac{\pi}{m^2}\right)-\int_0^\sigma\left[\frac{\partial}{\partial x}\left(\frac{\pi u}{m}\right)+\frac{\partial}{\partial y}\left(\frac{\pi v}{m}\right)\right]d\sigma \tag{3.3}$$

側向邊界條件爲假設垂直 (Normal) 於邊界的風爲零，即

$$V_{normal}=0 \qquad at\ the\ lateral\ boundary \tag{3.4}$$

又因爲絕熱系統，故設

$$\frac{\partial\theta}{\partial t}=\frac{\partial q}{\partial t}=0 \qquad at\ the\ lateral\ boundary \tag{3.5}$$

由於此濕 q 隨着高度減少得很快，吾人假設在上兩層的比濕幾近於零，而不予計算。

在上述方程式中，(3.2)，(2.3)，(2.4)，(2.6)，(2.7) 爲預報方程式，可計算π, u, v, T和q在下一時刻之值。而 (2.2_2)，(3.3) 式爲診斷方程式，可得$\phi, \dot{\sigma}$之診斷值 (diagnostic value)。

4. 運算範圍及網格結構

本文所探討的水平範圍在北緯10度和55度，東經85度和150度之間，如圖一所示。採用蘭勃特正角錐投影主要參考點在北緯30度，東經120度。在此區域中，東西方向分作19個網格點，南北方向分作20個網格點。網格點間之距離 d 爲240公里。

由於定差法係採用 Arakawa (Langlois, 1969) 之方法，其水平格子結構與該法相同。各變數在空間上爲相互交錯的 (Staggered)。π, ϕ, T, q, m, f 置於網格點上，u, v 置於網格中央（如圖二），垂直

方向分作四層，將σ八等分，頂端爲 $P_T=100mb$。u,v,ϕ 置於 $\sigma=1/8,3/8,5/8,7/8$ 四層，π,ϕ_s 分別指地表壓力變化和地表地形高度。溫度 T 於 $\sigma=0.5/8,2/8,4/8,6/8,7.5/8$ 五層。比濕 q 置於 $\sigma=4/8,6/8,7.5/8$三層，$\dot{\sigma}$ 置於 $\sigma=2/8,4/8,6/8$ 三層（如圖三）。

5. 控制方程式之定差式

將控制方程式改寫爲定差式時，必須使能量守恒。且基於圖二，圖三之網格結構，參考 Arakawa (Langlois, 1969) 之方法，可將定差式寫爲下列形式（絕熱，無摩擦）：

運動方程式：（在 $\phi=1/8,3/8,5/8,7/8$ 四層）

$$-\frac{\partial}{\partial t}u^*_{i,j,K}+Div_1(v^*u)_{i,j,K}+\frac{1}{\Delta\sigma}(u^*_{i,j,K+1}\dot{\sigma}_{i,j,K+1}-u^*_{i,j,K-1}\dot{\sigma}_{i,j,K-1})$$
$$+v^*_{i,j,K}\{f_{i,j}-[v_{i,j,K}(D_xm)_{i,j}-u_{i,j,k}(D_ym)_{i,j}]\}+G_x(\pi,\alpha,\phi)_{i,j,k}=0 \qquad (5.1)$$

$$-\frac{\partial}{\partial t}v^*_{i,j,k}+Div_1(v^*v)_{i,j,K}+\frac{1}{\Delta\sigma}(v^*_{i,j,K+1}\dot{\sigma}_{i,j,K+1}-v^*_{i,j,K-1}\dot{\sigma}_{i,j,K-1})$$
$$u^*_{i,j,k}\{f_{i,j}-[v_{i,j,K}(D_xm)_{i,j}-u_{i,j,K}(D_ym)_{i,j}]\}+G_y(\pi,\alpha,\phi)_{i,j,K}=0 \qquad (5.2)$$

其中 $\sigma=2/8,4/8,6/8$ 上的 u,v 可由 $\sigma=1/8,3/8,5/8,7/8$ 上的 u,v 作線性內插。

$$u^*_{i,j,k}=\frac{\bar{\pi}_{i,j}}{(\bar{m}_{i,j})^2}u_{i,j,k}$$
$$v^*_{i,j,k}=\frac{\bar{\pi}_{i,j}}{(\bar{m}_{i,j})^2}v_{i,j,k}$$
$$\bar{\pi}_{i+\frac12,j+\frac12}=\frac14(\pi_{i+1,j}+\pi_{i+1,j+1}+\pi_{i,j}+\pi_{i,j+1}) \qquad (5.3)$$
$$\bar{m}_{i+\frac12,j+\frac12}=\frac14(m_{i+1,j}+m_{i+1,j+1}+m_{i,j}+m_{i,j+1})$$

(5.2) 式中定差運算 Div_1,D_x,D_y,G_x,G_y 之定義分別如下 (Itoo, 1971)（參見圖四）

$$Div_1(V^*u)_{00}=1/6/d[(u^*_{1,\frac12}+u^*_{1,-\frac12}+u^*_{0,\frac12}+u^*_{0,-\frac12})(u_{1,0}+u_{00})$$
$$-(u^*_{0,\frac12}+u^*_{0,-\frac12}+u^*_{-1,\frac12}+u^*_{-1,-\frac12})(u_{0,0}+u_{-1,0})$$
$$+(v^*_{\frac12,0}+v^*_{-\frac12,0}+v^*_{\frac12,1}+v^*_{-\frac12,1})(u_{0,0}+u_{0,1})$$
$$-(v^*_{\frac12,-1}+v^*_{-\frac12,-1}+v^*_{\frac12,0}+v^*_{-\frac12,0})(u_{0,-1}+u_{0,0})]$$
$$+1/24/d[\{(u^*_{0,\frac12}+u^*_{1,\frac12}+u^*_{\frac12,1}+u^*_{\frac12,0})-(u^*_{0,\frac12}+v^*_{-\frac32,1}+u^*_{1,-\frac12}+v^*_{\frac32,0})\}$$
$$\times(u_{1,1}+v_{0,0})-\{(u^*_{-1,-\frac12}+u^*_{0,-\frac12}+v^*_{-\frac12,0}+v^*_{-\frac12,-1})-(u^*_{-1,\frac12}+v^*_{-\frac32,0}$$
$$+u^*_{0,-\frac32}+v^*_{-\frac12,-1})\}(u_{-1,-1}+u_{0,0})+\{(v^*_{-\frac12,1}-u^*_{0,\frac12}+v^*_{-\frac12,0}-v^*_{-\frac12,1})$$
$$-(v^*_{\frac12,1}-u^*_{0,\frac32}-u^*_{-1,\frac12}+v^*_{-\frac32,0})\}(u_{-1,1}+u_{0,0})-\{v^*_{\frac12,0}+v^*_{\frac12,-1}-u^*_{0,-\frac12}$$
$$-u_{1,-\frac12})-(v^*_{\frac32,0}-u^*_{1,\frac12}+v^*_{-\frac12,-1}-u^*_{0,-\frac32})\}(u_{1,1}+u_{0,0})$$
$$-(u^*_{1,\frac12}+u^*_{1,-\frac12})(u_{2,0}+u_{0,0})+(u^*_{-1,\frac12}+u^*_{-1,-\frac12})(u_{0,0}+u_{-2,0})$$
$$-(v^*_{\frac12,1}+v^*_{-\frac12,1})(u_{0,2}+u_{0,0})+(v^*_{\frac12,-1}+v_{-\frac12,-1})(u_{0,0}+u_{0,-2})] \qquad (5.4)$$

其中

$$u^*_{0,\frac12}=\frac14[(\frac{u}{m})_{0,1}+(\frac{u}{m})_{0,0}](\pi_{\frac12,\frac12}+\pi_{-\frac12,\frac12})$$
$$v^*_{\frac12,0}=\frac14[(\frac{v}{m})_{1,0}+(\frac{v}{m})_{0,0}](\pi_{\frac12,\frac12}+\pi_{\frac12,-\frac12})$$
$$(D_xm)_{i+\frac12,j+\frac12}=\frac{1}{2d}(m_{i+1,j+1}+m_{i+1,j}-m_{i,j+1}-m_{i,j})$$
$$(D_ym)_{i+\frac12,j+\frac12}=\frac{1}{2d}(m_{i,j}+m_{i+1,j}-m_{i,j+1}-m_{i+1,j+1}) \qquad (5.5)$$

Pressure gradient force:

$$G_x(\pi,\alpha,\phi)_{i+\frac{1}{2},\,j+\frac{1}{2},\,K}=\frac{1}{4d}\,\frac{1}{\overline{m}_{i,j}}\Big[\{(\pi_{i,j}+\pi_{i+1,j})(\phi_{i+1,j,K}-\phi_{i,j,K})$$
$$+(\pi_{i,j+1}+\pi_{i+1,j+1})(\phi_{i+1,j+1,K}-\phi_{i,j+1,K})\}$$
$$+\tfrac{1}{2}\{\sigma_{K-1}[(\pi_{i,j}\alpha_{i,j,K-1})+(\pi_{i+1,j}\alpha_{i+1,j,K-1})]$$
$$+\sigma_{K+1}[(\pi_{i,j}\alpha_{i,j,K+1})+(\pi_{i+1,j}\alpha_{i+1,j,K+1})]\}(\pi_{i+1,j}-\pi_{i,j})]$$
$$+\tfrac{1}{2}\{\sigma_{K-1}[(\pi_{i,j+1}\alpha_{i,j+1,K-1})+(\pi_{i+1,j+1}\alpha_{i+1,j+1,K-1})]$$
$$+\sigma_{K+1}[(\pi_{i,j+1}\alpha_{i,j+1,K+1})+(\pi_{i+1,j+1}\alpha_{i+1,j+1,K-1})]\}(\pi_{i+1,j+1}-\pi_{i,j+1})]$$
$$G_y(\pi,\alpha,\phi)_{i+\frac{1}{2},\,j+\frac{1}{2},\,K}=\frac{1}{4d}\,\frac{1}{\overline{m}_{i,j}}\Big[\{(\pi_{i+1,j}+\pi_{i+1,j+1})(\phi_{i+1,j,K}-\phi_{i+1,j+1,K})$$
$$+(\pi_{i,j}+\pi_{i,j+1})(\phi_{i,j,K}-\phi_{i,j+1,K})\}$$
$$+\tfrac{1}{2}\{\sigma_{K-1}[(\pi_{i+1,j}\alpha_{i+1,j,K-1})+(\pi_{i+1,j+1}\alpha_{i+1,j+1,K-1})]$$
$$+\sigma_{K+1}[(\pi_{i+1,j}\alpha_{i+1,j,K+1})+(\pi_{i+1,j+1}\alpha_{i+1,j+1,K+1})]\}(\pi_{i+1,j}-\pi_{i+1,j+1})$$
$$+\tfrac{1}{2}\{\sigma_{K-1}[(\pi_{i,j}\alpha_{i,j,K-1})+(\pi_{i,j+1}\alpha_{i,j+1,K-1})]$$
$$+\sigma_{K+1}[(\pi_{i,j}\alpha_{i,j,K+1})+(\pi_{i,j+1}\alpha_{i,j+1,K+1})]\}(\pi_{i,j}-\pi_{i,j+1}) \qquad (5.6)$$

流體靜力方程式

$$\phi_1-\phi_3=\pi\alpha_2\triangle\sigma+\tfrac{1}{4}\pi\alpha_{0.5}\frac{\triangle\sigma}{2}$$
$$\phi_3-\phi_5=\pi\alpha_4\triangle\sigma$$
$$\phi_5-\phi_7=\pi\alpha_6\triangle\sigma+\tfrac{1}{4}\pi\alpha_{7.5}\frac{\triangle\sigma}{2}$$
$$\phi_7-\tfrac{3}{4}\pi\alpha_{7.5}\frac{\triangle\sigma}{2}=\phi_8(x,y) \qquad (5.7)$$

連續方程式

$$\frac{\partial}{\partial t}\left(\frac{\pi_{i,j}}{m^2_{i,j}}\right)+Div_2(V^*)_{i,j,K}+\frac{1}{\triangle\sigma}\left(\frac{\pi_{i,j}}{m^2_{i,j}}\dot{\sigma}_{i,j,K+1}-\frac{\pi_{i,j}}{m^2_{i,j}}\dot{\sigma}_{i,j,K-1}\right)=0 \qquad (5.8)$$

其中
$$Div_2(V^*)_{i,j,K}=-\frac{1}{d}\left[u^*_{i+\frac{1}{2},\,j,K}-u^*_{i-\frac{1}{2},\,j,K}+v^*_{i,\,j-\frac{1}{2},K}-v^*_{i,\,j+\frac{1}{2},K}\right] \qquad (5.9)$$

$$\dot{\sigma}_{i,j,K+1}=\dot{\sigma}_{i,j,K-1}-\frac{m^2_{i,j}}{\pi_{i,j}}\triangle\sigma\left[Div_2(V^*)_{i,j,K}+\frac{\partial}{\partial t}\,\frac{\pi_{i,j}}{m^2_{i,j}}\right] \qquad (5.10)$$

$$\frac{\partial}{\partial t}\left(\frac{\pi_{i,j}}{m^2_{i,j}}\right)=-\triangle\sigma\sum_{K=1,3,5,7}\left[Div_2(V^*)_{i,j,K}\right] \qquad (5.11)$$

其中
$$\dot{\sigma}_0=\dot{\sigma}_8=0$$

熱力方程式（用於 K=0.5,2,4,6,7.5 五層）

$$\frac{\partial}{\partial t}\left(\frac{\pi_{i,j}}{m^2_{i,j}}T_{i,j,K}\right)+Div_3(V^*T)_{i,j,K}+\frac{1}{\triangle\sigma}\left[\frac{\pi_{i,j}\,\dot{\sigma}_{i,j,K+1}}{m^2_{i,j}}T_{i,j,K+1}-\frac{\pi_{i,j}\dot{\sigma}_{i,j,K-1}}{m^2_{i,j}}T_{i,j,K-1}\right]$$
$$-\frac{\pi^2_{i,j}\alpha_{i,j,K}\dot{\sigma}_{i,j,K}}{C_p m^2_{i,j}}-\frac{\sigma_K}{C_p}\pi_{i,j}\alpha_{i,j,K}\frac{\partial}{\partial t}\,\frac{\pi_{i,j}}{m^2_{i,j}}-\frac{\sigma_K}{C_p}H(\pi\alpha\tilde{V}\pi)_{i,j,K}=0,\ (K=2,4,6) \qquad (5.12)$$

$$\frac{\partial}{\partial t}\left(\frac{\pi_{i,j}}{m^2_{i,j}}T_{i,j,0.5}\right)+Div_3(V^*T)_{i,j,0.5}+\frac{2}{\triangle\sigma}\left(\frac{\pi_{i,j}}{m^2_{i,j}}\dot{\sigma}_{i,j,1}T_{i,j,1}\right)-\frac{\pi^2_{i,j}\alpha_{i,j,0.5}\dot{\sigma}_{i,j,0.5}}{C_p m^2_{i,j}}$$
$$-\frac{\sigma_{0.5}}{C_p}\pi_{i,j}\alpha_{i,j,0.5}\frac{\partial}{\partial t}\left(\frac{\pi_{i,j}}{m^2_{i,j}}\right)-\frac{\sigma_{0.5}}{C_p}H(\pi\alpha\tilde{V}\pi)_{i,j,0.5}=0 \qquad (5.13)$$

$$\frac{\partial}{\partial t}\left(\frac{\pi_{i,j}}{m^2_{i,j}}T_{i,j,7.5}\right)+Div_3(V^*T)_{i,j,7.5}-\frac{2}{\triangle\sigma}\left(\frac{\pi_{i,j}}{m^2_{i,j}}\dot{\sigma}_{i,j,7}T_{i,j,7}\right)-\frac{\pi^2_{i,j}\alpha_{i,j,7}\sigma_{5}\kappa_{i,j,7.5}}{C_p m^2_{i,j}}$$

$$-\frac{\sigma_{7.5}}{C_p}\pi_{i,j}\alpha_{i,j,7.5}\frac{\partial}{\partial t}\left(\frac{\pi_{i,j}}{m^2_{i,j}}\right)-\frac{\sigma_{7.5}}{C_p}H(\pi\alpha\tilde{V}\pi)_{i,j,7.5}=0 \qquad (5.14)$$

其中，假設 $\dot{\sigma}_{0.5}=\dot{\sigma}_2/4$，$\dot{\sigma}_1=\dot{\sigma}_2/2$，$\dot{\sigma}_3=(\dot{\sigma}_2+\dot{\sigma}_4)/2$

$\dot{\sigma}_5=(\dot{\sigma}_4+\dot{\sigma}_6)/2$，$\dot{\sigma}_7=\dot{\sigma}_6/2$，$\dot{\sigma}_{7.5}=\dot{\sigma}^6/4$

$V_{0.5}=V_1$，$V_{7.5}=V_7$

運算符號 $Div_3(V^*T)_{i,j,k}$ 及 $H(\pi\alpha\tilde{V}\pi)_{i,j,k}$ 分別

代表下列運算

$$Div_3(V^*T)_{i,j,k}=\frac{1}{4d}[(u^*_{i+\frac{1}{2},j,k-1}+u^*_{i+\frac{1}{2},j,k+1})(T_{i,j,k}+T_{i+1,j,k})$$
$$-(u^*_{i-\frac{1}{2},j,k-1}+u^*_{i-\frac{1}{2},j,k+1})(T_{i,j,k}+T_{i-1,j,k})$$
$$+(v^*_{i,j-\frac{1}{2},k-1}+v^*_{i,j-\frac{1}{2},k+1})(T_{i,j,k}+T_{i,j-1,k})$$
$$-(v^*_{i,j+\frac{1}{2},k-1}+v^*_{i,j+\frac{1}{2},k+1}(T_{i,j,k}+T_{i,j+1,k})] \qquad (5.16)$$

$$H(\pi\alpha\tilde{V}\pi)_{i,j,k}=\frac{1}{8d}[\{(\pi_{i,j}\alpha_{i,j,k})+(\pi_{i+1,j}\alpha_{i+1,j,k})\}(u_{i+\frac{1}{2},j+\frac{1}{2},k}$$
$$+u_{i+\frac{1}{2},j-\frac{1}{2},k})(\pi_{i+1,j}-\pi_{i,j})+\{(\pi_{i-1,j}\alpha_{i-1,j,k})+(\pi_{i,j}\alpha_{i,j})\}$$
$$\times(u_{i-\frac{1}{2},j+\frac{1}{2},k}+u_{i-\frac{1}{2},j-\frac{1}{2},k})(\pi_{i,j}-\pi_{i-1,j})+\{(\pi_{i,j}\alpha_{i,j,k})+(\pi_{i,j+1}\alpha_{i,j+1,k})\}$$
$$\times(v_{i+\frac{1}{2},j+\frac{1}{2},k}+v_{i-\frac{1}{2},j+\frac{1}{2},k})(\pi_{i,j}-\pi_{i,j+1})$$
$$+\{[\pi_{i,j-1}\alpha_{i,j-1,k})+(\pi_{i,j}\alpha_{i,j,k})\}(v_{i+\frac{1}{2},j-\frac{1}{2},k}+v_{i-\frac{1}{2},j-\frac{1}{2},k})$$
$$\times(\pi_{i,j-1}-\pi_{i,j})] \qquad (5.17)$$

上式中

$$u_{i,j,k}=\frac{1}{2}\left\{\frac{u_{i,j,k-1}}{m_{i,j}}+\frac{u_{i,j,k+1}}{m_{i,j}}\right\}$$

$$v_{i,j,k}=\frac{1}{2}\left\{\frac{v_{i,j,k-1}}{m_{i,j}}+\frac{v_{i,j,k+1}}{m_{i,j}}\right\}$$

水汽方程式，其表示方法與熱力方程式大致相同。

氣體定律 $P_{i,j,k}\alpha_{i,j,k}=RT_{i,j,k}$，k=0.5,1,2,……,7,7.5 (5.18)

$P_{i,j,k}=\sigma_k\pi_{ij}+P_T$ (5.19)

6. 初值化 (Initialization)

①各變數在P與σ坐標間之轉換

吾人所用的氣象資料是一九七五年六月十日0000Z七個等壓面(即850,700,500,300,250,200及100mb)上的高度場，海面壓力$P_{sea\ sfc.}$，地表溫度和三個等壓面（即850,700及500mb）上的溫度露點差。這些資料主要都在等壓面上，而在計算過程中，首先需用到地形表面的壓力，P_s和等σ面上的高度場，溫度場和濕度場等。因此必須利用等壓面上的資料及一轉換公式，來求得吾人所需的資料，在此吾人所用的轉換公式爲

$$(Z_\sigma)_k=\alpha_k-\beta_k lnP_k+r_k(lnP_k)^2 \qquad (6.1)$$

其中 α_k,β_k,r_k 由 P_{k-1},P_k,P_{k+1} 三等壓面及其上之高度場 Z_{K-1},Z_K,Z_{K+1} 求得。

①等σ面上的高度場$(Z\sigma)_k$由包含此σ的各等壓面及其相對應的 α,β,γ 值求得。

利用 (6.1)，和地形表面高度 Z_s，吾人可求得地形表面之壓力，P_s：

$$lnP_s=2(\alpha-Z_s)/(\beta+\sqrt{\beta^2-4r(\alpha-Z_s)}) \tag{6.2}$$

②溫度場：由高度場（在等壓面：1000,850,700,500,300,200 及 100mb上）利用流體靜力方程式，可求出其間的溫度場T：

$$T=\frac{g(Z_u-Z_L)}{Rln(P_L/P_u)} \tag{6.3}$$

Z_u和Z_L 表示與要算溫度場相鄰上、下兩層（upper, lower）之高度場。

再由轉換公式，將等壓面上的溫度場內插到等σ面上：

$$(T_\sigma)_K=\alpha_K-\beta_K lnP_K+r_K(lnP_K)^2 \tag{6.4}$$

③計算比濕 q，假設比濕與壓力之平方成一線性關係，即

$$q_k=aP_k^2+b \tag{6.5}$$

由上述溫度及溫度露點差，可得露點溫度T_d(°K)（在海面，850,700及500mb）。

由公式

$$q_k=\frac{6220.}{P_k}exp\left[20.33\left(\frac{T_d-273.2}{273.2}\right)-22.3816\left(\frac{T_d-273.2}{273.2}\right)^2-0.50464\right]$$

可得海面，850,700及 500mb 上之比濕，由 (6.5) 式可得各層相對應之 a，b 常數值。並由此可將 q_k 內插至等σ面上。

(2)風場V及ω

依向量原理，風場V可分爲旋轉部份V_ϕ (rotational part) 及發散部份 (divergent part) V_χ

$$V=V_\phi+V_\chi=K\times\nabla\phi+\nabla\chi \text{ (在P坐標上)} \tag{6.6}$$

由於風場和壓力場必須互相平衡，在原始方程式計算過程中方不致有內重力波(Internal grarity wave)等之干擾。故 V_ϕ由平衡方程式 (balance equation) 求得。V_χ 由 (quasi-geostrophic ω-eq.) 準地轉 ω 方程式及連續方程式求得：

$$S\nabla^2\omega+f_0^2\frac{\partial^2\omega}{\partial p^2}=fo\frac{\partial}{\partial p}(V_g.\nabla(f+\zeta_g))-\nabla^2(V.\nabla(\frac{\partial\phi}{\partial p}))$$
$$-fo\frac{\partial}{\partial p}(K\nabla^2\zeta)+\nabla^2(K\nabla^2\frac{\partial\phi}{\partial p}) \tag{6.7}$$

$$\nabla^2 x+\frac{\partial\omega}{\partial p}=0 \tag{6.8}$$

其中 S 爲靜力穩定度 (static stability)

$$S=-\alpha\frac{\partial ln\theta}{\partial p},\ \theta=-\frac{gp}{R}\left(\frac{p_0}{P}\right)^\kappa\frac{\partial Z}{\partial p} \tag{6.9}$$

f_0 爲科氏力之平均值，$K=10^5$，ϕ爲流線函數

χ爲 Potential velocity.

$$\nabla^2\phi=\nabla.(f\nabla\psi)-\frac{\partial}{\partial x}\left[m^2\left(\frac{\partial\psi}{\partial y}\frac{\partial^2\psi}{\partial x\partial y}-\frac{\partial\psi}{\partial x}\frac{\partial^2\psi}{\partial y^2}\right)\right.$$
$$\left.+\left\{\left(\frac{\partial\psi}{\partial x}\right)^2+\left(\frac{\partial\psi}{\partial y}\right)^2\right\}\frac{\partial}{\partial x}\left(\frac{m}{2}\right)^2\right]$$
$$-\frac{\partial}{\partial y}\left[m^2\left(\frac{\partial\psi}{\partial x}\frac{\partial^2\psi}{\partial x\partial y}-\frac{\partial\psi}{\partial y}\frac{\partial^2\psi}{\partial x^2}\right)\right.$$
$$\left.+\left\{\left(\frac{\partial\psi}{\partial x}\right)^2+\left(\frac{\partial\psi}{\partial y}\right)^2\right\}\frac{\partial}{\partial y}\left(\frac{m}{2}\right)^2\right] \tag{6.10}$$

由此可由高度場求得風場，再由內插公式

$$(V\sigma)_k=\alpha_k-\beta_k(lnP_k)+r_k(lnP_k)^2$$

求得等σ面上之風場。

7. 計算步驟

由上節，吾人將初始天氣資料初值化，使風場和氣壓場平衡後，內插到等σ面上。在σ坐標原始方程式模式中，作24小時的預測計算。其計算步驟如下：

(1)由 (5.11) ，tendency equation，吾人可得 $\partial(\pi/m^2)/\partial t$。

(2)由 (5.10) ，連續方程式，吾人可得$\dot{\sigma}$值。

(3)由 (5.18) ，氣體定律，吾人可得α值。

由 (5.7) ，流體靜力方程式，吾人可得ϕ值。

(4)由 (5.1) ， (5.2) ，運動方程式，吾人可得 $\partial(\pi V/m^2)/\partial t$

(5)由 (5.12) ， (5.13) ， (5.14) 熱力方程式，吾人可 $\partial(\pi T/m^2)/\partial t$

(6)由水汽方程式，求得 $\partial(\pi q/m^2)/\partial t$

(7)將(1)，(4)，(5)，(6)步驟中求得的 tendency value，對時間積分，求得下一時刻的 π, V, T, q 等值。

(8)第(1)到第(7)步驟重複做，至24小時爲止。

(9)將24小時計算的 V, T, q 等再依相同的轉換內插公式， (6.1) 式換算到等壓面上， 並由平衡方程式，計算出高度場，以與實際天氣比較。

8. 時間積分

在本文中所用的時間間隔爲 $\triangle T=6$ 分鐘，對於水平網格間距 $d=240$公里而言，合乎計算穩定條件。

時間積分 scheme 是採取 Euler-backward 及 Leapfrog方法合併使用，以五個 time steps 爲一單元中前三個 steps 用 Euler-backward method，後二個 steps 用 Leapfrog method。如此能避免 computational mode 之產生，對 physical mode 有 selective damping 之效果，並且不會太耗計算時間。Euler-backward method：

$$A^*=A^t+\triangle T(\frac{\partial A}{\partial t})^t$$

$$A^{t+1}=A^t+\triangle T(\frac{\partial A}{\partial t})^* \qquad (8.1)$$

Leapfrog method：

$$A^{t+1}=A^{t-1}+2\triangle T(\frac{\partial A}{\partial t})^t \qquad (8.2)$$

A^*, 表示猜測值 (tentative value).

9. 計算結果之分析與討論

初始天氣資料爲一九七五年六月十日及十一日 0000 Z， 經陳泰然教授主觀分析後的東亞地區天氣資料 (陳泰然，1977, Tech. Rep. No. Mei-Yu-001, NTU) 。七層 (1000,850,700,500,300,200及100mb) 的初期狀態天氣型態分別如下：

1000mb：日本東南海上附近有一低壓，槽線由此向西南延伸，經臺灣北部再向西北延伸至中國大陸西南之另一低壓。鄂霍次克海附近有一高壓中心，此高壓向西南延伸至韓國及遼東半島以西。其西蒙古附近有一低壓中心，低壓軸線大致是南北走向的。再向西，中國大陸西北又有一高壓中心。西太

平洋有一弱高壓。

850mb和700mb：日本東南海上，有一相當弱的低壓中心，槽線由此中心向西南延伸經臺灣北部東海面至位於華南之另一低壓中心，此槽線在 850mb 上者較 1000mb 上者北移，而 700mb 上此槽線又較 850mb 上者略偏北。700mb 和 850mb 上都可見一弱反氣旋，位於華北。故在上述槽線以北，普遍吹着東風和北風，而在槽線以南却主要是西南風，特別是臺灣附近尤其顯著。在 850mb 上的西南噴射氣流位於巴士海峽上空，而 700mb 的西南噴射氣流較 850mb 上者略向北移，橫跨臺灣中部。蒙古附近有一低壓中心，槽線由此中心向南延伸至華中。

500mb ： 主槽由日本海上空業已發展之低壓中心向西南延伸至臺灣東北，另一槽線由蒙古向南延伸，（略偏向西南），較之於 700和 850mb上者稍微傾斜。巴士海峽，南中國海一帶有一反氣旋中心，故在500mb上，臺灣附近盛行西北風。斜壓區位於北緯30度以北，噴射氣流在暖區，在此層上可見到典型的冷低壓（或槽）和暖高壓（或脊）型態。

300mb ： 此層環流系統與500mb上者非常相似。日本海上空有一低壓中心，蒙古一帶有另一低壓，其間有一脊。中國大陸西南有一高壓，弱風多出現於高低壓中心之間，沿著脊線亦有弱風，西北噴射氣流出現於中國大陸西北；西南噴射氣流由華東延伸至日本東南，成一帶狀。

200mb 及 100mb：此二層上的環流系統與300mb上的非常相似。低壓中心在日本海上空，槽線由此中心向西南延伸至臺灣以北之海面上。位置較300mb上者略偏東。中國大陸西南有一高壓，噴射氣流自青康藏高原以北至日本海一帶，以200mb上風速最強，比300mb上者還強。

而其中900,700,500,300mb四層高度場經平衡方程式模式初值化後的天氣型態（如圖十三至十六）。氣溫場如圖二十一至二十四。與上述原始天氣型態相近，僅300mb中國大陸西南之高壓經初值化後，向東發展，至臺灣東方之太平洋上。

24小時以後，即一九七五年，六月十一日0000Z 的實際天氣型態如下：

1000mb： 日本海附近之低壓中心略爲填塞，槽線由日本向西南延伸經巴士海峽至印度支那半島的低壓中心。此槽線較10日向東南移動。 鄂霍次克海高壓中心略爲發展， 脊線由此中心經庫頁島，韓國至華東沿海。另一高壓中心在華中，蒙古附近有二低壓中心。

850mb ： 日本東南海面有一低壓中心，槽線由此中心向西南延伸，經臺灣北部海面向西進入中國大陸西南之低壓中心。此槽線向南無明顯的移動。槽線以北，華中有一弱反氣旋，此反氣旋之西及東北皆各有一稍強之反氣旋，此時華中反氣旋比原來略爲增強，其西之反氣旋反而削弱，而其東北者強度大致保持不變。中國大陸北方，蒙古一帶有一低壓，較原來增強，槽線爲南北方向，向東移動約200公里。

700mb ： 日本上空有一弱低壓，槽線由此向西延伸，經臺灣北部海面，再向西北至華西，華中有一弱反氣旋。脊線由庫頁島一帶向西南延伸至華中後亦偏向西北走，至中國大陸西北。蒙古北方有一低壓槽，槽、脊線都較原來的位置略向東南移動約200多公里。

500mb ： 日本海上空之低壓略爲填塞，槽線由此中心向西南延伸至臺灣東部，較原來的位置向東移了 200多公里，脊線自庫頁島西方之大陸上向西南延伸至華中。其北端向東傾斜。脊之西，蒙古附近有一低壓，中心略爲填塞，槽線亦向西南延伸，並向東移。

300mb ： 日本海上之低壓中心向南移200多公里，強度大致維持不變。 蒙古北方之低壓發展，並向東移成一強度與前者相若之低壓中心，其間高壓脊向東移，強度亦未有太大之變化。

200mb ： 庫頁島東南至北海道北端海面上之低壓略爲填塞。蒙古北方之低壓略向東南發展，其間脊線向東移動。中國大陸西部之高壓系統範圍向南略爲擴展。

100mb ： 日本海上空之低壓略爲填塞，並向東移。中國大陸西方之高壓範圍擴展，增強。

經過σ坐標原始方程式模式，絕熱情況，24小時的計算， 地面壓力的變化（圖五及圖六）， 尚稱合理。但1000,850和700mb的天氣型態（如圖十一，十二）未能成功地模擬。500mb（如圖十）鄂霍次克海高壓脊移動速度較實際天氣慢，且其強度與範圍都較實際天氣小，日本海低壓位置偏北，槽線由此中心向西南延伸至臺灣東部海面上，其位置較實際位置偏東。鄂霍次克海高壓脊偏向西北，同時中國大陸北方之低壓亦向北退縮，中國大陸西部之高壓向西退縮。

爲了與P坐標原始方程式模式的計算結果比較，將上述初始資料放入P坐標原始方程式模式中（一九七六，蕭），作24小時之預測計算，該模式爲非絕熱系統，以簡單的參數化方法，考慮大幅度（Large scale）的潛熱及可感熱之作用，其結果如下：

900mb：此層的初始資料（如圖十六）是由1000mb，850mb和700mb內插而得。故24小時的計算結果（如圖二十）無法與實際天氣比較，但與其初始資料比較發現，原來在韓國北方之弱高壓逐漸發展成一高壓，脊線由此中心向西南延伸。中國大陸西南有一低壓，變化不大。中國大陸北方蒙古附近之低壓發展，形成低壓中心。在實際天氣中，1000mb及850mb，此低壓亦在增強。蒙古西方之高壓受此低壓之發展而被擠壓，向西退縮。西太平洋之高壓向西發展，至菲律賓東北方海面。其氣溫場見圖二十八。此層天氣型態之變化趨勢與實際天氣中1000mb及850mb之變化趨勢比較，是合理的。

700mb：如圖十九，低壓中心在日本海南端，槽線由此中心向西南延伸經臺灣北部海面，再向西延伸至中國大陸西部另一低壓。此槽線經24小時之運算，向南移動，速度較實際天氣較慢。中國大陸西都之低壓強度較實際天氣中的弱。蒙古附近一低壓中心，低壓槽爲南北走向，與實際天氣相同，移動速度亦與實際天氣中的相近。高壓脊由鄂霍次克海向西南延伸至華北，華北有一弱反氣旋。此高壓脊移動速度較實際天氣中的略慢。太平洋高壓向西南延伸至呂宋島附近，其範圍較實際天氣中的略大。氣溫場之計算（見圖二十七），一般而言，較實際氣溫低1～2°C， 唯中國大陸西南之低壓中心附近，氣溫較實際低7°C左右。

500mb：見圖十八日本海上空低壓中心向東移動的速度較實際略慢，中心強度較實際的強約20m。槽線由此中心向西南延伸至臺灣東部海面上。蒙古附近低壓強度較實際者弱，向南移動的速度也較慢。中國大陸西南之高壓系統減弱。華南、廣東附近有一高壓。一般而言，天氣型態，除移動速度較慢（24小時約慢100多公里）外，甚爲接近實際狀況。 氣溫場（見圖二十六）亦與實際氣溫場相近，除低壓中心氣溫較實際狀況低2°C，高壓中心氣溫較實際狀況高0.7～1°C，其餘幾乎與實際狀況一致。（例如蒙古低壓中心氣溫計算值爲257°K，而實際值爲258.8°K， 日本附近之低壓中心氣溫計算值爲255°K，而實際值爲257.8°K，鄂霍次克海高壓脊氣溫爲264°K， 而實際值爲263.7°K，廣東附近高壓中心氣溫計算值爲271°K，而實際值爲269.9°K）

300mb：見圖十七日本海上弱低壓中心，其預測強度與實際情況相近，移動速度比實際狀況略慢。中國大陸西北之弱低壓，比實際天氣系統運動較慢，強度較弱。其間之高壓脊強度與實際天氣相近。移動速度亦比實際狀況稍慢（24小時慢100多公里）， 中國大陸西南之高壓則向東伸展至臺灣東方之西太平洋上，與實際狀況比較，發展過甚。不過在計算之初，初始資料經平衡方程式模式初值化後，此高壓範圍就向東伸展至臺灣東方之西太洋上 。 計算的氣溫場（見圖二十五），鄂霍次克海高壓脊較實際狀況略低2.5°C，計算值爲234°K，實際值爲236.5°K， 日本海附近低壓中心氣溫計算值爲231°K，實際值爲228.7°K，較實際狀況略高2.3°C。中國大陸西南之高壓中心氣溫計算值爲247°K，實際值爲 246.7°K，僅略高 0.3°C。其餘亦與實際狀況相近，相差在±2°C左右。

在絕熱σ坐標與非絕熱P坐標原始方程式24小時的計算結果，發現：

(1)24小時的計算都相當穩定。顯示初始資料處理良好，且模式中對空間之差分和對時間的積分都合理。並顯示24小時的預測在有限區域內的計算是可行的。

(2) σ 坐標中能够便利地計算地表壓力變化，這是其特色之一，其計算結果合理。

(3)在非絕熱P坐標系中，四層的計算結果，無論天氣型態，槽脊線的形狀，位置都與實際天氣狀態接近，甚至氣溫場的誤差也在2°C左右。僅 Phase speed 的速度略爲落後，約24小時慢100多公里。

(4)在絕熱 σ 坐標中，上層（500mb以上）的計算結果較下層者好。下層受地表之摩擦作用、加熱作用及水汽潛熱釋放之影響很大，在未考慮這些因素之下，其計算結果不好。吾人將把加熱摩擦及擴散等作用加入，繼續探討其影響，及尋求改進之道。

References

Itoo, H. and Y. Isono, 1971: "Hemispheric Forecast with the Primitive Equation Model", Journal of the Meteorological Society of Japan, **49**, Special Issue. Dec, P.613~627.

Langlois, W.E., and H.C.W. Knok, 1969: "Description of the Mintz-Arakawa Numerical General Circulation Model", Uni. of California, Los Angeles, Numerical Simulation of Weather and Climate, Technical Report No. 3,P.1-95.

Philip, 1957: "A Coordinate System Having Some Special Advantage for Numerical Forecasting", J.Meteor, **14**, P.184~185.

Tai-Jen George Chen and Ching-Yen Tsay, 1977: "A Detailed analysis of a case of Mei-Yu System in the Vicinity of Taiwan". Tech. Rep. No. Mei-yu-001, Dept. of Atmos. Sci, NTU, Taipei, Taiwan, Rep. of China.

陳泰然，1977：臺灣梅雨平均結構之個案研究，大氣科學，第四期，P38~47

蕭錫璋，1976：有限區域原始方程式模式之初步探討，Ann. Rep. of Inst. of Physics, Academia Sinica, **6**,P.231~262.

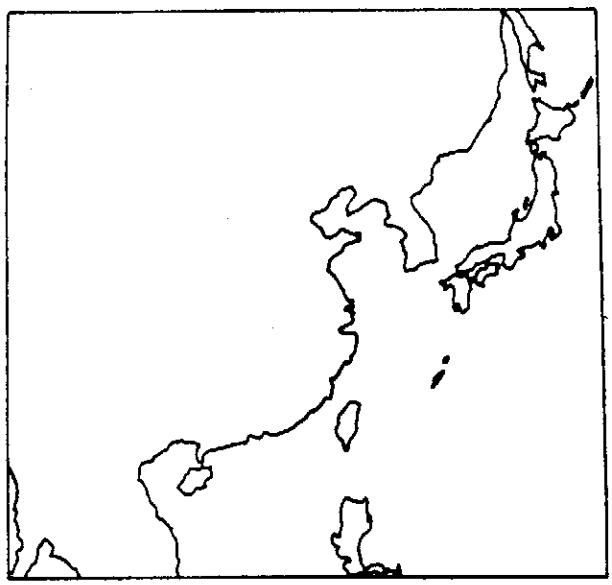

圖一　計算範圍

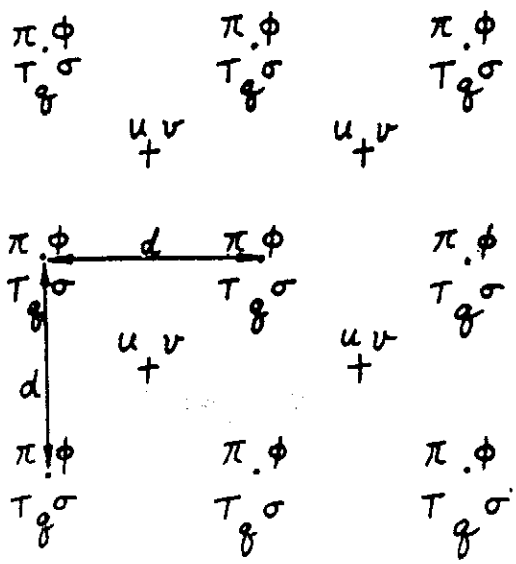

圖二　水平網格結構

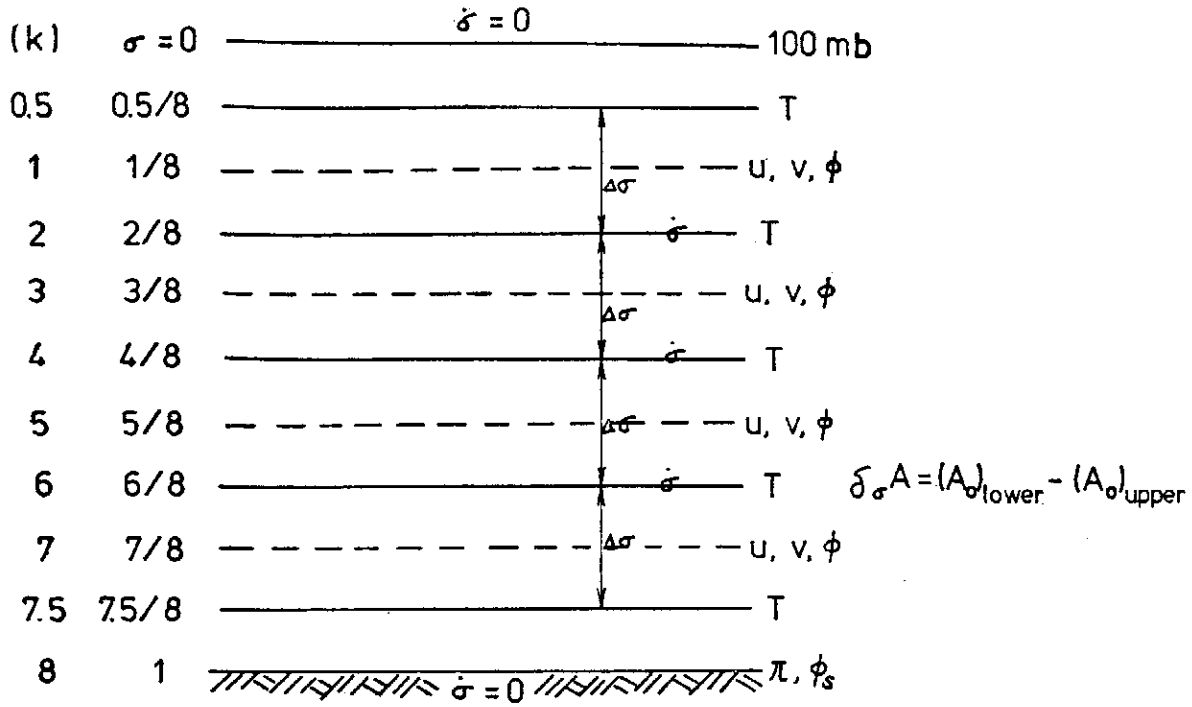

圖三　垂直分層結構

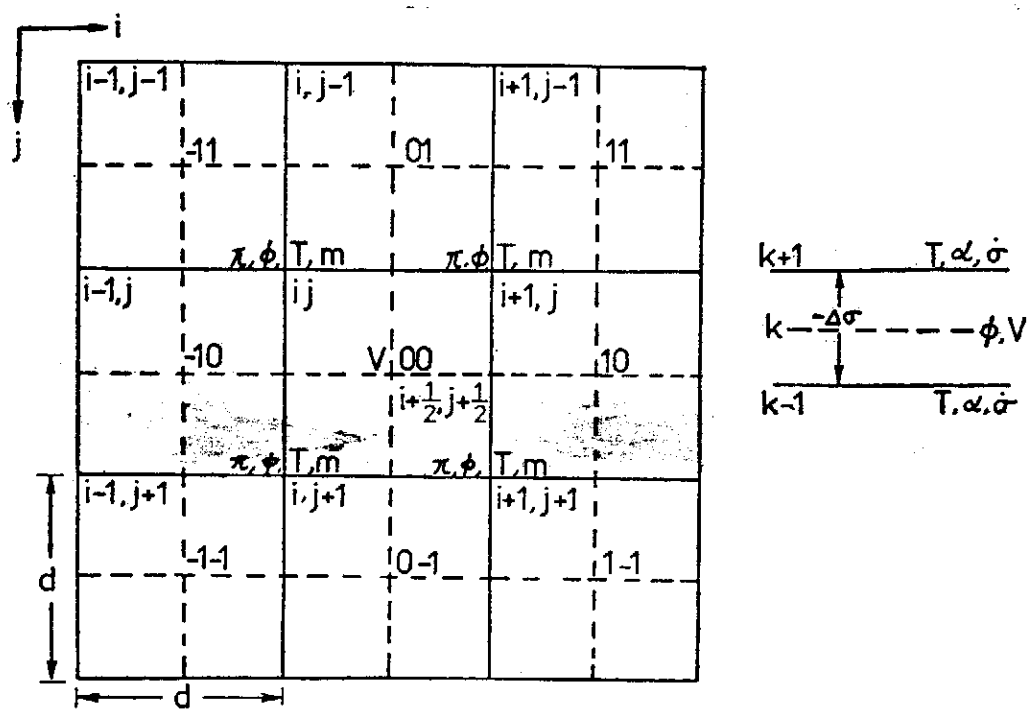

圖四　定差式中的網格結構

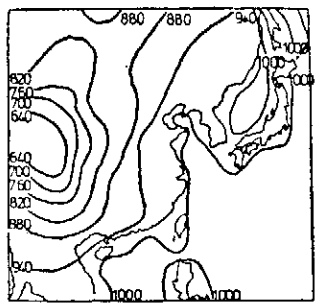

圖五　地表面壓力場（64年6月10日 0000z）初始值

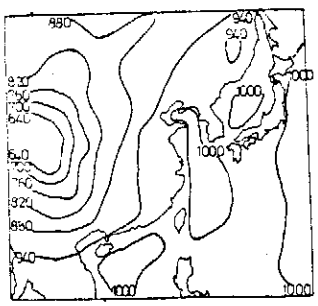

圖六　24小時後地表面壓力場之計算值（在σ坐標PE模式中）

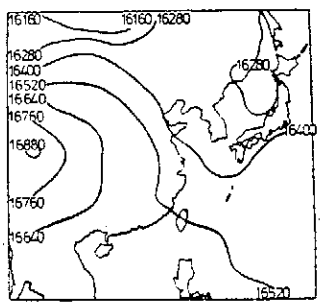

圖七　24小時後100mb高度場計算值（σ坐標PE模式中）

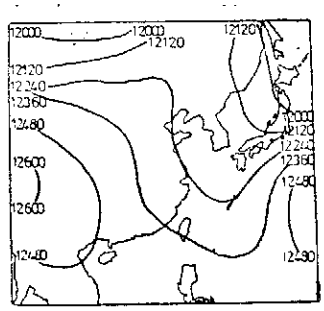

圖八　24小時後200mb高度場計算值（在σ坐標PE模式中）

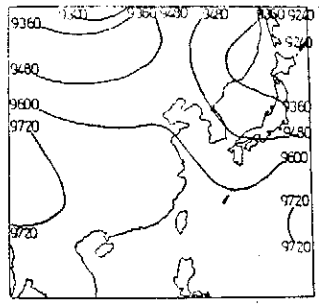

圖九　24小時後3300mb高度場計算值（在σ坐標PE模式中）

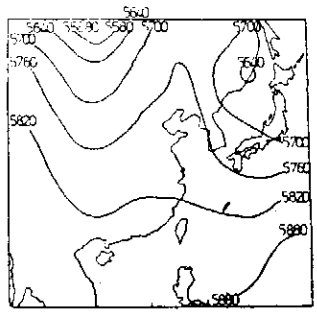

圖十　24小時後500mb高度場計算值（在σ坐標PE模式中）

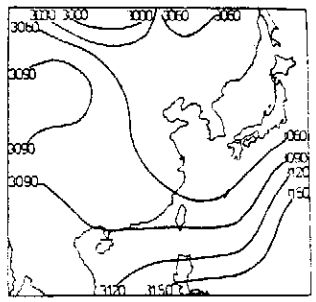

圖十一　24小時後700mb高度場計算值（在σ坐標PE模式中）

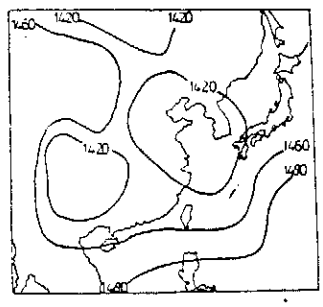

圖十二　24小時後850mb高度場計算值（在σ坐標PE模式中）

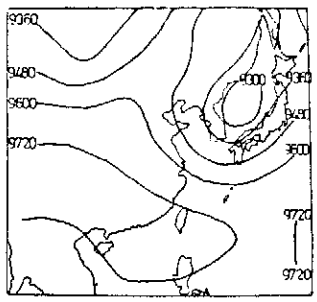

圖十三　在P坐標P E模式中初值化後300mb高度場之計算值

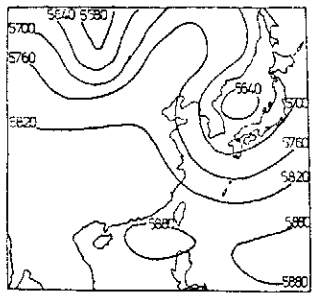

圖十四　在P坐標P E模式中初值化後500mb高度場之計算值

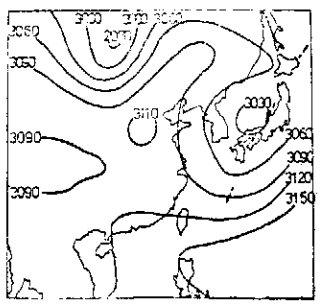

圖十五　在坐標P E模式中初值化後700mb高度場之計算值

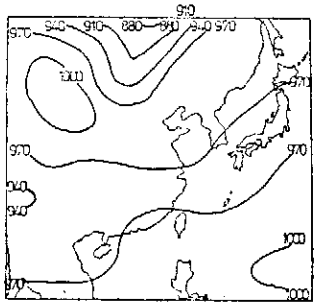

圖十六　在P坐標P E模式中初值化後900mb高度場之計算值

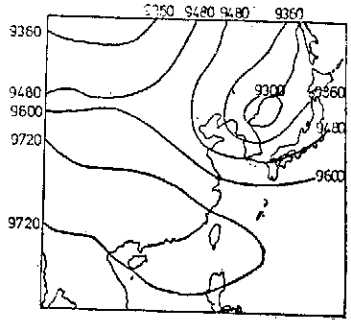

圖十七　在P坐標P E模式中24小時計算之300mb高度場

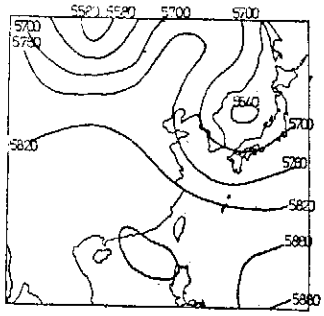

圖十八　在P坐標P E模式中24小時計算之500mb高度場

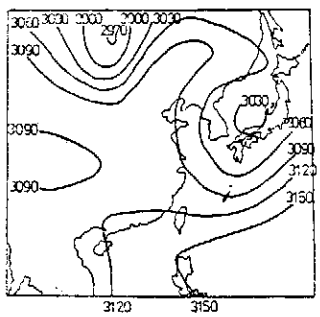

圖十九　在P坐標P E模式中24小時計算之700mb高度場

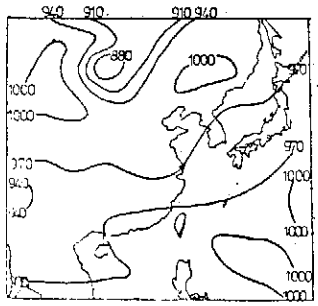

圖二十　在P坐標P E模式中24小時計算之900mb高度場

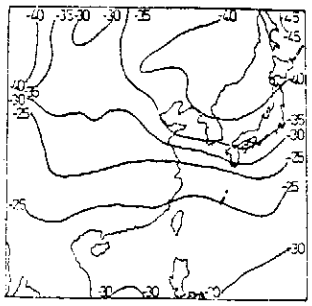

圖二十一　在P坐標P E模式中初值化後300mb之溫度場

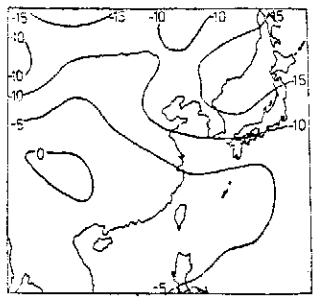

圖二十二　在P坐標P E模式中初值化後500mb之溫度場

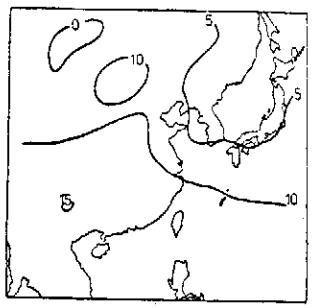

圖二十三　在P坐標P E模式中初值化後700mb溫度場

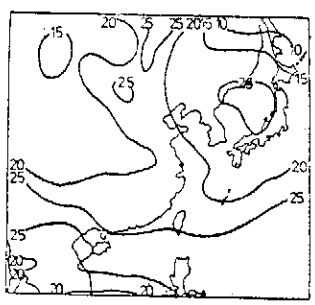

圖二十四　在P坐標P E模式中初值化後900mb溫度場

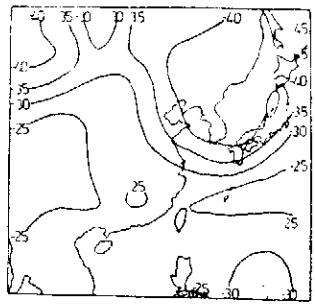

圖二十五　在P坐標P E模式中24小時計算後300mb溫度場

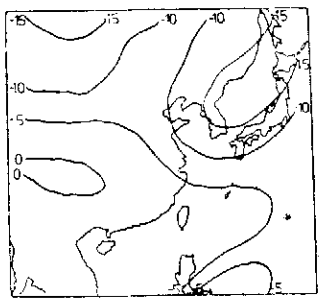

圖二十六　在P坐標P E模式中24小時計算後500mb溫度場

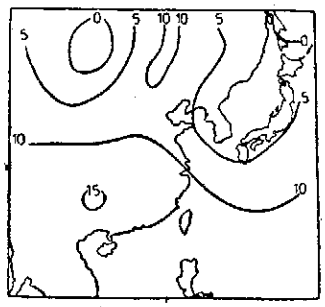

圖二十七　在P坐標P E模式中24小時計算後700mb溫度場

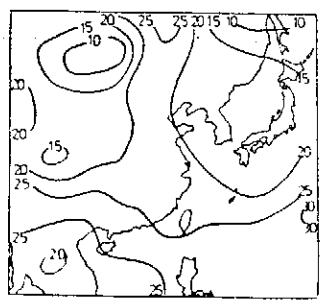

圖二十八　在P坐標P E模式中24小時計算後900mb溫度場

Annual Report of the Institute of Physics, Academia Sinica, Vol.7, 1977

潛水體之阻力試驗及其尺度效應之研究

汪群從　陳義男　陳正祐

摘要

本文目的爲設計一組試驗儀具，以測度潛水體模型之總阻力，並且探討顯示在小型寬4m，水深約2m之船糟進行5 ft 及7 ft 潛水體模型試驗時，適宜的考慮阻礙 (blockage) 效應及接近水面效應 (Near free surface effect) 後與 $DTMB$寬約15.5m，水深約7.7m之船糟中，9ft 潛水模型試驗數據比較，似無尺度效應，初步證實小型船糟使用5ft至7ft模型可供研討試驗使用。試驗同時提供沒水深度與直徑比 (d/D) 在3.03及4.27，潛水體接近水面時之阻力增加值，供設計參考之用。

* 本文發表於 NTU-INA-Tech. Rept. 61, June 1977.

Experimental Study of a 28,900 dwt Single-screw Multi-purpose Vessel

J.L. Hwang　C.T. Wang　C.M. Chung

Abstract

Geosim model Tests were conducted for a 28,900 dwt single-screw multi-purpose vessel. For model-ship correlation, three dimensional analysis method was introduced for full load condition power prediction, whereas two dimensional analysis method was used for sea trial condition power prediction.

For the vessel studied, the ship will be able to cruise around 19kt (MCR) at sea trial condition and aronud 16.40 kt (NOR) at full load condition at the engine output power provided the designed propeller be modified, i.e., the prodeller diameter and/or pitch be increased.

本文發表於 NTU-INA-Tech. Rept. 69, Augnst 1977

Annual Report of the Institute of Physics, Academia Sinica, Vol.7, 1977

Buoyant Surface Discharge and Small-Scale Oceanic Fronts: A Numerical Study*

Timothy W. Kao, Cheol Park, and Hsien-Ping Pao

Department of Civil Engineering, Catholic University of America, Washington, D .C. 20064

A study is made of the two-dimensional buoyant surface discharge into an ambient body of water. The numerical study is based on an initial boundary value problem using the full Navier-Stokes and dfifusion equations. A turbulence model using the Munk-Anderson parameterization formula for density straification effect is also incorporated. The results show the establishment of a surface density current with strong surface convergence and downwelling near the front. Comparison is made with the field experiments of Garvine and Monk on a small-scale oceanic front in Long Island Sound. Excellent agreement is obtained.

* This eaper has been published in J. of Geophysical Research, Vol.82, No.12, 1977,P. 1747~ 1752

Observations of Wave Motion and Upstream Influence in a Stratified Fluid

D. A. Hurdis
Assistant Professor,
Department of Mechanical Engineering,
The University of Maryland,
College Park, Md. ASME

H.-P. Pao
Professor,
Department of Aerospace and Atmospheric Sciences,
The Catholic University of America,
Washington, D. C.

Abstract

The disturbances created by the motion of a vertical flat plate within the density-gradient region between two superimposed liquid layers were examined both experimentally and numerically. An upsteam infuence, which from a balance of inertial and gravitational forces, was observed, and it was possible to predict the behavior of this influence with the numerical. The prediction included a description of the propagation of the upstream influence to steadily increasing distances from the flat plate and the shapes and magnitudes of velocity profiles.

* This paper has been published in J. of Applied Mechanics, Paper No. 76-APM-Q, P.1~5

Vortex Structure in the Wake of a Sphere*

Hsien-Ping Pao and Timothy W. Kao

Department of Civil Engineering, The Catholic University of America, Washington, D. C. 20064

Abstract

Results showing the three-dimensional vortex shedding structure when a sphere is towed at a constant velocity through a stratified fluid are presented. It is found tnat for small Richardson numbers (weak stratification) and Reynolds numbers in the range from 4×10^3 to 2×10^4 the vortex is shed three-dimensionally. However, stratification quickly and effectively inhibits the vertical motion and the initially turbulent wake collapses and reveals the vortex structure, reminiscent of a two-dimensional vortex street behind a circular cylinder when viewed from above. The structure is, however, distinctly three-dimensional. It is also found that the estimated vortex shedding frequency is in reasonable agreement with previously published results for a sphere in a homogeneous fluid. It is suggested that a weak stratification is an excellent means for revealing the vortex structure of a three-dimensional body in a homogeneous fluid, and that the vortex tube in the wake of a sphere in a homogeneous fluid has a closed-end double helical structure. Two branches of the double helix are continuously unwinding in an opposite sense from the formation region. Moreover, the present helical model satisfies Thompson' s circulation theorem in contrast to previously proposed helical models.

* This paper has been published in The Physics of Fluids, Vol.20, No.2, Feb, 1977, P.187~191.

Numerical Computation of a Stationary Two-Dimensional Vortex Flow in the Presence of a Barrier*

Robert R. Hwang, H.P. Pao and T.Y. Kou

Institute of Physics, Academia Sinica Nankang, Taipei, Taiwan

Abstract

In this study effect of barrier on the vortex is studied theoretically in terms of the understanding of the dynamical events associated with its blocking phenomena. A numerical model has been successfully developed for a stationary two-dimensional voretx flow in the presence of a barrier, using the full Navier-Stokes equations. The numerical results show the development of flow separation in the lee of the barrier and its formation of a secondary vortex behind the barrier. These results were compared favorably to the laboratory experiments and the field data on typhoons when encountering the island of Taiwan.

* This paper has been published in Atmospheric Science, Vol.4, May 1977, p. 28~37.

Annual Report of the Institute of Physics, Academia Sinica, Vol.7, 1977

The Effects of Mountains on a Typhoon Vortex as Identified by Laboratory Experiments Part II. Three Dimensional Barriers*

H. P. Pao, Robert R. Hwang and Jin Jso

Institute of Physics
Academia Sinica

Abstract

This paper continues the former study of the experimental performed series for investigating the interaction between the typhoon vortex and Taiwan island. An essentially two-dimesional free vortex in an otherwise uniform flow past a three-dimensional barrier is studied and three kinds of three-dimensional symmetrical models resembling the general shape of Taiwan are used. Results show that the phenomena of blocking and deflecting, and its moving path of the free vortex are similar for these three barriers. The vortex movement seems to be strongly dependent on the approaching path way of the vortex relative to the barrier. Comparisons are also made between the experimental results and field data. It is found that the flow patterns and the moving paths of the free vortex are resonably similar to the actual track of typhoon vortex. This suggests that the laboratory modeling may be a reasonable tool to predict the movement of typhoon vortex when it is in the vicinity of the island.

* This paper has been published in Proceedings of the Natonal Science Council,No.10, Part 1, May 1977, p. 251.

The Mixing Characteristics of Turbulent Buoyant Jets in Ambient Receiving Environments*

Paul Y.P. Kou[1], Robert R. Hwang[2] and C.S. Hung[3]

Abstract

The behavior of a set of heated water jets discharging into a shallow flowing environment was considered in a laboratory study. The relative effects of jet interaction and surface distortion were considered and three aspects of this problem singled out for particular attention: firstly, some means whereby stratified flow might be distinguished from mixed flow; secondly, the manner in which mixing varies with distance downstream from the discharge ports; thirdly, the flow regimes arising from combined mixing and buoyancy effects which can be expected in this type of flow system.

[1] Graduate School of Civil Eng., National Taiwan Univ., Taipei, Taiwan.
[2] Institute of Physics, Academia Sinica, Nankang, Taipei, Taiwan.
[3] M.S. of Civil Engineering Department, National Taiwan University.

* This paper has been published in Proceedings of the National Science Council No.10, Part 3, May 1977, p.195.

Annual Report of the Institute of Physics, Academia Sinica, Vol.7, 1977

Effects of Mountains on a Typhoon Vortex: A Laboratory Study*

H. P. Pao (鮑咸平)

The Catholic University of America, Washington, D. C.

and

R. R. Hwang (黃榮鑑)

Academia Sinica, Taipei, Taiwan

Abstract

In this study laboratory experiments have been performed by introducing a concentrated vortex which then interacts with a barrier resembling the gencral shape of the mountainons island of Taiwan. In the absence of the baerier the vortex is drifting at a constant speed along a flume, which is also the speed of the flowing water. No thermodynamic effects were provided for in the laboratory model, hence the effect of latent heat is entirely ignored.

The important governing parameters of the laboratory experiments are the Rossby number and the Reynolds number, both based on the circulation of the vortex. The basic objective of the present laboratory study is to find out whether such a laboratory modeling can reasonably simulate encountering event of a typhoon with the island of Taiwan.

When comparing the field data with the laboratory results, it is found that (i) the surface flow pattern of a typhoon when encountering the island can reasonably be simulated in the laboratory: such as secondary lows due to vortox shedding and flow separation, stagnation flow pattern, etc., (ii) the moving tracks of the vortex obtained from the laboratory are in close agreement with the real typhoon tracks

It is concluded that (i) when the typhoon vortex approaches the island of Taiwan thc mechanical encounter between the vortex and the mountain barrier is the sole dominant factor in the entire event. Therefore, the present laboratory model has provided a first order solution to the problem of typhoon movenent in the immediate vicinity of the island. The effects of the latent heat, the detailed secondary flow in the typhoon vortex and the Coriolis force can be considered as of secondary importance. (ii) Although the Reynolds number is only 10^4 in the laboratory which is much small than $10^{12}\sim10^{13}$ for actual typhoons, the similarity of the behavior and movement for typhoons and the vortex in the laboratory is remarkable. This seems to indicate that the Rossby number may be more important than the Reynolds number in this case, as long as the values of the Reynolds number in the laboratory are reasonably large. (iii) This laboratory modeling is certainly a valuable tool in studying the encounter of typhoons with the island. But this, by no means, can replace the field observation or numerical modeling. It is believed that the laboratory investigations are definitely complementary to the field observations, and that they will help to isolate certain important mechanisms and to untangle otherwise very complicated atmospheric flow phenomena, especially in the precsence of mountain barriers.

* This paper presented on 11th Technical Conference on Hurricanes and Tropical Meteorology of fhe American Meteo. Soc., Dec. 13-16, 1977 at Miami Beach, Florida.

Annual Report of the Institute of Physics, Academia Sinica, Vol.7, 1977

The Effect of a Barrier on a Two-dimensional Vortex Flow*

Robert R. Hwang and C. T. Wang
(黃榮鑑) (汪群從)

Institute of Physics
Academia Sinica

Abstract

In this study effect of a two-dimensional elliptical barrier on the vortex flow is studied theoretically in terms of the understanding of the dynamical events associated with its blocking phenomena. Using the full Navier-Stokes equaions, a numerical model based on the streamfunction/vorticity formulation has been developed for the computations of the laminar two-dimensional flow for a stationary vortex in the presence of a barrier as well as a moving vortex past a two-dimensional elliptical barrier. To the case of a moving vortex, the moving track of the vortex is specified which was obtained from the laboratory experiments. The numerical results show the development of flow seperation in the lee of the barrier and its formation of a secondary vortex behind the barrier. These results were compared favorably to the laboratory experiment on the vortex flow when encountering with the barrier considered.

* 本文發表於第一屆中國力學會議，民國六十六年十二月十七、十八。